Neurodegeneration in toxin-mediated demyelinating animal models of Multiple Sclerosis

Dissertation

for the award of the degree
"Doctor of Philosophy" (Ph.D.)
Division of Mathematics and Natural Sciences
of the George-August-Universität Göttingen

submitted by

Natalia Manrique Hoyos

born in

Cali, Colombia

Göttingen 2012

Members of the Thesis Committee:

Prof. Dr. Mikael Simons, Reviewer
        Max Planck Institute of Experimental Medicine
        Department of Neurology, University of Göttingen
Prof. Dr. Wolfgang Brueck, Reviewer
        Department of Neurobiology, Max Planck Institute for Biophysical Chemistry
Prof. Till Marquardt, Ph.D.
        Department of Neurogenetics, Max Planck Institute of Experimental Medicine

Date of the oral examination: 18 October, 2012

Affidavit

I hereby declare that this PhD thesis **"Neurodegeneration in toxin-mediated demyelinating animal models of Multiple Sclerosis"** has been written independently with no other aids or sources than quoted.

<div align="right">

Natalia Manrique Hoyos

September, 2012

Göttingen, Germany

</div>

Contents

List of Figures

Abbreviations

ANOVA	Analysis of variance
APC	Antigen presenting cell
APP	Amyloid precursor protein
APS	Ammonium persulfate
BSA	Bovine serum albumin
CNPase or CNP	2',3'-cyclic-nucleotide 3'-phosphodiesterase
CNS	Central nervous system
DD	Double demyelination
Distac	Distance in meters accumulated in 24 hours
Distmax	maximum distance per run
DNA	Deoxyribonucleic acid
EAE	Experimental autoimmune encephalomyelitis
ECD	Transmembrane domain
EDTA	Ethylenediaminetetraacetic acid
EGFP	Enhanced green fluorescent protein
EtBr	Ethidium bromide
ER	Endoplasmic reticulum
GPI	Glycosyl phosphatidylinositol
HEPES	4-(2-hydroxyethyl)-1-piperazineethanesulfonic acid
h	Hour(s)
HRP	Horse radish peroxidase
kDa	Kilodalton
L	liter
LFB/PAS	Luxol Fast Blue/ Periodic Acid Schiff
MAG	Myelin-associated glycoprotein
MBP	Myelin basic protein
min	Minute(s)
MOG	Myelin oligodendrocyte glycoprotein
MOSS	Motor Skill Sequence
MRI	magnetic resonance imaging

MS	Multiple Sclerosis
Nrun	number of individual runs in 24 hours
P14	Postnatal day 14
PAGE	Polyacrylamide gel electrophoresis
PFA	Paraformaldehyde
PBS	Phosphate buffered saline
PCR	Polymerase chain reaction
PLL	Poly-L-lysine
PLP	Proteolipid protein
pOLs	Primary oligodendrocytes
PI	Phosphatidylinositol
PLP	Proteolipid protein
PPMS	primary progressive Multiple Sclerosis
ROI	region of interest
RRMS	relapsing-remitting Multiple Sclerosis
RT	room temperature
RNase	Ribonuclease
ROI	Region of interest (microscopy)
RT	Room Temperature
SDS	Sodium dodecyl sulphate
s	Second(s)
sec	second(s)
SEM	Standard error of the mean
SD	single demyelination
SDS	Sodium dodecyl sulfate
SPMS	secondary progressive Multiple Sclerosis
TEMED	N'N'N'-tetramethylethylene diamine
Taq DNA polymerase	DNA polymerase from *Thermus aquaticus*
TMD	Transmembrane domain
Ttotal	accumulated running time in 24 hours
Vmax	maximum running velocity in revolutions per minute in 24 hours

DNA nucleotides purine or pyrimidine bases were codified as follows to describe DNA sequences:

A	Adenine
C	Cytosine
G	Guanine
T	Thymine

Acknowledgements

Abstract

Myelin is produced by a specialized membrane of oligodendrocytes in the CNS. This multilayered structure enwraps axons, providing them with trophic support and facilitates the fast transmission of electric signals. To study the short-term impact of demyelination, histological analysis was performed in a mouse model where myelinating oligodendrocytes are ablated by the expression of diphtheria toxin receptor in mature oligodendrocytes and systemic diphtheria toxin injection. We observed that it results in a fatal disease where demyelination of white matter tracts is accompanied by microglia activation and axonal damage. We demonstrated that this model is therefore well suited for studying demyelination-mediated axonal injury and myelin degradation in the short term.

To investigate the impact of episodes of reversible demyelination on long-term locomotor performance and neuro-axonal integrity, cuprizone-treated animals were monitored using motor skill sequence (MOSS), to observe whether a functional recovery was attained and maintained in the long-term. Despite complete apparent recovery, treated animals exhibited late-onset motor impairment and ongoing acute axonal damage. This model mimics many of the aspects of axonal pathology observed in chronic progressive MS and might therefore be useful in studying the factors initiating, sustaining or compensating axonal damage.

Finally, since myelin neuroprotection most likely involves a direct communication between axons and oligodendrocytes, proteomic analysis of myelin fractions enriched in axo-glial regions was performed to identify novel candidates involved in axo-glial interaction in the context of myelin biogenesis. A battery of functional assays was established and use to evaluate identified candidates to determine their role in axoglial communication and myelin formation. We identified that some members of the IgLON family bound to both oligodendrocytes and axons. We observed that these proteins have no effect on the

migration, proliferation, differentiation of oligodendrocyte precursor cells. However, we observed that one member, Ntm negatively impacts the early stages of myelination.

Chapter 1

Introduction

1.1 CNS Myelin biology

1.1.1 CNS organization

The central nervous system (CNS), composed of the brain and the spinal cord, controls the behavior of bilaterian organisms. It integrates sensory inputs and conveys signals produced by specialized cells to either generate a motor output, communicate to the endocrine system, or carry out learning and memory processes (Kandel et al., 2000). The CNS is comprised of a heterogeneous population of cells, classified into neurons and glia (Virchow, 1846; Verkhratsky and Butt, 2007). Neurons convey messages by the transmission of electric signals along specialized processes, called axons. This triggers a release of neurotransmitters at a specialized junction between neurons called the synapse, where information is transmitted directionally from the pre-synaptic axon terminal to the post-synaptic neuron. The type and abundance of neurotransmitter released and receptors present on the postsynaptic membrane determines the response elicited in the apposing cell (Cajal, 1894; Jessell and Kandel, 1993).

Despite the fundamental role of neurons, the majority of the CNS is composed of glial cells. They form a heterogeneous group of cells that closely interact with neurons. In the vertebrate CNS, glial cells are traditionally classified into microglia, and macroglia; the latter mainly composed of ependymal cells, astrocytes and oligodendrocytes (Verkhratsky and Butt, 2007). Microglia are of mesodermal origin, migrating into the brain early during

development, and perform both as immune cells and macrophages in the CNS (Kreutzberg, 1996). Ependymal cells line the ventricles and central canal and are responsible for the production of cerebrospinal fluid (CSF). Astrocytes interact closely with synapses, maintaining ionic balance and providing trophic support, among other functions (Kandel et al., 2000). Finally, oligodendrocytes form myelin by wrapping their processes around axons in the CNS (Bunge et al., 1962).

1.1.2 Myelination process

Myelin, a specialized membrane, wraps repeatedly around axons and is produced by oligodendrocytes in the CNS (Bunge et al., 1962). Oligodendrocyte precursor cells (OPCs), also termed oligodendrocyte-type 2 astrocyte (O-2A) progenitors, originate during development mainly from the subventricular zones in the brain and the ventral region of the spinal cord (Reynolds and Wilkin, 1988; Compston et al., 1997). OPCs express the gangliosides GD3 and A2B5, as well as the intermediate filament Vimentin. They can also be identified by their expression of NG2 chondroitin sulphate proteoglycan or platelet-derived growth factor α receptor (Levine et al., 2001). They proliferate and migrate throughout the brain and spinal cord. Upon axonal contact, a transition into a premyelinating state is induced, identified by the expression of the surface marker O4, as well as GalC, PLP, and its smaller isoform, DM20 (Levine et al., 2001; Verkhratsky and Butt, 2007).

Following axonal ensheathment, several layers are loosely wrapped around the axon, followed by a drastic cytoplasmic extrusion and compaction of the layers of myelin, called lamellae. The compacted cytoplasmic region between two membranes is called the major dense line, and the space between two opposed membranes, facing the extracellular space, is called the intraperiod line. In mice, this process begins at birth and fully compacted myelin can be found few days later. Myelination peaks at around postnatal day 20 and most myelination is complete by postnatal day 60 (Baumann and Pham-Dinh, 2001). In humans, myelin formation begins mid-gestation and is complete around the third postnatal year (Parazzini et al., 2002). In the peripheral nervous system (PNS), where myelin is formed by Schwann cells, an axonal diameter of minimum 0.2 µm is a critical parameter for an axon to become myelinated. In the CNS, even though an axon with a diameter smaller than 0.2 µm is also unlikely to be myelinated, it is believed that additional factors contribute to the onset of myelination. For instance, the adhesion protein NCAM

has been found to inhibit myelination and its downregulation is necessary for myelination onset, while L1 increases oligodendrocyte survival and myelination *in vitro* (Verkhratsky and Butt, 2007; Fewou et al., 2007; Laursen et al., 2009).

1.1.3 Myelin structure

As the myelin sheath extends along an axon, it undergoes molecular and structural specialization. A single segment is composed of domains differing in their structure, level of compaction, size, and protein/lipid composition. The formation of myelin involves the close aposition between the oligodendrocyte and axonal membranes, as well as the coordinated establishment of intercellular protein complexes. The axo-glial communication facilitates the formation of the molecular and structural domains that characterize a myelin segment, such as the clustering of sodium channels at the internode, the formation of the paranodal loops and the segregation of potassium channels to the juxtaparanodes (Poliak and Peles, 2003; Salzer et al., 2008). The paranodes are found at each edge of the myelin segment and are of special interest as they contain adhesion proteins that form axo-glial contact sites (Baumann and Pham-Dinh, 2001).

For instance, Neurofascin155 is expressed in the paranodes by oligodendrocytes and interacts with the Contactin-Caspr1 complex (Tait et al., 2000), expressed on the axonal side. Neurofascin loss results in the disorganization of the paranodes, degeneration of myelinated axons, ataxia and premature death (Pillai et al., 2009). Therefore, these proteins are crucial in the correct formation of myelin, and the survival of those axons. In general, myelin can be classified into compacted and non-compacted areas. The compacted areas are found between the inner and outer tongue along the internode, and consist of closely apposed layers of myelin, with a minimal cytoplasmic content. The non-compacted areas comprise the inner and outer tongue of myelin, paranodes and juxtaparanodes.

1.1.4 Myelin composition

Myelin is formed by a specialized membrane, which has a specific protein and lipid composition. In contrast to the plasma membrane, regularly composed of 50% lipids and 50% proteins in dry weight, myelin is enriched in lipids, which make up to 80% of the dry weight, with the remaining 20% contributed by proteins (Pfeiffer et al., 1993). Lipids enriched in myelin include galactocerebroside and sulfogalactosylceramide. Cholesterol is

also a very abundant lipid in myelin, as cholesterol, phospholipids, and glycolipids are found in molar ratios ranging from 4:3:2 to 4:4:2 (Baumann and Pham-Dinh, 2001).

The major proteins enriched in myelin are proteolipid protein (PLP) and myelin basic protein (MBP), which together comprise around 80% of the total myelin protein composition (Campagnoni and Macklin, 1988). Other proteins found in myelin are myelin oligodendrocyte glycoprotein (MOG), myelin-associated glycoprotein (MAG), and myelin-associated oligodendrocytic basic protein (MOBP), 2',3'-Cyclic-nucleotide 3'-phosphodiesterase (CN-Pase), Neurofascin155 and Claudin 11 (Baumann and Pham-Dinh, 2001). The distribution of these proteins varies between areas. The layer closely in contact with the axon, or adaxonal membrane, is enriched in MAG and runs along the internodal length. MBP and PLP are found mostly in compacted areas of myelin, while the paranodes and juxtaparanodes present Neurofascin 155 and Tag1, respectively, as depicted in Figure 1.1 (Poliak and Peles, 2003; Salzer, 2003; Aggarwal et al., 2011). *In vitro*, this distribution is in part determined by the restriction of proteins with a bulky cytoplasmic termini to non-compacted areas of myelin (Aggarwal et al., 2011). However, the mechanism for protein segregation in the multilayered myelin structure in *in vivo* is still unclear.

1.1.5   General function of myelin

Due to its tight and compacted structure, myelin provides high resistance electric insulation for axons, which results in the fast and saltatory conduction of electric signals from one myelin-free area to the next (Pfeiffer et al., 1993). These areas within the axon are called nodes of Ranvier, where an accumulation of voltage-gated sodium channels can be found. This facilitates the renewal of the action potential at the nodes and the further transmission of the electric signals along the axon (Salzer, 1997).

In addition to contributing to the amplification and faster propagation of the action potential along the axon, myelin can influence other internal processes in the axon, such as fast axonal transport and axonal diameter regulation (de Waegh et al., 1992). Most importantly, it has been found that myelin can be relevant for short- and long-term axonal preservation and survival. It has been found that a late-onset neurodegeneration occurs in mice lacking several myelin proteins, even when at a structural level, myelin appears
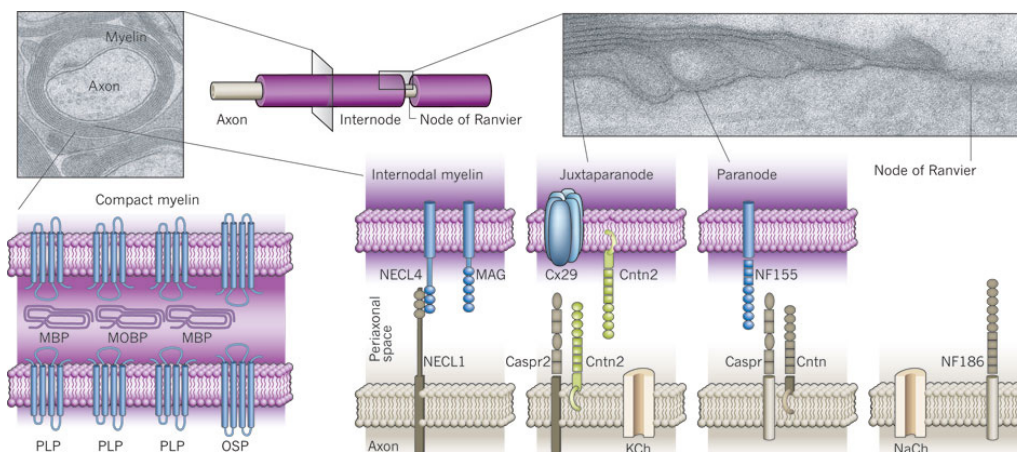
Figure 1.1: General myelin structure and protein distribution at the axo-glial junction. Structural and molecular arquitecture of myelin in the CNS. Direct axo-glial junctions can be found in the paranodal and juxtaparanodal areas, where intercellular protein contents are located. Caspr, contactin-associated protein; Cntn, contactin (Cntn2 is also known as Tag1); Cx29, connexin 29 kDa; KCh, fast potassium channels; MAG, myelin-associated glycoprotein; MBP, myelin basic protein; MOBP, myelin oligodendrocyte basic protein; NaCh, voltage-gated sodium channels; NECL, nectin-like protein/synCAM; NF155/186, neurofascin 155 kDa/186 kDa; OSP, oligodendrocyte specific protein or Claudin 11; PLP, proteolipid protein. The figure is adapted from Nave (2010). Reprint by permission from Macmillan Publishers Ltd: Nature, copyright (2010).

normal (Nave and Trapp, 2008). This suggests that it has a nurturing role in addition to serving as an insulating surface.

1.2 Myelin disorders

The suboptimal formation of myelin during development, or dysmyelination, results in several clinically relevant disorders (Verkhratsky and Butt, 2007). For instance, a duplication or missense mutation of the Plp1 gene, results in Pelizaeus-Merzbacher disease, characterized by hypomyelination and presenting a wide phenotypic range, from mild spasticity to an early lethality (Pham-Dinh et al., 1993). Also, myelin alterations have been associated to different psychiatric diseases, including depression and schizophrenia (Fields, 2008).

Proper myelin function depends not only on its formation, but also on the efficiency of its repair mechanisms. During normal aging, several myelin anomalies have been identified. These are mainly vacuolization, accumulation of cytoplasm along the major dense line, formation of redundant myelin and lamellae disruption (Peters, 1996). This results in an altered insulation and abnormal electric propagation along the axon, which can affect neural circuits necessary for complex behavior (O'Sullivan et al., 2001). A decrease in neuronal connectivity between brain regions could be responsible for the cognitive decline observed in aging (Peters, 2002). However, most of the attention directed towards myelin formation and repair has been due to disabling diseases such as multiple sclerosis.

1.2.1   Multiple sclerosis

1.2.1.1   Immunopathology

Multiple sclerosis (MS) is the most common disabling disease in young adults. In its early stages, this autoimmune disease is characterized by an inflammatory reaction against myelin in the CNS. The infiltration of lymphocytes and monocytes across the blood-brain barrier (BBB), which initiate an inflammatory response, results in demyelination and axonal loss along multifocal lesions in the CNS, as shown in Figure 1.2 (Trapp et al., 1998; Noseworthy et al., 2000; Friese et al., 2006). A major contribution comes from autorreactive CD4+ T cells that generate proinflammatory cytokines and chemokines, resulting in the activation of local microglia and infiltrated macrophages (Martin et al., 1992; Sospedra and Martin, 2005).

CD8+ T cells also have been found to invade the CNS and contribute to the cytotoxicity and inflammation observed in MS (Friese and Fugger, 2005). Different lesion patterns have been described, and in many lesions demyelination seems to be caused by the inflammation mediated by T-cell and macrophages/microglia with or without antibody deposition (lesion pattern I-II). However, lesions where demyelination seems to take place due to a primary oligodendroglial dysfunction (lesion patterns III-IV) were also found (Lucchinetti et al., 2000). This could suggest the existence of independent mechanisms of demyelination across different subgroups or stages of MS. Although the etiology of MS is still unclear, it is believed that a combination of genetic predisposition and environmental factors and

viral infections ultimately contribute to trigger the disease (Hemmer et al., 2002; Gold et al., 2006).
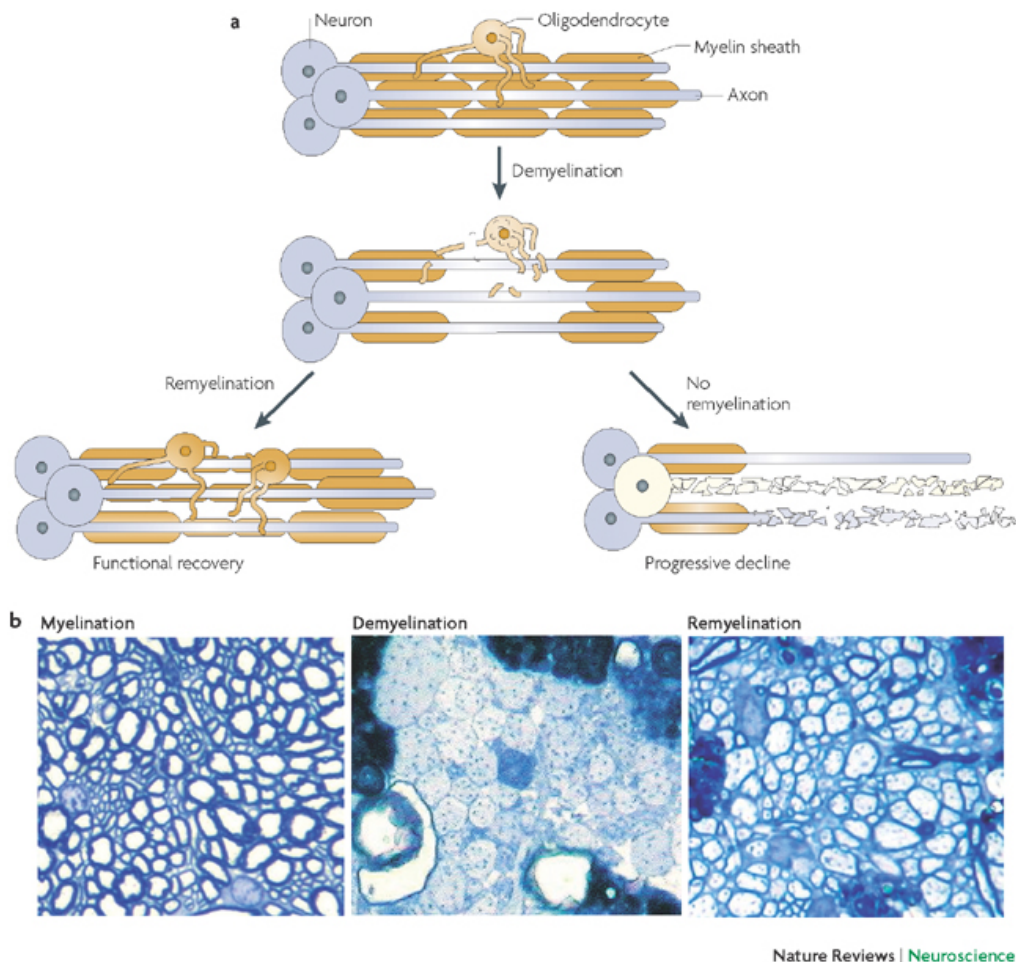
Figure 1.2: Demyelination in the CNS. Following demyelination and oligodendrocyte death, a thinner and shorter myelin sheath can be formed in the nude regions of affected axons by re-myelination. The axons that remain demyelinated are prone to degenerate. The figure is adapted from Franklin and Ffrench-Constant (2008). Reprint by permission from Macmillan Publishers Ltd: Nature, copyright (2008)

1.2.1.2   Symptoms and progression

The most frequent symptoms in MS are loss of motor function, sensory impairment, fatigue and cognitive deterioration (Noseworthy et al., 2000). The Kurtzke Extended Disability Status Scale or EDSS is used to quantify the level of disability and ambulatory state of

MS patients, and ranges from 0.0 (normal) to 10.0 (death due to MS). It defines seven functional systems (FS): pyramidal, cerebellar, brainstem, sensory, bowel/bladder, visual, cerebral and other which are analysed separately (Kurtzke, 1983). It is used to describe the course of MS and is often used as a readout of the effectiveness of therapeutic approaches in clinical trials.

Approximately 85% of patients initially present a series of discrete inflammatory episodes with reversible clinical symptoms, called relapsing-remitting MS (RRMS) (Confavreux et al., 1980; Weinshenker et al., 1989). MS is usually detected in the second or third decade of life and after a median time of 19 years after initial diagnosis, approximately 70% of the patients suffer a transition into secondary progressive MS (SPMS) (Noseworthy et al., 2000). Secondary progression is usually defined as a period of continous clinical worsening, persisting for at least six months. Only about 10-15% of patients present a progressive increase in neurological disability from the initial onset, called primary progressive MS or PPMS (Sospedra and Martin, 2005).

Since progressive MS results in the patient's permanent disability, it is clinically relevant to elucidate the mechanisms triggering the transition into the progressive stage. One of the most significant factors associated with progressive MS is age, with the conversion occurring at a mean age of 39 years (Kremenchutzky et al., 2006). In addition, location of new lesions can help predict future disability, with lesions in the frontal lobe correlated with cognitive deficits and in the brain stem with motor defects (Wybrecht et al., 2012). Once a disability threshold is reached, measured as a score of 4 in the EDSS, these variables no longer influence the course of the disease (Confavreux et al., 2003; Vukusic and Confavreux, 2007). Surprisingly, the speed at which patients develop neurological deficits in progressive MS is remarkably similar between patients (Confavreux et al., 2000; Rovaris et al., 2006).

Thus, the onset of progressive MS does not appear to be exclusively determined by the inflammatory load that arises during the relapsing-remitting course of the disease. Even though the initial relapsing-remitting stage of the disease is considered to be highly vari-

able and unpredictable, the progressive phase seems to follow a common path (Antel et al., 2012). All of these findings raise the question of how chronic progressive MS is triggered and whether non-inflammatory mechanisms play a crucial role independent from the number of relapses. In addition, it is likely that aging processes themselves might be relevant for the initiation of the progressive phase of the disease (Tutuncu et al., 2012). However, the exact pathways involved in this transition remain unclear.

1.2.1.3 Therapeutic approaches

Several therapies have been developed and approved to ameliorate MS symptoms. Currently, the drugs approved for the treatment of MS treatments include glatiramer acetate and IFN-ß, along with second-generation drugs such as sphingosine-1-phosphate receptor agonist (Fingolimod), a humanized monoclonal antibody against alpha 4 integrin called Natalizumab and Mitoxantrone (Rovaris et al., 2006; Yadav and Bourdette, 2012).

Glatiramer acetate, also known as Copolymer 1 or Copaxone, is a mixture of synthethic polypeptides that reduces the inflammatory response and was found to decrease relapse frequency and severity in RRMS patients (Johnson et al., 1995). IFN-β is a cytokine which reduces the number and appearance of active lesions and the overall disease burden defined as the cumulative lesion area in MS patients (Group, 1993; Paty et al., 1993). Fingolimod (FTY720) is a sphingosine-1-phosphate receptor agonist that sequesters lymphocytes in lymph nodes, inhibiting their distribution and infiltration of the CNS. This anti-inflammatory property has been shown to reduce relapse frequency in RRMS patients, however it does not improve disease progression (Cohen et al., 2010).

A humanized monoclonal antibody against alpha-4 integrin commercially known as Natalizumab has been re-approved for MS treatment due to its effective immunomodulatory function despite its rare but potentially fatal side effects. It binds to $\alpha 4 \beta 1$ and $\alpha 4 \beta 7$ integrin molecules on the surface of lymphocytes and blocks their interaction with endothelial cells, preventing their transmigration across the blood-brain barrier and immune cells infiltration of the CNS (Polman et al., 2006). Finally, mitoxantrone is a synthetic compound approved for the treatment of leukemia that inhibits T cell, B cell and macrophage proliferation, as well as decreases pro-inflammatory cytokine secretion and antibody production

(Fox, 2004). Most of the approved treatments target the modulation of the autoimmune response and are therefore mostly directed towards controlling the acute inflammatory episodes of relapsing-remitting or early MS. However, they do not appear to have a neuroprotective or a disease-modifying effect in non-relapsing progressive MS stages (Rovaris et al., 2006; Ransohoff, 2012).

1.2.2 Demyelinating animal models

To study demyelination and its consequences *in vivo*, several animal models have been established to resemble different traits of MS. Among the diverse models, the most common approach involves the induction of an autoimmune reaction against myelin components or the use of cytotoxic substances that result in loss of oligodendrocytes.

1.2.2.1 Experimental Autoimmune Encephalomyelitis (EAE)

The most widespread MS model is the Experimental Autoimmune Encephalomyelitis or EAE. It is based on the induction of auto-reactive T cells to proliferate and cross the blood-brain barrier. This is attained by either an "active" or a "passive" immunization. The active immunization involves injecting mice, rats or non-human primates with either myelin protein epitopes (frequently the 35-55 amino acid residues of the MOG peptide), or myelin/spinal cord preparations, usually in Complete Freund's Adjuvant (Steinman, 1999; Friese et al., 2006). T cells that are reactive against these components proliferate and cross the brain-blood barrier, where they are reactivated by MHCII-expressing macrophages or dendritic cells, which act as antigen-presenting cells (APC). This reactivation triggers a T cell-mediated inflammatory reaction against myelin, resulting in focal demyelinating lesions and cytokine release. There is an important contribution from microglial activation and proliferation, which release NO and other cytotoxic factors and contribute to the severity of the disease (Heppner et al., 2005). Passive immunization consists of the transfer of isolated autoreactive T cells to a naive recipient, which results in a similar BBB infiltration and inflammatory response (Mokhtarian et al., 1984).

EAE is one of the most widely used MS models due to the induction of an autoimmune reaction specifically against myelin components which results in demyelination and motor phenotype that resembles the clinical symptoms of MS patients. Certain variations of the EAE model, depending on the epitope and the mice strain used, can result either in a

single or repeated demyelinating events, which resemble the common relapsing-remitting pattern of MS. This makes EAE seem ideal for the trial of novel therapeutical approaches. However, most of the treatments that have been described to have a beneficial effect in preclinical EAE studies have been shown to have either none or sometimes even adverse effects in MS patients (Steinman, 1999; Friese et al., 2006). However, it has been useful in the development of glatiramer acetate, Mitoxantrone, and Natalizumab, described in the previous section (Teitelbaum et al., 1971; Ridge et al., 1985; Yednock et al., 1992).

Another disadvantage of the EAE model for MS is that the assessment of remyelination is difficult since demyelinating lesions are variable in localization and timing. In addition, it seems to overestimate the role of CD4+ T cells, as B and CD8+ T cells show a minimal involvement in EAE, opposed to what has been observed in MS patients (Ransohoff, 2012). Due to the nature of the model, EAE has been useful in testing and developing therapies that ameliorate the acute inflammatory stages of the disease via immunomodulation, but has provided little contribution to the understanding of MS progression (Nakahara et al., 2012). Clearly, additional models of MS are necessary to understand processes that are not sufficiently represented in EAE.

1.2.2.2 Cuprizone

Cuprizone (bis-cyclohexanone-oxaldihydrazone) is a chemical compound commonly used as a copper-chelating agent. Feeding mice with 0.2-0.5% cuprizone for at least three weeks results in oligodendrocyte death and demyelination. The induced demyelination is most prominent in the corpus callosum and superior cerebellar peduncle, where more than 90% of axons are affected (Blakemore, 1973a). As a result of the myelin debris that results from oligodendroglial death, there is a massive proliferation and activation of astrocytes and microglia (McMahon et al., 2002). This reaction occurs without disruption of the blood-brain barrier or infiltration of the immune system (Matsushima and Morell, 2001). This resembles, to a certain extent, pattern III MS lesions of a primary oligodendropathy (Lucchinetti et al., 2000). After cuprizone is removed from the diet, an extensive formation of new myelin, or remyelination, can be observed in 5 to 6 weeks (Merkler et al., 2005; Blakemore, 1973b). However, if the cuprizone treatment is increased to 12 weeks or more, insufficient remyelination and epileptic seizures can be observed (Hoffmann et al., 2008).

The exact mechanism of cuprizone-induced apoptosis in oligodendrocytes remains unknown, but it is believed to be related to a copper deficiency caused by the chelating property of the toxin. Cuprizone has been shown to inhibit copper-dependent enzymes like cytochome oxidase and monoamine oxidase, and appears to decrease the activity of several mitochondrial respiratory complexes, in particular complex IV (Matsushima and Morell, 2001; Pasquini et al., 2007). It also arrests OPCs maturation, inhibiting remyelination and therefore, increasing the severity and duration of the demyelinating insult (Cammer, 1999). Since this model involves minimal infiltration by the immune system and acts to preserve the integrity of the blood-brain barrier, it is widely used as a model of de- and re-myelination. Due to its reliable timing and location it is especially useful in elucidating the mechanisms involved in myelin clearance and remyelination, independent of the side effects commonly observed in an immune-derived inflammation and cytotoxicity.

1.2.2.3 Diphtheria-toxin oligodendrocyte ablation and other models

Necrotic lesions can be induced by the local injection of diphtheria toxin (DT). The susceptibility to this toxin varies among species: humans, rabbits and guinea pigs have been found to be very sensitive to the toxin, while rats and mice have been shown to be highly resistant (Pappenheimer and Gill, 1973). This susceptibility depends on the expression of high-affinity DT receptors, which are either scarce or absent in the cells of resistant species (Middlebrook and Dorland, 1977; Naglich et al., 1992). Elevated concentrations of diphtheria toxin are necessary to induce cytotoxicity in resistant cells, requiring more than 100-fold concentration of the toxin to elicit the same response as in sensitive cells. The toxin acts by binding to its receptor and triggering its internalization. The toxin is subsequently cleaved and one of the proteolytic products, Fragment A, is liberated into the cytoplasm. This fragment inactivates the elongation factor EF-2 by ADP-ribosylation (Collier, 1967; Honjo et al., 1969), resulting in translation arrest and inhibition of new protein synthesis, ultimately leading to apoptotic cell death. It has been found that a single DT molecule is capable of killing a eukaryotic cell (Yamaizumi et al., 1978).

Resistant cells can be sensitized to DT by inducing the expression of the primate diphtheria toxin receptor, the heparin-binding epidermal growth factor-like (HB-EGF) precursor (Naglich et al., 1992; Saito et al., 2001). iDTR transgenic mice have been created by the introduction of a gene encoding the DT receptor with a lox-P flanked stop cassette in its

open reading frame. Upon Cre-mediated recombination, the stop cassette is removed and the functional DT receptor is expressed. By crossing these mice with lines expressing Cre recombinase under cell-lineage specific promotors, targeted cell ablation can be induced through the injection of DT (Buch et al., 2005).

In another approach, a floxed LacZ within the gene encoding DT Fragment A allows the expression of the catalytically active DT-A upon Cre-mediated recombination. This active DT Fragment A has the capacity of inducing cell death in the absence of a functional receptor, since the expression takes place from within the targeted cell (Brockschnieder et al., 2004). Mice carrying the *iDTR* gene and expressing Cre under the *Mog* promotor express a functional diphtheria toxin receptor solely in mature oligodendrocytes. The injection of DT in these mice has been shown to result in a massive oligodendrocyte death and systemic demyelination (Buch et al., 2005). On the other hand, the expression of diphtheria toxin A subunit in an inducible PLP-Cre mouse line results also in the apoptotic death of mature oligodendrocytes (Traka et al., 2010). Other cytotoxic demyelinating models include the local injection of ethidium bromide (Blakemore, 1982) or lysolecithin (Hall, 1972).

Viruses have been proposed to be a factor contributing to the onset of MS, presumably creating an autoimmune response triggered by a molecular mimicry or recognition of some myelin proteins epitopes as foreign due to an infection in the past (Chastain and Miller, 2011; Owens et al., 2011). Some of the evidence supporting this idea originates from viral models of inflammatory demyelination, including the infection with human endogenous retrovirus (HERV) expressing recombinant syncitin (Antony et al., 2004), the A59 strain of mouse hepatitis virus (Lavi et al., 1984), the Semliki-Forest virus (Amor et al., 1996) and Theiler's murine encephalomyelitis virus (Sato et al., 2009).

1.3 Neuroprotective function of myelin

In addition to its insulating properties, myelin has been found to be essential for long-term axonal survival. Alterations in myelin composition can trigger neurodegeneration (Nave and Trapp, 2008). For instance, mice lacking myelin-associated glycoprotein (MAG),

2',3' - cyclic nucleotide 3- phoshodiesterase (CNPase) and proteolipid protein (PLP) form structurally almost normal myelin, but develop late-onset, chronic progressive neurodegeneration (Griffiths et al., 1998; Yin et al., 1998; Lappe-Siefke et al., 2003). Axonal swelling, transections and an impairment of axonal transport occur in these mice, highly reminiscent of the changes found in MS lesions (Ferguson et al., 1997; Trapp et al., 1998; Kornek et al., 2000). Interestingly, *shiverer* mice, which lack myelin basic protein (MBP), form only small amounts of myelin. Even though this results in severe behavioral phenotype, with epileptic seizures, tremors and premature death (Roach et al., 1983; Popko et al., 1987), they do not exhibit conspicuous signals of axonal damage or degeneration (Griffiths et al., 1998). This raises the possibility that, although unmyelinated axons can survive on their own, axons that indeed are myelinated require an intact sheath for their maintenance, and they may require trophic support due to their isolation from external metabolite sources (Nave and Trapp, 2008).

1.3.0.4   Remyelination and myelin repair

Following demyelination, the damaged myelin is not repaired but can be replaced through a process called remyelination, which restores saltatory conduction and trophic support to the axon (Smith et al., 1979). Immature oligodendrocyte precursors migrate to demyelinated areas, and after a process closely resembling OPC maturation during development, they extend processes that surround the unmyelinated axons and form a new myelin sheath (see **Figure** 1.3). This myelin is normally thinner, with shorter internodes (Franklin and Ffrench-Constant, 2008). Remyelination efficiency decreases with time in MS (Wolswijk, 1998; Franklin, 2002), and different demyelinating animal models show that age negatively influences the recruitment and differentiation of OPCs after demyelination (Shields et al., 1999; Sim et al., 2002).

Two steps are crucial for remyelination to occur: the recruitment of OPCs to the demyelinated area, followed by their differentiation and maturation into myelinating cells. Several factors leading to differentiation inhibition and therefore remyelination impairment have been identified (Huang et al., 2011). For instance, myelin debris inhibits OPC differentiation; therefore its clearance is crucial for remyelination efficiency (Kotter et al., 2006; Pohl et al., 2011). This inhibition seems to involve the activation of Fyn-Rho-ROCK and protein Kinase C pathways (Baer et al., 2009). Hyaluronan deposition has been found

in EAE and chronic MS lesions, and inhibits OPC differentiation through its binding
to toll-like receptor 2 (TLR-2) in OPCs (Sloane et al., 2010). In addition, semaphorins
have been suggested as regulatory molecules in remyelination. While Semaphorin 3A has
been identified as a repulsive signal and differentiation inhibitor for OPCs, Semaphorin
3F serves as a chemoattractant (Williams et al., 2007; Piaton et al., 2011). Therefore,
through a balance and timing of the expression of these two molecules, the recruitment
and differentiation extent of OPCs within a demyelinated lesion can be coordinated.

Diverse pathways inducing OPC differentiation have been identified. While LINGO-1, Wnt
and Notch1 pathways inhibit differentiation (John et al., 2002; Mi et al., 2005), activation
of retinoid X receptors (RXR) induce it (Huang et al., 2011). In MS, remyelination
failure has been associated to OPC differentiation impairment and to a lesser extent to
insufficient recruitment (Wolswijk, 1998; Chang et al., 2002; Sim et al., 2002). As it
is crucial to elucidate ways to promote remyelination as a therapeutic approach in MS,
targeting these pathways can help modulate the onset and extent of OPC differentiation
and help determine the factors that may pose as barriers or inhibitors of this process.

1.3.0.5   Axonal damage in myelin diseases

A decrease in the efficiency of remyelination has been associated to increased axonal dam-
age (Kuhlmann et al., 2002; Irvine and Blakemore, 2006; Hampton et al., 2012). Failure
in remyelination results in a greater extent of axonal loss after demyelination, supporting
the idea that myelin also provides the axons with trophic support (Irvine and Blake-
more, 2008). There is abundant evidence showing that chronically demyelinated axons
will degenerate due to a lack of glial support (Lindner et al., 2009). Since remyelination is
initiated by recruited OPCs that undergo differentiation, the steps involved in migration,
proliferation and maturation of OPCs can determine the clinical outcome of a demyelinat-
ing event. Remyelination has been found to fail in advanced stages of MS, but the reasons
are unclear. It has been proposed that either the glial scar formed in lesions affects myeli-
nation by mature, differentiated OPCs or the OPCs have an intrinsic problems achieving
complete differentiation and myelination (Levine et al., 2001).
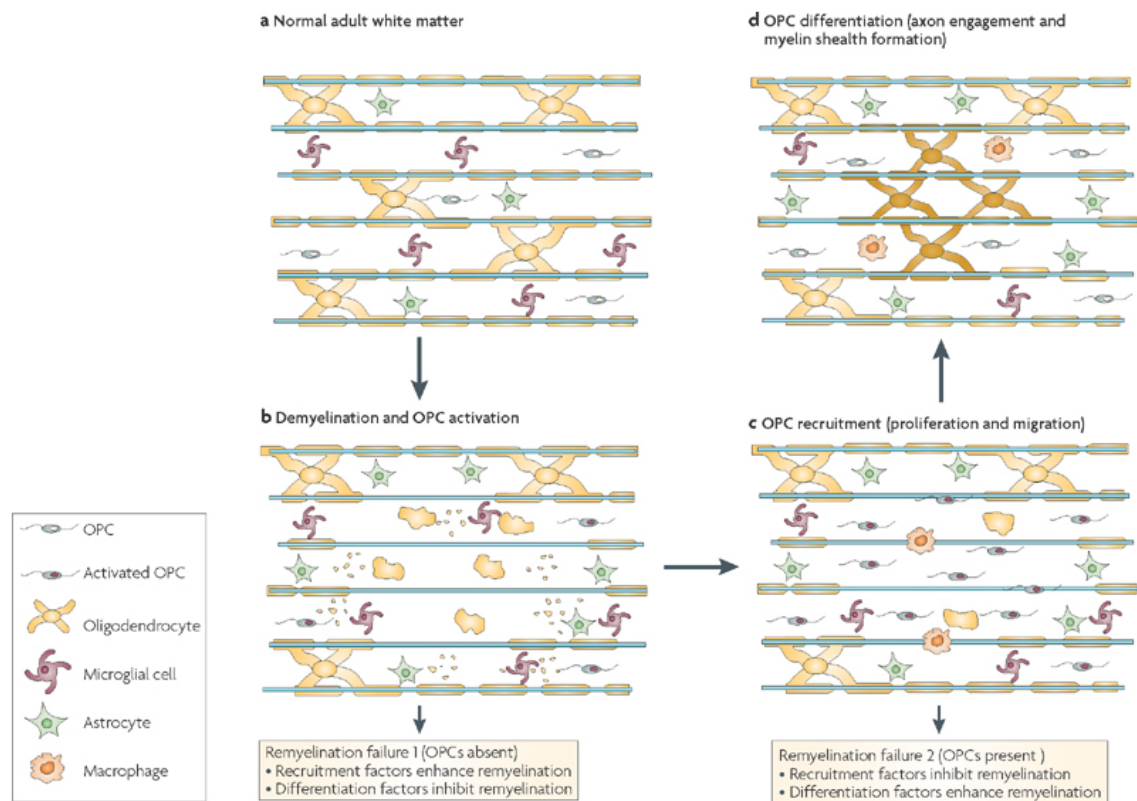
Figure 1.3: Remyelination in the CNS. Following demyelination, oligodendrocyte precursor cells (OPC) migrate to the demyelinated area and undergo differentiation and remyelination. When recruitment or differentiation of OPC is inhibited, remyelination will be arrested or delayed. The figure is adapted from Franklin and Ffrench-Constant (2008). Reprint by permission from Macmillan Publishers Ltd: Nature, copyright (2008)

Axonal dysfunction and transection has been widely identified in MS lesions (Ferguson et al., 1997; Trapp et al., 1998; Bitsch et al., 2000; Kuhlmann et al., 2002). It has also been shown that small axons are more vulnerable to damage than bigger axons (Evangelou et al., 2001). In fMRI studies, a decrease in the relative concentration of N-acetylaspartate (NAA), measured as the NAA/Creatine ratio (Na/Cr), is thought to reflect axonal injury and is measured using brain MRSI (Matthews and Arnold, 2001). This method has also detected axonal injury not only in areas of demyelination but also in normal appearing white matter (NAWM) (Narayanan et al., 1997; Miller et al., 2003). The accumulation of amyloid precursor protein or APP, is widely used as an evidence of defects in fast axonal

transport and reflects acute axonal dysfunction. APP accumulation has been detected in MS acute lesions as well as on the border of chronic lesions (Ferguson et al., 1997). Axonal damage, evidenced by APP accumulation, is also observed in animal models after acute as well as chronic demyelination (Kornek et al., 2000; Lindner et al., 2009).

The damage induced in axons as a consequence of demyelination can be exacerbated when accompanied by inflammation. Inflammation levels have been shown to directly correlate with the extent of axonal loss (Ferguson et al., 1997; Trapp et al., 1998; Frischer et al., 2009). Inflammation itself can induce mitochondrial dysfunction and irreversible axonal damage even if demyelination does not occur (Nikic et al., 2011). Therefore, an early control of inflammation can reduce the subsequent axonal loss (Bitsch et al., 2000). However, even though anti-inflammatory treatments help to mitigate the severity of damage in the primary stages of MS, it is not clear whether they are able to delay the transition into a secondary progressive stage of MS. Thus, it seems that the natural course of the disease is not solely dependent on inflammation (Confavreux et al., 2003; Brück, 2005).

Reactive oxygen and nitrogen species (ROS and RNS) derived from macrophages/microglia can result in mitochondrial pathology and initiate focal axonal degeneration (Smith et al., 2001; Nikic et al., 2011). It is believed that the nitric oxide (NO) and other cytotoxic products produced by microglia contribute significantly to the blockade of axonal signal transmission and oligodendrocyte death observed in demyelinating lesions (Pasquini et al., 2007).

Even though some axonal damage has been found to be reversible (Stefano et al., 1995; Meyer zu Hoerste et al., 2010), it is believed that the vast majority of the axonal injury in plaques and normal appearing white matter is irreversible (Evangelou et al., 2000). The terminal formation of ovoid structures in axons stained for neurofilament has indicated the transection of axons in demyelinated lesions (Trapp et al., 1998).

1.3.0.6   Mechanisms of functional recovery

Despite the fact that remyelination restores trophic support and normal axonal function to a great extent, axonal loss does occur during the initial stages of MS and its animal models (Kuhlmann et al., 2002; Merkler et al., 2006). However, a functional recovery of clinical symptoms has been observed to occur after demyelination, despite the irreversible axonal loss in the CNS, where axonal regeneration is limited. Similar to what occurs in spinal cord injury, an important fraction of the recovery after demyelination is due to the resolution of inflammation and the reversibility of the conduction blockage in axons. In addition, remyelination and an increased axonal sodium channel expression are mechanisms that have been proposed to contribute to the functional recovery after inflammatory brain injuries (Waxman and Ritchie, 1993; Brück et al., 2003).

If axonal transection occurring as the result of an inflammatory attack is substantial and irreversible, these mechanisms cannot completely account for the functional recovery in patients. Despite considerable axonal loss in initial inflammatory stages of MS, the clinical recovery observed in RRMS patients indicate that symptoms do not directly correlate to initial loss of axons (Compston and Coles, 2008). Only in progressive MS stages, a correlation between ongoing neurodegeneration and irreversible clinical disability is evident (Trapp et al., 1999; Bjartmar and Trapp, 2003). This suggests the existence of compensatory mechanisms that allow for the re-establishment of the circuits necessary for complex motor and cognitive performance. It has been found that cortical adaptation may help compensate the outcome of axonal injury in MS and mitigate the clinical phenotype (Reddy et al., 2000).

Neuroplasticity is thought to allow the formation of circuits in the learning and execution of complex motor tasks. Reddy and colleagues (2000) found that as axonal injury increases, there is a decreased lateralization of sensorimotor cortex (SMC) activation of MS patients when performing a finger tapping exercise. No mirror movements in the opposite hand were detected to account for a contribution of ipsilateral SMC activation. This suggests that there is an increase in the ipsilateral SMC activation during the control of the fingers in order to perform the task at a speed comparable to healthy patients. This decrease in contralateral activation is markedly correlated with an increased axonal

injury, indicating that this reorganization is a mechanism to maintain a normal cognitive and motor performance and can serve as a marker of short term disability (Faivre et al., 2012).

Other evidence of functional reorganization in MS patients has been reported. The hyper-activation of task-related and additional brain structures has been reported to compensate for areas with impaired activation and to preserve cognitive performance. However, it has been proposed that an accumulation of structural damage can result in a 'burn-out' of the possible adaptive mechanisms and limit the extent of cortical reorganization (Rocca et al., 2010). In simple motor tasks, initially a higher activation of the associated area is observed, and with the disease progression this increase in activity becomes bilateral, and finally additional, compensatory brain areas are recruited to perform the same simple task (Rocca et al., 2005).

Axonal loss may be compensated for many years during relapsing demyelination before a threshold is reached and compensatory mechanisms are exhausted. Axonal loss might therefore be one of the crucial factors responsible for the conversion of RRMS to SPMS and the resulting progression of clinical disability (Trapp and Nave, 2008). Remyelination is thought to reduce the reliance on compensatory mechanisms and prolong the conversion progressive MS by at least temporarily restoring axonal function and maintenance, however the long-term impact of remyelination on functional recovery and thus neuronal integrity is not well understood.

To study the short-term impact of demyelination, histological analysis was performed in a mouse model where myelinating oligodendrocytes are ablated by the expression of diphtheria toxin receptor in mature oligodendrocytes and systemic diphtheria toxin injection. In addition, cuprizone-treated animals were monitored using motor skill sequence (MOSS), to investigate the impact of episodes of reversible demyelination on long-term locomotor performance and neuro-axonal integrity. Through this study we attempted to elucidate the impact of demyelination in axonal preservation and the role of remyelination in the functional recovery in the long term.

Chapter 2

Materials and Methods

2.1 Materials

2.1.1 Chemicals and consumables

The chemicals used in this study were purchased from Sigma-Aldrich or AppliChem, unless otherwise specified. Cell culture consumables and biochemistry reagents were purchased from Falcon and Eppendorf.

2.1.2 Antibodies

Table 2.1: Antibodies used during this study

Target	Application	Reference
APP	Mouse IgG	Chemicon
βIII Tubulin	Mouse IgG	Promega
CD3	Rat	Serotec
CNPase	Mouse IgG	Sigma
Fc (human)	Rabbit	Jackson Laboratories
GFAP	Rabbit	Promega
Iba1	Rabbit	Wako Chem. GmbH
Mac3	Rat	Pharmingen
MAG (clone 513)	Mouse	(Poltorak et al., 1987)
MBP	Rabbit	DakoCytomation
MOG (clone 8-18-C5)	Mouse IgG	Millipore
myc-tag	Mouse IgG	Cell Signalling
myc-tag	Rabbit	Upstate

Nerofilament200, clone N52	Mouse IgG	Sigma
Neurofilament 160	Mouse IgG	Novocastra
Neurofilament 200	Mouse IgG	Novocastra
Neurofilament 68	Mouse IgG	Chemicon
Neurofascin	Rabbit	Abcam
NeuN	Mouse IgG	Chemicon
NogoA, clone 11C7	Mouse IgG	(Liebscher et al., 2005)
O1	Mouse IgM	(Sommer and Schachner, 1981)
PLP (3F4)	Mouse IgG	K. Nave, MPI of Exp. Med., Göttingen, Germany
PLP (AA3)	Mouse IgG	K. Nave, MPI of Exp. Med., Göttingen, Germany

Anti-mouse, anti-rat and anti-rabbit horse radish peroxidase (HRP)-conjugated secondary antibodies used for Western blot were purchased from Dianova. Fluorescence secondary antibodies were purchased from Dianova and Invitrogen.

2.1.3 Commercial Kits

Table 2.2: Commercially available kits

Kit	Application Producer	
Spin Tissue Midi Kit	DNA extraction for genotyping	Invitek
In situ cell detection kit	TUNEL assay	Roche
CytoSelect 24-Well Cell Migration Assay, 8 μm	Migration assay	CellBioLabs
NucleoSpin Plasmid Quick-Pure	DNA purification, Miniprep	Macherey-Nagel
NucleoBond Xtra EF	DNA purification, Midiprep	Macherey-Nagel
NucleoSpin Gel and PCR clean up	DNA extraction and purification	Macherey-Nagel
Protein A HP Spin Trap Columns	Fc-fusion protein purification	GE Healthcare

2.1.4   DNA plasmids and primers

2.1.4.1   DNA plasmids

Vectors, commercial and previously published plasmids are listed below.

Table 2.3: Acquired DNA constructs used in this study

Construct	Vector	Description/Application	Source
EGFP-Tmem10	pcDNA3.1(-)	Expression of EGFP tagged Tmem TMD, used for cloning of EGFP-tagged proteins	Shweta Aggarwal
myc-Tmem10-MBP	pcDNA3.1(-)	myc-tagged Tmem TMD and MBP sequence, used for cloning of myc-tagged proteins	Shweta Aggarwal
EGFP-C1	EGFP-C1	expression of EGFP in mammalian cells	Clontech
Necl1-Fc	pSX	Expression of Fc fusion Necl1	(Spiegel et al., 2007)
Necl4-Fc	pCX	Expression of Fc fusion Necl4	(Spiegel et al., 2007)
pcDNA3.1(+)	pcDNA3.1(+)	vector for mammalian expression	Invitrogen
Lsamp	pENTR233.1	Lsamp cDNA *Mus musculus*	Genecopoeia
Lsamp	pExpress1	Lsamp cDNA *Rattus norvegicus*	OpenBiosystems
Opcml	pYX-Asc	Opcml cDNA *Mus musculus*	OpenBiosystems
Ntm	pCMV-Sport6	Igsf8 cDNA *Mus musculus*	OpenBiosystems
MCAM	pCMV-Sport6	MCAM cDNA *Mus musculus*	OpenBiosystems
Igsf8	pCMV-Sport6	Igsf8 cDNA *Mus musculus*	OpenBiosystems
LGI3	pYX-Asc	LGI3 cDNA *Mus musculus*	OpenBiosystems
Plekhb1	pCMV-Sport6	Plekhb1 cDNA *Mus musculus*	OpenBiosystems
Ntm shRNA	psi nU6	RNAi mouse Ntm (MSH040231)	Genecopoeia
Lsamp shRNA	psi nU6	RNAi mouse Lsamp (MSH041371)	Genecopoeia
Opcml shRNA	psi nU6	RNAi mouse Opcml (MSH042052)	Genecopoeia
Control shRNA	psi-nU6	control shRNA (CSHCTR001)	Genecopoeia

Constructs generated in this study are listed below.

Table 2.4: Cloned DNA constructs used in this study

Construct	Vector	Description
myc-Lsamp	pcDNA3.1(-)	myc-tagged full length Lsamp
myc-Opcml	pcDNA3.1(-)	myc-tagged full length Opcml
myc-Ntm	pcDNA3.1(-)	myc-tagged full length Ntm
myc-MCAM	pcDNA3.1 (-)	myc-tagged full length MCAM
EGFP-Lsamp	pcDNA3.1(-)	EGFP-tagged full length Lsamp
EGFP-Opcml	pcDNA3.1(-)	EGFP-tagged full length Opcml
EGFP-Ntm	pcDNA3.1(-)	EGFP-tagged full length Ntm
EGFP-MCAM	pcDNA3.1 (-)	EGFP-tagged full length MCAM
Lsamp-Fc	pcDNA3.1(+)	Fc-fusion of Lsamp ECD
Opcml-Fc	pcDNA3.1(+)	Fc-fusion of Opcml ECD
Ntm-Fc	pcDNA3.1(+)	Fc-fusion of Ntm ECD
MCAM-Fc	pcDNA3.1(+)	Fc-fusion of MCAM ECD
Igsf8-Fc	pcDNA3.1(+)	Fc-fusion of Igsf8 ECD
Plekhb1-Fc	pcDNA3.1(+)	Fc-fusion of Plekhb1 ECD
LGI3-Fc	pcDNA3.1(+)	Fc-fusion of LGI3 ECD
Necl1-Fc	pcDNA3.1(+)	Fc-fusion of Necl1 ECD
Necl4-Fc	pcDNA3.1(+)	Fc-fusion of Necl4 ECD

2.1.4.2   DNA primers for cloning

The primers for cloning were designed using the software ApE. The general rule for primer design used was selecting a sequence that would have between 18 and 30 bp, if possible over 50 %GC content and that would end in C or G. The list of used primers is shown ahead. Designed primers were synthesized by ACGTLab, DNA core facility at the Max Planck Institute of Experimental Medicine.

Primer	Sequence	Description
22040	5'-AAAAAAGCTTACCATGGGCGTCCCT AGCC -3'	Igsf8 ECD fwd for pCX

Primer	Sequence	Description
22041	5'-AAAAGAGCTCGGTATCCACAGCATG CGTG -3'	Igsf8 ECD rev for pCX
22043	5'-AAAAGGGCCCTCTAGATCATTTACCC -3'	Fc rev pCX
22044	5'-AAAAGAGCTCGGAGGAGGAGGAGAT CCCCGTCGTGCATCTATC -3'	Fc fwd pCX glycine linker
22710	5'-AAAAGCTAGCACCATGTACCATCCC GC-CTACTGG -3'	Opcml ECD fwd for pCX NheI
22712	5'-AAAAGCTAGCACCATGGTCGGGAGA GTTC -3'	Lsamp ECD fwd pCX NheI
22714	5'-AAAAGCTAGCACCATGGGGGTCTGT GGGTACC -3'	Ntm ECD fwd for pCX NheI
22894	5'-AAAAGCTAGCGGAGGAGGAGGAGA TCCC -3'	beginning Fc fraction fwd
22895	5'-AAAAGCTAGCTCTGGAGGCCGAGTT TACAC -3'	Opcml rev NheI
22896	5'-AAAAGCTAGCGATTCCTCTCACCGA CCCG -3'	Lsamp rev NheI
22897	5'-AAAAGCTAGCCCTCCTTGATGTCCCA TTGTTGAC -3'	Ntm rev nheI
22898	5'-AAAAGCTAGCACCATGGGCCGGGC -3'	Necl4 NheI fwd
22899	5'-AAAAGCTAGCGGAACCGATGTCTGAG CCTC -3'	Necl4 NheI rev
23303	5'-AAAAGCTAGCCACCATGGAGACAGA -3'	Necl 1 fwd NheI
23304	5'-AAAAGCTAGCCGTACTGGAGGATGAG GGCAC -3'	Necl 1 rev NheI
23761	5'-AAAAGCTAGCACCATGGGGCTGCCCA AACTG -3'	MCAM ECD fwd NheI
23762	5'-AAAAGCTAGCACCTTTGCTCTCTGGCT GTG -3'	MCAM ECD rev NheI
23763	5'-AAAAGCTAGCACCATGAGCCCGGCAA CCCC -3'	Plekhb1 fwd NheI
23764	5'-AAAAGCTAGCTGAGCTGTAGCAGGGG TCC -3'	Plekhb1 rev NheI
23765	5'-AAAAGCTAGCACCATGGCCGGGCTAC GAGC -3'	LGI3 fwd NheI

Primer	Sequence	Description
23766	5'-AAAAGCTAGCGGCACTAAGGTCCACC ACAAC -3'	LGI3 rev NheI
24673	5'-AAAACTCGAGACATTTGCTGAGAAGG CAGAAC -3'	Lsamp full XhoI rev
25006	5'-AAAAAGCGCTGGAGGAGGAGGAGTTC GCAGCGTGGATTTTAACC -3'	EGFP Lsamp AfeI fwd
25007	5'-AAAACTTAAGTTAACATTTGCTGAGAAG GCAGAAC -3'	EGFP Lsamp AflII rev
25450	5'-AAAAAGCGCTGTTCGCAGCGTGGATTT TAACC -3'	Lsamp AfeI fwd
25451	5'-AAAAAGCGCTGGAGATGCCACCTTTCC CAAAG -3'	Opcml AfeI fwd
25452	5'-AAAACTCGAGTCAAAACTTGATGAAGA AGTGGGC -3'	Opcml XhoIrev
25453	5'-AAAAAGCGCTCGTAGCGGAGATGCCAC C -3'	Ntm AfeI fwd
25454	5'-AAAACTCGAGTCAAAATTTGAGGAGCA GGTGTAAGAC -3'	Ntm XhoI rev
25557	5'-AAAACTTAAGTCAAAACTTGATGAAGAA GTGGGC -3'	Opcml AflIIrev
26691	5'-AAAAAGCGCTGTGCCAGGAGAGGAAAA GCAG -3'	Mcam afeI fwd
26692	5'-AAAACTCGAGATGCCTCAGATCGATGTAT TTCTCTC -3'	Mcam xhoI rev full length
26693	5'-AAAACTTAAGCTTTCAATGCCTCAGAT CGATGTATTTCTCTC -3'	Mcam AflII rev full length

2.1.4.3 Primers for genotyping

Table 2.5: Primers for *MOGiCre/iDTR* genotyping

Number	Name	Sequence
14932	MogCre1, fwd	CTTCTTGGAGGAAACGGACATG
14933	Cre7, rev	CATCAGCTACACCAGAGACGGAAATC
14935	MogEx2-1, fwd	GACAATTCAGAGTGATAGGACCAGGGTATC
14936	MogEx2-3, rev	GGTCAATCTACCTACAGGTCATTTGA
14930	WSS-F, fwd	GGCTACTGCTGACTCTCAACATT
14931	DTR-R, rev	TCATGGTGGCGAATTCGAT
14927	Rosa FA, fwd	AAAGTCGCTCTGAGTTGTTAT
14929	SpliAcB, rev	CATCAAGGAAACCCTGGACTACTG
14928	RosaRA, rev	GGAGCGGGAGAAATGGATATG

2.1.5 Commercially available components, buffers and media

2.1.5.1 Commercial solutions and media

Media	Producer
B27 supplement	Gibco/Invitrogen
DMEM for Primary cell culture	Gibco/Invitrogen
DMEM for cell line culture	PAA
Fetal Calf Serum (FCS)	PAA
GlutaMAX™-I supplement	Gibco/Invitrogen
Horse Serum	PAA
Trypsin/EDTA	Lonza GmbH
Luxol Fast Blue Solvent	ClinTech
LB Medium	AppliChem
LB-Agar plate	AppliChem
OptiMEM-I Media	Invitrogen
PBS	PAA
Poly-L-Lysine (PLL)	Sigma
Penicillin/Streptomycin (Pen/Strep) 100×	Gibco/Invitrogen
Protease inhibitors cocktail Complete	Roche

10× PBS (phosphate buffered saline)

80 g	NaCl
2 g	KCl
14.4 g	Na$_2$HPO$_4$ (or 18.05 g Na$_2$HPO$_4$ · 2H$_2$O)
2.4 g	KH$_2$PO$_4$

Add dH$_2$O to 1 L and adjust pH to 7.05-7.11

2× HBSS (Hanks' balanced salt solution)

4 g	NaCl
0.1775 g	KCl
0.095 g	Na$_2$HPO$_4$· 7H$_2$O)
0.675 g	Glucose
2.5 g	Hepes-free acid

Add dH$_2$O to 250 mL and adjust pH to 7.05-7.11

The modified SATO medium, termed Super SATO, was used for the culture of primary oligodendrocytes and neurons.

Super SATO medium

2 %	B27-supplement
1 %	Horse serum
110 μg/mL	pyruvate
500 pM	tri-iodo-thyronine
520 nM	L-thyroxine
1×	Pen/Strep
1×	GlutaMAX™

in DMEM (Gibco/Invitrogen) with high glucose and without glutamine

2.1.6 Software

The software used for primer design, sequence analysis, data acquisition and processing are stated in Table 2.6.

Table 2.6: Software used in this study

Software	Application	Source/Manufacturer
Adobe Illustrator CS3	Image processing	Adobe Systems, Inc.
Adobe Photoshop CS3	Image processing	Adobe Systems, Inc
ApE	DNA analysis and editing	Wayne Davis, University of Utah
Dotslide System	Light microscrope images acquisition	Olympus GmbH
EndNote	Bibliography manager	Thomas Reuters
GraphPad Prism	Statistical analysis and graph production	http://www.graphpad.com/
ImageJ	Image processing and analysis	http://rsbweb.nih.gov/ij/
Leica Confocal Software	Confocal images acquisition	Leica Microsystems, Mannheim, Germany
LaTeX and TeXworks	Document writing and editing	http://www.latex-project.org/
LSM software	Confocal images acquisition	Zeiss, Inc.
Mendeley	Bibliography manager	http://www.mendeley.com/
Mirax Midi	Scanning and imaging	Zeiss, Inc.
Phobius	Signal peptide prediction	http://phobius.sbc.su.se/
Scaffold	Mass spectrometry data analysis	Proteome Software Inc.
SigmaPlot 11	Statistical analysis	Systat Software GmbH
SPPS 11.0	Statistical analysis	IBM
TMHMM	Protein trasmembrane prediction	http://www.cbs.dtu.dk/services/TMHMM/

2.2 Methods

2.2.1 Molecular Biology

DNA amplification for genotyping of mice used in the study, as well as for the cloning of expression plasmids was performed by polymerase chain reaction (PCR) (Mullis et al., 1986). The concentration of double stranded DNA was performed by diluting the samples 1:100 in ddH$_2$O in UV cuvettes (Eppendorf), and the absorbance at 260 nm with a BioPhotometer plus spectrophotometer (Eppendorf).

2.2.1.1 Genotyping

A small fraction of the mice tail tips were taken for genotyping. The extraction of DNA was performed using the Invitek Spin Tissue Kit following the manufacturer's recommendations. The DNA was eluted in 50 μL and kept at -20 °C for further use. For genotyping

the DNA was amplified using polymerase chain reaction, or PCR (Mullis et al., 1986), using GoTaq DNA polymerase (Promega, Mannheim, Germany) employing the primers found in Table 2.5. Designed primers were synthesized by ACGTLab, DNA core facility at the Max Planck Institute of Experimental Medicine.

PCR mix was prepared per sample as follows:

12.3 μL bidistilled water
4μL 5X buffer
0.96 μL MgCl2 (25mM)
1μL dNTPs (10mM mix of 2,5mM each)
0.5 μL from each primer (10pmol/μL stock)
0.8 μL DNA (0.05-1 μg)
0.2 μL Taq polymerase (5u/μL)

The PCR protocol used for genotyping was performed using a T3000 Thermocycler Kombi (Biometra), as follows:

Table 2.7: Primers for *MOGiCre/iDTR* genotyping

Stage	Temperature	Time
Initial denaturation	94℃	2 minutes
35 cycles of:		
Denaturation	94℃	30 seconds
Annealing	According to primer pair	1 minute
Extension	72℃	1 minute
Final Extension	72℃	5 minutes

The following pairs of primers were used for each allele:

MOGiCre
Primers: Mogicre1 & Cre7
Annealing temperature: 58℃
Expected length of amplified segment: 800 bp

MOG

Primers: MogEx2-1 & MogEx2-3

Annealing temperature: 58℃

Expected length: 370 bp

iDTR

Primers: WSS-F & DTR-R

Annealing temperature: 60℃

Expected length: 695 bp

R26Ri

Primers: RosaFA, SpliAcB & Rosa RA

Annealing temperature: 60℃ Expected length: wildtype 624 bp. iDTR 242 bp. A heterozygous mouse would have both bands.

2.2.1.2   DNA amplification for cloning

For cloning the different constructs described in listed in the previous section (Table 2.8), we amplified DNA fragments by PCR using with Phusion polymerase (2X Phusion High-Fidelity PCR Master Mix with HF Buffer, Finnzymes).

Table 2.8: PCR with Phusion Polymerase mix

Component	Amount
2X Phusion mix containing:	25 μL
-0.2 mM dNTPs	
-1 X Phusion HF Buffer	
-1 X Phusion High-Fidelity DNA Polymerase	
Primer 1 (10 pmol/μL stock)	2.5 μL
Primer 2 (10 pmol/μL stock)	2.5 μL
DNA (10 ng/μL)	1μL
DMSO	1,5 ul (3%)
ddH$_2$O (add to 50 μL)	17.5 μL

3% DMSO is suggested as a PCR additive to facilitate the denaturation of templates rich in GC. The general PCR protocol used was:

Table 2.9: PCR protocol for cloning using Phusion polymerase

Component	Temperature	Time
Initial denaturation	98℃	3 min
25 cycles of:		
Denaturation	98℃	10 sec
Annealing	Lowest melting temperature (Tm) of primers+3℃	15 sec
Elongation	72℃	Low complexity DNA (e.g. plasmid) 15 sec/kb. Complex genomic DNA: 30 sec/kb
Final Elongation	72℃	10 min

Agarose gel electrophoresis

Plasmids and PCR products were run in 1-2% Agarose gel in $1\times$ TAE buffer with 0.5 mg/mL ethidium bromide (Sharp et al., 1973) for the separation and visualization of DNA fragments. Chambers assembled by the Feinmechanik Service Department at the Max Planck Institute for Experimental Medicine were used for electrophoresis in $1 \times$ TAE buffer. The DNA was visualized by transillumination using Intas Gel Documentation System (Intas Science Imaging Instruments GmbH).

10X TAE (1 L)

  48.4 g   Tris base

11.4 mL   Acetic acid

20.0 mL   0.5 M EDTA

Adjust to 1 L with ddH$_2$O, pH $\sim$ 8.5

After agarose gel electrophoresis, DNA fragments were extracted with NucleoSpin Gel and PCR Clean-up kit (Macherey-Nagel) following manufacturer's instructions, and eluted in 15 μL.

DNA concentration determination

The concentration of DNA fragments and plasmids was determined measuring the absorbance at 260 nm of 1 μL of DNA diluted in 49 μL of H$_2$O, using a BioPhotometer plus (Eppendorf). The formula used was:

$$\text{Concentration of DNA } (\mu g/mL) = A_{260} \times \text{dilution factor} \times 50 \ \mu g/mL \qquad (2.1)$$

2.2.1.3   DNA digestion with restriction enzymes

Digestion of DNA fragments were done using restriction enzymes, due to their ability to cleave DNA fragments according to specific sequences (Arber and Linn, 1969). Restriction enzymes were purchased from New England Biolabs and Fermentas. A typical reaction was prepared as follows:

Table 2.10: Digestion with restriction enzymes

Component	Reaction	Vector	Control
10X buffer	3 μL	3μL	3μL
DNA	4 μg (1 μg/μL Midiprep) or 15 μL PCR elution	4 μg (Midiprep)	4 μg (Midiprep)
BSA 10X	3μL	3μL	3μL
Water	18-19 μL/8 μL	18-19 μL	19-20 μL
Enzyme(s)	1 μL each	1 μL each	

The mixture was left for 1 hour generally at 37℃ unless specified for a particular enzyme. When required, vector dephosphorylation was performed by adding, after digestion, 3 μL 10X Antarctic phosphatase buffer and 1 μL Antarctic phosphatase (New England Biolabs) to the digestion mix, leaving at 37℃ for 1 hour and heat inactivating for 5 minutes at 65℃ .

2.2.1.4   DNA Ligation

Digested fragments were ligated using T4 DNA ligase (Fermentas) as follows:

Ligation reaction

10× buffer	1 μL
T4 DNA Ligase	1μL
ATP(100mM)	1μL
Digested vector DNA	50-400 ng
Digested insert	1:1-5:1 to vector[1]
fill with H$_2$O to 10 μL	

The mix was incubated for at least 1h at RT, or overnight at 4℃ and used for bacterial transformation.

2.2.1.5   Transformation of *E. coli*

For transformation, 50-100 μL of DH5$_{alpha}$ *E. coli* (Subcloning Efficiency DH5$_{alpha}$, Invitrogen) were thawn on ice. 5-10 μL of ligation (or 0.5 μg of plasmid DNA for retransformation) were added, mixed gently and incubated 30 min on ice. The mix was subjected to a heat shock for 40 seconds at 42 ℃ and left for 2 minutes on ice. Then, 800 μL of LB medium were added and the cells were shaken at 37℃ for 1h. Afterwards, the cells were centrifuged for 2 minutes at 2000 rpm, most of the supernatant was removed, leaving $\sim$ 200 μL. The cells were resuspended and added to to LB-Agar plates (LB-Agar 40 g dissolved in 1 L H$_2$O) containing 100 μg/mL ampicillin, 50 μg/mL kanamycin or 50 μg/mL spectinomycin, according to the antibiotic resistance cassette incorporated to the vector of the mixture.The plates were incubated at 37℃ for 16-18 h. For plasmid purification, *E. coli* samples of colonies grown in antibiotic-containing plates were picked with autoclaved pipette tips, added to appropriate antibiotic-containing LB media (25 g LB-Medium per 1 L H$_2$O) and grown at 37 ℃ for 16-18 h.

2.2.1.6   Plasmid DNA amplification and purification

Cultures of transformed DH5$_{alpha}$ *E. coli* (Subcloning Efficiency DH5$_{alpha}$, Invitrogen) were grown in antibiotic-containing LB media H$_2$O) with constant shaking. The cells

---

[1]molar ratio

were centrifugated at 4 000 g for 15 min at 4℃ and DNA purification was performed using NucleoBond Xtra Midi EF Kit (Macherey-Nagel) following manufacturer's instructions. Eluted DNA was reconstituted in sterile H_2O.

To check ligation effectivity by restriction enzyme digestion and sequencing, *E. coli* samples of colonies grown in antibiotic-containing plates were picked with autoclaved pipette tips and grown in 3 mL LB containing the appropriate antibiotic for selection and grown at 37℃ for 16-18 h with constant shaking. Plasmid DNA was purified from these cultures using NucleoSpin Plasmid QuickPure Kit (Macherey-Nagel) according to manufacturer's recommendations.

2.2.2   Cell culture

2.2.2.1   Primary cultures

Primary oligodendrocyte cultures were prepared from the brain of postnatal day 0-2 rats or mice as described previously (Trajkovic et al., 2006). After removing the meninges, the neonatal brain hemispheres were digested with 0.25% trypsin,and cultured in Eagle 's basal medium with 10% horse serum on poly-L-lysine (PLL)-coated flasks at 37 ℃. Oligodendroglial cells were harvested from 8-10 day old mixed glia culture using mechanical dissociation. Cells were cultured on PLL-coated dishes or glass coverslips in Super SATO medium (DMEM containing 1% horse serum, B27 supplement, L-thyroxine, tri-iodothyronine, glutamine, pyruvate, and penicillin/streptomycin, see materials section for protocol).

To obtain primary neuronal cells, mixed brain culture from embryonic day 16 mice was prepared as previously described (Fitzner et al., 2006). Cells were cultured in Super SATO medium for two weeks to acquire confluent differentiated neurons.

To prepare a coculture of neurons and oligodendrocytes, neurons were cultured in a 12-well plate for 2 weeks as described above. The media was exchanged for fresh Super SATO media and 60 000 oligodendrocyte precursor cells were added per well and allowed to grow for 5 days.

2.2.2.2   Cell line culture

Human Embryonic Kidney (HEK) 293T cells (Graham et al., 1977) were used for production of Fc-fusion soluble proteins and binding assays. The cells were cultured in high glucose DMEM, 1 × GlutaMAX, 10% FCS and 100 U/mL penicillin and streptomycin. The cells were split 2-3 times per week after trypsinization with 0.05% trypsin/EDTA (Lonza GmbH). For Fc-fusion protein production, the media was exchanged for 1% FCS media.

2.2.2.3   Mammalian cells transfection and RNAi

Transfection of primary cultures and HEK cells was done using Lipofectamine® 2000 (Invitrogen). For cells cultured in 12 well plates, the following reaction was prepared per well: Per each coverslip in 12-well plates 1.6 μg of plasmid DNA was mixed with 100 with 100 μL OptiMEM-I (Invitrogen). Separately, 4 μL Lipofectamine2000 reagent were mixed with 100 μL OptiMEM. After 5 min incubation, both solutions were mixed and incubated for 20 min at RT. The 200 μL solution was added dropwise to the cells and left at least overnight before analysis.

Knockdown of exogenously expressed Lsamp, Opcml and Ntm (IgLON family) in HEK 293T cells was done in 6-well dishes by mixing 250 μL OptiMEM with 0.5 μg of myc-tagged IgLON protein and 3 μg shRNA plasmid (see Materials section for details). 250 μL of OptiMEM was mixed with 10 μL Lipofectamine 2000 in a separate vial and incubated for 5 min at RT. The two solutions were mixed gently, incubated for 20 min at RT and added dropwise to HEK 293T cells grown on PLL-coated 6-well dishes. After 3 days, the cells were scraped and prepared for analysis by Western blot.

2.2.2.4   Preparation of cell lysates for Western blot

To prepare cell lysates for analysis by Western blot, the culture medium was removed and the cells were washed once with PBS. An appropriate volume of Lysis buffer (2% NP-40, 0.2% SDS, 1 mM EGTA in PBS supplied with protease inhibitors) was added and the cells were detached using a cell scraper (Sarstedt), while being kept on ice. The samples were then centrifuged at 10 000 g for 10 min and the supernatant was used for protein concentration measurement using Bradford assay (Bradford, 1976). The samples were mixed with equal volume of 2 × sample buffer (20% glycerol, 4 mM EDTA, 4% SDS, 4%

2-mercaptoethanol, 0.05% Bromophenol blue and 100 mM Tris-HCl pH 6.8) and stored at -20℃ until further analysis.

HEK cells were transfected with Calcium Phosphate method based on the formation of a calcium phosphate-DNA precipitate which is uptaken by cells by endocytosis (Wigler et al., 1977; Abrahams and Van der Eb, 1975). For soluble Fc-fusion production, cells were cultured in 20 cm culture dishes in 25 mL media per dish. A typical transfection reaction for one dish was prepared as follows:

Transfection reaction

DNA (1 μg/μL)	12 μg
pEGFP-C1 DNA (1 μg/μL)	0.5μL
H_2O	887μL
$CaCl_2$ (2.5 M)	100 μL
2 × HBSS	1 mL

mix softly, add dropwise to cells

2.2.3   Fc-fusion protein purification

Soluble Fc-fusion proteins were purified using Protein A HP Spin Trap columns (GE Healthcare), following manufacturer's instructions. Briefly, HEK cells were transfected as described in the previous section. After 2-3 days, the supernatant was collected, and centrifuged for 15 min at 4 000 g at 4℃. 1× Complete Protease Inhibitor Cocktail (Roche) was added to the supernatant and then concentrated using Amicon Ultra-15 Centrifugal Filter Units (Millipore) according to manufacturer's recommendations. The final volume of 2 mL was diluted in equal volume of binding buffer (20 mM sodium phosphate, pH 7.0). Briefly, the storage solution from the column was removed by centrifugation for 30 s at 100 g. The column was equilibrated adding 600 μL of binding buffer, centrifuged for 30 s at 100 g. Then, 600 μL of the antibody solution were added, incubated for 4 min while gently mixing and then centrifuged for 30 s at 100 g. This procedure was repeated until all the volume was loaded on the column. Then the column was washed twice adding 600 μL binding buffer and centrifuging for 30 s at 100 g. Two collection tubes per sample were prepared for eluted fractions, each one containing 30 μL of neutralizing buffer . The proteins were eluted twice by adding 400 μL of elution buffer (0.1 M glycine-HCl, pH 2.7),

mixing by inversion, placing the column in a 2 mL microcentrifuge tube containing 30 μL neutralizing buffer (1 M Tris-HCl, pH 9.0) and centrifuged for 1 min at 50 g. The proteins were aliquoted and kept at -20°C .

2.2.4   Myelin isolation and purification

We isolated different fractions of myelin from C57BL6 mice (1-6) or human sample (7):

1. Standard compact myelin preparation in discontinous sucrose gradient, 0.32M/0.85M interphase.

2. Myelin isolated from postnatal day 14 (P14) brain homogenate, in discontinuous sucrose gradient, 0.32M/0.85M interphase.

3. Purified myelin solubilised with 1% TritonX overnight and bound to ConcanavalinA beads

4. Purified myelin bound to WGA beads.

5. Myelin isolated from brain homogenate subjected to an initial hyposmotic shock with water and then subjected to a continuous gradient, fraction 0.9-1M sucrose.

6. Myelin isolated from brain homogenate subjected to an initial discontinuous gradients and collected from 0.32-1.2M interphase and subsequently subjected to a continuous sucrose gradient. Collected from Fraction 3, or 0.9-1 M sucrose.

7. Glycoprotein from human myelin preparation, subjected to a lentil-lectin column (Mathey et al., 2007), was kindly provided by Edgar Meinl (Max Planck Institute of Neurobiology, Munich).

2.2.4.1   Myelin isolation by centrifugation in discontinous sucrose gradient

Compact myelin from 3-months-old mice (sample 1, 3 and 4) and 14-days-old mice (sample 2) were isolated based on a protocol previously described (Norton and Poduslo, 1973), with slight modifications. All the steps were done on ice using a SW41 Ti rotor in an Optima XL-70 ultracentrifuge (Beckman Coulter, USA). Homogenized brain tissue was placed over a discontinuous sucrose gradient (0.32 M and 0.85 M sucrose for fractions in a preparation buffer containing 5 mM EDTA and 10 mM Hepes, pH 7.4) and centrifuged for 30 minutes at 75 000 g. The interface between the two sucrose gradients was recovered and diluted in ten volumes of ice-cold water, and centrifuged for 20 minutes at 75 000 g. The pellet was subjected twice to hypo-osmotic shock by resuspension in ice-cold water and 10 minutes centrifugation steps at 12 000 g. The pellet was resuspended on 0.32 M sucrose in preparation buffer and overlaid on 0.85 M sucrose (in preparation buffer) to

create a new gradient as the one mentioned above. The previous centrifugation steps were repeated and the final purified myelin pellet was resuspended in preparation buffer and kept at -20℃ for futher use.

2.2.4.2   Myelin isolation by centrifugation in continous sucrose gradient

A continous sucrose gradient was prepared as follows: Using a long needle, 1 mL of 0.6 M sucrose in preparation buffer (5 mM EDTA and 10 mM Hepes pH 7.4) was laid in the bottom of a ultracentrifuge tube (Thinwall, Ultra-Clear™, 344059, Beckmann Coulter). Then, successive 1.5 mL layers of sucrose with increasing molarity (0.7, 0.8, 0.9, 1.0, 1.1 and 1.2 M) were added. The tube was left for 3 hours at room temperature to allow the formation of a continous gradient. Then, samples 5 and 6 were prepared by overlaying either brain homogenate (sample 5) or myelin from a 0.32 /1.2 M sucrose interphase (sample 6) onto the continuous sucrose gradient described above. The samples were centrifuged at 75 000 g for 1 hour using a SW41 Ti rotor in an Optima XL-70 ultracentrifuge (Beckman Coulter, USA). The overlay remains and the first mL of the continous gradient were removed. Afterwards, 6 fractions of 1.5 mL each were taken, diluted in ice cold water and centrifuged for 1 hour at 75 000 g. Subsequently, the pellet was subjected twice to hypo-osmotic shock by resuspension in ice-cold water and 10 minutes centrifugation steps at 12 000 g, resuspended in preparation buffer and kept at -20℃ for further use.

2.2.4.3   Glycoprotein enrichment by WGA and ConA columns

To isolate glycoprotein-rich myelin fractions using Wheat Germ Agglutinin (WGA) lectin resin, purified myelin from adult mice was obtained as stated in section 2.1.1. The myelin suspension was passed through a 26G gauge needle 10 times and bound to a Wheat Germ Agglutinin (WGA) column (Pierce Glycoprotein Isolation Kit, WGA, Thermofisher) following manufacturer's instructions. After washing, the beads were retrieved, resuspended in sample buffer and boiled for 10 minutes at 70℃ . The supernatant was retrieved and kept at -20℃ for further use. To isolate myelin glycoproteins using Concanavalin A lectin resin, purified myelin from adult mice was initially obtained as stated in section 2.1.1. The myelin was spun down and resuspended in a solution of 0.1% Triton X in PBS for solubilization. The supernatant was then loaded onto a ConA column (Pierce Glycoprotein Isolation Kit, ConA, Thermofisher) according to manufacturer's instructions. After

washing, the ConA beads were retrieved, resuspended in sample buffer and boiled for 10 minutes at 70℃ .

2.2.4.4   Human myelin glycoprotein enrichment

Glycoproteins were isolated from human myelin preparation with lentil-lectin affinity chromatography according to the manufacturer's guidelines (GE Healthcare) as described previously (Mathey et al., 2007).

2.2.5   SDS-PAGE and Western Blotting

Protein analysis by Western Blot was performed by SDS-PAGE as described earlier (Burnette, 1981; Laemmli, 1970). The polyacrylamide gels comprising of stacking and resolving gels were self-cast with composition described in Table 2.11. Equal amounts of protein from each sample were mixed in a 1:1 volume proportion with 2X loading buffer (10% glycerol, 2 mM EDTA, 2% SDS, 144 mM ß-mercaptoethanol, 50 mM Tris-HCl and 0.02% bromophenol blue), heated for 10 min at 70℃ and loaded onto 12% SDS-PAGE gel. For each gel, 3.5 μL of pre-stained protein ladder was loaded into one of the lanes. Electrophoresis was performed at 100V in the running buffer (190 mM glycine, 25 mM Tris and 0.1% SDS). The proteins were transferred from the polyacrylamide gel onto a Protan nitrocellulose membrane (Whatman GmbH, Germany) using a semi-dry procedure, for 1 hr at 100 V in the transfer buffer (20 mM Tris base, 153 mM glycine, 20% methanol).

Table 2.11: Components for Western Blot gels

Stacking gel		Resolving gel	
H$_2$O	1.21 mL	H$_2$O	1.66 mL
30% Acrylamide solution	0.27 mL	30% Acrylamide solution	2.04 mL
Stacking buffer (0.5 M Tris-HCl, pH 6.8)	0.5 mL	Resolving buffer (1.5 M Tris-HCl, pH 8.8)	1.3 mL
10% SDS	20 μL	10% SDS	50 μL
10% APS	20 μL	10% APS	50 μL
TEMED	3 μL	TEMED	2 μL

The correct transfer of protein was confirmed by fast reversible staining of protein bands by immersing the membrane in 0.1% Ponceau S in 5% acetic acid solution for five minutes and thereafter washing it with distilled water. The blot was blocked with 4% milk powder in PBS for 1 hr at RT followed by overnight incubation with appropriate pri-

mary antibody diluted in PBS containing 0.1% Tween-20 (PBST). After washing three times for 10 minutes with 0.1% PBST, the membranes were incubated with the appropriate horseradish peroxidase-conjugated secondary antibody diluted in PBST for 1 hour at room temperature. The blots were washed three times for 10 minutes with PBST and subjected to a mixture of equal parts of peroxide solution and luminol enhancer solution detection reagents (Thermo Scientific, Pierce). The blots were later exposed to light sensitive CL-XPosure films (Thermoscientific) and developed in a Kodak X-OMAT 1000 image processor. Images of the films were prepared using Adobe Photoshop software (Adobe Systems, Mountain View, CA).

2.2.5.1 Protein concentration determination

The protein concentration of cell lysate preparations, myelin preparations and purified proteins was determined by using Bradford assay (Bradford, 1976), and BCA Protein Assay (Pierce, Thermo Scientific) following manufacturer's instructions. The absorbance at 562 nm of the mixtures was measured with a 96-well plate MRXTc Revelation reader (Dynex Technologies).

2.2.6 *In vitro* assays

2.2.6.1 Immunocytochemistry

For immunolabeling, cells were fixed with 4% paraformaldehyde (PFA) for 15 min at room temperature before permeabilization with 0.1% Triton X-100 in PBS for 1 min. The blocking solution (2% BSA, 0.2% Fish gelatine, and 2% FCS in PBS) was then added to fixed cells for 30 min at RT. The primary antibodies diluted in blocking solution were added for 1 h at RT or overnight at 4℃ . After washing three times with PBS, cells were incubated with secondary antibodies for 1 h at RT. Finally, the coverslips were washed with PBS and mounted onto a glassslide with a drop of Mowiol solution (2.4 g Mowiol, 6 g Glycerol, 6 mL H2O, 12 mL 0.2 M Tris/HCl pH 8.5) and were kept in at 4℃ in the dark. When required, nuclei were stained with 4',6-diamidino-2-phenylindole (DAPI).

2.2.6.2 Paraformaldehyde (PFA) solution for fixation

Paraformaldehyde (PFA) 16% stock solution was prepared by dissolving 16 g PFA in 70 mL H_2O, heating at 60℃ adding NaOH pellets until the solution became clear. Then, 10 mL 10 × PBS were added and pH was adjusted to 7.4. Water was added to a total

volume of 100 mL. Aliquots of the solution were then stored at -20℃ . Working solution of 4% PFA in PBS was prepared by diluting 50 mL of PFA stock solution in 150 mL of 1× PBS and stored at 4 ℃ .

2.2.6.3   Mowiol solution for immunocytochemistry

Mowiol was used as the mounting medium after immunocytochemistry. The solution was prepared in the following way: 2.4 g Mowiol was added to 6 g glycerol and 6 mL H_2O. The mixture was stirred for seveeral hours at room temperature. Then, 12 mL 0.2 M Tris-HCl (pH 8.5) was added and then incubated at 60 ℃ for 10 min. The solution was centrifugated at 4000 g for 15 min, aliquoted an kept at -20 ℃ until further use.

2.2.6.4   Binding assay

For binding assays, supernatant from transfected HEK cells were retrieved and centrifuged 10 min at 5000 rpm. Per each 18 mm coverslip of neuronal or oligodroglial culture, 150 μL of media were mixed with 1.5 μL of Cy3-conjugated anti-human Fc antibody (Dianova) and incubated for 30 min at RT. Then, the mix was added to each coverslip and incubated for 20 min at RT in a humid chamber (Feinmechanik Service Department, Max Planck Institute for experimental medicine). Finally, the coverslips were washed 3 times with PBS and the cells were fixed with 4% PFA for 15 min at RT.

2.2.6.5   Proliferation assay

For proliferation assays, 30 000 oligodendrocyte precursor cells (OPC) per well were plated in a 24-well plate on PLL-coated coverslips. 10 μg/mL of the Fc-fusion proteins were then added to the wells. The cells were allowed to settle down and were fixed after 8 hours, and stained for the OPC marker A2B5. We used 100 ng/mL PDGF as a positive control of proliferation.

2.2.6.6   Migration assay

Migration assays were performed using CytoSelect 24-Well Cell Migration and Invasion Assay (8 μm, Colorimetric Format). Briefly, the chamber membranes were coated by placing each insert on 400 μL PLL (100μg/mL) for 1 h at 37℃ and washed 2 times with PBS. A cell suspension of 1 000 000 oligodendrocyte precursor cells per mL was prepared in serum-free Super SATO. 500 μL of serum-free super SATO media containing 10 μg/mL

Fc-fusion proteins, 100 ng/mL PDGF or equal volume PBS were added to the lower well of the migration plate. Next, 300 μL of OPC suspension were added to the inside of each insert, and incubated 8 hours at 37 ℃ . Then, the media from the inside of the insert was removed, cotton-tipped swabs were used to remove the interior of the inserts to remove non-migratory cells. The insert was transferred to a clean well containing 400 μL of Cell Stain Solution and incubated for 10 minutes at room temperature. After allowing the inserts to air dry, migratory cells were counted with a Nikon Ti-E brightfield microscope.

2.2.6.7   Differentiation assay

To observe whether the presence of soluble IgLON in the media can influence the growth and differentiation of oligodendrocytes *in vitro*, OPC were grown for 4 days in media with 30 μg/mL of IgLON Fc-fusion proteins on PLL-coated coverslips, and then fixed with 4% PFA.

2.2.6.8   Adhesion assay

Glass coverslips in a 24-well plate were coated with 500 μL of a solution with 10 μg/mL of donkey anti-human Fc antibody (Dianova) in 50 mM Tris-HCl (pH 9.0) and left overnight at 4℃. Then, the coverslips were washed 3 times with supplement-free DMEM and 500 μL of a solution containing 10 μg/mL of Fc-fusion protein in 0.2% BSA/PBS. After 1h of incubation at 37℃ , the coverslips were washed 3 times with DMEM and fresh Super SATO media was added. PLL coating (100 μg/mL was used as a positive control to verify the quality of the primary oligodendrocyte preparation. After washing and placing new media, 25 000 OPC were plated and allowed to grow for four days, and fixed with 4% PFA.

2.2.6.9   Myelination assay

Primary neurons were plated on a 12-well plate and grown for two weeks in super SATO media. After exchanging for new media, 60 000 OPC were added to each well and allowed to grow for 5 days, before fixation with 4% PFA.

2.2.7   Toxin-induced oligodendrocyte death and demyelination

2.2.7.1   Diphtheria toxin-mediated oligodendrocyte ablation

Animal experiments were conducted in accordance with animal protection laws approved by the Government of Lower Saxony, Germany. 10-week-old MOGi-Cre/iDTR mice (Buch et al., 2005; Hovelmeyer et al., 2005) were injected intraperitoneally with 400 ng of diphtheria toxin (DT, Merck) in PBS once a day for seven days. Age- and sex-matched MOGi-Cre/iDTR mice injected with PBS, and MOGi-Cre mice (lacking the iDTR allele) injected with DT were used as controls.

2.2.7.2   Cuprizone-induced de- and remyelination

8-weeks-old C57Bl6 male mice were used in the experiment here described. The animals were divided into three groups, named according to the applied treatment as double demyelination (DD), single demyelination (SD) and Control. DD animals were fed with 0.25% cuprizone (Sigma, St Louis, MO, USA) in milled chow (Ssniff) for 5 weeks, followed by normal diet for 4 weeks to allow recovery. Subsequently they received 0.25% cuprizone diet for 5 weeks, which was then replaced by normal diet for the remaining of the experiment. Animals in SD group received normal diet for 9 weeks (until the start of the second demyelinating event of group DD) and then were fed with 0.25% cuprizone for 5 weeks and finally with normal diet for the remaining of the experiment. Age-matched controls received normal diet without cuprizone throughout the entire experiment (see **Figure** 3.10).

2.2.7.3   Behavioral test: Motor Skill Sequence

Assessment of motor performance following remyelination was done using Motor Skill Sequence (MOSS) as previously described (Liebetanz and Merkler, 2006). Separate analysis were performed 6, 20 and 28 weeks after cuprizone was removed from the diet following the first demyelination in SD group and second demyelination in DD group. For every analysis, each animal was transferred to an individual cage containing a running wheel, and for 14 days the animals were allowed to run voluntarily in training wheels composed of regularly-spaced crossbars.
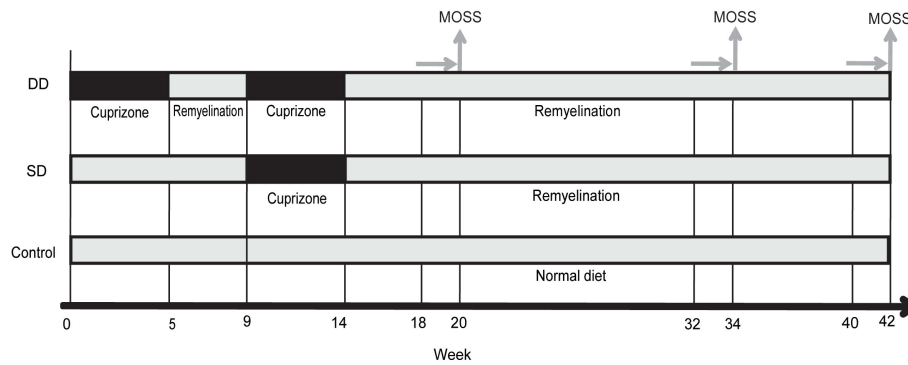
Figure 2.1: Experimental design of cuprizone treatment. 8-week-old mice were fed cuprizone for 5 weeks, were then allowed to recover for 4 weeks and finally received cuprizone for 5 more weeks (double demyelination, or DD). A second group of mice (single demyelination, or SD) were fed cuprizone for 5 weeks simultaneous to the second demyelination of the DD group as indicated. Animals were switched to a normal diet for 28 weeks until the end of the experiment. Age-matched controls were fed with a normal diet throughout the experiment. Motor Skill Sequence analysis (MOSS) was performed at the times indicated. Animals were first habituated to training wheels composed of regularly spaced crossbars for two weeks. Subsequently, running performance on complex wheels was recorded for an additional week.

Following the training period, the training wheel was replaced by a "complex" wheel containing irregularly-spaced crossbars and the animals were allowed to run voluntarily for seven consecutive days. Activity in the individual wheels was recorded automatically with a rotation sensor connected to the wheel axis. The following parameters were monitored continuously: maximum running velocity in revolutions/minute (Vmax), accumulative distance in meters (Distac), the number of individual runs (Nrun) and the maximum distance per run (Distmax). Each parameter was calculated online and the results were logged once daily (12 am). Thus, Distac and Nrun represent the values accumulated during the last 24 h, whereas Vmax and Dmax represent maximum values achieved within the last 24 h.

2.2.8   Perfusion and tissue processing

Animals were sedated with a 14% chloral hydrate intraperitoneal injection, perfused transcardially and fixed with 4% paraformaldehyde (PFA) with a Heraeus SR70 peristaltic pump (0.2-0.5 mL/sec). After perfusion the brain and spinal cord were immersed in 4% PFA overnight. Tissue was processed as described previously (Merkler et al., 2005; Mason et al., 2001). After paraffin embedding in a HMPII embedder (Microm), paraffin blocks

were created in a Microm AP280 Embedding Center. Then, 3 μm thick sections of the brain, spinal cord, spleen and liver were obtained with a Microm HM400 microtome, laid on glass slides and left overnight at 37℃

2.2.8.1   Human brain tissue

Human brain biopsies of four patients with MS were obtained from the collection of the Department of Neuropathology at the Georg-August University. Its use for scientific purposes was in accordance with the guidelines of the institutional ethics committee and the study was approved by the ethics committee of the University of Göttingen (Göettingen, Germany).

2.2.8.2   Histological analysis

The extent of demyelination induced by diphtheria toxin injection or cuprizone treatment was assessed scoring the animals from 0 (no demyelination) to 3 (complete demyelination) in sections stained with Luxol fast blue–periodic acid Schiff (LFB–PAS) (Hiremath et al., 1998).

Bielchowsky's silver staining for axons (Cobb and Bielschowsky, 1925) was performed as follows: Paraffin embeded tissues were deparaffinize and hydrated in distilled H_2O. After washing 3 times in dH_2O, sections were placed in 50 mL 20% silver nitrate solution for 20 min and washed 3 times in dH_2O. 10 mL of concentrated 32% ammonium hydroxide were added dropwise while stirring to 50 mL 20% silver nitrate solution to form silver hydroxide solution. Then, the section were incubated in silver hydroxide solution for 15 min in the dark and washed in 0.1% ammonium hydroxide 3 times. Then 1.4 mL of developer solution (20 mL 37% formaldehyde, 100 mL dH_2O, 2 drops 65% nitric acid and 0.5 g citric acid) to 50 mL 20% silver hydroxide solution, and the sections were stained in this solution until they turned brown with a golden background. The reaction was stopped washing with dH_2O 3 times. Then the sections were placed in 2% sodium thiosulfate for 2 min. Finally, the sections were washed with dH_2O, dehydrated with alcohol and xylene and mounted with DePeX (Serva).

2.2.8.3 Immunohistochemistry

Immunohistochemistry was performed using antibodies against neuronal nuclei (NeuN Chemicon), mature oligodendrocytes (NogoA, (Liebscher et al., 2005)), macrophages or activated microglia (Mac3, Pharmingen), astrocytes (GFAP, Promega), T-cells (CD3, Serotec) and axonal damage with amyloid precursor protein (APP, clone 22C11; Chemicon) followed by labelling with biotinylated secondary antibodies. Avidin-biotin technique with 3,3-diaminobenzidine was used for visualization.

A general protocol for 3,3-diaminobenzidine (DAB) visualization method was the following: The sections were deparaffinized, and hydrated in distilled H_2O. When necessary, epitope retrieval was done in 10 mM sodium citrate buffer (pH 6.0), microwaved 5 times for 3 minutes and allowed to cool down. After washing with dH_2O, endogenous peroxidase were blocked by incubation in 3% H_2O_2 for 20 min at 4℃ and washed with PBS. When relevant, 1:100 Fab Goat-anti-Mouse antibody in 10% FCS was added to the sections and incubated for 1 h at RT in a humid chamber, and washed with PBS. Blocking was performed with 10% FCS/PBS for 1h at RT and primary antibodies were added to the sections overnight at 4℃ . Then, the sections were washed with PBS and incubated with biotinylated secondary antibodies for 1h at RT. After washing with PBS, the sections were incubated with 1:1000 ExtrAvidin-Peroxidase (Sigma) in 10% FCS for 1h at RT. The sections were washed with PBS and placed in a solution of 49 mL PBS, 1mL DAB (25 mg/mL, Sigma) and 40 μL 30% H_2O_2. After washing with distilled H_2O, the slides were immersed 5 times in Haemalum (Harris) Solution (Sigma-Aldrich), and then washed with running tap water for 10 min. After washing with distilled H_2O, the sections were dehydrated with increasing percentage of alcohols, placed in Xylol (Chemie Vertrieb GmbH) and mounted with DePeX.

For fluorescence immunohistochemistry, the following protocol was used: The sections were deparaffinized, and hydrated in distilled H_2O. When necessary, epitope retrieval was done in 10 mM sodium citrate buffer (pH 6.0), microwaved 5 times for 3 minutes, allowed to cool down and washed with dH_2O. When relevant, 1:100 Fab Goat-anti-Mouse antibody in 10% FCS was added to the sections and incubated for 1 h at RT in a humid chamber, and washed with PBS. Blocking was performed with 10% FCS/PBS for 1h at RT and primary antibodies were added to the sections overnight at 4℃ . Then, the sections were washed with PBS and incubated with 488- or Cy3-conjugated antibodies (Invitrogen or

Dianova) and incubated for 1h at RT. After washing with PBS, nuclei were stained by placing 100 μL per slide of DAPI (4'6-diamidino-2-phenylindole-2HCl) 1:10 000 dilution for 15 minutes at RT. The sections were washed with PBS, distilled H_2O and mounted in fluorescence mounting medium (Dako).

Histopathological analysis was performed on PFA-fixed sections from brain biopsies of patients with documented progressive MS. All tissue blocks (n= 6 blocks from 4 patients) were selected if signs of remyelination (judged by LFB/PAS staining) were observed. Fluorescence immunohistochemistry was performed for MBP and APP as described above.

To assess axonal preservation, images of each side of the midsagittal line of the corpus callosum from coronal sections stained with NF200 were obtained under equal acquisition parameters with a confocal microscope (LSM 510, Carl Zeiss MicroImaging, Inc) and the signal intensity was analysed with Image J. Histological sections stained with anti-APP counterstained with Haemalaum Solution (Sigma-Aldrich), and of NeuN antibody and were scanned using the Mirax Midi System (Carl Zeiss MicroImaging, Jena, Germany). Confocal microcopic images were aquired with Carl Zeiss LSM 510 microscope with a 63$\times$ oil plan-Apochromat objective, or with a Leica TCS SP2 AOBS confocal laser scanning setup.

2.2.8.4   Semi-automated axonal counts

Callosal axons were evaluated on sagittal neurofilament stained brain sections (Pan-Neuro filament using a pool of anti-NF 160 (Novocastra), anti-NF200 (Novocastra) and anti-NF60 (Chemicon). Images of transversally cut axons were obtained by a Zeiss LSM 510 laser scanning microscope coupled to a Zeiss Axiovert 100 M inverted microscope equipped with a 63x/1.4 oil immersion objective. Callosal axons were captured in 3 to 5 randomly selected, non-overlapping areas (146.2 x 146.2μm2) per animal. Confocal stacks (thickness of 1.2–3.7 μm; interval of 0.41 μm) were scanned in the z-direction (Software LSM 510; Zeiss) and 3 to 5 overlapping stacks composed 1 layer using Fiji. Axons were counted in an area of at least 5 600 μm2 per animal using a custom-programmed script in Cognition Network Language–based on the Definiens Cognition Network Technology platform (Definiens Developer XD software; Definiens).

In brief, neurofilament- positive axons were detected based on their contrast to the image background signal. To adapt for potential variable background staining levels, the area surrounding potential axonal structures was segmented and the mean intensity difference between the structures was calculated. Neurofilament- positive structures displaying a signal difference higher than 8 from their surroundings were classified as axons (for detailed formula see the Definiens Developer XD 1.5.2 Reference book). Complementary, adjacent sections were stained using Bielschowsky's silver impregnation technique and sections were scanned using Zeiss Mirax Virtual Slide Scanner (Carl Zeiss MicroImaging GmbH). The thickness of the corpus callosum was then measured using a Mirax Slide Viewer (Carl Zeiss MicroImaging GmbH). Axonal numbers were subsequently calculated by multiplying axonal densities (expressed as axons per square millimeter) with the thickness of the corpus callosum of a given animal. Staining and analysis were performed by Tanja Jürgens, Geneva University Hospital.

2.2.8.5   Neuronal numbers semi- automated analysis

Sections stained for neuronal nuclei with NeuN antibodies were scanned as described above. Neuronal numbers were automatically counted using a script in Cognition Network Language based on Definiens Cognition Network Technology ® platform (Definiens Developer XD software, Munich, Germany). Briefly, the cortical region of interest was drawn manually and NeuN positive cells were detected based on color criteria. After finer segmentation to discriminate between nucleus and cytoplasm, the object was classified as a NeuN-positive cell if the soma was below a certain size and had 0-1 nucleus. If more than one nucleus was detected within one soma, the object was split using each nucleus as seed to grow into the surrounding cytoplasm, stopping if growing borders converged or the cytoplasmic border was reached. Finally, the total number and density of NeuN-positive cells was calculated. Quantification was performed by Mario Kreutzfeldt, Geneva University Hospital.

2.2.8.6   Electron microscopy

Electron microscopy (EM) was performed according a modified protocol as earlier described (Merkler et al., 2005). Briefly, mice were fixed by transcardial perfusion with 4% paraformaldehyde and 2.5% glutaraldehyde in 0.1 M phosphate buffer containing 0.5% NaCl. The tissue was embedded in epon and corpus callosum were cut and stained with

toluidine blue. The tissue was then trimmed and reoriented so that ultrathin cross sections of midline corpus callosum could be cut and treated with uranyl acetate and lead citrate. The sample area was selected at low magnification in the electron microscope (2500x) before systematically recording images of the corpus callosum at 16000x magnification using a CCD camera (MegaView III, Soft Imaging System). Axon diameters and myelin sheath thicknesses of at least 300 axons (¿0.35 μm in diameter) were measured from each animal using CellF software (Olympus Soft Imaging Solutions GmbH, Germany), and were used to calculate the g-ratio (axon diameter/fibre diameter) as described previously (Coetzee et al., 1996).

2.2.9   Proteomic analysis

2.2.9.1   Mass spectrometry

Mass spectrometry analysis of myelin samples were analyzed by nanoliquid chromatography coupled to tandem mass spectrometry (LC-MS/MS) on a Thermo LTQ XL Orbitrap (Thermo Fisher Scientific, Bremen, Germany) coupled to an Agilent 1100 series LC-system. Peak lists of all MS samples were searched against the National Center for Biotechnology Information (NCBI) non-redundant RefSeq database www.ncbi.nlm.nih-.gov./RefSeq/ (Pruitt et al., 2003) using Mascot (Matrix Science, London, UK). Mascot was set up to search the nr_240211 database (selected for Homo sapiens, 558660 entries) (only "mascot_daemon_merge (F009486)") assuming the digestion enzyme trypsin and the nr_240211 database (selected for Mus, 471874 entries) (only samples "mascot_daemon_merge (F009472)", "mascot_daemon_merge (F009473)", "mascot_daemon_merge (F009474)", mascot_daemon_merge (F009475), "mascot_daemon_merge (F009476)" and mascot_daemon _merge (F009477)) also assuming trypsin. Mascot was searched with a fragment ion mass tolerance of 0,60 Da and a parent ion tolerance of 10,0 PPM. Oxidation of methionine and iodoacetamide derivative of cysteine were specified in Mascot as variable modifications. Mass spectrometry analysis was done by Monika Raabe, department of Analytical Mass Spectrometry, Max Planck Insititute for Biophysical Chemistry, Goettingen.

For protein identification, Scaffold (version Scaffold_3.0.9.1, Proteome Software Inc.) was used to validate MS/MS based peptide and protein identifications. Peptide identifications were accepted if they could be established at greater than 80% probability as specified by the Peptide Prophet algorithm (Keller et al., 2002). Protein identifications were accepted

if they could be established at greater than 50% probability and contained at least 2 identified peptides. Protein probabilities were assigned by the Protein Prophet algorithm (Nesvizhskii et al., 2003). Proteins that contained similar peptides and could not be differentiated based on MS/MS analysis alone were grouped to satisfy the principles of parsimony.

2.2.9.2   In-silico screening

A candidate list from the results of the proteomic analysis of myelin was made by selecting proteins predicted to have transmembrane regions using the software TMHMM `http://www.cbs.dtu.dk/services/TMHMM/` (Krogh et al., 2001) and/or signal peptide using the software Phobius `http://phobius.sbc.su.se/` (Käll et al., 2004). Functional information was searched at the UniProt database (The UniProt Consortium, 2008).

2.2.10   Statistical analysis

For two-groups comparison, a Student's t-test was used. For more than two groups, a one-way ANOVA was performed, followed by a Tukey test for pairwise comparisons, when applicable. A p level of <0.05 was considered significant in all tests. All values are expressed as mean ±SEM. To analyse the effect of the cuprizone treatment on wheel running skills (MOSS) a two-factorial repeated measurements ANOVA, with treatment and time course as the independent variables and the respective wheel-running parameter serving as dependent variable was applied. If ANOVA indicated significant differences for the main effect of treatment, Fisher's LSD post hoc tests were applied. For histological analysis a one-way ANOVA was perfomed, followed by Tukey test for pairwise comparisons, when applicable. A p valuel of ¡0.05 was considered significant in all tests. Statistics were calculated using SPPS 11.0 (IBM), GraphPad Prism (GraphPad Software, Inc.) or SigmaPlot software (Systat software, Inc.).

Chapter 3

Results

Multiple Sclerosis (MS) is a demyelinating disorder that results in motor and cognitive decline. Axonal loss occurs throughout the disease, especially in the initial inflammatory stages, where the immune system breaches the blood-brain barrier (BBB) and starts to attack the myelin sheath. Even though axonal loss appears to be driven by the cytotoxic inflammatory reaction against myelin, axons continue to present signals of damage and be lost in chronic stages of the disease when inflammation is minimal (Kuhlmann et al., 2002). This could suggest that a long-term damage could be induced by the disruption of the axo-glial contact and integrity of myelin.

The purpose of this study was to observe the consequences of oligodendrocyte death and myelin loss on axonal preservation. To discern the consequences of the myelin loss from the cytotoxic effect of an autoimmune reaction against myelin, which occurs in experimental autoimmune encephalomyelitis (EAE), we used toxin-based demyelinating models that did not involve infiltration of the immune system in the CNS. To study the short- and long-term effect of demyelination on axons, we induced mature oligodendrocyte ablation by diphtheria toxin and cuprizone.

3.1   Targeted Ablation of Oligodendrocytes Triggers Axonal Damage

3.1.1   Diphtheria-toxin-induced oligodendrocyte ablation and demyelination in MOGi-Cre/iDTR mice

Diphtheria toxin causes apoptosis of cells that express a functional DT receptor or cells that express the catalitically active fragment A of diphtheria toxin. In order to induce mature oligodendrocyte death, we used MOGi-Cre/iDTR mice, which express the DT receptor in myelinating cells. We used heterozygote mice for both the MOGi-Cre and iDTR alleles (see genotyping sample of MOGi-Cre/iDTR mice in **Figure** 3.1). It has been shown previously that intraperitoneal injection of these animals 3 times a day for 7 days with 100 ng of DT results in massive oligodendrocyte death after $\sim$ 30 days (Buch et al., 2005). To explore the consequences of this process on axonal integrity, we injected 10-week-old MOGi-Cre/iDTR mice with 400 ng DT daily for 7 days. We modified the protocol to reduced the frequency in mice injection, and therefore decided to increase the amount of DT injected. As controls, we injected the same volume of PBS to age- and sex-matched MOGi-Cre/iDTR mice and the same amount of DT to MOGi-Cre mice, lacking the iDTR allele.
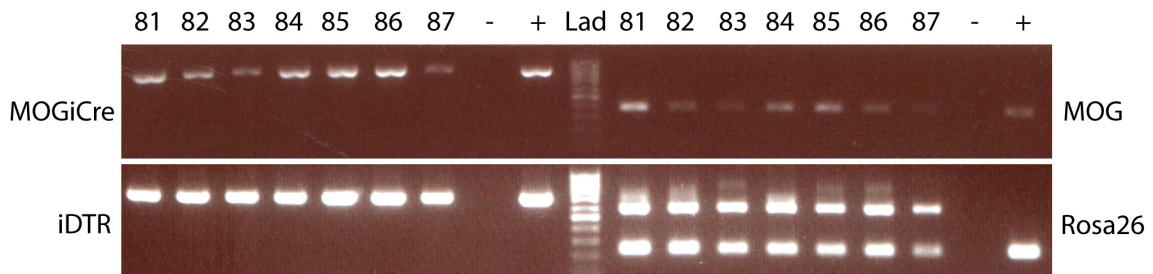
Figure 3.1: Genotyping of MOGi-Cre/iDTR mice animals used in diphtheria toxin-induced oligodendrocyte ablation. Sample of MOGi-Cre/iDTR mice genotyping of heterozygote animals used in diphtheria toxin-induced oligodendrocyte ablation. PCR products were run in 2% agarose gel at 100V and visualized by transilumination and ethidium bromide. See the methods section for details.

We observed, in accordance with Buch et al. (2005), that after approximately 30 days, MOGi-Cre/iDTR mice injected with DT presented clinical symptoms such as weight loss, tremor and unbalanced gait and occassional death. Due to the severity of the disease, the

animals were sacrificed and processed for tissue analysis. A similar phenotype was observed in animals that were injected with 200 ng DT once a day for seven days, although clinical symptoms were observed around 45 days post injection (data not shown).

To confirm the ablation of oligodendrocytes, coronal sections were stained for the oligodendrocyte marker NogoA and NogoA positive cell densities in the corpus callosum were quantified (**Figure** 3.2). Indeed, the density of oligodendrocytes in MOGi-Cre/iDTR mice (280 ± 25) was significantly reduced compared to MOGi-Cre/iDTR mice injected with PBS (878 ± 82) and MOG-iCre mice injected with DT (707 ± 29), indicating the successful oligodendrocyte ablation induced by DT in MOGi-Cre/iDTR mice.
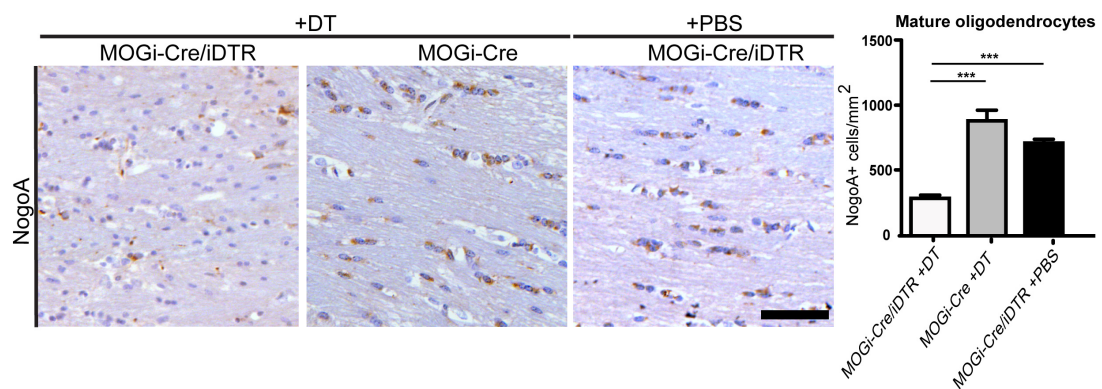
Figure 3.2: **Oligodendrocyte ablation induced with Diphtheria Toxin in MOGi-Cre/iDTR mice.** MOGi-Cre/iDTR mice were injected with 400 ng diphtheria toxin (DT) daily, for 7 days. After 30 days, the number of oligodendrocytes was assessed by NogoA staining. A decrease in oligodendrocyte number was observed in MOGi-Cre/iDTR mice treated with DT (left panel), compared to DT-treated MOGi-Cre animals as control (middle panel) and MOGi-Cre/iDTR animals treated with PBS (right panel). For quantification one-way ANOVA was performed, followed by pairwise Tukey test. Statistical significance is represented with asterisks (n=3-9, $**$p=0.01, $***$p=0.001). Scale bar, 100 μm.

The extent of demyelination 30 days after injection was assessed by staining coronal sections with LFB-PAS and classifying the signal in the corpus callosum using a standardized scale, from 0 (no demyelination) to 3 (complete demyelination) (Hiremath et al., 1998). Moderate demyelination was observed in MOGi-Cre/iDTR mice treated with DT, in accordance with the reduction of oligodendrocyte abundance (**Figure** 3.3).
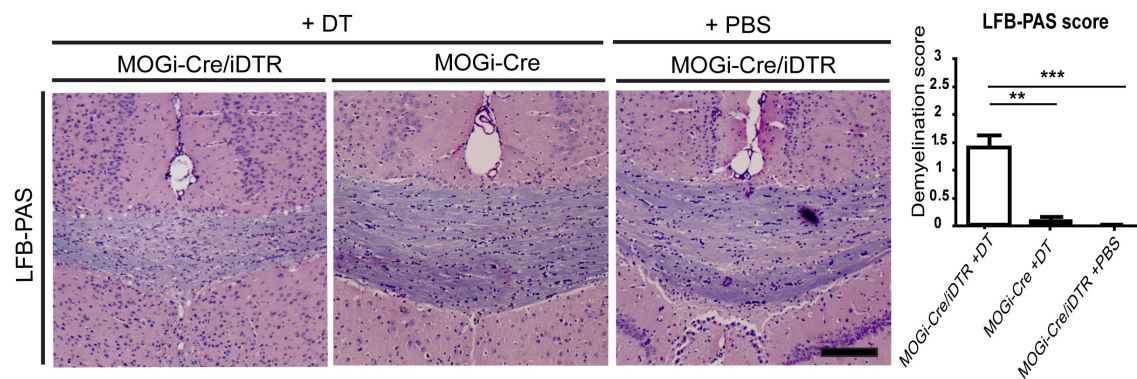
Figure 3.3: **Demyelination induced with Diphtheria Toxin in MOGi-Cre/iDTR mice.** The level of myelination was assessed 30 days after DT treatment by LFB-PAS staining in coronal sections of MOGi-Cre/iDTR mice (left panel), DT-treated MOGi-Cre animals as control (middle panel) and MOGi-Cre/iDTR animals treated with PBS (right panel). For quantification one-way ANOVA was performed, followed by pairwise Tukey test. Statistical significance is represented with asterisks (n=3-9, $**p<0.01$, $***p<0.001$). Scale bar, 100 μm.

3.1.2   Astrogliosis and immune system response

To evaluate the reaction by other glial populations upon oligodendrocyte death and demyelination, we measured astrogliosis by staining with GFAP antibodies (**Figure** 3.4). We observed a significant increase in astrocyte population in demyelinated animals (378 $\pm$ 24 GFAP+ cells per mm^2) in comparison with MOGi-Cre animals treated with DT (152 $\pm$ 13 GFAP+ cells per mm^2) and MOGi-Cre/iDTR animals treated with PBS (120 $\pm$ 23 GFAP+ cells per mm^2).

A typical feature of demyelinating lesions is an increase population of activated microglia/macrophages. We quantified the macrophage/microglia activation by staining coronal sections with Mac3 antibodies (**Figure** 3.5). We detected a significant increase of this population in DT-treated MOGi-Cre/iDTR mice in demyelinated animals (513 $\pm$ 75 Mac3+ cells per mm^2) in comparison with MOGi-Cre animals treated with DT (101 $\pm$ 8 Mac3+ cells per mm^2) and MOGi-Cre/iDTR animals treated with PBS (84 $\pm$ 21 Mac3+ cells per mm^2).
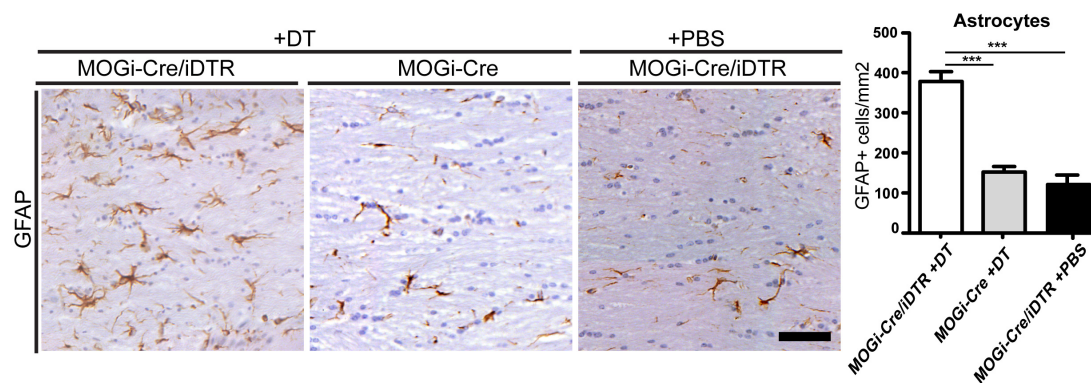
Figure 3.4: **Astrogliosis in Diphtheria toxin-induced oligodendrocyte ablation.** Coronal sections from MOGi-Cre/iDTR mice treated with DT (left panel), DT-treated MOGi-Cre animals as control (middle panel) and MOGi-Cre/iDTR animals treated with PBS (right panel) were stained for astrocytes (GFAP). Quantification of astrocyte density in central corpus callosum is shown as mean ± SEM (n=3-7). If ANOVA indicated significant differences in the main effect (p<0.05), Tukey test pairwise comparison was applied. Statistically significant differences are indicated by asterisks ($**$p <0.01, $***$p <0.001). Scale bar: 50 μm.

Finally, to determine whether a demyelinating event is sufficient to trigger an infiltration of the immune system through the BBB, we used CD3 antibodies to stain T cells. No infiltration of T cells was observed in any of the groups (data not shown).

3.1.3   DT-induced ablation of oligodendrocytes triggers axonal damage

To analyze the changes in the axonal composition and integrity of the corpus callosum, we stained coronal sections with antibodies against high-molecular weight neurofilament (NF200) and measured its thickness. In addition, we measured the NF200 signal, which has been shown to be decreased in demyelinated MS lesions and can reflect a cytoskeletal disorganization in axons (Lovas et al., 2000).

We did not observed evidence of corpus callosum atrophy (ANOVA p>0.05). However, there was a decrease in neurofilament signal density in MOGi-Cre/iDTR mice injected with DT (signal density 31.5 $\pm$ 2.9 gray value per μm) compared to MOGi-Cre/iDTR mice injected with PBS (878 $\pm$ 82 gray value per μm) and MOG-iCre mice injected with DT (707 $\pm$ 29 gray value per μm), which indicates axonal abnormality (**Figure** 3.6).

Damaged axons can be identified by the accumulation of amyloid precursor protein (APP), possibly as a consequence of axonal transport disruption or even the irreversible transection of an axon in the CNS. APP positive axons are frequently found in MS lesions and are taken as a measure of axonal damage (Kuhlmann et al., 2002; Trapp and Nave, 2008). We
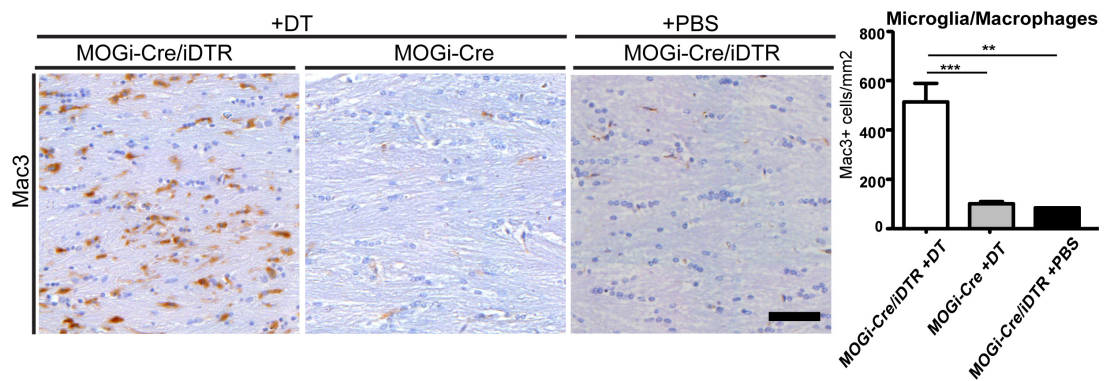
Figure 3.5: **Microglia activation in Diphtheria toxin-induced oligodendrocyte ablation.** Coronal sections from MOGi-Cre/iDTR mice treated with DT (left panel), DT-treated MOGi-Cre animals as control (middle panel) and MOGi-Cre/iDTR animals treated with PBS (right panel) were stained for macrophages and activated microglia with Mac3 antibodies. Quantification of macrophage/microglia density in central corpus callosum is shown as mean ± SEM (n=3-7). If ANOVA indicated significant differences in the main effect (p<0.05), Tukey test pairwise comparison was applied. Statistically significant differences are indicated by asterisks (∗∗p <0.01, ∗∗∗p <0.001). Scale bar: 50 μm.

observed a massive accumulation of APP in the corpus callosum of MOGi-Cre/iDTR mice treated with DT (89 ± 15 positive axons per μm^2), while it was virtually absent in the control groups. (**Figure** 3.7). This indicated that demyelination of the corpus callosum results in axonal damage and possible loss.

3.1.4   No neuronal death detected upon oligodendrocyte ablation

Since there was significant axonal damage in MOGi-Cre/iDTR mice treated with DT, we next examined whether this resulted in detectable neuronal death. We stained neuronal nuclei using NeuN antibodies, and counted the total number of cortical neurons in coronal sections. We did not observe a significant reduction in neuronal abundance (**Figure** 3.8). However, it should be considered that small amounts of localized neuronal death may not be detected when assessing the total number of neurons in our semi-automated method. Therefore, we assessed the number of apoptotic neurons. We stained coronal sections with NeuN antibodies for neuronal nuclei and performed a fluorescein-12-deoxy-UTP nick-end labeling (TUNEL) staining to detect apoptotic cells. We did not observe any apoptotic neurons in any of the groups (**Figure** 3.9). Therefore, DT-induced oligodendrocyte depletion triggered massive axonal damage, but did not result in neuronal death.
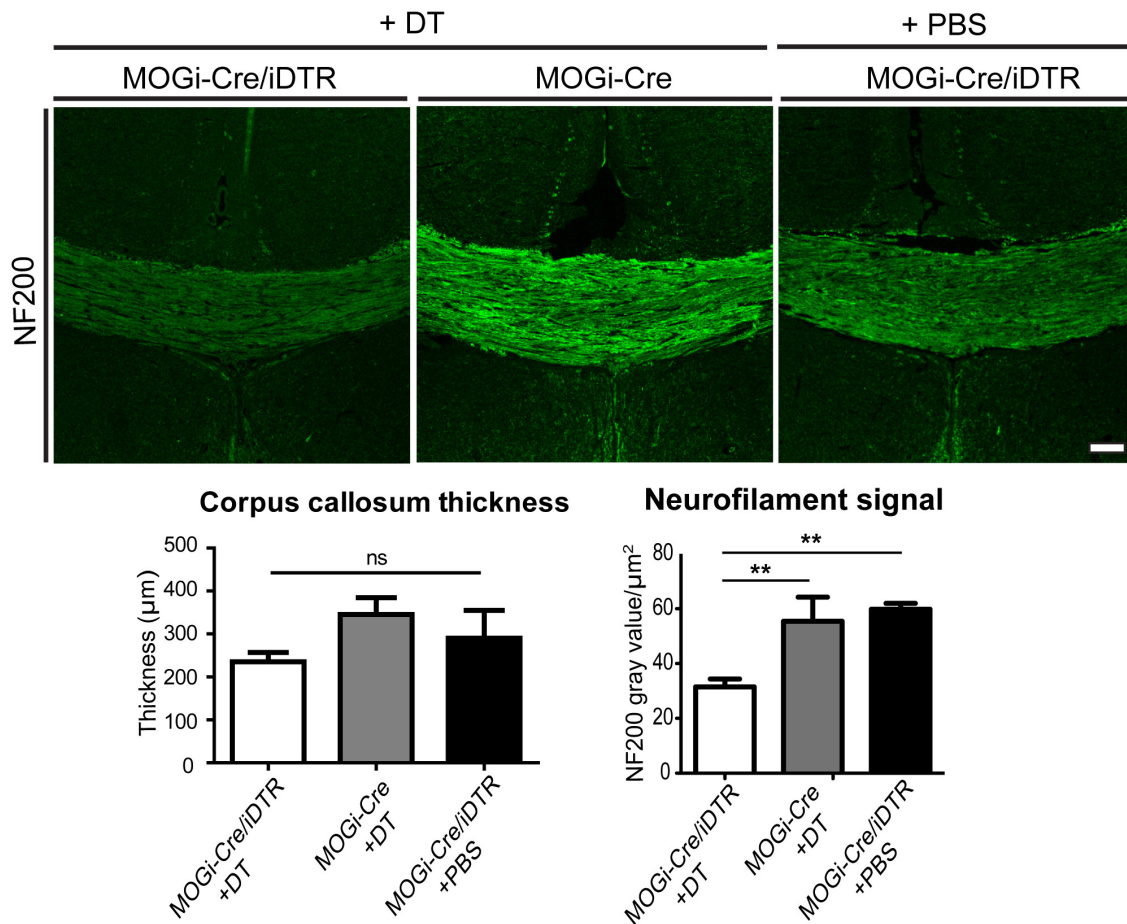
Figure 3.6: **Reduction in neurofilament signal density in DT-induced demyelination.** A decrease of neurofilament signal density (NF200),was observed in MOGi-Cre/iDTR mice treated with DT (left panel), compared to DT-treated MOGi-Cre animals as control (middle panel) and MOGi-Cre/iDTR animals treated with PBS (right panel). Quantifications are shown as mean and SEM (n=3-10). One way ANOVA was performed, followed by pairwise Tukey test. Significance is represented with asterisks ($**p{<}0.01$, $***p{<}0.001$). Scale bar, 100 μm. ns: non-significant.
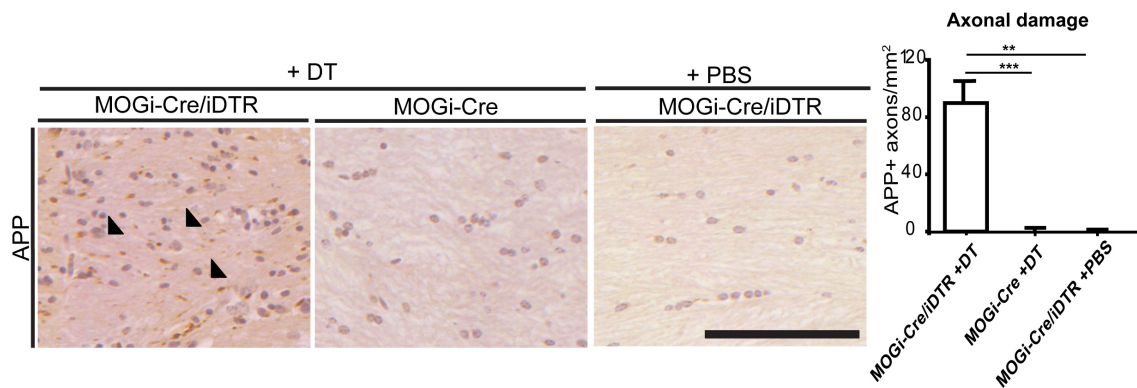
Figure 3.7: **Axonal damage as a consequence of Diphtheria toxin treatment in MOGi-Cre/iDTR mice.** An increase in axonal damage (evidenced by APP accumulation) was observed in MOGi-Cre/iDTR mice treated with DT (left panel), compared to DT-treated MOGi-Cre animals as control (middle panel) and MOGi-Cre/iDTR animals treated with PBS (right panel). Quantifications are shown as mean and SEM (n=3-10). One way ANOVA was performed, followed by pairwise Tukey test. Significance is represented with asterisks (∗∗p<0.01, ∗∗∗p<0.001). Scale bar, 100 μm.
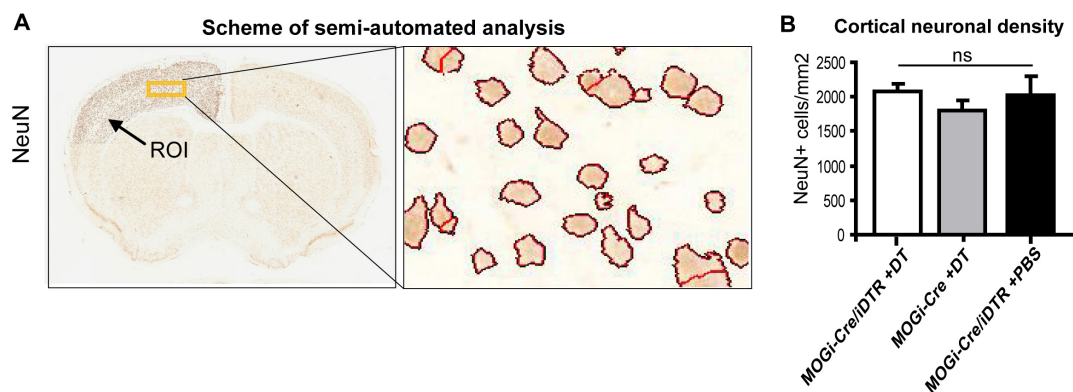
Figure 3.8: **Oligodendrocyte depletion with DT does not affect cortical neuronal density.** Coronal sections were stained for neuronal nuclei with NeuN antibodies, scanned with Mirax Midi System and automatically counted using Definiens Developer XD software in the indicated region of interest (ROI). One way ANOVA was performed, no statistically significant difference in neuronal density was observed between the groups. Also, no significant difference was found in cortical volume between the groups (p>0.05). An average of 10104 NeuN+ were counted per animal. Quantifications represent mean and SEM (n= 8 MOGi-Cre/iDTR mice treated with DT, 5 DT-treated MOGi-Cre animals as control (middle panel) and 3 MOGi-Cre/iDTR animals treated with PBS, ns: not significant).
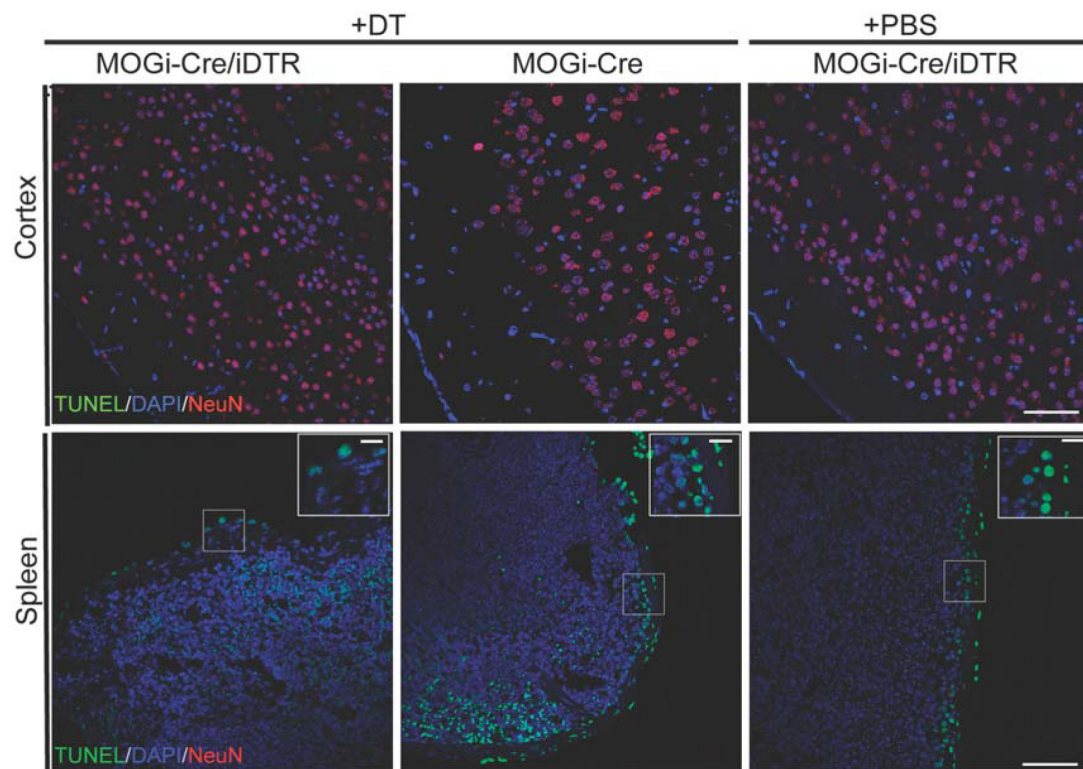
Figure 3.9: **No neuronal apoptosis observed after DT-induced oligodendrocyte ablation.** Coronal sections of cortex from MOGi-Cre/iDTR mice treated with DT (left panel), DT-treated MOGi-Cre animals as control (middle panel) and MOGi- Cre/iDTR animals treated with PBS (right panel) were stained for TUNEL and NeuN 30 days after injection. Sections of the spleen of the respective groups were used as positive control for the TUNEL stainings. Colocalisation of DAPI and TUNEL-positive cells is shown as an inset for each group. Scale bar: 50μm, for inset 10 μm.

3.2   Late motor decline after accomplished remyelination in murine cuprizone model

3.2.1   Long-term analysis of cuprizone-induced de- and remyelination

We used the toxin cuprizone to study the long-term effect of demyelination on axonal preservation and motor functional recovery. Feeding mice with 0.2-0.3% cuprizone (Sigma-Aldrich) for 5-6 weeks results in massive demyelination of white matter tracts in the brain, mainly the corpus callosum. Removing cuprizone from the diet for more than 3 weeks results in extensive remyelination. To observe the difference in the effect of a single or repeated demyelinating events, we submitted a group of male mice for 2 cycles of 5 weeks of 0.25% cuprizone, allowing 4 weeks of recovery in between (named "DD" or "double demyelination" group). In addition, another group of age- and sex-matched mice (named "SD" or "single demyelination" group) were submitted to a single demyelinating event by feeding them with cuprizone for 5 weeks (simultaneous with the second cycle of cuprizone in the DD group). A control group received normal milled chow. For a scheme of the experimental design, see **Figure** 3.10.
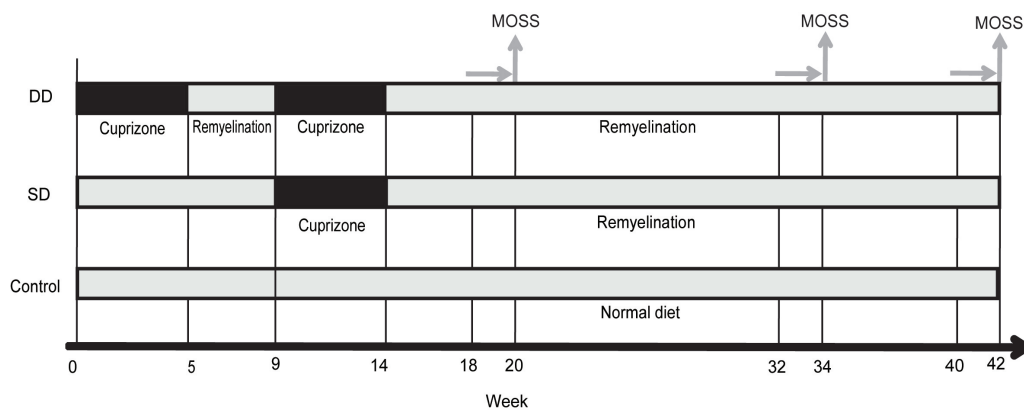
Figure 3.10: Experimental design of cuprizone treatment. 8-week-old mice were fed cuprizone for 5 weeks, were then allowed to recover for 4 weeks and finally received cuprizone for 5 more weeks (double demyelination, or DD). A second group of mice (single demyelination, or SD) were fed cuprizone for 5 weeks simultaneous to the second demyelination of the DD group as indicated. Animals were switched to a normal diet for 28 weeks until the end of the experiment. Age-matched controls were fed with a normal diet throughout the experiment. Motor Skill Sequence analysis (MOSS) was performed at the times indicated. Animals were first habituated to training wheels composed of regularly spaced crossbars for two weeks. Subsequently, running performance on complex wheels was recorded for an additional week.

The effectivity of the demyelinating paradigm using cuprizone was evaluated by staining coronal sections with Luxol Fast Blue - Periodic Acid Schiff (LFB-PAS) staining and assessing myelination level with a scale ranging from 0 (no demyelination) to 3 (complete demyelination). We confirmed that demyelination occurred after each cuprizone treatment, and extensive remyelination was observed 28 weeks after the cuprizone was removed from the diet. As expected, the control group, which received normal milled chow, presented no demyelination (**Figure** 3.11).
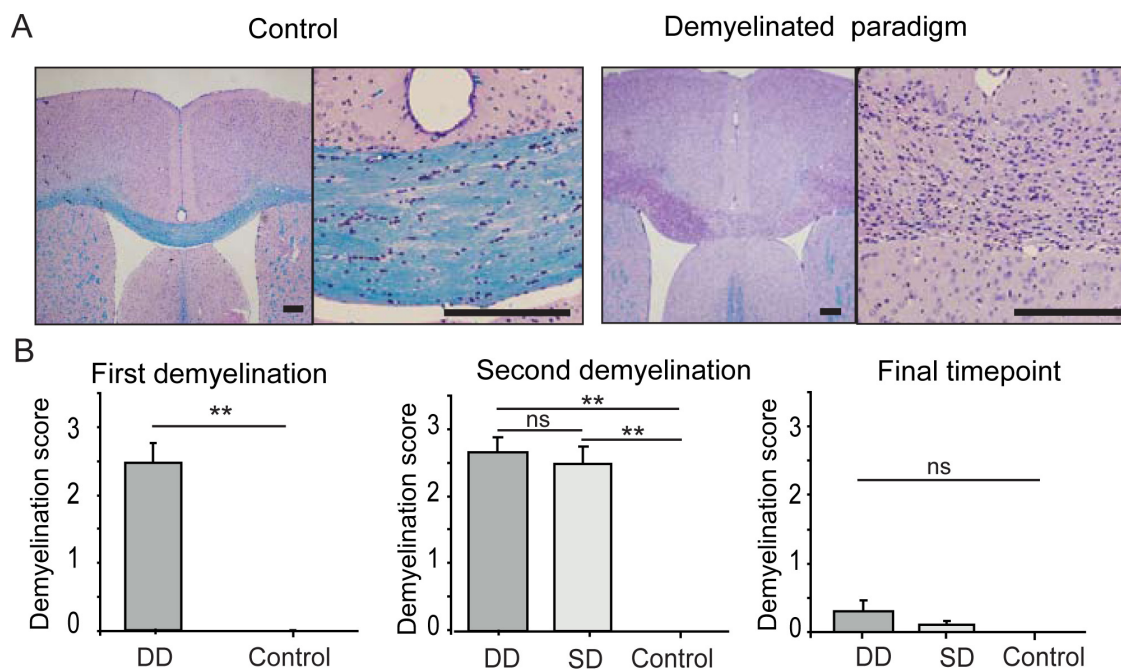
Figure 3.11: **Cuprizone-induced demyelination and remyelination.** (A) Representative LFB/PAS-stained corpus callosum of untreated control (left) and after 5 weeks of cuprizone treatment (right). Extensive callosal demyelination is evident in the right panel. Scale bar: 200 μm. (B) Semi-quantitative analysis of callosal demyelination (n=3-9 animals per group) and compared to age-matched control (n=2-6). A score of 3 corresponds to maximal demyelination, a score of 0 represents no detectable demyelination. For the first demyelination (left), a *t*-test was applied. For second demyelination (center) and final time point (right), if ANOVA indicated significant differences in the main effect ($p<0.05$), Tukey test pair-wise comparison was applied. $**p <0.01$. Data shown as mean + SEM. DD: Double demyelination, SD: Single demyelination. First demyelination: week 5, second demyelination: week 14, final time point: week 42 (see also Fig. 1a).

3.2.2   Late motor decline after accomplished remyelination

To understand whether demyelination can have long-term consequences on the function of the affected axons despite remyelination, we used a motor skills test called Motor Skill Sequence (MOSS). It has been shown that MOSS is useful in assessing behavioral outcome as an indication of the changes in the functional state of the corpus callosum (Schalomon and Wahlsten, 2002; Liebetanz and Merkler, 2006). In this test, mice are allowed to voluntarily run in "complex" wheels with irregularly spaced crossbars following a 2-week training period in regular wheels in individual cages. Since the animals need to constantly adapt the step length in the complex wheels, this movement requires a bi-hemispherical coordination that involves the corpus callosum, as it is the largest white matter tract connecting both cortical hemispheres. The time, velocity and running events are recorded automatically 24 hours a day during seven days. The number of runs, time spent running and accumulated distance are considered to reflect the animal's motivation and fitness, whereas the maximum velocity (Vmax) and maximum distance (Dmax) accomplished during a running bout reflect the highest performance in bi-hemispherical motor coordination.

We assessed the running performance of the mice on three occasions during recovery: 6 weeks, 20 weeks and 28 weeks after cuprizone was removed from the diet (see **Figure** 3.10). At the first time point of MOSS analysis (6 weeks after cuprizone removal), the maximal velocity and maximal accumulated distance in one run were reduced in treated animals compared to controls (**Figure** 3.12, left panel). This confirms previous findings that showed reduced maximal coordination capacity after 6 weeks of recovery in the cuprizone model, measured by MOSS (Liebetanz and Merkler, 2006). No differences were observed between the SD and the DD groups. At 20 weeks of recovery, there was no significant difference in any of the parameters measured by MOSS between the treated and control animals (**Figure** 3.12, central panel). This may indicate that extended remyelination or compensation mechanisms through cortical plasticity contribute to a functional recovery after cuprizone treatment. Strikingly, in the final time point of MOSS evaluation, 28 weeks after recovery, animals treated with cuprizone once again exhibited a decreased performance in the Vmax and Dmax measurements (**Figure** 3.12, right panel). No difference was detected between the SD and DD groups. This indicates that, regardless of the number of demyelinating events, in the long-term cuprizone treated animals entered a phase of motor decline, revealing latent functional deficits as a consequence of oligodendrocyte death and myelin loss.
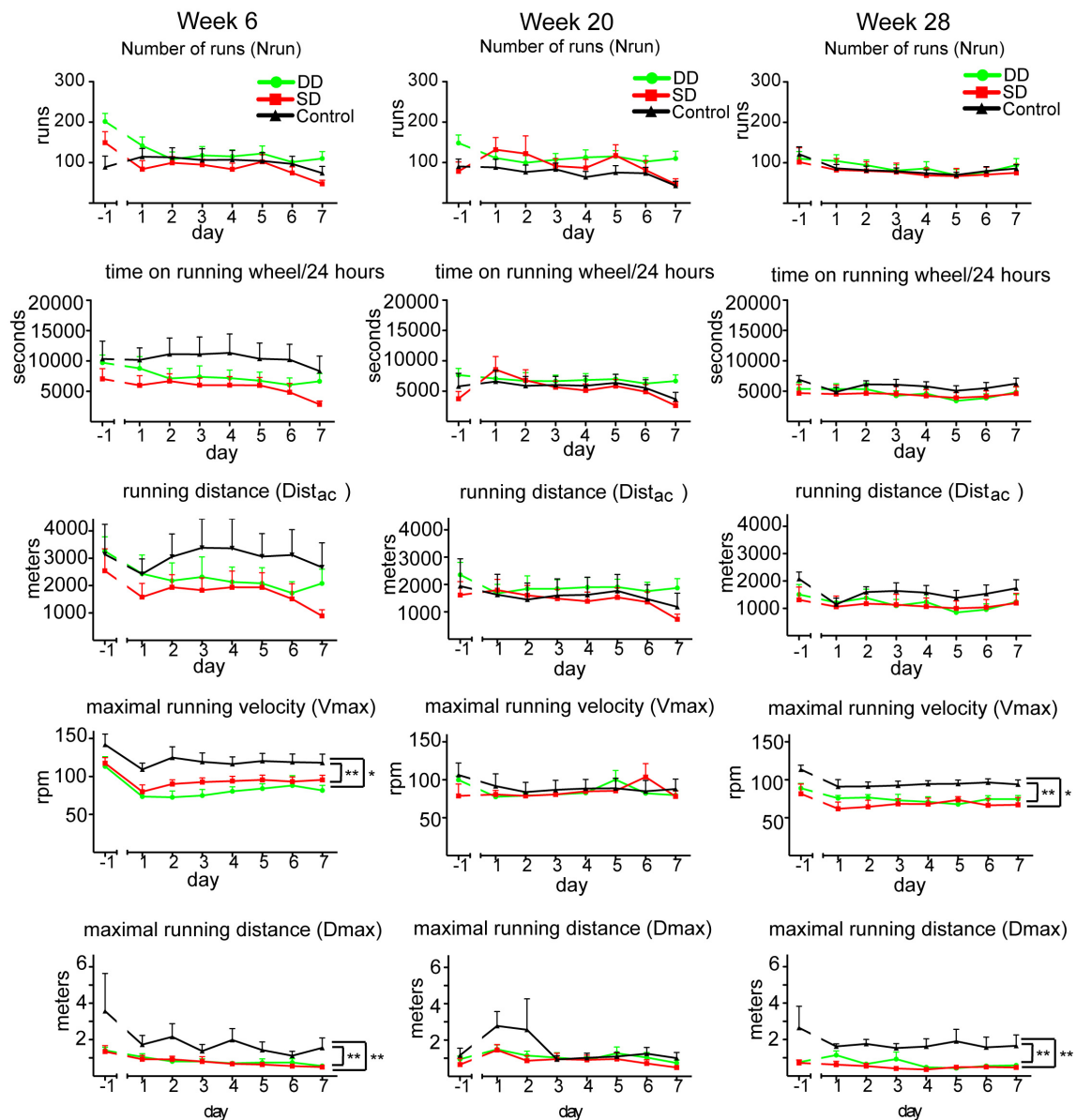
Figure 3.12: **Late-onset latent motor deficits as measured by wheel running performance after remyelination.** Animals received one (shown in red) and two (shown in green) cycles of cuprizone to induce demyelination and were allowed to recover for 28 weeks during which MOSS performance was compared to age- and sex-matched controls (shown in black). Recording was preceded by a two-week training session (day -1: performance of last day on training wheels, for details see material and methods). Complex wheel performance (day 1 to 7) is shown as follows: 6 weeks (left panels), 20 weeks (central panels) and 28 weeks (right panels) after cuprizone withdrawal. Differences between the cuprizone and control group with regard to wheel running performance were calculated by repeated measurements ANOVA. If ANOVA indicated significant differences in the main effect ($p < 0.05$), Fisher's LSD post-hoc tests were applied. $*p < 0.05$, $**p < 0.01$, rpm: revolutions per minute (n=8-12 animals per group). DD: Double demyelination, SD: Single demyelination. $Dist_{ac}$: distance in meters accumulated in 24 hours; Dmax: maximum distance per run; Nrun, number of individual runs in 24 hours; Vmax: maximum running velocity in revolutions per minute in 24 hours.

3.2.3   Cortical thickness and neuronal preservation after cuprizone treatment

To assess the anatomical and histological aspects of the late-onset motor decline observed in cuprizone-treated animals, we measured the cortical thickness, as atrophy could be related to the functional impairment observed in this study. We measured three regions, which we defined as medial, paramedial and lateral (**Figure** 3.13). We only observed a significant difference in the paramedial thickness, which could be induced by the conspicuous ventricular enlargement observed in the treated animals rather than structural atrophy of the cortex.
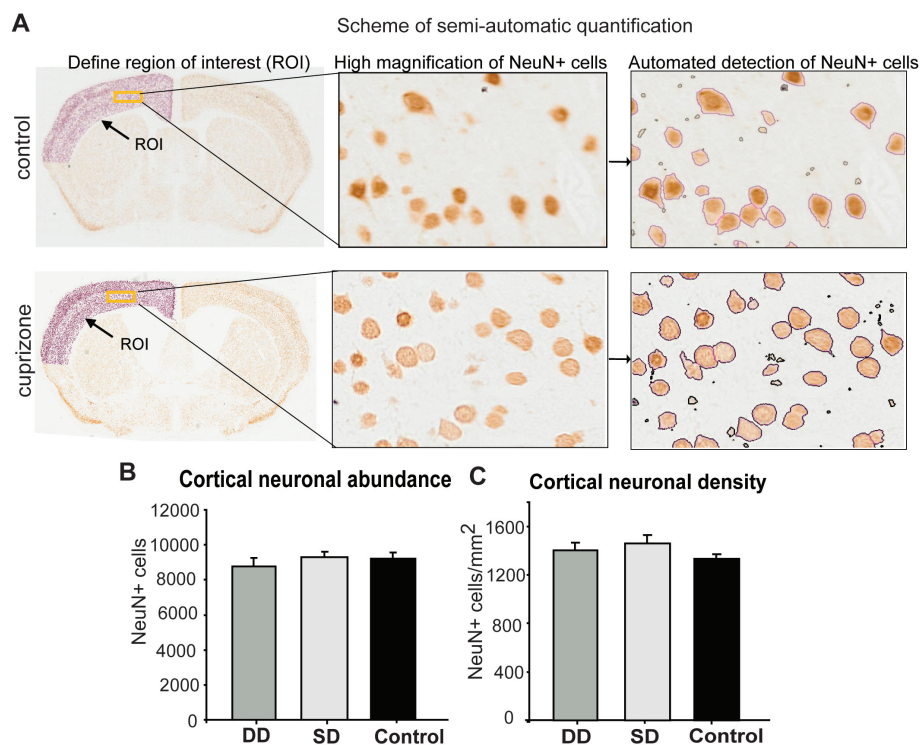
Figure 3.13: **NeuN-positive neuronal cell bodies within the cerebral cortex are not lost following 28 weeks after stopping cuprizone treatment.** (A) Sections were stained for neuronal nuclei with NeuN antibodies, scanned and automatically counted using Definiens Developer XD software in the indicated ROI. (B) Number of cortical neurons in treated groups and controls are shown as the mean + SEM. (C) Density of cortical neurons is shown as the mean + SEM.

To confirm whether the cuprizone treatment resulted in a significant neuronal loss, we stained coronal sections with NeuN antibodies to indicate neuronal nuclei. The abun-

dance of neurons in the cortex at a global level within a particular section was calculated semiautomatically using a custom-made software (for further information refer to the methods section). Similar to the DT model, we did not observe any difference in neuronal numbers between the treated samples nor compared to control (**Figure** 3.14).
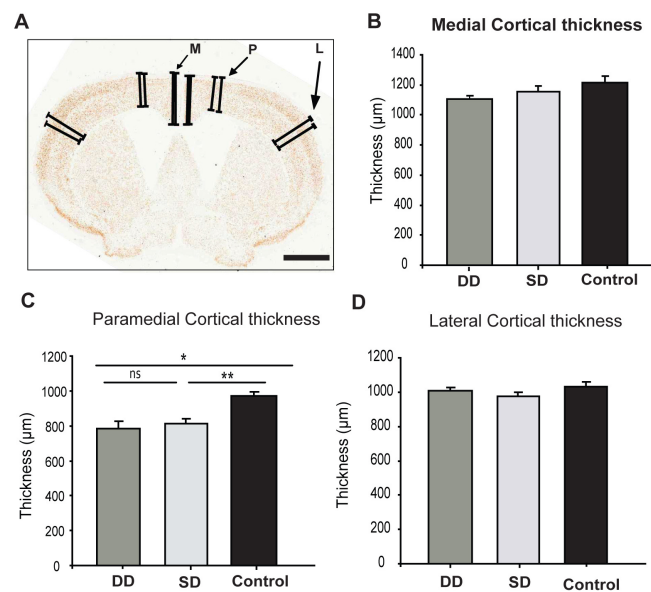
Figure 3.14: **Cortical thickness is largely unchanged after cuprizone treatment.** (A) Scheme showing the different regions where cortical thickness was determined, defined as medial (M), paramedial (P) and lateral (L). Cortical thickness was measured in the medial (B), in the paramedial (C) and the lateral region (D). Scale bar: 1mm (n =5-9, error bars represent SEM. Statistically significant differences are indicated by asterisks. If ANOVA indicated significant differences in the main effect (p <0.05), Tukey test pairwise comparison was applied. ns: not significant, ∗p <0.05, ∗∗ p <0.01. ANOVA: analysis of variance; DD: double demyelinated group, ROI: region of interest; SD: single demyelinated group; SEM: standard error of the mean.

3.2.4 Ultrastructural evaluation after cuprizone treatment

We used electron microscopy to evaluate the ultrastructural consequences of cuprizone treatment and remyelination efficiency 28 weeks after cuprizone removal. This allows for the analysis of myelin at a single-axon level and a more quantitative assessment of remyelination efficiency (see **Figure** 3.15).

6 wks remyelination   28 wks remyelination (DD) 28 wks remyelination (SD)   Control
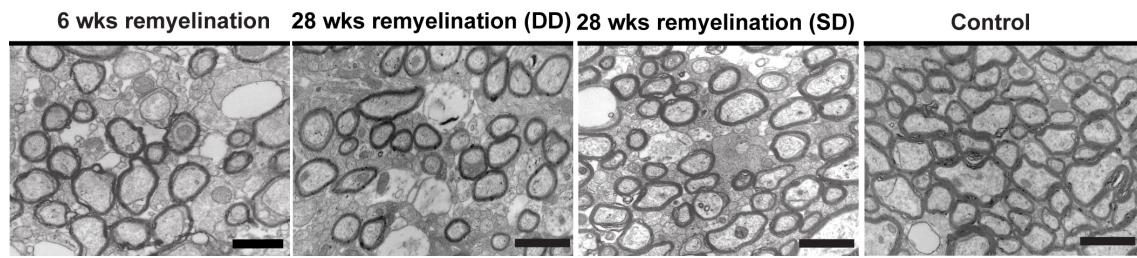
Figure 3.15: **Overview of remyelination after cuprizone treatment.** Electron microscopy of the corpus callosum after 6 weeks of remyelination, as well as after 28 weeks of recovery for double demyelinated (DD), single demyelinated (SD) and control animals are shown. Scale bar = 1 μm

We quantified the percentage of myelinated axons after 6 weeks of remyelination, 28 weeks after remyelination in the SD and DD group, as well as in the control (see **Figure** 3.16, panel A). We defined a threshold of myelin sheath thickness of 15 nm in order to consider an axon to be myelinated (considering that the axonal membrane thickness is of approximately 5-10 nm). In addition, as axons below 200 nm tend to be unmyelinated in the CNS, we set up a conservative threshold and only considered axons that had a diameter larger than 350 nm. We observed an increase in the fraction of unmyelinated axons after 6 weeks of remyelination (23.3% $\pm$ 2.5), as well as the DD group after 28 weeks of recovery (26% $\pm$ 8.7), compared to control (5.9% $\pm$ 1.2). After 28 weeks of recovery, the SD group also presented a tendency of increase in the fraction of unmyelinated axons, but did not reach statistical significance (20% $\pm$ 8.4, p=0.68).

In addition, we measured the g-ratio (axon diameter/ fiber diameter) of axons with a diameter larger than 350 nm, which described the myelin thickness relative to the axonal diameter. The g-ratio tends to increase after remyelination, reflecting how the newly formed myelin tends to be thinner than the original. Indeed, we observed an increase of the g-ratio after remyelination (ANOVA p <0.05, 6 weeks: 0.80 $\pm$ 0.008, DD: 0.8$\pm$ 0.012, SD: 0.77 $\pm$ 0.018, control: 0.73$\pm$0.010). The g-ratio increase was statistically significant in remyelinated animals after 6 weeks of recovery and after 28 weeks of recovery (DD group), compared to control. There was a trend towards an increased g-ratio in the SD group as well, but it did not reach statistical significance (p=0.12). There was no statistical significance between the cuprizone-treated groups.
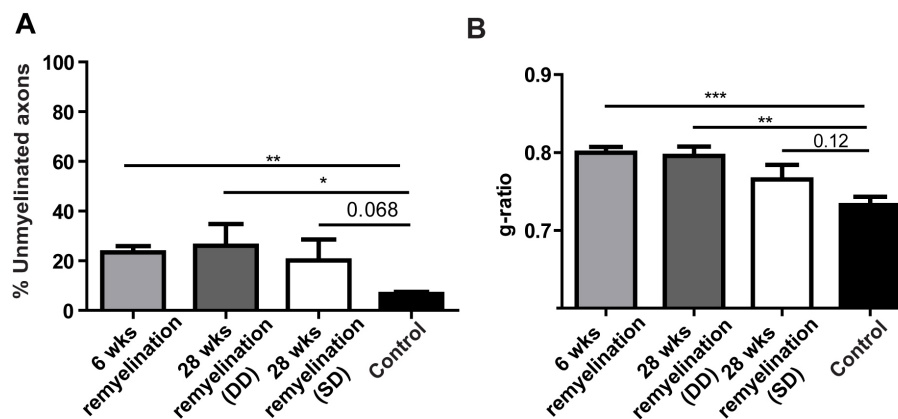
Figure 3.16: **Ultrastructural analysis of long-term effects of cuprizone-induced demyelination of myelin in corpus callosum.** (A) Percentage of non-myelinated fibers as compared to controls (mean + SEM) (B) Axonal diameter to the fiber diameter (g-ratio) in treated groups and controls is shown as the mean + SEM. If ANOVA indicated significant differences in the main effect ($p<0.05$), Tukey test pair-wise comparison was applied ($*p<0.05$, $**p <0.01$, $***p <0.001$) DD: double demyelinated; SD: single demyelinated; SEM: standard error of the mean.

Although cuprizone-treated animals tended to present thinner myelin sheaths (as seen by the displacement of the g-ratios distribution towards higher values), there was a prominent increase in the population of fibers with a g-ratio of approximately 1 in the treated groups compared to control, corresponding to unmyelinated or hypomyelinated axons (see **Figure 3.17**).

3.2.5   Corpus callosum atrophy and axonal loss

We studied the integrity of the corpus callosum at 28 weeks of recovery. First, we stained coronal sections with heavy-molecular weight neurofilament antibodies (NF200) and measured the thickness of the corpus callosum around the midline. In addition to a significantly decreased thickness of the corpus callosum in the treated groups, a reduction of the neurofilament signal intensity was evident (**Figure** 3.18).
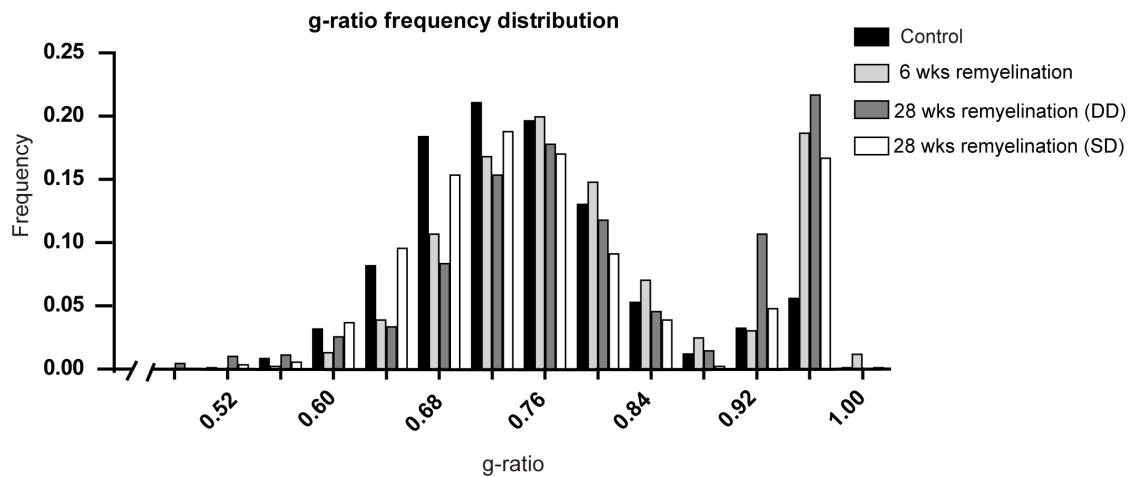
Figure 3.17: G-ratio distribution shows incomplete remyelination. Distribution of g-ratios in the corpus callosum after cuprizone-induced demyelination is shown for treated and control groups. n=3-11 animals per group, >300 axons, >350 nm in diameter per animal.
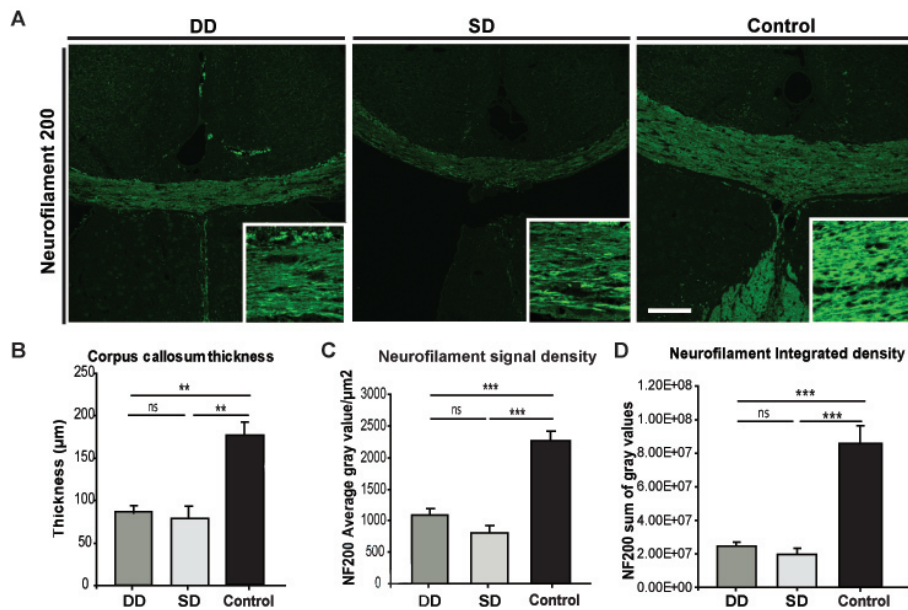
Figure 3.18: Effect of demyelination on corpus callosum integrity. Cuprizone-induced demyelination results in a decrease in neurofilament signal and corpus callosum atrophy, as seen 28 weeks after cuprizone treatment removal. (A) Representative images (overview: 100x, insets: 400x magnification) of coronal sections stained for neurofilament 200 (NF200) from double demyelinated (DD), single demyelinated (SD) and control animals are shown. Insets show high magnification of NF200-stained corpus callosum. (B) Quantitative analysis of corpus callosum thickness as determined MBP staining and image analysis. Mean (C) and integrated (D) density of NF200 signal in the corpus callosum of the different groups is shown as the mean ± SEM (n=5–9). Statistically significant differences are indicated by asterisks. If ANOVA indicated significant differences in the main effect (p<0.05), Tukey test pair-wise comparison was applied (∗∗p <0.01, ∗∗∗p <0.001). Scale bar = 100μm.

We then calculated the number of axons crossing the corpus callosum at the midline. For this, we used sagital sections, where myelin was stained with the Bielchowski method, and axons were stained using pan-Neurofilament antibodies (**Figure** 3.19). The number of axons per area were determined by densitometry, and the total axons were calculated by multiplying the axonal density by the corpus callosum thickness. As expected, axonal numbers in remyelinated animals after 6 weeks of recovery were decreased compared to control. Interestingly, the axonal abundance was further decreased after 28 weeks of recovery, compared to the 6 weeks recovery time point.
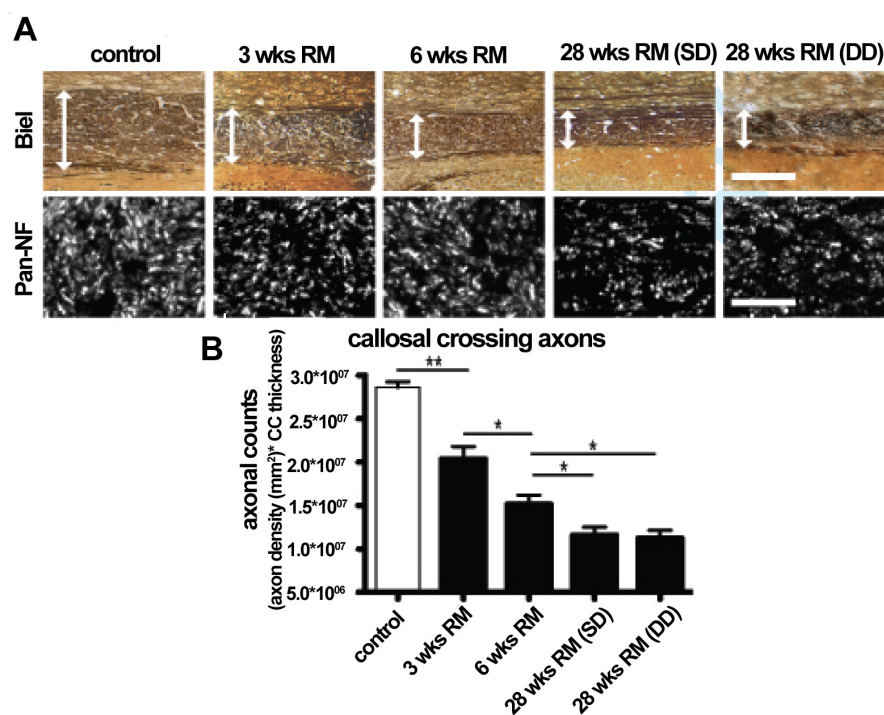
Figure 3.19: **Extensive axonal loss in cuprizone-induced demyelination.** (A) Upper panel: The thickness of the corpus callosum (CC) was determined on sections stained by Bielschowsky's silver impregnation (Biel, extent of CC indicated by double arrows). Lower panel: Axonal densities were determined on confocal images of pan-neurofilament (PAN-NF)-stained adjacent sections within CC. (B) Callosal axonal numbers were calculated by multiplying axonal densities (expressed as axons per mm^2) by the thickness CC of a given animal. Bars represent mean + SEM. Statistically significant differences are indicated by asterisks. If ANOVA indicated significant differences in the main effect ($p < 0.05$), Tukey test pair-wise comparison was applied (*$p < 0.05$, **$p < 0.01$). RM= Remyelination; wks= weeks; ns= not significant). Scale bar upper row in A = 120 μm, lower row = 25 μm. The quantifications were performed by Tanja Jürgens, Medical University Geneva, Switzerland.

Furthermore, we observed enlarged mitochondria in axons, supporting the idea of ongoing axonal pathology ~ 6 months after cuprizone had been removed from the diet (see **Figure 3.20**).
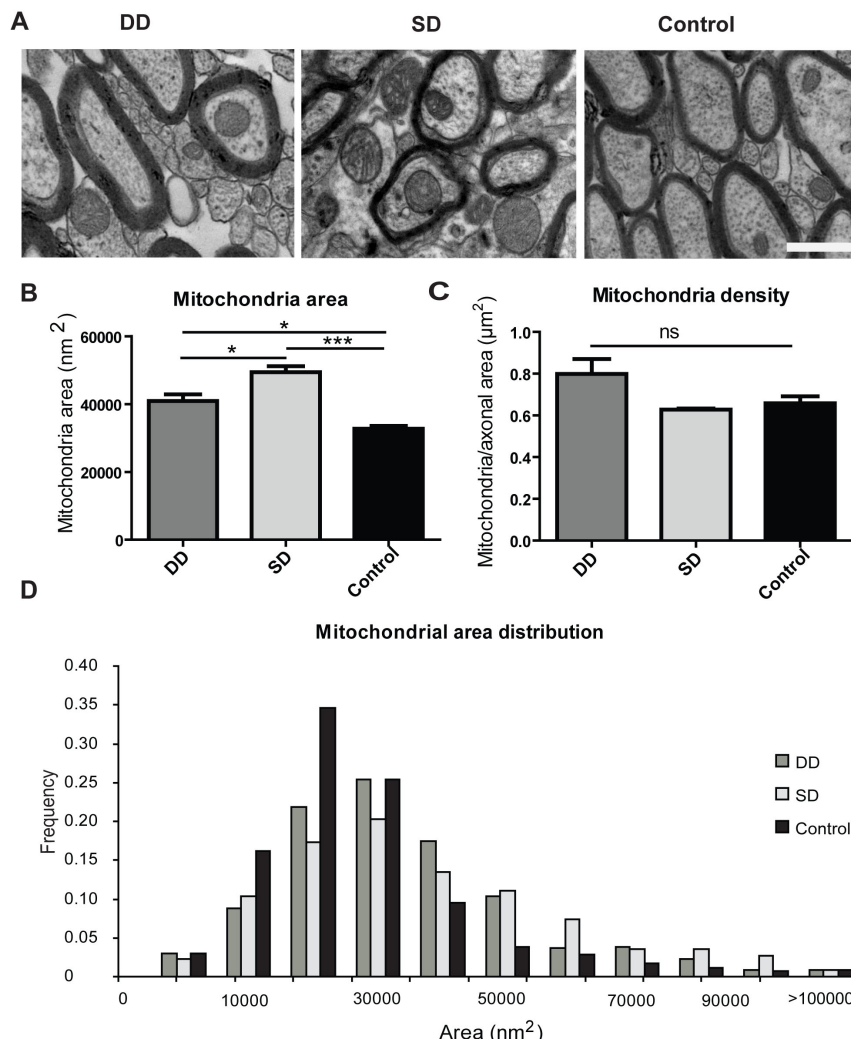
Figure 3.20: **Mitochondrial size and density in remyelinated axons.** Mitochondrial transverse area and frequency was quantified with electron microscopy. (A) Sample image of mitochondria in micrograph. Scale bar: 250 nm. (B) Mitochondrial area was measured for treated (DM and SM) and control groups. (C) The mitochondrial density was defined as the number of mitochondria found per axonal area (mitochondria/axonal μm^2). An area of 681.4 μm^2 was analysed per animal. n=3 animals per group, error bars represent standard error of the mean (SEM). (If ANOVA indicated significant differences in the main effect (p<0.05), Tukey test pairwise comparison was applied $*p < 0.05$, $***p < 0.001$, ns: not significant).

3.2.6 Long-term axonal damage in cuprizone-treated mice

Previous studies have shown that cuprizone treatment results in axonal damage, as determined by the accumulation of the acute axonal injury marker APP within axons (Irvine and Blakemore, 2008). APP accumulation is regarded as a transient and reversible feature. and is regarded as a transient feature. After 6 months of normal diet following cuprizone treatment, APP-positive axons were still detectable in the corpus callosum of mice, albeit at a low level (see **Figure** 3.21). Therefore, we found evidence for ongoing axonal degeneration long after the demyelinating trigger had been removed.
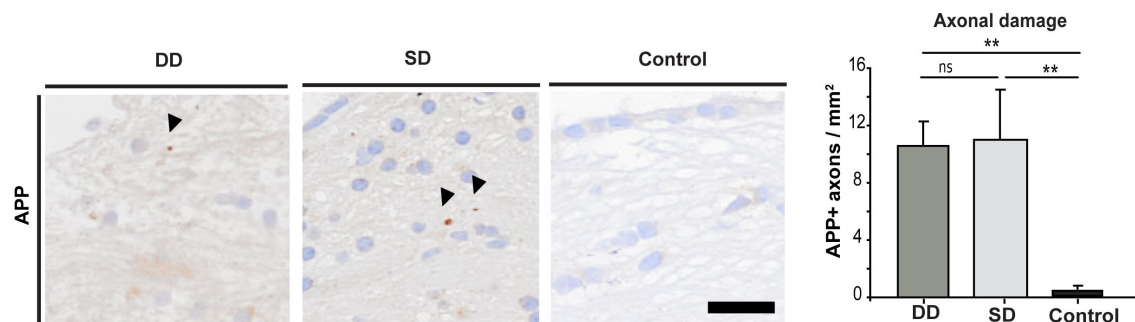
Figure 3.21: **APP-positive axons can be detected in chronic remyelinated lesions.** Coronal sections were analyzed in the medial part of the corpus callosum by immunohistochemistry with an antibody against amyloid precursor protein (APP). Arrowheads indicate examples of APP-positive structures. Scale bar: 20 μm. Quantification of APP-positive axons in central corpus callosum is shown as mean $\pm$ SEM (n=5–9). Statistically significant differences are indicated by asterisks; if ANOVA indicated significant differences in the main effect (p<0.05), Tukey test pair-wise comparison was applied ($\ast\ast$ p <0.01, ns: not significant).

Since remyelination is considered to protect axons from degeneration (Irvine and Blakemore, 2008), we quantified the proportion of damaged (APP+) axons that were unmyelinated in cuprizone-treated animals 28 weeks after cuprizone removal, when remyelination would be expected to be accomplished. Interestigly, we observed that a fraction of the APP+ axons (within a 1 μm-thick sagittal section) were surrounded by an MBP+ myelin sheath (19% for DD and 27% for SD; see **Figure** 3.22).

3.2.7 Axonal damage in MS chronic lesions

To compare our models to what occurs in MS, we also evaluated the proportion of unmyelinated versus myelinated APP+ axons in remyelinated lessions in 6 lesions within 4 different MS patients with documented progressive MS (average disease duration 17.2 $\pm$
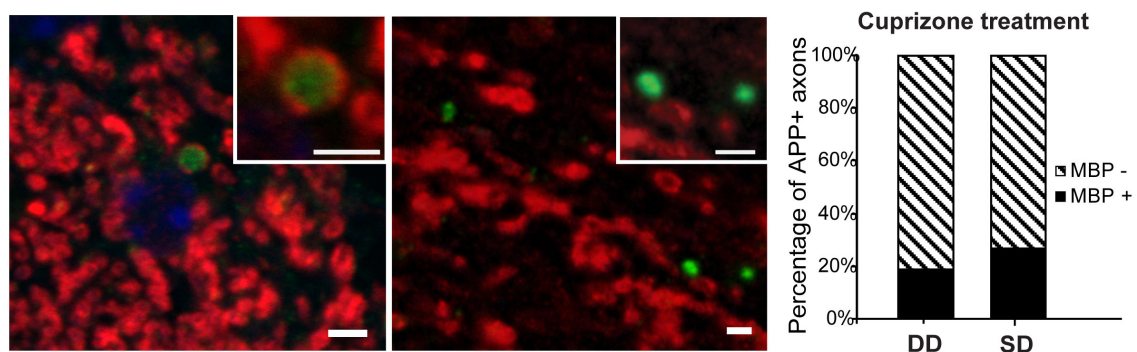
Figure 3.22: **Myelin ensheathment of APP-positive axons.** Sections were stained by immuno-histochemistry with antibodies against APP (green) and MBP (red). Left image shows an example of an MBP-positive ring surrounding an APP-positive axon. Right image displays an example of an APP-positive axon lacking MBP. Scale bar: 2 μm. (D) Quantification of the percentage of myelinated and unmyelinated APP-positive axons in central corpus callosum of cuprizone-treated groups, n=5–9 per group. DD: double demyelination group, SD: single demyelination.

4.7 years). We found that around 14% of APP+ axons were surrounded by an MBP+ myelin sheath, similar to what we observed in our cuprizone-treated animals (see **Figure 3.23**).
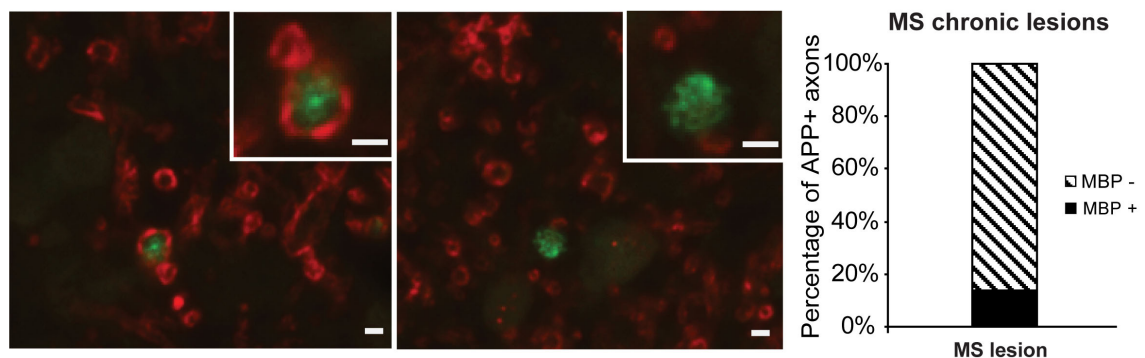
Figure 3.23: **APP-positive axons can be detected in chronic remyelinated lesions in MS.** MS autopsy lesions showing extensive remyelination and with known long clinical history of progressive MS (average disease duration 17.2±4.7 years) were stained by immunohistochemistry with antibodies against APP (green) and MBP (red). Left image shows an example of an MBP-positive ring surrounding an APP-positive axon. Right image displays an example of an APP-positive axon lacking MBP. Scale bar: 2 μm (F) Quantification of the percentage of myelinated and unmyelinated APP-positive axons in lesions of progressive MS patients, n=5 MS cases. Quantifications performed by Doron Merkler, Geneva University Hospital, Switzerland).

3.2.8 Astrogliosis and microglia activation ∼ 6 months after cuprizone treatment

To understand associated cellular responses in the context of ongoing axonal damage and functional deficits 28 weeks after cuprizone removal, we carried out different histological analysis to assess the other glial populations in the corpus callosum. Astrogliosis was still evident at this final time point in treated animals compared to control (**Figure** 3.25). In addition, macrophage/microglia activation was still relatively elevated in cuprizone-treated groups (**Figure** 3.24). Once more, we did not detect any differences between the SD and DD groups.
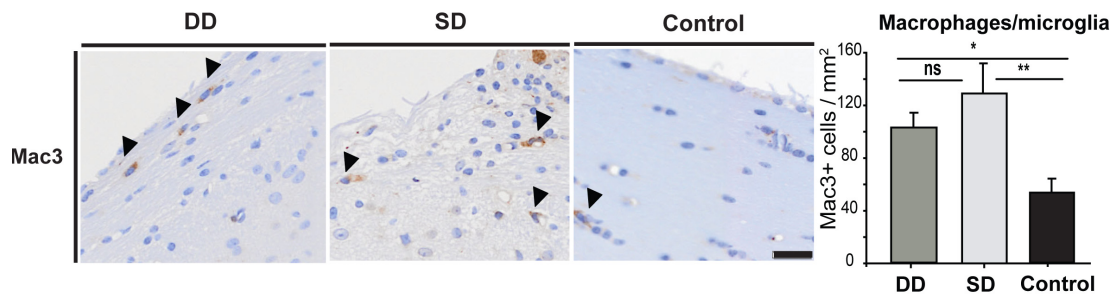
Figure 3.24: Microglia activation ∼ 6 months after cuprizone-induced demyelination. (A) Coronal sections from double demyelinated (DD), single demyelinated (SD) and control animals were analyzed in the medial part of the corpus callosum and stained for microglia/macrophages (Mac3). Arrowheads indicate examples of positively stained cells. (B) Quantification of microglia/macrophage density in central corpus callosum is shown as mean + SEM (n=5–9). Statistically significant differences are indicated by asterisks (If ANOVA indicated significant differences in the main effect (p<0.05), Tukey test pair-wise comparison was applied, ∗p <0.05, ∗∗p <0.01, ns: not significant). Scale bar: 20 μm.

Microglia help in the clearance of myelin and cell debris that arise as a consequence of demyelination, but can also secrete pro-inflammatory molecules that can have a cytotoxic effect both in oligodendrocytes and axons. Indeed, it is thought that in MS the levels of axonal damage are somewhat correlated to microglia activation levels. We observed an apparently similar trend in microglia activation and axonal damage through the duration of the experiment (**Figure** 3.26). As to whether an increase in these populations is either a cause or a consequence of degenerative processes is still under debate. Therefore, it should be carefully interpreted in the context of the prolonged axonal damage described in this study.
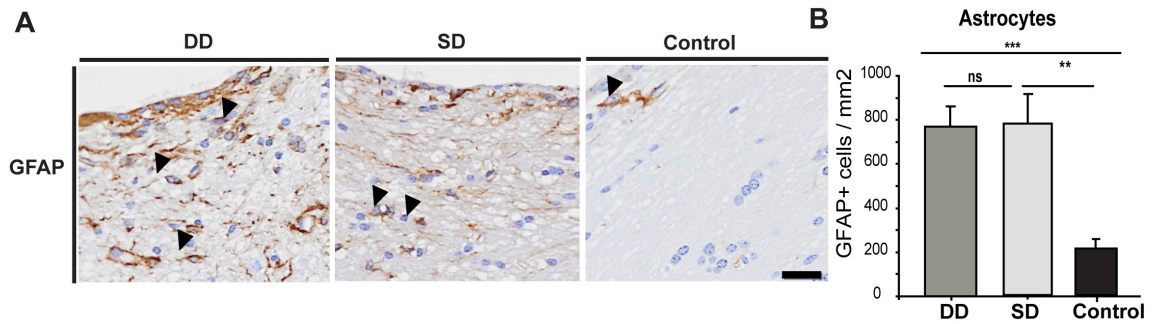
Figure 3.25: **Astrocytosis ∼ 6 months after cuprizone-induced demyelination.** (A) Coronal sections from double demyelinated (DD), single demyelinated (SD) and control animals were analyzed in the medial part of the corpus callosum and stained for astrocytes (GFAP). Arrow heads indicate examples of positively stained cells. (B) Quantification of astrocyte (GFAP) density in central corpus callosum is shown as mean + SEM (n=5–9). Statistically significant differences are indicated by asterisks (If ANOVA indicated significant differences in the main effect (p<0.05), Tukey test pair-wise comparison was applied, ∗∗p <0.01, ∗∗∗p <0.001, ns: not significant). Scale bar: 20 μm.
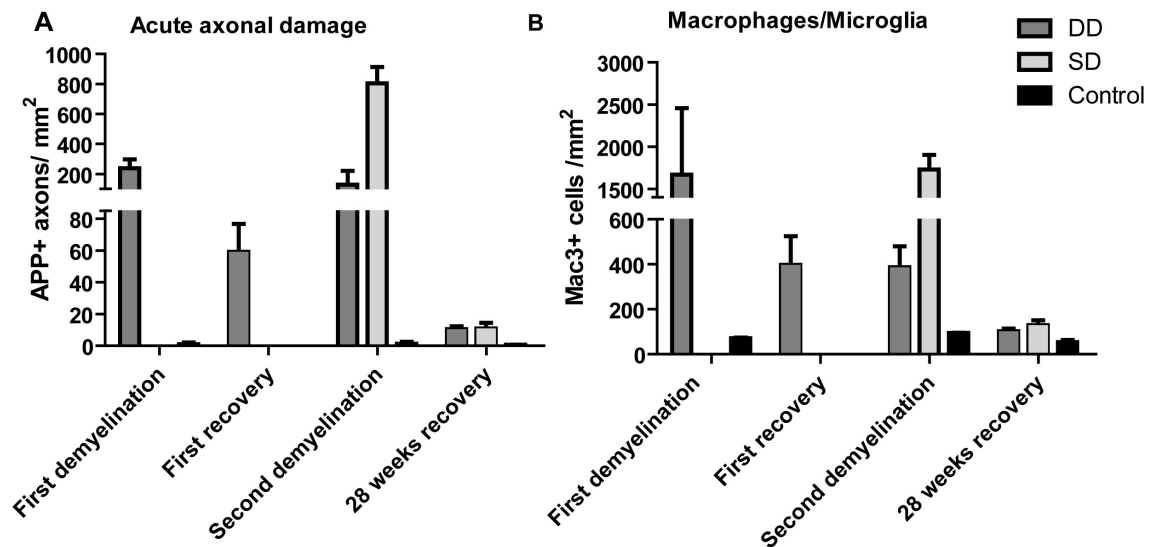
Figure 3.26: **Longitudinal APP accumulation and microglia activation after cuprizone.** Immunohistochemistry for APP as a marker of axonal damage (A) and Mac3 as a marker of macrophages and activated microglia (B) during cuprizone treatment and recovery. Coronal sections were analysed in the medial part of the corpus callosum.

It is believed that the cuprizone model preserves the integrity of the blood-brain barrier. However, to assess if demyelination can trigger by itself an infiltration of immune cells

into the CNS, we searched for the presence of T cells staining with CD3 antibodies in the brain. As in the DT model, we did not observe any conspicuous T cell infiltration in the treated groups compared to control (data not shown).

In summary, our findings indicate that late-onset locomotor dysfunction can be observed long after cuprizone-induced de- and remyelination. This is accompanied by a reduction of callosal axons and a low level of still ongoing axonal degeneration.

3.3   Protein screening for candidates involved in myelination

Proteins localized at contact sites between axons and myelin have been found to be important in the formation and stability of myelin and axonal survival. These sites are usually enriched with adhesion molecules involved in axo-glial communication and molecular organization of the axonal and myelin membranes. Some of these proteins have been identified and are well characterized, such as Neurofascin 155 in oligodendrocytes and the Contactin/Caspr complex at the axonal membrane (Peles and Salzer, 2000). To explore at a cellular level the interaction between oligodendroglia and axons, we isolated fractions of myelin enriched in glycoproteins, as well as periaxonal, and paranodal/juxtaparanodal regions, which are in close apposition to the axolemma.

3.3.1   Myelin fractions isolation and purification

Based on its specific density, myelin can be isolated by subjecting it to centrifugation in a discontinuous sucrose gradient (Matthieu et al., 1973). The majority of the myelin fraction can be collected at the interphase between 0.32 and 0.85 M of sucrose solution (Norton and Poduslo, 1973), and most of it is composed by compact myelin, of which MBP and PLP are the major proteins. In this fraction, an enrichment of myelin proteins can be observed compared to brain homogenate (**Figure** 3.27, panel A). However, the regions in direct contact with the axons (paranodes, juxtaparanodes and periaxonal area) are composed of non-compacted areas with cytoplasm and cytoskeletal components, and therefore tend to float in slightly heavier fractions (**Figure** 3.27, panel B).

As myelin tightly wraps around axons, a close contact between the glial and axonal membrane is created. In these regions, specialized cell adhesion molecules coordinate the formation of the node of Ranvier, paranodes and juxtaparanodes. Many proteins involved in cell-to-cell adhesion and communication contain contain heavily glycosylated extracellular domains, and therefore can be isolated using lectin proteins such as Concanavalin A or Wheat Germ Agglutinin (WGA), which bing strongly to glycosylated motifs in these proteins (**Figure** 3.28).
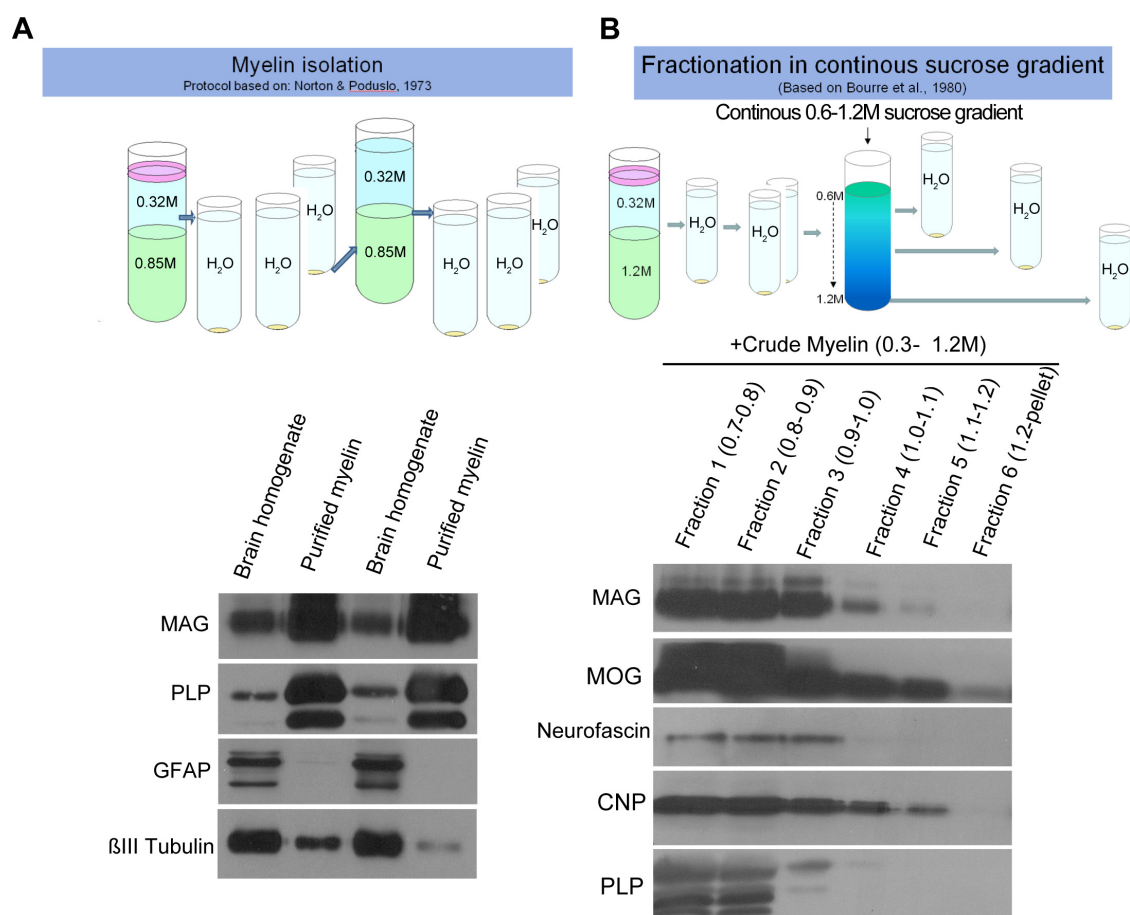
Figure 3.27: **Myelin isolation by sucrose gradient centrifugation.** (A) Myelin is isolated by adding brain homogenate to a discontinuous 0.32 M and 0.85 M sucrose gradient and retrieving the resulting interphase after centrifugation. The recovered material is then diluted in water and centrifuged. The pellet is submitted to two subsequent hyposmotic shocks with water, obtaining "crude myelin". The pellet is resuspended and overlaid on a new gradient, repeating the previous steps to obtain "purified" myelin). The Western blot shows the enrichment of myelin-associated proteins (MAG and PLP) and de-enrichment of astrocyte (GFAP) and neuronal (βIII tubulin) material. (B) Myelin can be fractionated according to the floatability properties of the different domains of myelin, with compacted areas (rich in PLP and MBP) floating at lower densities than non-compact areas (enriched in MAG, CNP and Neurofascin). Briefly, crude myelin can be subjected to a continuous sucrose gradient and centrifuged. The different fractions are retrieved using equal volumes and the components are washed with water and centrifuged to obtain a pellet. MAG: myelin associated glycoprotein, PLP: proteolipid protein, MBP: myelin basic protein, GFAP: glial fibrillary acidic protein, MOG: myelin oligodendrocyte glycoprotein, CNP: 2',3'-Cyclic-nucleotide 3'-phosphodiesterase.
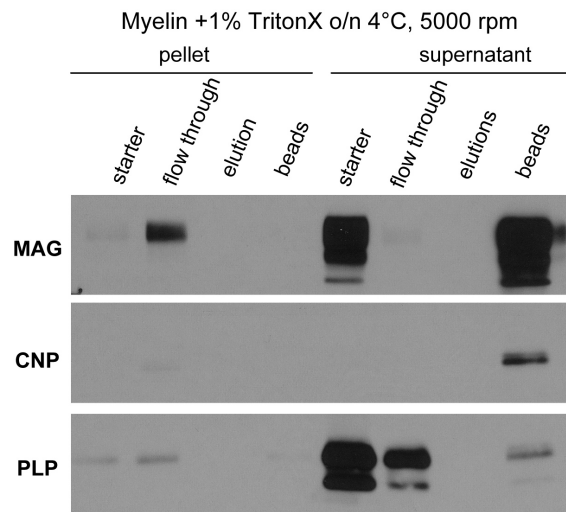
Figure 3.28: **Myelin-associated glycoprotein isolation using lectin beads.** Myelin proteins are solubilized with 0.1% Triton and spun down. For comparison, both the insoluble pellet and the supernatant were bound to lectin beads (Glycoprotein Isolation Kit, Concanavalin A, Thermofisher). Enrichment of non-compact proteins (MAG and CNP) can be observed compared to PLP. MAG: myelin associated glycoprotein, PLP: proteolipid protein, CNP: 2',3'-Cyclic-nucleotide 3'-phosphodiesterase.

Taking advantage of the different densities of compact and non-compact myelin, and the glycosylation of cell adhesion molecules associated to it, we used several different approaches to enrich these fractions. We used continuous and discontinuous sucrose centrifugation, WGA and ConA columns for glycoprotein isolation, as well as myelin isolated at postnatal day 14, before compaction of myelin is complete. We evaluated the distribution of compact and non-compact myelin proteins compared to the classical myelin preparation (Norton and Poduslo, 1973) where compact myelin proteins are preferentially enriched. This sample was not included in proteomic analysis, but rather kept as a sample for comparison in the quality control of the preparations (**Figure** 3.29).

In summary, we isolated different fractions of myelin from C57/BL6 mice (1-6) or human brain samples (7):

1. Standard compact myelin preparation in discontinous sucrose gradient, 0.32 M/0.85 M interphase (Norton and Poduslo, 1973).

2. Myelin isolated from postnatal day 14 (P14) brain homogenate, in discontinuous sucrose gradient, 0.32M/0.85M interphase.

3. Purified myelin solubilised with 1% Triton X-100 o/n and bound to ConA beads

4. Purified myelin bound to WGA beads.

5. Myelin isolated from brain homogenate subjected to an initial hyposmotic shock with water and then subjected to a continuous gradient, fraction 0.9-1 M sucrose.

6. Myelin isolated from brain homogenate subjected to an initial discontinuous gradients and collected from 0.32-1.2 M interphase (crude myelin) and subsequently subjected to a continuous sucrose gradient. Collected from Fraction 3, or 0.9-1 M sucrose.

7. Glycoprotein from human myelin preparation, subjected to a lentil-lectin column (Mathey et al., 2007), kindly provided by Edgar Meinl (Max Planck Institute of Neurobiology, Munich).
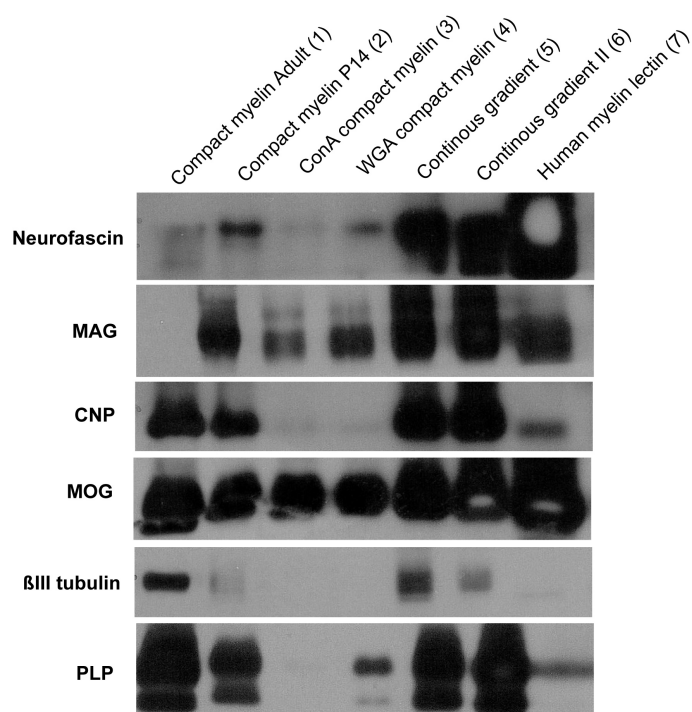
Figure 3.29: **Western blot of myelin-enriched fractions for proteomics.** Enrichment of non-compact proteins (Neurofascin, MAG, CNP and MOG) compared to compact myelin protein (PLP) and axonal proteins (βIII tubulin). Sample 1: Adult myelin, 0.32/0.85 M interphase. Sample 2: P14 myelin 0.32/0.85 M interphase. Sample 3: Adult myelin treated with Triton X 0.1% and bound to ConA beads. Sample 4: Adult myelin bound to WGA beads. Sample 5: Adult brain homogenate subjected to sucrose continuous gradient, fraction corresponding to 0.9-1.0 M. Sample 6: Adult myelin taken from 0.32/1.2 interphase and then subjected to a sucrose continous gradient, fraction corresponding to 0.9-1.0 M. Sample 7: Human myelin glycoproteins eluted using a lentil-lectin column. MAG: myelin associated glycoprotein, PLP: proteolipid protein, MOG: myelin oligodendrocyte glycoprotein, CNP: 2',3'-Cyclic-nucleotide 3'-phosphodiesterase.

3.3.2   Proteomic analysis

The samples were analyzed by mass spectrometry and 6 lists, with a total of 1904 proteins, were obtained. As stated above, the compact enriched myelin fraction (Sample 1) was not analyzed as it was used for quality control comparison by western blot. We then screened the lists by identifying the proteins predicted to have a transmembrane domain with the TMHMM Software or have a signal peptide with the Phobius software. We selected the proteins that were present in two or more lists, except for the human sample list, which was analyzed separately. We then manually selected candidates according to literature search or functional information available at the UniProt database (The UniProt Consortium, 2008). We discarded the proteins that have already been intensively described, as MAG, Contactin, Caspr and Necl4, among others. A summary of the selected candidates is presented below.

Accession number	Identified Proteins	List	Unique peptides (sum)
gi|119571963	ADAM metallopeptidase domain 11, isoform CRAa	human	5
gi|1709301	amyloid precursor-like protein 1	human	9
gi|16306530	cadherin-10 preproprotein	human	2
gi|119571613	carboxypeptidase D, isoform CRAb	human	7
gi|119613874	CD46 antigen, complement regulatory protein, isoform CRAf	human	2
gi|18640734	contactin-associated protein-like 5 precursor (CNTP5)	human	5
gi|13435361	desmocollin-1 isoform Dsc1a preproprotein (DSC1)	human	2
gi|32189434	immunoglobulin superfamily member 8	4 (+human)	29 (+19)
gi|109658490	Insulin receptor	human	2
gi|116295258	integrin alpha-2 precursor (CD49B)	human	6
gi|27363458	leucine-rich repeat and fibronectin type-III domain-containing protein 4 (LRFN4)	human	6
gi|148665587	limbic system-associated membrane protein (Lsamp)	4	22
gi|14192943	multiple epidermal growth factor-like domains protein 10 precursor (MEG10)	human	4
gi|145701025	multiple epidermal growth factor-like domains protein 8	human	9
gi|163965382	neural cell adhesion molecule 2 isoform a (NCAM2)	2	9
gi|119630409	neural cell adhesion molecule 2, isoform CRAa	human	44
gi|27151644	neurotrimin (HNT)	(+human)	8 (+2)

Accession number	Identified Proteins	List	Unique peptides (sum)
gi|148707097	nicastrin	2	5
gi|119608548	olfactomedin 1, isoform CRAa	human	18
gi|152013069	PCDH9 protein	human	13
gi|119606585	plexin domain containing 2, isoform CRAc	human	2
gi|189065500	predicted: melanoma cell adhesion molecule (MCAM)	human	11
gi|156523248	proline-rich transmembrane protein 2	3	10
gi|148699102	protein tyrosine phosphatase, receptor type, D	2	9
gi|119603966	protein tyrosine phosphatase, receptor-type, Z polypeptide 1, isoform CRAa	human	19
gi|148728162	receptor-type tyrosine-protein phosphatase isoform 1 precursor (PTPRJ)	human	10
gi|5729718	trophoblast glycoprotein (TPBG)	human	2
gi|110626109	tyrosine-protein phosphatase non-receptor type substrate 1 isoform 1	3 (+ human)	13(+26)
gi|158256874	unnamed protein product	human	4
gi|221041684	unnamed protein product	human	2
gi|22760207	unnamed protein product	human	8
gi|170014689	VPS10 domain-containing receptor SorCS2 precursor (SORC2)	human	6

3.3.3   Expression of candidates in HEK 293T cells and binding assay

From our proteomic analysis of glycoprotein-enriched and non-compact myelin fractions we generated a list of candidate proteins by transmembrane and signal peptide prediction. We then created a soluble version of each candidate, cloning the signal peptide and predicted extracelular domain and tagging it with a human Fc fragment for detection. The exclusion of the transmembrane domain thus results in the protein being secreted by transfected HEK 293T cells, and the soluble proteins were then retrieved by collecting the supernatant.

Subsequently, a binding assay was used as a screening method to detect potential interaction of selected candidates with neurons or oligodendrocytes (as some of the axonal components may be isolated along with myelin). The assay was performed by adding the soluble version of the candidate proteins to neurons and oligodendendrocyte-enriched cultures. As positive controls, we used Necl1-Fc and Necl4-Fc, which bind strongly to oligodendrocytes and axons, respectively (Spiegel et al., 2007).

We evaluated the expression and secretion of Necl1, Necl4 and candidate proteins by analysis of the supernatant of transfected HEK cells by western blot (see example in **Figure** 3.30).
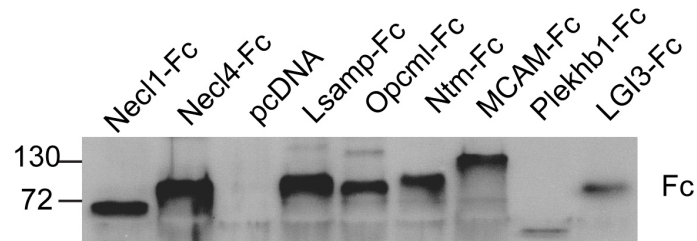
Figure 3.30: **Western blot of Fc-fused candidate proteins.** pcDNA is the empty vector, used as negative control. The soluble proteins consisted of the signal peptide and extracellular domain, fused to a human Fc fragment for detection. The proteins are retrieved from the supernatant of transfected HEK 293T cells and detected using an antibody against human Fc fragment. Necl: Nectin-like protein, Lsamp: limbic system-associated membrane protein, Opcml: opioid binding protein/cell adhesion molecule-like, Ntm: neurotrimin, MCAM: melanoma cell adhesion molecule, Plekhb1: pleckstrin homology domain containing, family B (evectins) member 1: LGI3: leucine-rich repeat LGI family, member 3.

To evaluate whether the expressed soluble proteins retained their normal interaction properties, we took the supernatant from transfected HEK 293T cells, incubated it with Cy3-conjugated anti-Fc antibody and added it to live cells for 20 minutes. **Figure** 3.31 shows a sample of a binding assay using Necl1 and Necl4 as controls.Using this binding assay as a screening tool, we screened for the candidates as Igsf8, MCAM, Plekhb1 and LGI3, and did not observe binding (see example for Igsf8 in **Figure** 3.32).

We decided to take MCAM-Fc as a negative control for the functional assays, to discard unspecific effect of a soluble Fc-fusion protein.However, we saw binding of one of our candidates, limbic system-associated membrane protein to both neurons and oligodendrocytes (Lsamp, **Figure** 3.33).

The Lsamp-Fc fusion protein did not appear to bind to astrocytes. Uptake by microglia was observed, but was considered unspecific as it occured with all proteins that were added microglia and can, thus, be attributed to its phagocytic properties (**Figure** 3.34). This suggests that the binding to oligodendrocytes and neurons observed is specific.
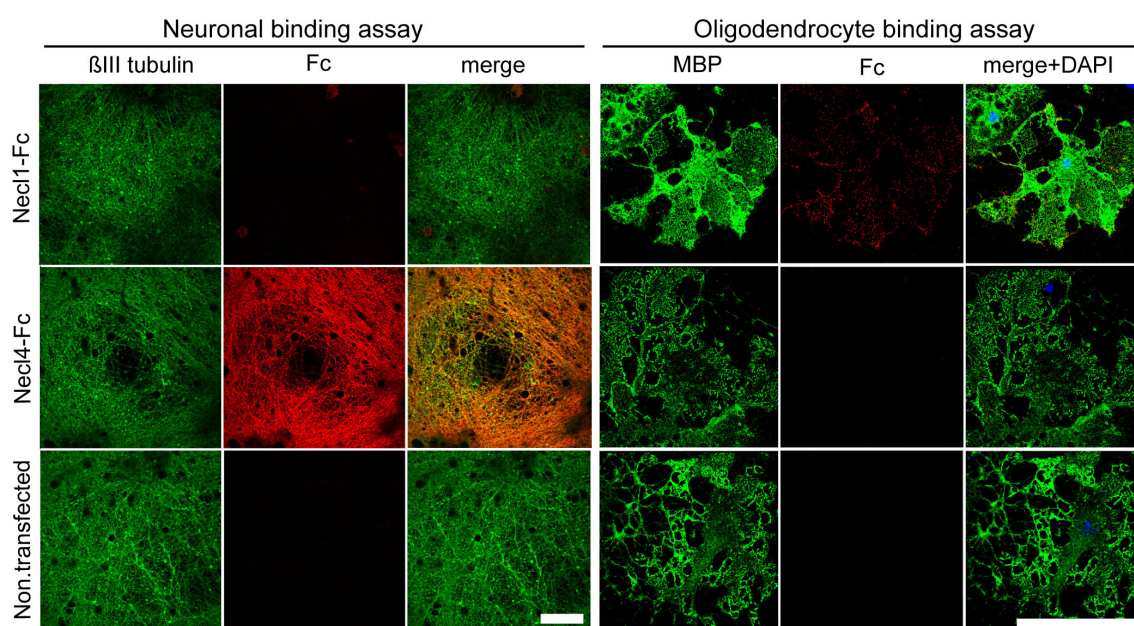
Figure 3.31: Binding assay of Necl1-Fc and Necl4-Fc as controls. Soluble versions of Necl1 and Necl4, consisting of the extracellular domain fused to a human Fc fragment were tagged with Cy3-conjugated anti- Fc antibodies and added to neuronal and oligodendrocyte cultures. As described previously, Necl1-Fc binds extensively to oligodendrocytes, stained with MBP, whilst Necl4-Fc binds to neurons, stained with βIII tubulin (Spiegel et al., 2007). Scale bar: 50μm.
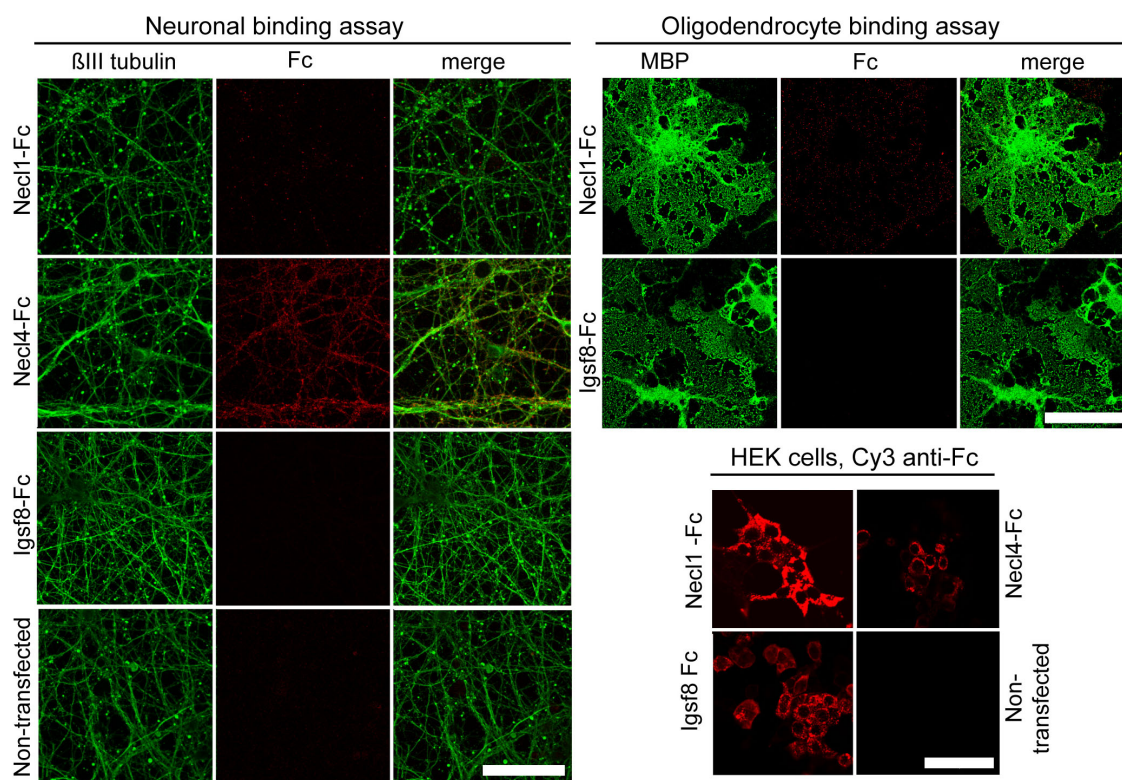
Figure 3.32: Immunoglobulin family member 8 (Igsf8) binding assay. Binding assay of Igsf8 to neurons and oligodendrocytes, using Necl1-Fc and Necl4-Fc as controls. Soluble Fc-fusion proteins were added to neuronal and oligodendrocyte cultures. No binding of Igsf8 was observed to oligodendrocytes (MBP) nor neurons (βIII tubulin). Transfected HEK 293T cells were stained with Cy3-conjugated anti-Fc antibodies to reveal the expression of the proteins within the cell. Scale bar: 50μm.
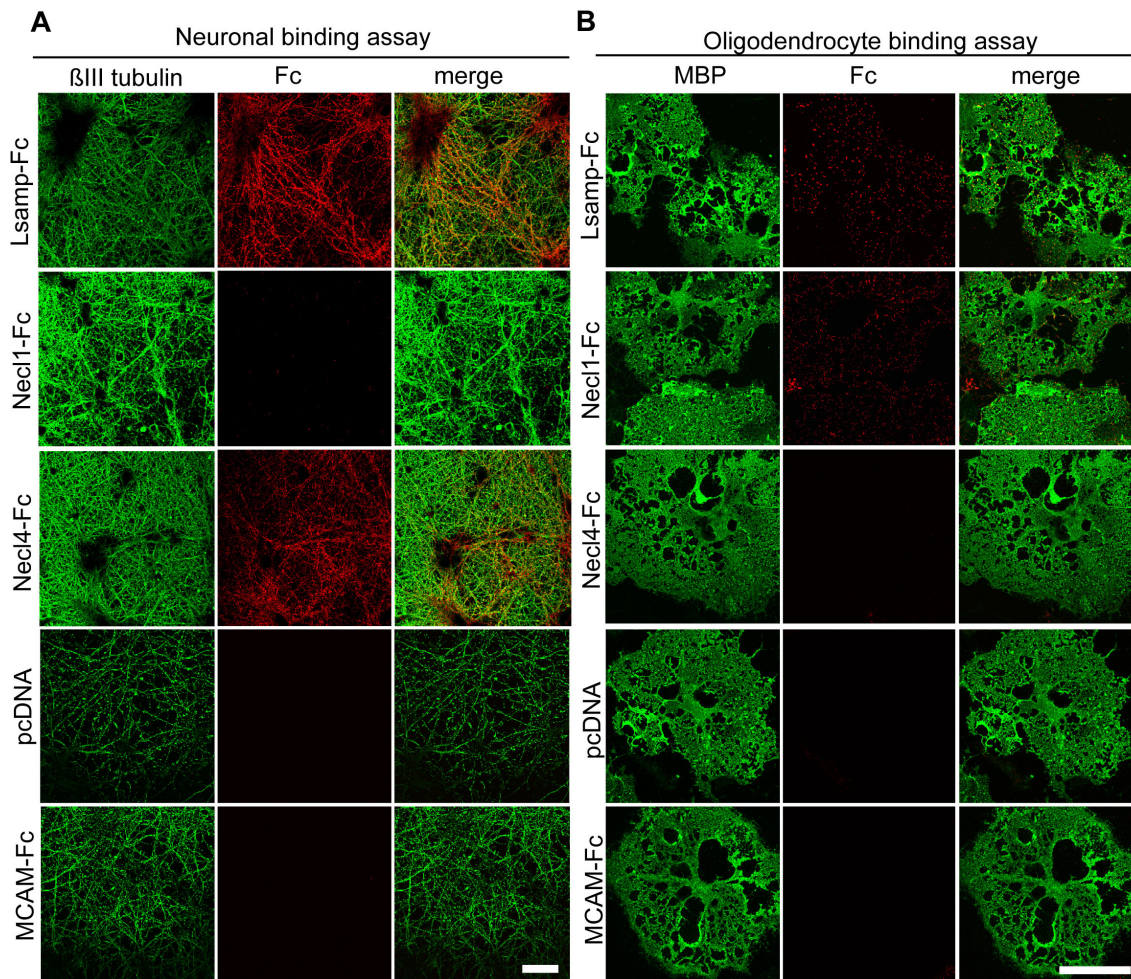
Figure 3.33: **Limbic system-associated membrane protein (Lsamp) binding assay.** Binding assay of Lsamp to primary neuronal and oligodendrocyte culture, using Necl1-Fc and Necl4-Fc as controls. Soluble versions of the proteins, consisting of the extracellular domain fused to a human Fc fragment were tagged with Cy3-conjugated anti-Fc antibodies and added to neuronal and oligodendrocyte cultures. Positive binding of Lsamp to both oligodendrocytes (MBP) and neurons (βIII tubulin) was observed. Scale bar: 50 μm
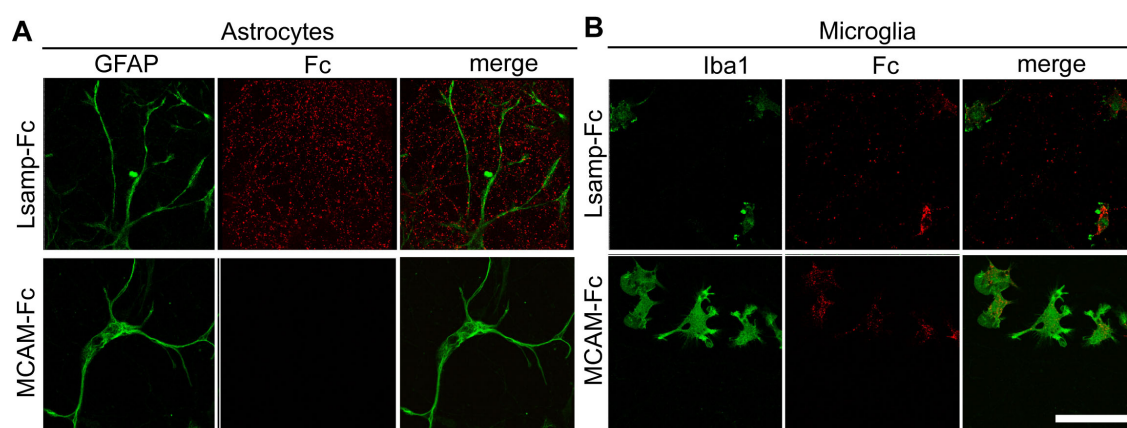
Figure 3.34: **Lsamp does not bind to astrocytes and is uptaken by microglia.** Binding assay of Lsamp to primary astrocytes and microglia culture present in primary neuronal cultures,using MCAM-Fc as control. No binding to astrocytes (GFAP) was observed. Microglia uptake of both Lsamp-Fc and MCAM-Fc is shown. Scale bar: 50 μm

Both candidate proteins Lsamp and Neurotrimin (here termed Ntm) belong to the GPI-anchored family IgLON, and Lsamp has been previously identified in other myelin proteomic and transcriptomic analysis (Nielsen et al., 2006; Jahn et al., 2009a). We therefore decided to include a third member of the family Opcml, to analyze whether the binding property is shared among the family. Opcml was found in the proteomic screening but failed to pass the first transmembrane prediction by TMHMM and Phobius and was not initially included in the candidate list.

However, as the IgLON family is GPI-anchored, they are anchored to the membrane and can be involved in cellular communication as they can associate to transmembrane proteins to trigger intracellular responses (Simons and Toomre, 2000). Lsamp, Opcml and Ntm have previously been described as neuronal proteins that appear to regulate neurite growth and interact with members of the same family, forming both homophilic and heterophilic complexes (Lodge et al., 2000; Gil et al., 2002; Reed et al., 2004). Concordantly, we observed that the three proteins bound to neurons (**Figure** 3.35).
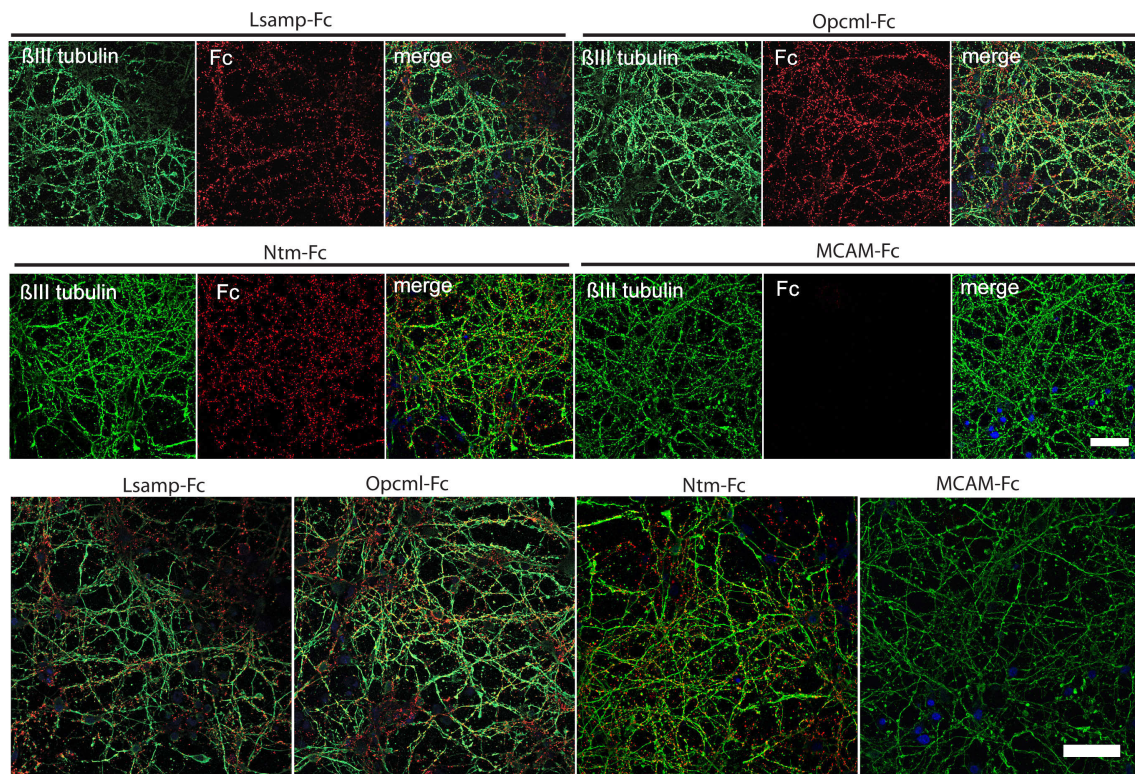
Figure 3.35: Neuronal binding assay with proteins of the IgLON family. Proteins of the IgLON family, Lsamp, Opcml and Ntm were used for binding assays with primary neuronal culture, using MCAM-Fc as negative control. Soluble versions of the proteins, consisting of the extracellular domain fused to a human Fc fragment were tagged with Cy3-conjugated anti-Fc antibodies and added to neuronal and oligodendrocyte cultures. Positive binding of Lsamp, Opcml and Ntm to neurons (βIII tubulin) was observed. Scale bar: 50 μm

The confirmation of the interaction of IgLON candidates with neurons primary culture shows that our fusion proteins were biologically functional. We therefore proceeded to repeat the binding assay with Lsamp, Opcml and Ntm in oligodendrocytes, using MCAM-Fc as a negative control. To protect the integrity of the oligodendrocyte lipid-rich myelin sheets for our binding assay, we did a surface staining against the oligodendrocyte marker O1, which requires no permeabilization. We saw binding of Lsamp, Opcml and Ntml (**Figure** 3.36).
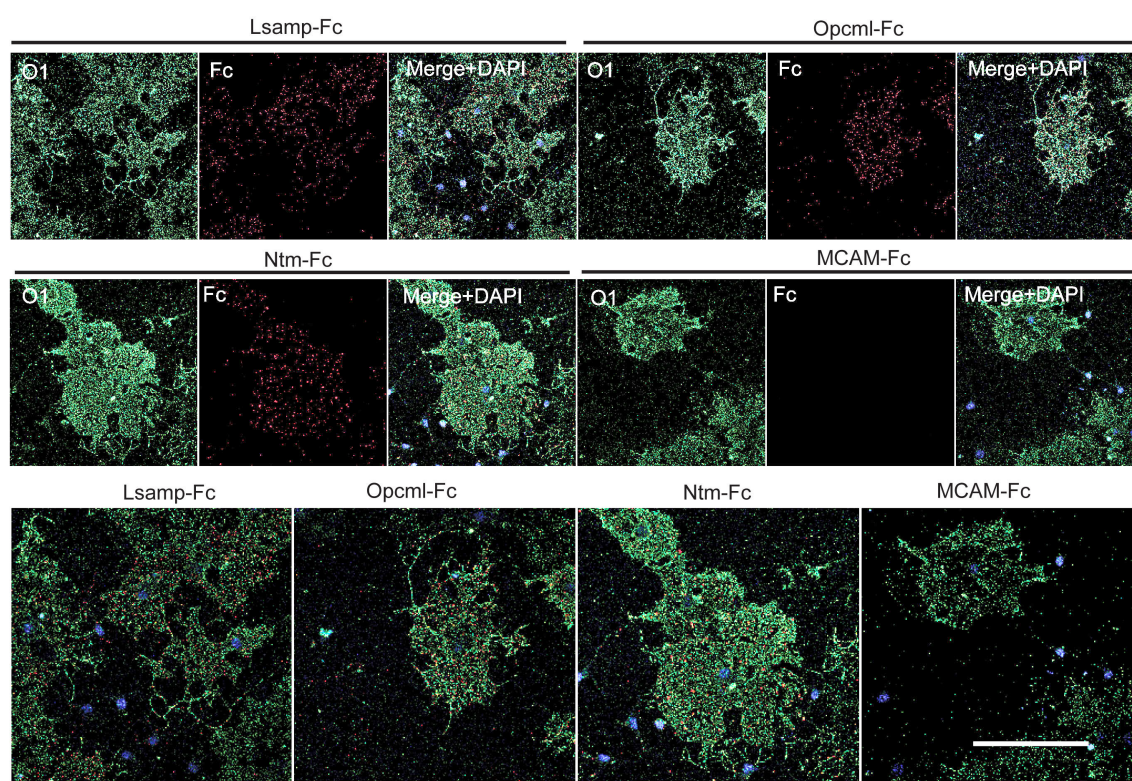
Figure 3.36: **Oligodendrocyte binding assay with proteins of the IgLON family.** Proteins of the IgLON family, Lsamp, Opcml and Ntm were used for binding assays with primary oligodendroglial culture,using MCAM-Fc as negative control. Soluble versions of the proteins, consisting of the extracellular domain fused to a human Fc fragment were tagged with Cy3-conjugated anti-Fc antibodies and added to neuronal and oligodendrocyte cultures. Positive binding of Lsamp, Opcml and Ntm to oligodendrocytes (MBP) was observed. Scale bar: 50 μm

To confirm that the IgLON proteins are interacting with other members of their family, we transfected HEK 293T cells with full length Lsamp tagged with EGFP. Then we added the soluble proteins and visualized them with a Cy3-conjugated Fc antibody. We indeed observe how there is interaction of Lsamp with the other members of the family, as well as itself (**Figure** 3.37). No binding was observed adding MCAM-Fc or adding the IgLON

proteins to HEK 293T cells transfected only with EGFP, confirming the specificity of the interaction. Similar results where observed when expressing the full length of Opcml and Ntm (data not shown).
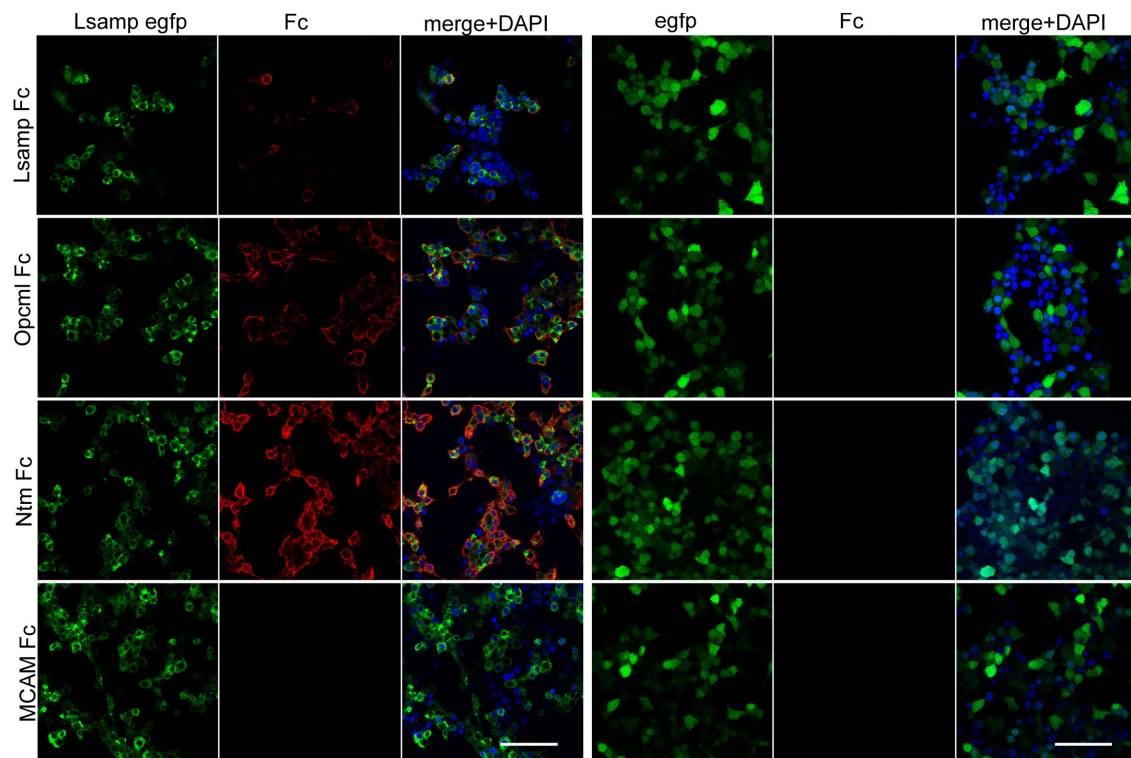
Figure 3.37: **IgLON fusion proteins interact with members of their family.** Lsamp-Fc, Opcml-Fc and Ntm-Fc were added to HEK 293T cells transfected with full length Lsamp-EGFP, using MCAM as negative control. IgLON proteins bound to HEK 293T cells expressing full length Lsamp but did not bind to HEK cells transfected with EGFP. Scale bar 100μm

To test the specificity of commercially available antibodies we transfected HEK 293T cells with myc-tagged full length proteins, and tested different shRNA to knockdown the expression of the proteins, using scramble shRNA and untransfected HEK 293T cells as negative controls. Unfortunately, the antibodies commercially available have not been useful in elucidating the expression of the IgLON candidates the different cell types, as they seem to give unspecific signals which do not facilitate the expression analysis (**Figure** 3.38).

To analyze the distribution of exogenously expressed Lsamp, Opcml and Ntm in oligodendrocytes, we transiently transfected primary oligodendrocytes with full-length version of these proteins, with a myc tag in the N-terminus. We observed that the proteins entered the compact, MBP positive myelin-like sheets (**Figure** 3.39).
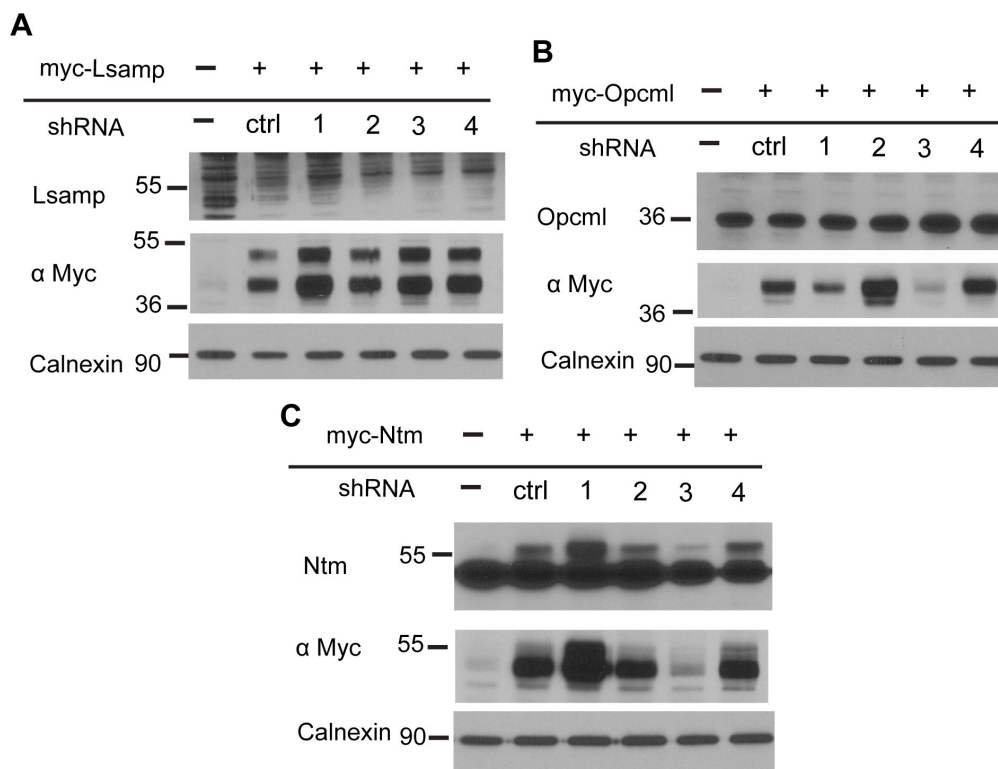
Figure 3.38: **Knockdown of exogenously expressed IgLON proteins in HEK 293T cells.** HEK 293T cells were transfected with myc-tagged full length Lsamp, Opcml and Ntm. Knockdown was attempted using four shRNA constructs, a scramble shRNA as control. Knockdown was assessed staining against myc, and commercially available antibodies for Lsamp (Biozol), Opcml (Biozol) and Ntm (Millipore) were used to validate the specificity of their signal. Only Ntm seemed to reflect the pattern obtained by myc antibodies, but presents a stong unspecific band at approximately 50 KDa.
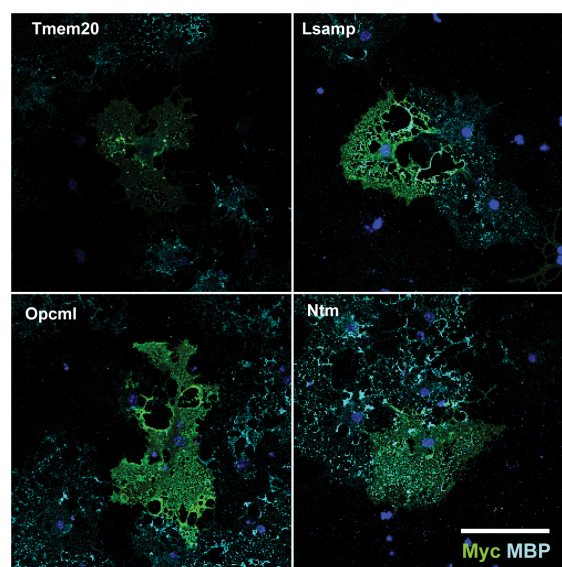
Figure 3.39: **Exogenous expression of IgLON proteins in oligodendrocytes.** Myc-tagged full length Lsamp, Opcml and Ntm localized to MBP-positive myelin sheets in mature oligodendrocytes in vitro. Scale bar: 50 μm.

3.3.4   Functional assays

We proceeded to establish different functional assays to determine whether IgLON proteins can influence the intrinsic processes in oligodendrocyte life cycle, or the interaction with neurons for myelination. We tested the effect of Lsamp, Opcml and Ntm, as well as MCAM (as negative control) to test the effect of the presence of these proteins in the media on oligodendrocyte proliferation, differentiation, migration, adhesion and myelination.

Proliferation assay

First, we plated 30 000 oligodendrocyte precursor cells (OPC) per well in a 24-well plate on PLL-coated coverslips. We added 10 μg/mL of the Fc-fusion proteins to the wells, fixed the cells after 8 hours and stained them for the OPC marker A2B5. We used 100 ng/mL PDGF as a proliferative agent. We did not see any effect of the IgLON proteins on the proliferation of OPC or the proportion of OPC in culture (**Figure** 3.40).
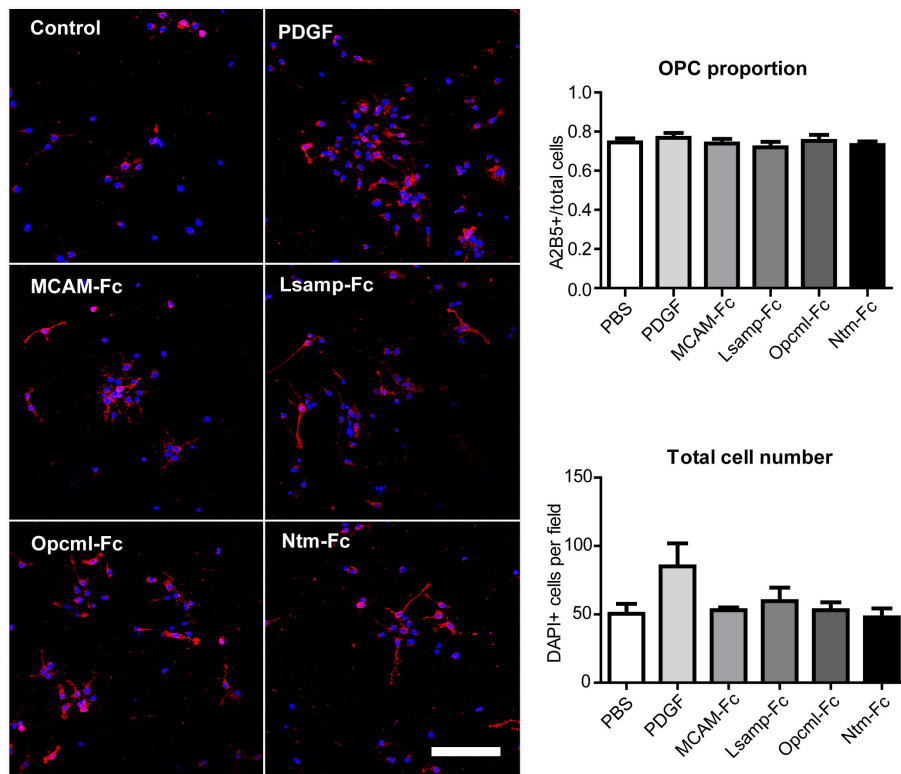
Figure 3.40: **IgLON family proteins do not influence OPC proliferation** OPC were seeded after shaking and fixed after 8 hours. No offect in cell numbers or OPC proportion was observed. PDGF was used as proliferative factor. OPC: Oligodendrocyte precursor cell (n=3). Scale bar: 100μm

Migration assay

We used a modified Boyden-chamber to study the effect of IgLON candidates on the migration of OPC (CytoSelect 24-Well Cell Migration and Invasion Assay, 8 μm Colorimetric Format). We added 300 000 OPC to each inner well in the migration chamber and allowed the cells to settle down. The membrane in the well has pores with 8 μm diameter, that allow the cells to migrate towards chemoattractants on the other side. We added 10 μg/mL of the Fc-fusion proteins to the wells to the media on the outer part of the well. We used 100 ng/mL PDGF as a chemoattractant. PBS was used as a negative control. After 8 hours we did not see any effect of IgLON proteins in the migration of the OPC (**Figure** 3.41).
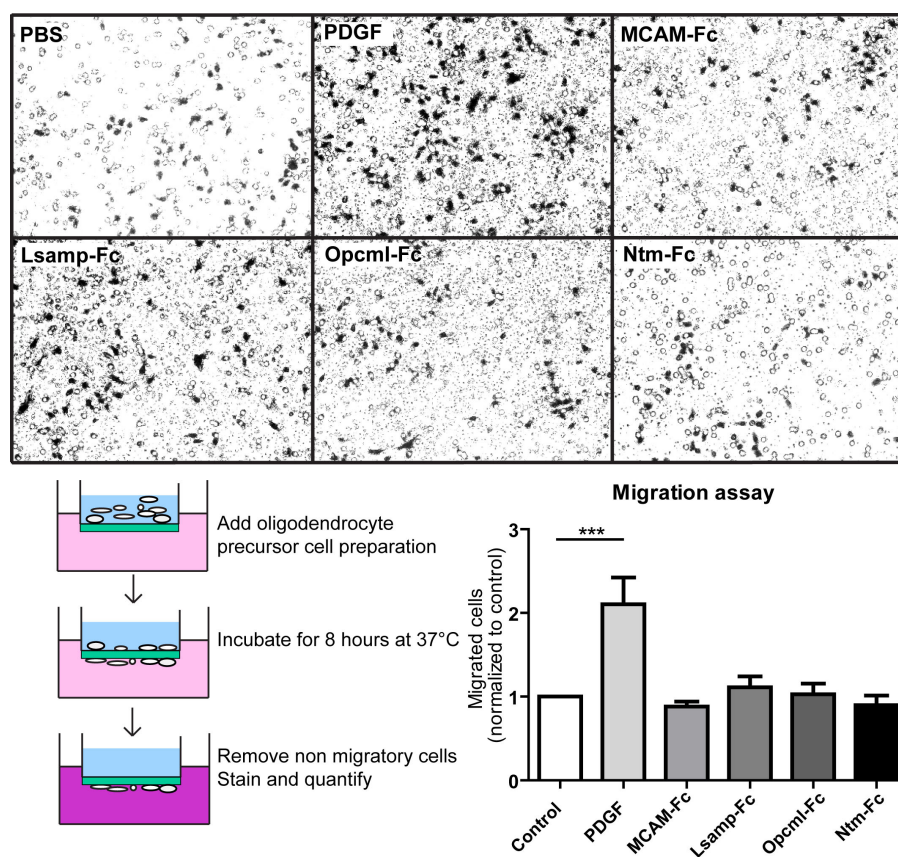
Figure 3.41: Proteins of the IgLON family do not induce OPC migration OPC were seeded after shake in a boyden chamber with 8 μm wide pores and allowed to freely migrate for 8 h in the presence of 10 μg/mL of Fc-fusion IgLON proteins. No effect was observed in the migration of OPC compared to negative control. PDGF (100 ng/mL) was used as a chemoattractant and PBS was used as a negative control (n=4).

Differentiation assay

To observe whether the presence of soluble IgLON in the media could influence the growth and differentiation of oligodendrocytes *in vitro*, we allowed OPC to grow on PLL-coated coverslips for 4 days in the presence of 30 μg/mL of IgLON Fc-fusion proteins. We did not see any change in the proportion and density of oligodendrocytes, nor in the normalized MBP signal per cell, suggesting that cell size also was not affected (**Figure** 3.42).
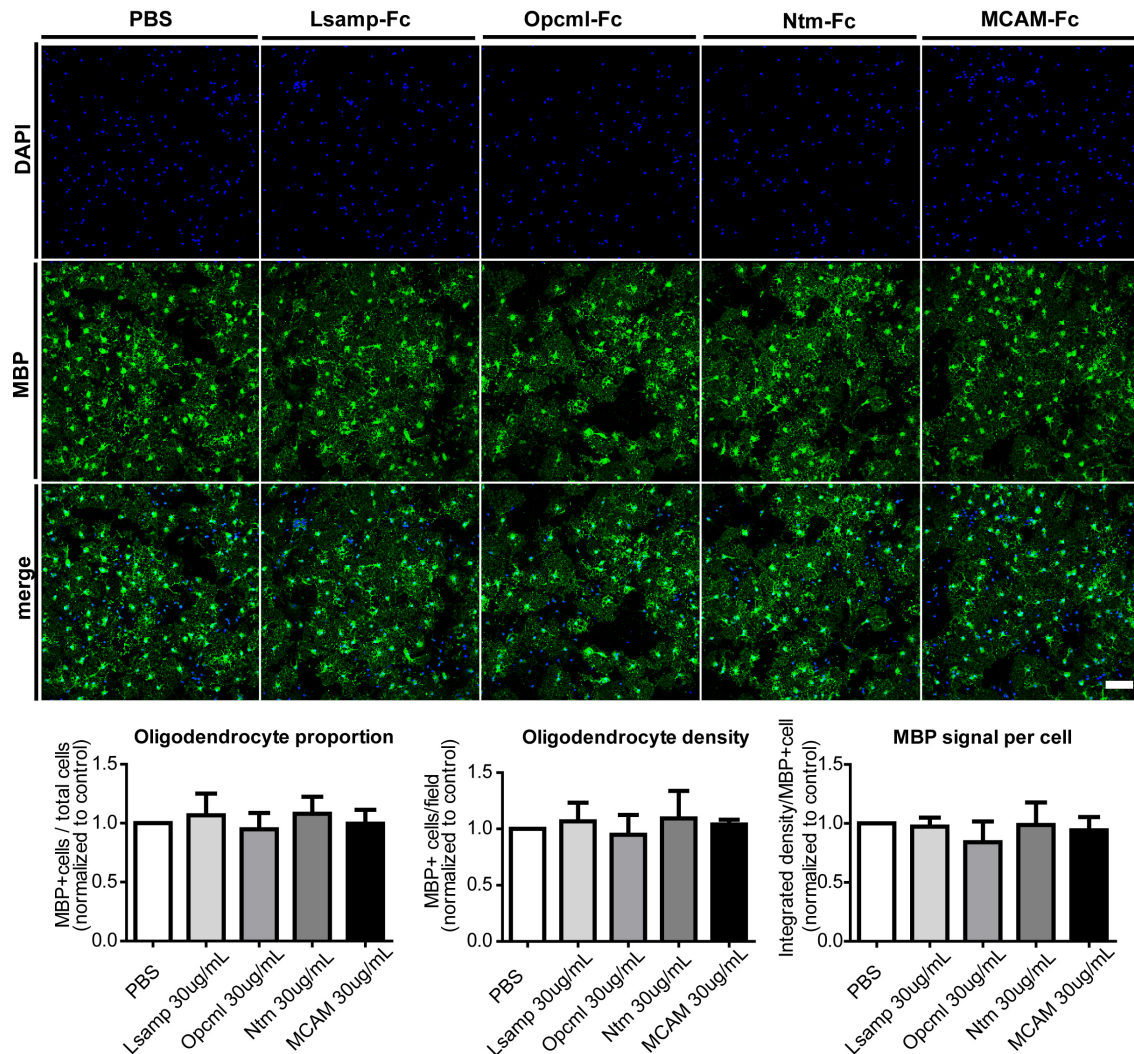
Figure 3.42: IgLON proteins do not influence OPC differentiation. OPC were seeded after shake and were allowed to grow for four days in the presence of 30 μg/mL IgLON-Fc fusion proteins, using MCAM-Fc and PBS controls. No difference in cell number, OPC proportion nor MBP integrated signal per cell as cell size indication was observed (n=3). Scale bar: 100 μm.

Adhesion assay

We hypothesized that a neuronal molecule involved in axoglial contact would provide an adhesive surface for oligodendrocytes. Therefore, we coated coverslips with the Fc-fusion candidates. As controls, we used PLL to verify the quality of the culture and the axonal protein Necl1-Fc, to confirm the functionality of the assay. OPC were allowed to grow for 4 days (**Figure** 3.43). We observed that the number and size of oligodendrocytes in the Necl1-Fc sample was comparable to that to PLL coated coverslips, indicating the robustness of the assay. Even though the oligodendroglial size in the IgLON samples showed a tendency to increase, it did not reach statistical significance.
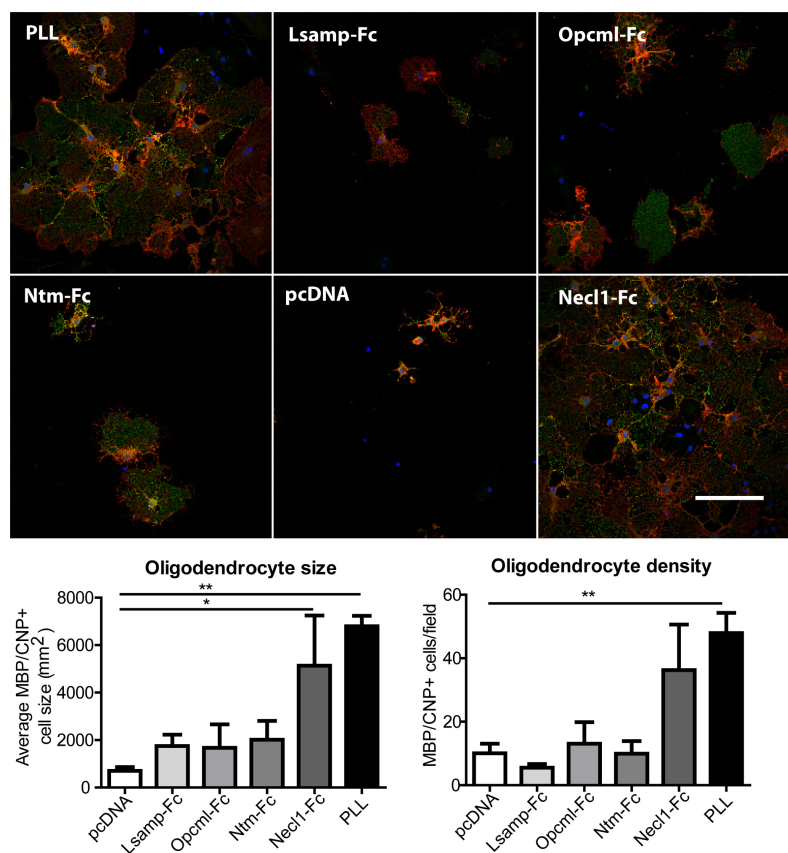
Figure 3.43: **IgLON family proteins adhesion assay.** Coverslips were coated with 5 μg/mL Fc-fusion proteins and OPC were plated and allowed to adhere and grow for 4 days. PLL and Necl1-Fc coating were used as positive controls. The purified supernatant of HEK 293T cells transfected with an empty vector (pcDNA) and MCAM-Fc were used as negative control. ANOVA <0.05, Dunnet post-hoc test with pcDNA as control (n=3). $*$p <0.05, $**$p <0.01. Scale bar: 100 μm.

Myelination assay

A myelinating co-culture can be established *in vitro* by adding OPC to primary neuronal culture previously grown for two weeks. Myelinating oligodendrocytes are identified by counting the percentage of MBP+ oligodendrocytes that form tubular, perpendicular structures, following the axonal path. Non-myelinating oligodendrocytes tend to form myelin sheets, display ramified processes that bifurcate at angles smaller than 90 degrees or do not develop processes at all (**Figure** 3.44).
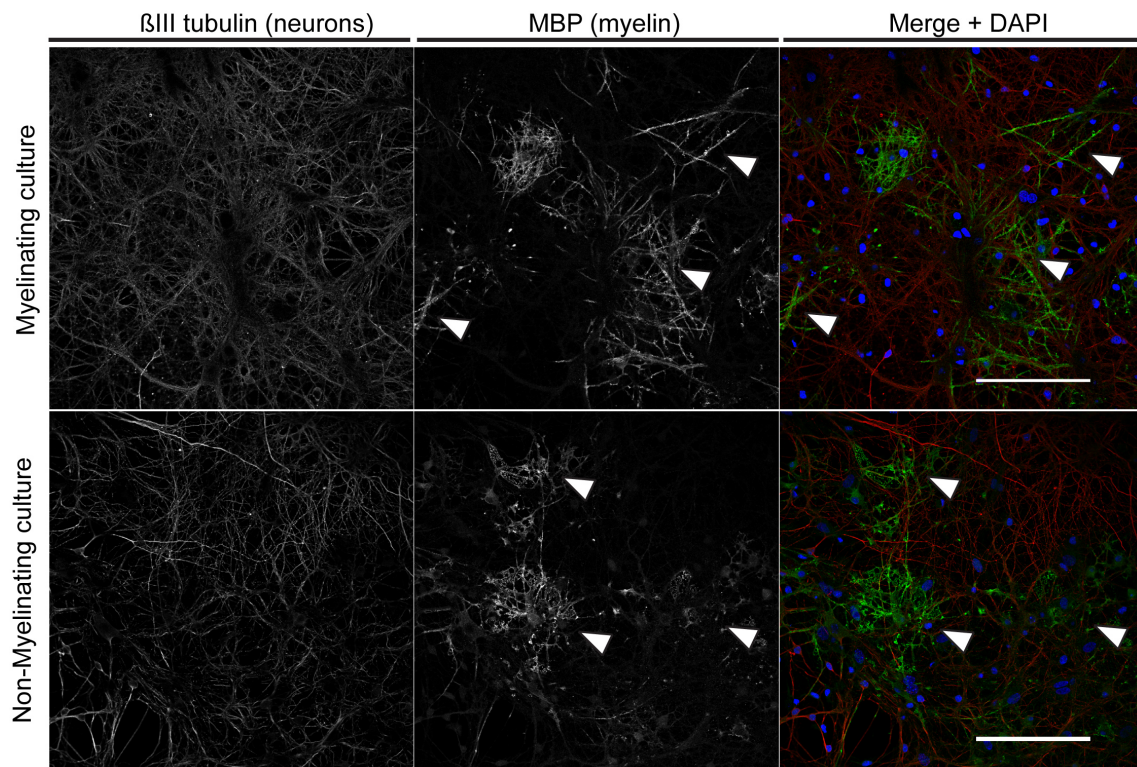
Figure 3.44: **Example of myelinating and non-myelinating coculture.** Myelinating oligodendrocytes form perpendicular, MBP-positive tubular structures. Non-myelinating oligodendrocytes typically form MBP-positive sheets, numerous processes bifurcating repeatedly and at less than 90 °C, or no processes at all. Examples are indicated with arrow heads. Scale bar: 100 μm.

To assess the ability of oligodendrocytes to initiate myelination in the presence of IgLON soluble proteins, we added 10 μg/mL of protein to primary neuronal cultures prepared at E16 and allowed them to grow for two weeks. We then added OPC to the neurons and continued to culture for 5 days. We observed a decrease in myelination efficiency in the presence of Ntm-Fc (**Figure** 3.45). This indicates a possible role of Ntm in the

communication between axons and glia that may have impact on myelination *in vitro*. It is known for proteins of the IgLON family to be involved in the guidance and extension of neurites but this is the first evidence of their function involving glial cells. Further studies can test the effect of IgLON downregulation in an *in vivo* mammalian system.
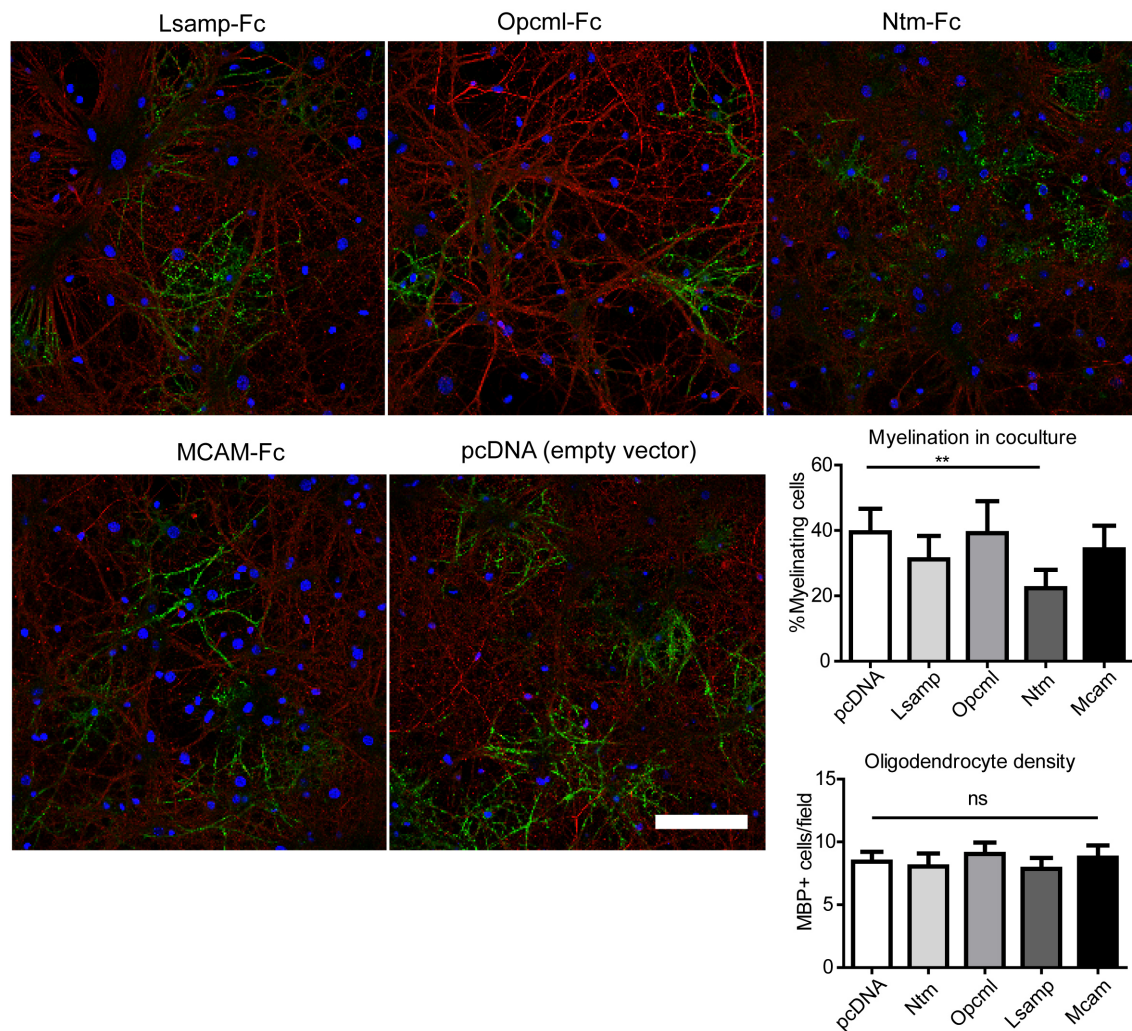
Figure 3.45: **Myelination assay in co-culture system with IgLON proteins.** Neuron and oligodendrocyte cocultures were allowed to grow for 5 days in the presence of 10 μg/mL IgLON-Fc fusion proteins. The purified supernatant of HEK 293T cells transfected with an empty vector (pcDNA) and MCAM-Fc were used as negative control. ANOVA $<$0.05, Dunnet post-hoc test was performed comparing the samples against pcDNA as control. $**$p $<$0.01, ns: not significant. Scale bar: 100 μm.

Chapter 4

Discussion

In this study, we analysed the short-and long-term consequence of oligodendrocyte ablation and demyelination on axonal preservation in two animal models of MS. It has been proposed that myelin may have a nurturing role in addition to its structural function as an insulating surface that allows the fast transmission of electric signals along the axon (Nave and Trapp, 2008). We used models that preserved the integrity of the BBB to prevent the infiltration of the immune system into the CNS. We focused on the corpus callosum because it is the main white matter tract in the brain connecting the two cortical hemispheres. Disruption of this structure results in functional deficits that can be assessed using senstitive motor tests (Liebetanz and Merkler, 2006). We observed that both cuprizone- and diphtheria toxin-induced oligodendrocyte death led to significant demyelination in the corpus callosum. This was accompanied by axonal damage, evidenced by APP accumulation and a decrease in neurofilament signal in both of the models. In the long term, cuprizone-induced demyelination was followed by remyelination and a transient functional performance similar to control animals, which ultimately gave way to a late motor decline, analyzed by the MOSS complex wheel running paradigm.

4.1   Acute axonal damage as a consequence of oligodendro- cyte ablation

Multiple sclerosis (MS) is a disease that involves an autoimmune attack against myelin, accompanied by inflammation and axonal damage. In most of the cases it initiates with discrete episodes of infiltration of immune cells into the CNS and a localized breakdown of the blood-brain barrier. This is accompanied by clinical symptoms that include motor and sensory impairment and fatigue. Acute episodes result in the formation of multifocal lesions, giving the disease its name. However, these acute episodes are usually followed by a partial or complete recovery, in a pattern termed relapsing-remitting multiple sclerosis (MS). With time, patients tend to enter a progressive phase, characterized by a steady worsening of symptoms without recovery, including decreased mobility and cognitive decline (Trapp et al., 1998; Noseworthy et al., 2000; Friese et al., 2006). It appears this late stage is somewhat independent of inflammation, and is instead related to a ongoing axonal loss and neurodegeneration, accounting for the clinical worsening of the patients (Confavreux et al., 2003; Brück, 2005). It has been proposed that remyelination serves as a neuroprotective mechanism, which not only prevents axonal loss related to a demyelinating event by protecting the axon from a toxic environment but also seems to provide axons with required trophic support (Trapp et al., 1998).

It has been widely accepted that MS is initiated by an autoimmune response against myelin epitopes, the consequence of which is demyelination, oligodendrocyte loss and axonal damage. However, in recent years, this hypothesis of MS pathogenesis has been questioned, as evidenced by oligodendrocyte abnormality and demyelination in early MS lesion, before immune infiltration can be detected (Barnett and Prineas, 2004). This has opened the debate as to whether the inflammatory response is the cause or the consequence of the demyelination and axonal pathology observed. Many anti-inflammatory therapies have been developed to reduce the relapse rate and severity in early stages of MS. However, these therapies do not necessarily delay the onset and advancement of the progressive stages of the disease, pointing to the possibility that MS initiation and progression is not entirely dependent on inflammatory processes (Brück, 2005; Nakahara et al., 2012).

To study the different aspects of multiple sclerosis, numerous animal models have been developed in the recent decades. Each of these models have proven to be useful in under-

standing the diverse aspects and mechanisms of myelin pathology. Most have addressed the control of an autoimmune response directed against myelin, as in EAE, or a direct insult against oligodendrocytes, as in toxin-mediated oligodendrocyte death. Although the main underlying question regarding the origin and mechanism of the autoimmune response against myelin remains, the different studies to date have tried to address the four major aspects in the therapeutic approach to MS: how to decrease demyelination, promote remyelination, control immune-driven cytotoxicity and inflammation, and how to protect axons from permanent damage.

4.1.1 Diphtheria toxin-mediated oligodendrocyte ablation

One recent approach involves the coordinated induction of oligodendrocyte death using diphtheria toxin (DT) in mice. As murine cells are naturally resistant to the toxin, it is necessary to either force the expression of the DT receptor, or induce the expression of the diphtheria toxin catalytically active fragment A, or DT-A, to trigger cell death. Brockschnieder and colleagues (2004) reported the expression of DT-A, by Cre-mediated recombination under the control of the CNP promoter. As CNP is readily expressed in mature oligodendrocytes and oligodendrocyte precursor cells (Chandross et al., 1999), this resulted in the overall arrest of developmental myelination and early lethality (Brockschnieder et al., 2004). Therefore, several models of systemic diphtheria toxin-induced oligodendrocyte ablation have been developed in recent years that involve temporal control of demyelination onset and allow its study in adult mice (Buch et al., 2005; Traka et al., 2010; Pohl et al., 2011; Oluich et al., 2012). Buch and colleagues (2005) described a method of oligodendrocyte ablation through expression of DTR by recombination induced by Cre recombinase expressed under the MOG promoter. They reported a massive demyelination in the corpus callosum and cerebellum but did not explore the consequences on axonal preservation any further (Buch et al., 2005).

We used this model to specifically trigger the death of mature oligodendrocytes by injecting diphtheria toxin (DT) in MOG-iCre/iDTR mice, whose myelinating oligodendrocytes express the DT receptor (Buch et al., 2005). We observed that after approximately 30 days, most animals became severely ill, displaying tremor, hind limb paralysis and, on occassion, death (data not shown). We observed moderate demyelination, accompanied by a decreased number of mature oligodendrocytes in the corpus callosum of MOG-iCre/iDTR mice treated with DT but not in MOG-iCre/iDTR mice treated with PBS or MOG-iCre

mice (lacking DTR expression) treated with DT. This indicates the specific ablation of DTR-expressing mature oligodendrocytes and demyelination induction.

The demyelination level observed in diphtheria-toxin induced oligodendrocyte ablation has varied among studies. While some have reported extensive demyelination along the CNS (Buch et al., 2005; Traka et al., 2010; Pohl et al., 2011), others have reported that oligodendrocyte abundance in the corpus callosum was unchanged despite reductions in other regions of the CNS (Oluich et al., 2012). Injections of intraperitoneal DT may not diffuse uniformly and therefore may not reach all areas of the CNS evenly or at the same time. However, in our investigation, injection of DT was sufficient to induce a reduction in oligodendrocyte number and degree of myelination. The fact that we injected higher amount of DT (400 ng daily for 7 days vs a single 200 ng dose) could also explain the increased effect in our system.

Indeed, a recently published study (Locatelli et al., 2012a) explored DT models in further detail. In addition to observing widespread oligodendrocyte death, microglia activation and astrogliosis, in agreement with our study, no acute infiltration from the immune system was detected in any of DT-mediated demyelination models (Buch et al., 2005; Traka et al., 2010; Pohl et al., 2011; Locatelli et al., 2012a; Oluich et al., 2012). This casts doubt on the hypothesis of an oligodendrogliopathy as being sufficient to elicit an immune response, at least within this short time frame. However, we did observe, as did the other mentioned studies, an increase in microglia activation and proliferation. In most MS models, it is believed that in addition to the induced demyelination, microglia activation can contribute to the harm inflicted on oligodendrocytes and axons possibly through the production of NO, cytokines and ROS (Smith et al., 2001).

Indeed, we found a significant amount of acute axonal damage, evidenced by a significant accumulation of APP and decreased neurofilament signal. This is in accordance to most DT-induced demyelination studies published so far (Pohl et al., 2011; Oluich et al., 2012). Surprisingly, contradicting results have been reported using similar models of DT-A expression upon Cre-mediated recombination using either PLP-CreERT (Traka et al., 2010) or PLP-CreERT2 (Pohl et al., 2011). Traka et al. (2010) reported that despite the massive demyelination and microglia activation generated in their model, no axonal loss was observed in the optic nerve or the spinal cord, and remyelination was prompt and

widespread. Pohl et al. (2011), who used the same model, did observe axonal damage and loss, and a delay in myelin debris clearance, which was shown to correlate to a lower remyelination efficiency (Kotter et al., 2006; Baer et al., 2009). These discrepancies could be due to differences in either the recombination efficiency due the use of the more sensitive Cre recombinase Cre-ERT2 instead of Cre-ERT (Indra et al., 1999), higher amounts of tamoxifen injected, or simply the fact that slightly older animals were used in one of the studies (Pohl et al., 2011).

Traka et al. (2010) reported that older animals did not remyelinate efficiently and did not appear to recover in contrast to the phenotype they observed in younger animals. It is possible that the greater severity of symptoms in the models involving DT injection in comparison to those involving DT-A expression within the target cell, can be in part due to a delayed clearance of the DT. This delay could cause the continued depletion of oligodendrocyte precursors undergoing differentiation in an attempt to remyelinate. As a single molecule of DT is sufficient to induce apoptosis in a cell (Yamaizumi et al., 1978), the system is very sensitive to residual DT, possibily prompting the animal to miss the critical time window in which remyelination can protect axons from degeneration (Crawford et al., 2009). On the contrary, in the inducible models that involve tamoxifen-mediated recombination, once the effect of the tamoxifen treatment is over, the precursors can freely differentiate and remyelinate. However, it should be noted that in the other studies using Cre-ERT-induced DT-A expression, this recovery was not observed (Pohl et al., 2011). The amount of tamoxifen and the efficiency of recombination can therefore determine the clinical outcome of the model.

The clinical phenotype induced by diphtheria toxin-mediated oligodendrocyte ablation is not changed in mice lacking or with reduced functional lymphocytes, or when enhancers of inflammation were added (Pohl et al., 2011; Locatelli et al., 2012b). This indicates that in the DT-induced demyelination model, this process is independent of the adaptive immune system. Most importantly, these results show that, at least in the short term, oligodendrocyte death and demyelination are not sufficient to trigger an autoimmune response against myelin, but can trigger microglia activation and axonal damage. Interestingly, Pohl et al. (2011) report that the areas with the lowest levels of remyelination, presented the highest axonal pathology. Unfortunately, none of these studies can discard or quantify, at this point, the extent of the axonal damage induced by activated microglia. Rather they sup-

port the idea that remyelination indeed appears to have a neuroprotective function. The fact that we did not observe any axonal or clinical phenotype in DT-treated Mogi-Cre mice that lacked the DTR allele shows the robustness of the model and discards any unspecific cytotoxic effect of the toxin itself.

Due to the severity of the disease, the animals had to be sacrificed before we were able to study the remyelination and long-term consequences of demyelination in this model. This fatal monophasic phenotype has also been found in similar diphtheria toxin models, where no recovery was observed (Pohl et al., 2011; Oluich et al., 2012). Only Traka et al. (2010) reported a complete motor and clinical recovery in young animals. This discrepancy could be explained by the reasons stated above. Although our model has not allowed us to address the long-term consequences of demyelination in the future it could be useful in addressing the question of how to mitigate axonal damage as a consequence of demyelination.

4.2 Late motor decline and axonal damage in cuprizone model

To analyze the long-term consequences of myelin loss on axonal preservation and functional recovery, we attempted to understand the long-term consequences of early cuprizone-induced demyelination in mice. The aim of this study was to establish an animal model that mimics some aspects of progressive MS, characterized by late-onset progressive neurological deficits, often in the absence of active inflammation (Kremenchutzky et al., 2006; Lassmann et al., 2007; Miller and Leary, 2007). Remyelination has been shown to be extensive in the cuprizone model (Blakemore, 1973b), but the long-term impact of myelin repair on neuro-axonal function is not known.

4.2.1 Functional recovery and late onset motor decline after remyelination

Due to the localized and reversible demyelination induced in the cuprizone model, it has been difficult to detect phenotypes related to the myelination and functional state of the corpus callosum, especially after remyelination. A deficit in the prepulse inhibition of acoustic startle response has been reported, but only during cuprizone feeding (Xu et al., 2009, 2010). After recovery, a decreased anxiety and increased interactive behavior, as well

as a higher frequency of falls in the rotarod test have been reported (Franco-Pons et al., 2007; Hibbits et al., 2009). However, the interactive behaviour test should be done in naive animals and is most likely not optimal for longitudinal studies (Bolivar et al., 2007). On the other hand, the rotarod test is not likely to be solely related to the myelination status of the corpus callosum, as differences were observed after 6 weeks of remyelination but not at 6 weeks of cuprizone feeding, when demyelination is much higher (Franco-Pons et al., 2007). In addition, it is difficult to target and follow the specific brain structures correlated with these behaviors.

Impaired performance in complex running wheel tests has been described in mice with genetically-absent or surgically removed corpus callosum (Schalomon and Wahlsten, 2002). The corpus callosum consists of the axons of cortical projection neurons and facilitates the communication of both the cerebral hemispheres, and the associative connectivity, to execute complex motor and cognitive tasks. Most of these axons are myelinated and therefore make up the largest white matter structure in the placental mammalian brain (Aboitiz and Montiel, 2003; Fame et al., 2010). One of the few methods shown to detect latent deficits in animals after remyelination in the cuprizone model is the motor skill analysis or MOSS (Liebetanz and Merkler, 2006). In this test, mice ran voluntarily in wheels with irregularly spaced crossbars, therefore requiring a constant step length adaptation and bi-hemispherical coordination.

To analyze the long-term effect and functional recovery of cuprizone-induced demyelination, a motor skills evaluation was performed three times over a period of 28 weeks using the MOSS running test (Liebetanz and Merkler, 2006). In this study, we reproduced earlier findings showing that latent motor deficits in MOSS parameters, such as maximum velocity (Vmax) and maximum distance (Dmax) are still evident after 6 weeks of recovery following cuprizone diet (Liebetanz and Merkler, 2006). We further re-examined the animals 14 weeks later (i.e. 20 weeks after cuprizone treatment removal). Locomotor performance of remyelinated animals was indistinguishable to age-matched controls by MOSS at this time point. These results indicate that remyelination together with, most probably, neuroplastic processes, can fully compensate functional disability after a demyelinating insult.

To further investigate whether functional recovery remained stable in the long-term, we repeated MOSS analysis at 28 weeks after cuprizone removal. At this latest time point, remyelinated animals, independent of single or repeated exposure to cuprizone, displayed deteriorated locomotor performance as compared to age-matched controls in the coordinative parameters Vmax and Dmax. Similar to earlier time points, no differences were detected in parameters assessing general motivation and/or fitness compared to controls and no differences in any of the parameters were observed between the treated groups.

These data show that mice fed with cuprizone recover completely as measured by MOSS, but develop late-onset functional deficits at advanced age. One possibility could be that after the initial deficiency detected after 6 months, the treated animals entered a steady state, and their performance level is ultimately reached by the decreased performance of control animals due to aging, and this could account for the similar performance of all groups 20 weeks after cuprizone removal. However, with time, cuprizone- treated animals exhibited a continued decline, evidenced in the last timepoint of the MOSS analysis. Although it is not possible to describe the rate of the decline beyond the three time points analyzed, the data show that there is indeed a late-onset motor decline observed in the treated mice between 20 and 28 weeks of cuprizone treatment.

A decline in performance after a period of stability in the first 20 weeks could be explained by two independent factors: compensatory mechanisms that facilitate the functional recovery and a steady accumulation of structural damage. A tipping of the balance between these two processes upon reaching a certain threshold may unmask latent damage. Such a mechanism has been proposed to explain the functional recovery in MS patients during relapsing-remitting stages of the disease and the irreversible clinical decline observed in the progressive phases (Trapp et al., 1998; Bjartmar and Trapp, 2003). Four components appear to be involved in maintaining this balance and contribute to the clinical readout: axonal damage, resolution of inflammation, remyelination,and cortical plasticity.

4.2.2   Axonal damage as a driver of motor decline

Most of the axonal damage induced by cuprizone-mediated demyelination occurs during the treatment, and decreases during recovery (Hoehn et al., 2008; Lindner et al., 2009). In our study, axonal damage, measured by APP accumulation, was at a maximum after 5 weeks of cuprizone treatment (Figure 3.26). It is intriguing, however that even at

$\sim$ 6 months after the treatment with cuprizone was ceased, APP-positive axons are still detected. Even more interestingly, some of these APP-positive axons were still surrounded by a myelin sheath. Furthermore, we also observed enlarged mitochondria in axons in this last time point, $\sim$ 6 months after cuprizone had been removed from the diet, providing further evidence of persisting axonal pathology (Kiryu-Seo et al., 2010).

The axonal damage described in our model may be the result of several processes. First, it is possible that cuprizone-mediated toxicity is not selective to oligodendrocytes, but may also work directly against the axon, as many axons are lost during the treatment with cuprizone. There is mounting evidence that axonal damage most importantly decreases with remyelination efficiency and increases with the level of microglia activation (Irvine and Blakemore, 2008; Tsiperson et al., 2010; Yoshikawa et al., 2011). Inflammation level and axonal damage correlate in acute and chronic MS lesions (Bitsch et al., 2000; Kuhlmann et al., 2002). Microglia are known to perform dual roles that have beneficial positive and detrimental consequences for axonal survival. Accordingly, understanding the pathways that stimulate/inhibit one response over the other would be useful in modulating the net contribution of microglia to a demyelinating episode, in order to preserve axonal integrity (Hanisch and Kettenmann, 2007).

On one hand, microglia act as macrophages, clearing myelin debris, which is necessary for efficient remyelination to occur. On the other hand, activated microglia release cytokines and NO. These can contribute to a reversible blockage of axonal conduction, exacerbate the inflammatory effects and lead to axonal damage and subsequent loss (Smith et al., 2001; Aboul-Enein et al., 2006). Therefore, it is possible that the low yet sustained presence of astrocytes and microglia observed in our study can contribute to the low ongoing damage. The decrease of axonal counts observed in our study, suggests that microglia presence could be induced by an ongoing axonal degeneration and could be contributing to debris clearance without the production of harmful pro-inflammatory signals (Neumann et al., 2009).

Following axonal transection, regeneration in the CNS is considerably limited, due to the presence of inhibitory factors in the extracellular space. Oligodendrocyte molecules such as NogoA, MAG and OMgp have been identified as axonal growth inhibitors (Kotter et al., 2006; Baer et al., 2009). These three molecules bind to the Nogo receptor (NgR)

present in axons, which associates with the receptor p75 and LINGO-1 (Wang et al., 2002; Mi et al., 2004) and is responsible for neurite outgrowth inhibition and prevents axonal regeneration in the CNS (Fournier et al., 2001). In addition, myelin debris and associated proteins have also been found to inhibit oligodendrocyte differentiation, a crucial step for remyelination to occur (Kotter et al., 2006; Syed et al., 2008). A failure in remyelination has been repeatedly associated to an increased axonal loss in the cuprizone model and progressive MS, and is currently one of the major targets in MS treatment (Smith, 2006; Franklin and Ffrench-Constant, 2008; Irvine and Blakemore, 2008).

Further evidence that supports the idea that myelin integrity itself may be necessary for axonal maintenance stems from studies showing that mice lacking different myelin-specific proteins suffer from late-onset neurodegeneration, despite the fact the myelin appears structurally normal (Griffiths et al., 1998; Lappe-Siefke et al., 2003). In different demyelinating animal models, age can negatively affect the recruitment and differentiation of OPCs after demyelination (Shields et al., 1999; Sim et al., 2002), resulting in a decreased remyelination capacity and more extensive axonal damage (Hampton et al., 2012). In our study, we observed an extensive yet incomplete demyelination. In addition to the expected increase in the g-ratio, due to a thinner myelin sheath formed after remyelination, we observed that a population of axons (approximately 26%) remained unmyelinated.

Aside from decreasing neuronal energy demands by facilitating saltatory conduction, myelin regulates the axonal diameter (de Waegh et al., 1992), fast axonal transport (Edgar et al., 2004), and the molecular organization of the nodes of Ranvier (Peles and Salzer, 2000). Therefore, chronically demyelinated axons undergo alterations in structure and function, demand more energy and become more vulnerable to degeneration (Irvine and Blakemore, 2008; Lindner et al., 2009). Despite the axonal loss observed after cuprizone treatment, remyelination seems to contribute to the axonal preservation of remaining axons, as the majority of the APP-positive axons observed after 6 months appeared unmyelinated.

However, it is striking that, in both the cuprizone model at 6 months after treatment removal, as well as in chronic lesions from MS patients there was a constant fraction of axons that displayed APP accumulation yet had a surrounding myelin sheath. It could be possible that the axon is not myelinated along its entire length and the pathology is

caused by insufficient myelination in adjacent regions. This is difficult to prove due the fact that axons crossing the corpus callosum can be over 2 mm long (Wahlsten, 1984), and the tightly packed structure of the corpus callosum that precludes quantifying the fraction of an entire axon that is myelinated.

Another option is, that despite the fact that remyelination contributes to axonal preservation and functional recovery (Duncan et al., 2009), alterations to the newly formed myelin, such as the change in thickness, internodal length and protein or lipid composition, could compromise axonal survival in the long term. Minor alterations in myelin membrane composition can trigger neurodegeneration (Nave and Trapp 2008). Thus, it could be possible that the changes in myelin composition occurring after episodes of demyelination and remyelination are sufficient to induce neuronal dysfunction that only become apparent when mice age.

Interestingly, similar changes in the proteome of myelin from animals that have undergone remyelination and in myelin from old animals has been found (Manrique-Hoyos et al., 2011). This does not exclude the possibility that the minor alterations occurring in remyelinated myelin results in subtle changes in axonal function that may only become functionally relevant after a certain age. In addition, the induction of two episodes of cuprizone-induced demyelination in our study did not increase late-onset axonal dysfunction and motor decline in our model compared to a single demyelination. This finding indicates that the critical threshold is already reached after one round of demyelination and remyelination. Interestingly, in MS the onset of the progressive phase is independent of number of relapses and age is the most important risk factor that determines when chronic progressive MS is set off (Confavreux et al., 2003; Kremenchutzky et al., 2006).

While the reversible disability observed during initial inflammatory episodes is caused in part by a transient conduction block due to the edema that accompanies the infiltration through the BBB, in chronic stages or SPMS the progressive disability seems to be correlated with irreversible axonal degeneration. It is widely accepted that axonal loss is a key determinant for permanent disability beginning at disease onset and correlating with the degree of inflammation within lesions in patients with MS (Bitsch et al., 2000; Bjartmar and Trapp, 2003) and can be observed both in inflammatory and chronic demyelination (Trapp et al., 1998; Dutta et al., 2006). In this study, we showed that a cuprizone-induced

demyelination causes a massive axonal loss in the corpus callosum without a reduction of cortical neuronal soma. Interestingly, in MS axonal loss is more frequently found than loss of neuronal cell bodies (Trapp and Nave, 2008). We measured massive axonal loss, evidenced by the shrinkage of the corpus callosum thickness, a decrease in neurofilament signal and in axonal counts. This loss seems to continue occurring beyond 6 weeks of remyelination indicating a progressive axonal loss.

The capacity of cortical adaptation after injury has been demonstrated in both experimental models and in MS patients. These studies have shown cortical adaptive changes occurring concurrently with the progression of axonal injury (Reddy et al., 2000; Faivre et al., 2012). Once structural damage is so extensive that compensation mechanisms are insufficient to correctly execute a given task, functional deficit will become evident. If the axonal pathology is indeed more frequent early in disease, it is possible that the brain has a greater capacity to compensate and is able to recover from early axonal damage. As axonal loss continues and the brain ages, a critical threshold may be reached, where compensatory mechanisms are exhausted, and clinical symptoms reappear, unmasking the long-term consequences of the demyelinating insult (Bjartmar and Trapp, 2003; Trapp et al., 1999).The mechanisms limiting the extent of compensation of axonal pathology that ultimately triggers the transition from RRMS to SPMS remain unclear.

4.2.3   Relevance of MS animal models and final remarks

A major difficulty when studying animal models of MS is that the etiology of the disease and its progression mechanisms are largely unknown. The translation of experimental findings into effective treatment of MS patients has been mostly limited to the inflammatory stages of the disease (Steinman, 1999; Steinman and Zamvil, 2006). The different animal models of MS attempt to recreate the different components and courses of the disease but none has satisfactorily captured all aspects of MS and therefore do not guarantee successful translation of experimental results to applications in a clinical setting. In addition, the inbred nature of most of the animals used in MS models generates a rather homogeneous immunological background and response, which does not reflect the reality of the human population afflicted by MS.

Since each MS model appears to address different aspects of the disease, combinations of several models have been used as attempts to integrate the different mechanisms and

processes observed in MS. However, the outcome is frequently unexpected and complicates the analysis and interpretation of the results. For instance, the combination of selective ablation of a cell lineage in mice using diphtheria toxin is limited to models that do not involve an immunization of mice like EAE, since it has been found that immunization of mice results in the sensitization to DT (Holmes, 2000; Meyer zu Hoerste et al., 2010). On the other hand, the clinical course of DT-induced demyelination is not modified by the repression or exacerbation of the immune response, as the demyelination and axonal loss appears to occur independently of the adaptive immune system (Pohl et al., 2011; Locatelli et al., 2012a). Surprisingly, in one combinatorial experiment it was found that a pre-treatment with cuprizone prior to EAE induction by MOG injection significantly ameliorated the clinical score and decreased the autoimmune inflammation (Maña et al., 2009).

While the use of several models may be able to capture more features of a highly complex disease such as MS, each model carries distinct disadvantages. In our case, one of the disadvantages of the cuprizone model is that the exact underlying mechanism is not clear. Although it appears to selectively trigger oligodendrocyte death, it can also affect liver metabolism, as well as some T cell activity (Emerson et al., 2001). This may complicate investigations of the immune reaction in demyelination caused by primary oligodendropathy. The DT model presented in this work allows for highly specific widespread oligodendrocyte death but its severity does not allow the study of remyelination and functional recovery, which is extensive in MS. Therefore, it is crucial to further explore and develop new models that resemble MS in its immunopathology and clinical course, or carefully interpreting the results when combining more than one of the existing models.

In the past, several hypothesis regarding the etiology of the MS have been proposed. However, none have been able to account for the majority of the symptoms nor the diversity of cases. Genetic, environmental, viral, and lifestyle factors have been proposed as contributors to the susceptibility and triggering of the disease. Even though it has widely assumed that MS is primarily an autoimmune disorder, the possibility of a primary oligodendrogliopathy as the cause of MS has been proposed. Additionally, the possibility that MS is actually a group of diseases that share similar symptoms has emerged (Owens et al., 2011; Gourraud et al., 2012; Nakahara et al., 2012; Stys et al., 2012).

4.3   Proteomic screening of candidates for axoglial communication

Large-scale proteomic and transcriptomic analysis have proven to be powerful tools for the identification of myelin-associated proteins (Colello et al., 2002; Taylor et al., 2004; Jahn et al., 2009b), genes involved in oligodendrocyte differentiation (Nielsen et al., 2006; Cahoy et al., 2008; Baer et al., 2009), proteins relevant in myelin structural organization (Werner et al., 2007) or proteome changes after remyelination (Werner et al., 2010). We have performed an extensive proteomic analysis of myelin fractions aimed to identify proteins involved in axo-glial communication.

Except for the first layer, which is in direct contact with the axon, the majority of myelin is composed by a highly compacted, lipid-rich membrane layers. This facilitates the isolation of myelin domains in a sucrose gradient, based on their light density. We observed an enrichment of MAG and Neurofascin, characteristic of the periaxonal and paranodal/nodal regions respectively, at a slightly heavier fraction (0.9 M-1.0 M) than that usually used to isolate myelin (0.32-0.85 M) (Norton and Poduslo, 1973). The enrichment of non-compact proteins in the 0.9-10 M fraction is congruent with the myelin peak observed in *shiverer* mice at approximately 0.85-0.9 M sucrose (Bourre et al., 1980). As shiverer mice lack MBP and thus compact myelin, it indicates that non-compact myelin tends to float a that density.

We included myelin isolated on the postnatal day 14 (P14) in our proteomic analysis, since at this time-point myelination is still ongoing. Therefore, proteins important for initial axo-glial contact are assumed to be present, and compacted myelin represents a smaller fraction than in mature myelin. In addition, we successfully isolated myelin-associated glycoproteins using different lectin beads (ConA and WGA for mouse myelin, and lectin-lentil for human myelin). This combined analysis of myelin fractions resulted in a total of 1904 identified proteins. This database was taken as the starting point for the selection of novel candidates in axo-glia communication and myelination.

First, we selected candidates that were predicted to contain a signal peptide and a trans-membrane domain, as it would be expected that proteins involved in axo-glial communication are exposed at the cell surface in order to interact with adjacent cells. However, this

method can result in the exclusion of GPI-anchored proteins despite the fact that they are indeed exposed to the extracelullar space. GPI-anchored proteins lack a transmembrane domain in their mature form but present a hydrophobic stretch, which is cleaved in the ER as a post-translational modification and replaced with glycosylphosphatidylinositol. Fatty acids from phosphatidyl-inositol group allow the anchoring of the protein to the exterior face of the cell membrane. A glycosphingolipids and cholesterol-enriched environment such as myelin favors the targeting of this type of proteins (Krämer et al., 1997).

In addition, as GPI-anchored proteins can act as cell-adhesion molecules or associate in *cis* to proteins that can trigger downstream cascades and generate responses in the cell, they should be considered potential candidates. Indeed, PSA-glycosylation of the glial GPI-anchored protein NCAM-120 inhibits myelin formation. Also, the axonal protein Contactin, which interacts with Caspr and Neurofascin-155 in the orfanization of the paranodes (Tait et al., 2000; Rios et al., 2000), is a GPI-anchored protein as well.

Although the presence of the hydrophobic stretch in GPI-anchored proteins in occasions resulted in the prediction of a transmembrane domain in our analysis, it was inconsistent. Even though all proteins from the IgLON family are GPI-anchored, Lsamp was predicted to have a transmembrane, Opcml was not, and Neurotrimin had incongruous results: while it was not predicted to have a transmembrane domain in the mouse samples, the human Neurotrimin isoform 2 did. Even though TMHMM and Phobius resulted useful in the prediction of transmembrane domains, GPI-anchored proteins would require additional prediction method to detect them consistently, as big-PI Predictor `http://mendel.imp.ac.at/gpi/cgi-bin/gpi_pred.cgi`(Eisenhaber et al., 1999).

Following our proteomic analysis, we established a battery of functional assays to help elucidate the role of candidate proteins in the axoglial communication. In the present study, we used the IgLON family proteins Lsamp, Opcml and Ntm as candidates, and used Necl1, Necl4 and MCAM-Fc as controls. These methods are intended to be used also as future assay battery for other novel candidates in axo-glial communication. IgLON proteins have previously been described to be expressed in neurons and mediate neurite outgrowth regulation (Gil et al., 1998; Lodge et al., 2000; Reed et al., 2004). However, they have been suggested to have additional roles in recognition and cell adhesion (McNamee

et al., 2002). As they have previously been shown to be expressed in neurons, we focused on developing functional assays to determine the response on oligodendrocytes.

We evaluated the effect of our candidate proteins on the intrinsic behavior and development of oligodendrocytes by analyzing changes in proliferation, migration and differentiation patterns. We did not observe any significant changes in these processes induced by IgLON proteins. Adhesion and myelination assays were performed to evaluate the effect of the candidates on the interaction between oligodendrocytes and neurons. While we did not observe a significant effect on the adhesion of oligodendrocytes, we observed a reduction in myelination in samples where Ntm-Fc was added to the media.

The addition of a soluble fusion protein can inhibit intercellular communication blocking binding sites or it could trigger a response in the cell it binds to. The reduction in myelination efficiency could be explained in different ways: either the soluble protein blocks binding sites involved in myelination initiation (interaction interference), it induces oligodendrocytes to not myelinated but rather enter the default sheet formation (effect on oligodendrocytes), or it exerts an effect on axonal organization that hinders myelination to occur (effect on axons). This type of assay has been useful to elucidate the role of Necl4 in myelination in the PNS (Spiegel et al., 2007) and L1 in CNS myelination (Laursen et al., 2009). Our results propose Ntm as an interesting candidate in axo-glial interaction and further analysis remain to be done to elucidate the mechanism and specific role of the protein. Assays inducing neuronal downregulation of the proteins would facilitate understanding their role.

Myelin is a highly compacted structure, and it has been found that proteins with a cytoplasmic domain larger than 30 aminoacids are excluded from the compact, MBP-positive sheets in oligodendrocytes *in vitro*; PLP tagged with intracellular EGFP is also restricted from entering compact myelin *in vivo* (Aggarwal et al., 2011). GPI-anchored glycoproteins can theoretically freely diffuse along myelin compacted and non-compacted areas, allowing the incorporation of glycoproteins along myelin. This could facilitate the establishment of intercellular contact sites or theoretically, inter-lamellar adhesion. Even though the exogenous expression of full length constructs showed that the IgLON proteins distribute throughout compact, MBP-positive areas in primary oligodendrocytes, the actual expression and distribution patterns remain to be elucidated. The interaction

molecule(s) expressed in oligodendrocytes, which could be, but is not limited to, a member of the IgLON family itself, remains to be identified.

It is important to highlight that the exploratory approach of this study implies the selection of proteins that are not yet fully described, or even known. Therefore, the availability of functional antibodies can be limited and has been one of the principal difficulties encountered. The characterization of the expression profile of a candidate allows to identify the type of cell, the moment in development where the protein is expressed, and facilitates the selection of relevant functional assays. However, the development and acquisition of antibodies for a large number of proteins during a screening process is not feasible.

For this reason, we established a binding assay as a screening method and a set of functional tests that can be applied universally to any candidate protein as long as it has a known aminoacid sequence, using tags as Fc and myc, which allow the detection and purification of the protein. Therefore a battery of tests presented in this study is a useful method to evaluate potential candidates previous to antibody generation (when commercially unavailable), and *in vivo* gene silencing. In addition, the proteomic database generated by the analysis of myelin fractionation and glycoprotein isolation provides a valuable source of novel candidates of axo-glial communication and myelination in the CNS.

Chapter 5

Summary and conclusions

In demyelinating diseases like multiple sclerosis (MS), myelin is damaged but can be replaced by a thinner myelin sheath. Remyelination restores saltatory conduction and is thought to contribute to the functional recovery in MS. However, even if remyelination is extensive, most patients enter a progressive phase with continuous accumulation of neurological deficits (SPMS), questioning the role of myelin on the long-term survival of axons.

Two toxin-based demyelinating models, which do not involve an autoimmune response or blood-brain barrier disruption, were used to study the effect of demyelination on axonal integrity. To study the short-term impact of demyelination, histological analysis was performed in samples from a mouse model where myelinating oligodendrocytes are ablated by the expression of diphtheria toxin receptor in mature oligodendrocytes and systemic diphtheria toxin injection. We observed, in accordance to studies using similar models, that the animals became severely ill, and that demyelination of the corpus callosum was accompanied by microglia activation and axonal damage. We showed that the use of systemic oligodendrocyte ablation through the targeted effect of diphtheria toxin is an effective and highly specific model of demyelination. However, due to its clinical severeness it was not possible to observe remyelination and recovery of the animals. Therefore, this model is very useful in studying the most acute stages of demyelination and could be used to develop strategies to minimize the extent of axonal damage and cytotoxic inflammatory response resulting from oligodendrocyte death and myelin loss.

In addition, to analyse the consequence of demyelination in the long-term, we used the cuprizone model of de- and remyelination. We aimed at establishing an animal model that mimics aspects of progressive MS, which is characterized by late-onset progressive neurological deficits, often in the absence of active inflammation. This model induces demyelination most prominently in the corpus callosum and superior cerebellar peduncle, does not involve the infiltration of the immune system through the blood-brain barrier, and is associated with extensive remyelination and recovery. We observed that after one or two demyelinating events, animals recovered to an extent that they became undistinguishable from age-matched controls. However, they presented late-onset motor impairment, showing that functional recovery was not permanent and latent consequences become detectable in the long-term. Single and repeated cuprizone-induced demyelinating events have shown similar long-term functional motor readouts.

These functional deficits were accompanied by a substantial loss of axons in the corpus callosum and extensive, but incomplete remyelination.These findings suggest that there is a yet unknown trigger of axonal dysfunction at late stages of remyelination. Both unmyelinated and myelinated axons exhibit acute damage evidenced with APP accumulation. This is a non-inflammatory model of demyelination with ongoing axonal damage in both acute and chronic stages, making it especially useful for testing neuroprotective treatment strategies. The use of models in which de- and remyelination are restricted to defined/reproducible areas of the CNS can facilitate the study of axonal preservation and functional recovery after remyelination.

Finally, we successfully generated an extensive list of 1904 proteins potentially associated to myelin axo-glial contact sites and a set of functional assays to choose and evaluate the role of candidate proteins in oligodendrocyte life-cycle and myelin formation *in vitro*. We have identified a family of proteins (IgLON) as potential candidates that appear to interact with both neurons and oligodendrocytes, with the presence of soluble neurotrimin having a negative effect on myelination efficiency *in vitro*. Further exploration of their role *in vivo* is necessary to the elucidate their function in myelination in the CNS.

Chapter 6

Appendix: Complete myelin proteomics list

6.0.1 Complete list of proteins identified in myelin samples analysed with LC-MS/MS.

In summary, we isolated different fractions of myelin from C57/BL6 mice (1-5) or human brain samples (6) and analyzed them with mass spectrometry:

1. Myelin isolated from postnatal day 14 brain homogenate in a discontinuous sucrose gradient ("P14 (myelin)"), 0.32M/0.85M interphase (Norton and Poduslo, 1973).

2. Purified myelin solubilised with 1% Triton X-100 overnight and bound to ConA beads ("ConA myelin")

3. Purified myelin bound to WGA beads ("WGA myelin").

4. Myelin isolated from brain homogenate subjected to an initial hyposmotic shock with water and then subjected to a continuous gradient, fraction 0.9-1 M sucrose ("Continuous (myelin)").

5. Myelin isolated from brain homogenate subjected to an initial discontinuous gradients and collected from 0.32-1.2 M interphase (crude myelin) and subsequently subjected to a continuous sucrose gradient. Collected from Fraction 3, or 0.9-1 M sucrose ("Continuous (brain)").

6. Glycoprotein from human myelin preparation , subjected to a lentil-lectin column (Mathey et al., 2007), kindly provided by Edgar Meinl, Max Planck Institute of Neurobiology, Munich ("Human Myelin").

The complete list of proteins identified based on unique peptide count is included. The electronic version of the list as a spreadsheet is found at the folder \\em-filer\ag-simons \Manrique\proteomics at the server of the Max Planck Institute of experimental medicine, Göttingen.

#	Accession Number	Identified Proteins (1904)	P14 (myelin)	Continous (brain)	Continous (myelin)	ConA (myelin)	WGA (myelin)	Human myelin
1	gi|4507729	tubulin beta-2A chain [Homo sapiens], gi|3385	29	34	22	7	0	28
2	gi|148692349 (+2)	ATPase, Na+/K+ transporting, alpha 3 polypep	49	64	61	11	21	0
3	gi|6755901 (+1)	tubulin alpha-1A chain [Mus musculus], gi|1156	28	36	18	6	4	22
4	gi|13591880 (+1)	myelin proteolipid protein [Rattus norvegicus],	9	12	14	9	10	12
5	gi|11935049 (+1)	keratin 1 [Homo sapiens], gi|39794653|gb|AAF	0	0	0	0	0	53
6	gi|69885032	myelin basic protein isoform 1 [Mus musculus]	12	18	20	12	2	0
7	gi|148670605 (+2)	cyclic nucleotide phosphodiesterase 1, isoform	37	41	41	31	14	0
8	gi|187956886 (+2)	Spna2 protein [Mus musculus]	78	161	90	0	10	0
9	gi|126012562 (+1)	prolow-density lipoprotein receptor-related prot	0	0	0	0	0	133
10	gi|4501885 (+6)	actin, cytoplasmic 1 [Homo sapiens], gi|66715(	24	23	14	7	7	23
11	gi|119611400	tenascin R (restrictin, janusin), isoform CRA_a	0	0	0	0	0	46
12	gi|6680748 (+1)	ATP synthase subunit alpha, mitochondrial pre	18	48	52	20	14	0
13	gi|55959403	neurofascin homolog (chicken) [Homo sapiens	0	0	0	0	0	62
14	gi|37360088 (+1)	mKIAA0778 protein [Mus musculus], gi|148707	15	43	38	0	0	0
15	gi|15804371 (+5)	thioredoxin [Escherichia coli O157:H7 EDL933	4	4	4	4	4	4
16	gi|117938332	spectrin beta chain, brain 1 isoform 1 [Mus mu	64	117	85	0	0	0
17	gi|158260531 (+2)	unnamed protein product [Homo sapiens]	0	0	0	0	0	43
18	gi|119581085 (+3)	keratin 10 (epidermolytic hyperkeratosis; kerat	0	0	0	0	0	37
19	gi|47132620	keratin, type II cytoskeletal 2 epidermal [Homo	0	0	0	0	0	40
20	gi|22094075	ADP/ATP translocase 2 [Mus musculus], gi|170	6	25	32	0	3	0
21	gi|55956899	keratin, type I cytoskeletal 9 [Homo sapiens], g	0	0	0	0	0	31
22	gi|6981602	syntaxin-binding protein 1 [Rattus norvegicus],	22	42	26	5	3	13
23	gi|23272966 (+3)	Atp5b protein [Mus musculus]	14	24	25	18	12	0
24	gi|134288917	cytoplasmic dynein 1 heavy chain 1 [Mus muso	72	124	12	0	0	0
25	gi|120538513 (+2)	Contactin 2 (axonal) [Homo sapiens]	0	0	0	0	0	47
26	gi|225735584 (+1)	hexokinase-1 isoform HK1 [Mus musculus], gi|	15	37	61	0	0	0
27	gi|26339872	unnamed protein product [Mus musculus]	0	45	55	0	2	0
28	gi|56788381 (+3)	myelin-oligodendrocyte glycoprotein isoform al	0	0	0	0	0	19
29	gi|33438248 (+2)	mKIAA0034 protein [Mus musculus]	46	72	26	0	0	0
30	gi|119603966 (+5)	protein tyrosine phosphatase, receptor-type, Z	0	0	0	0	0	19
31	gi|86792778	dipeptidyl aminopeptidase-like protein 6 isoforr	0	0	0	0	0	41
32	gi|119607840 (+1)	tenascin C (hexabrachion), isoform CRA_a [Hc	0	0	0	0	0	58
33	gi|119630409 (+1)	neural cell adhesion molecule 2, isoform CRA_	0	0	0	0	0	44
34	gi|496140	AMPA selective glutamate receptor [Mus muso	2	19	9	0	0	0
35	gi|4507157	sortilin-related receptor preproprotein [Homo sa	0	0	0	0	0	61
36	gi|10720404 (+2)	RecName: Full=Voltage-dependent anion-sele	9	23	24	0	5	0
37	gi|300680975	RecName: Full=Lectin alpha chain; Contains: I	2	0	0	3	2	2
38	gi|262118282	plexin-A1 precursor [Homo sapiens], gi|313104	0	0	0	0	0	50
39	gi|27369581	calcium-binding mitochondrial carrier protein A	6	34	39	5	2	0
40	gi|28373117	contactin-1 isoform 1 precursor [Homo sapiens	0	0	0	0	0	49
41	gi|148747424 (+1)	ADP/ATP translocase 1 [Mus musculus], gi|219	6	17	17	2	2	0
42	gi|117606275 (+1)	excitatory amino acid transporter 2 isoform 2 [N	10	19	15	0	0	0
43	gi|55926127	spectrin beta chain, brain 2 [Mus musculus], gi	14	62	67	0	0	0
44	gi|189054749 (+2)	unnamed protein product [Homo sapiens]	0	0	0	0	0	35
45	gi|112363107	neurofilament medium polypeptide [Mus muscu	31	45	7	0	0	0
46	gi|164448632 (+1)	neural cell adhesion molecule 1 isoform 3 [Mus	28	23	12	0	6	0
47	gi|119600163 (+1)	activated leukocyte cell adhesion molecule, isc	0	0	0	0	0	34
48	gi|123230374	dynamin 1 [Mus musculus]	26	40	36	3	0	0
49	gi|39204499	neurofilament light polypeptide [Mus musculus	31	41	15	0	0	0
50	gi|148689581 (+4)	mCG10343, isoform CRA_c [Mus musculus]	4	17	17	0	2	0
51	gi|122065897 (+3)	RecName: Full=Plectin; Short=PCN; Short=PL	0	138	4	0	0	0
52	gi|62201487 (+1)	Glyceraldehyde-3-phosphate dehydrogenase [	16	21	8	3	0	0
53	gi|5174735 (+1)	tubulin beta-2C chain [Homo sapiens], gi|2216	7	10	6	2	0	5

54	gi|1815649 (+2)	telencephalin precursor [Homo sapiens]	0	0	0	0	0	28
55	gi|148667088 (+4)	ATPase, Ca++ transporting, plasma membrane	16	44	24	0	0	0
56	gi|164607137	guanine nucleotide-binding protein G(o) subun	15	21	15	7	0	0
57	gi|39104626 (+1)	mKIAA0968 protein [Mus musculus]	10	24	12	0	0	0
58	gi|40254595	dihydropyrimidinase-related protein 2 [Mus mu	25	26	10	0	0	0
59	gi|18079339 (+2)	aconitate hydratase, mitochondrial precursor [N	14	33	35	0	0	0
60	gi|148668412 (+1)	synapsin I, isoform CRA_b [Mus musculus]	17	27	23	0	0	0
61	gi|229892316 (+1)	NADH-ubiquinone oxidoreductase 75 kDa sub	5	31	35	3	9	0
62	gi|6754036	aspartate aminotransferase, mitochondrial [Mu	8	25	23	0	0	0
63	gi|21361322 (+1)	tubulin beta-4 chain [Homo sapiens], gi|319819	6	8	6	0	0	6
64	gi|12963615 (+1)	tubulin beta-3 chain [Mus musculus], gi|145966	11	15	5	0	0	0
65	gi|94721261	2',3'-cyclic-nucleotide 3'-phosphodiesterase [H	0	0	0	0	0	26
66	gi|23503267 (+1)	ectonucleotide pyrophosphatase/phosphodiest	0	0	0	0	0	23
67	gi|157738645	plexin-A4 isoform 1 [Homo sapiens], gi|108860	0	0	0	0	0	35
68	gi|16445029 (+1)	immunoglobulin superfamily member 8 [Homo	0	0	0	0	0	19
69	gi|148539957	alpha-internexin [Mus musculus], gi|17390900|	23	39	10	0	0	0
70	gi|55770878	neuronal pentraxin-1 precursor [Homo sapiens	0	0	0	0	0	25
71	gi|6651380 (+2)	NgCAM-related related cell adhesion molecule	0	0	0	0	0	37
72	gi|12846616 (+3)	unnamed protein product [Mus musculus]	11	11	6	0	0	0
73	gi|261278070	AMPA-selective glutamate receptor 3 flop type	0	8	4	0	0	0
74	gi|21361116 (+2)	versican core protein isoform 1 precursor [Hom	0	0	0	0	0	18
75	gi|13242237 (+3)	heat shock cognate 71 kDa protein [Rattus nor	29	33	19	0	0	0
76	gi|6755965	voltage-dependent anion-selective channel pro	3	13	17	0	0	0
77	gi|6753138 (+1)	sodium/potassium-transporting ATPase subun	9	14	11	3	4	0
78	gi|22267442 (+1)	cytochrome b-c1 complex subunit 2, mitochond	8	21	27	8	10	0
79	gi|148694984 (+2)	glycerol phosphate dehydrogenase 2, mitocho	0	38	42	0	0	0
80	gi|262527579 (+2)	RecName: Full=Voltage-dependent calcium ch	0	0	0	0	0	24
81	gi|16307541 (+1)	Atp1a1 protein [Mus musculus]	17	25	20	4	0	0
82	gi|113722116 (+3)	plexin-A2 precursor [Homo sapiens], gi|251757	0	0	0	0	0	38
83	gi|6981600	syntaxin-1B [Rattus norvegicus], gi|13259378|r	7	20	10	0	0	0
84	gi|124286811 (+1)	neurofilament heavy polypeptide [Mus muscul	19	33	4	0	0	0
85	gi|6678197 (+1)	synaptotagmin-1 [Mus musculus], gi|1174545|s	13	22	10	0	0	0
86	gi|6681273	elongation factor 1-alpha 2 [Mus musculus], gi|	14	13	8	7	0	0
87	gi|124244033 (+1)	microtubule-associated protein 1A isoform 1 [M	19	45	0	0	0	0
88	gi|124487263	gamma-aminobutyric acid type B receptor sub	0	4	0	0	0	0
89	gi|3334470	RecName: Full=Myelin-associated glycoprotein	7	8	15	13	5	0
90	gi|32015 (+1)	alpha-tubulin [Homo sapiens], gi|1333692|emb	3	7	3	0	0	3
91	gi|171543853	microtubule-associated protein 1B [Mus muscu	18	45	4	0	0	0
92	gi|148665587 (+2)	limbic system-associated membrane protein [N	7	8	5	0	2	0
93	gi|18426911	tyrosine-protein phosphatase non-receptor typ	0	0	0	0	0	26
94	gi|119588266 (+6)	hCG1990378, isoform CRA_c [Homo sapiens]	0	0	0	0	0	30
95	gi|1195531 (+1)	type I keratin 16 [Homo sapiens]	0	0	0	0	0	19
96	gi|12025532 (+2)	V-type proton ATPase 116 kDa subunit a isofo	11	26	8	0	0	0
97	gi|148667815 (+1)	mCG121680 [Mus musculus]	24	27	0	0	0	0
98	gi|28395018	junction plakoglobin [Mus musculus], gi|83305	8	9	12	12	4	0
99	gi|6005854	prohibitin-2 isoform 2 [Homo sapiens], gi|1267	5	19	22	0	0	12
100	gi|31981562 (+1)	pyruvate kinase isozymes M1/M2 [Mus muscu	22	25	3	0	0	0
101	gi|148666993 (+2)	inositol 1,4,5-triphosphate receptor 1, isoform (	8	48	8	0	0	0
102	gi|183396771 (+2)	60 kDa heat shock protein, mitochondrial [Mus	16	29	31	4	0	0
103	gi|78214312	ATP synthase subunit b, mitochondrial precurs	2	18	21	3	2	0
104	gi|10946574 (+2)	creatine kinase B-type [Mus musculus], gi|4172	16	17	6	0	0	0
105	gi|19526960	dynamin-like 120 kDa protein, mitochondrial is	0	19	38	0	0	0
106	gi|6680045 (+1)	guanine nucleotide-binding protein G(I)/G(S)/G	14	15	14	0	2	9
107	gi|15030102 (+1)	Sdha protein [Mus musculus]	6	18	34	3	0	0
108	gi|148680322	ankyrin 2, brain, isoform CRA_b [Mus muscul	6	40	9	0	0	0

109	gi|115511052 (+1)	myosin-Va [Mus musculus]	5	43	10	0	0	0
110	gi|6755588	synaptosomal-associated protein 25 [Mus mus	17	20	14	0	0	2
111	gi|21311845	mitochondrial glutamate carrier 1 [Mus muscul	4	12	14	0	0	0
112	gi|119597945 (+1)	ADAM metallopeptidase domain 10, isoform C	0	0	0	0	0	22
113	gi|84000448	glial fibrillary acidic protein isoform 2 [Mus mus	3	24	18	0	0	0
114	gi|116256510 (+2)	AP-2 complex subunit alpha-1 isoform b [Mus	18	34	13	0	0	0
115	gi|56206143 (+1)	oxoglutarate dehydrogenase (lipoamide) [Mus	8	25	38	0	0	0
116	gi|113199771 (+2)	myelin-oligodendrocyte glycoprotein [Mus mus	5	11	11	9	6	0
117	gi|158635979 (+2)	sarcoplasmic/endoplasmic reticulum calcium A	14	25	10	0	0	0
118	gi|31982186	malate dehydrogenase, mitochondrial precursc	18	25	24	0	0	0
119	gi|10835015 (+4)	gamma-aminobutyric acid type B receptor subt	0	0	0	0	0	18
120	gi|148679695 (+1)	cytochrome c oxidase subunit IV isoform 1, iso	3	17	18	0	0	0
121	gi|6671539	fructose-bisphosphate aldolase A isoform 2 [M	22	21	8	0	0	0
122	gi|16580128 (+2)	dihydrolipoamide S-acetyltransferase precursc	6	18	19	0	2	0
123	gi|28173550	septin-7 [Mus musculus]	12	16	13	7	0	0
124	gi|24233554 (+2)	excitatory amino acid transporter 1 [Mus musc	3	10	9	0	0	0
125	gi|119608548 (+1)	olfactomedin 1, isoform CRA_a [Homo sapiens	0	0	0	0	0	18
126	gi|148671850 (+1)	mCG13557, isoform CRA_c [Mus musculus]	3	18	20	2	0	0
127	gi|148702861 (+1)	fatty acid synthase, isoform CRA_a [Mus musc	30	33	6	0	0	0
128	gi|31543349 (+1)	vesicle-fusing ATPase [Mus musculus], gi|146:	15	31	22	0	0	0
129	gi|7106439 (+2)	tubulin beta-5 chain [Mus musculus], gi|27465!	4	5	2	0	0	3
130	gi|7861733 (+1)	low density lipoprotein receptor related protein-	0	0	0	0	0	38
131	gi|119395754 (+2)	keratin, type II cytoskeletal 5 [Homo sapiens],	0	0	0	0	0	15
132	gi|124487407 (+1)	protein bassoon [Mus musculus]	0	41	2	0	0	0
133	gi|189386 (+3)	oligodendrocyte-myelin glycoprotein [Homo sa	0	0	0	0	0	13
134	gi|16128817	glutaredoxin 1, redox coenzyme for ribonucleo	2	3	4	2	2	2
135	gi|148689693	mCG13663, isoform CRA_b [Mus musculus]	11	19	10	0	0	0
136	gi|56205559	myosin, heavy polypeptide 10, non-muscle [Mu	13	50	18	0	0	0
137	gi|13470090	ras-related protein Rab-3C [Mus musculus], gi|	8	14	6	0	2	0
138	gi|118200813 (+2)	cytochrome c oxidase subunit II [Mus musculu:	4	7	7	0	0	0
139	gi|178855 (+5)	apolipoprotein J precursor [Homo sapiens]	0	0	0	0	0	21
140	gi|148692167 (+2)	sirtuin 2 (silent mating type information regulat	12	15	20	8	2	0
141	gi|12840425 (+2)	unnamed protein product [Mus musculus]	4	11	17	0	0	0
142	gi|27552760 (+2)	mitochondrial import receptor subunit TOM70 [	0	23	32	0	0	0
143	gi|119588218 (+1)	hCG2036598, isoform CRA_a [Homo sapiens]	0	0	0	0	0	18
144	gi|148692928 (+1)	glutamate dehydrogenase 1 [Mus musculus]	11	23	15	0	0	0
145	gi|7106335	keratin, type I cytoskeletal 17 [Mus musculus],	5	4	7	5	4	0
146	gi|148696104 (+1)	creatine kinase, mitochondrial 1, ubiquitous, is	6	12	19	9	0	0
147	gi|28972652	mKIAA1176 protein [Mus musculus]	6	20	8	0	0	0
148	gi|119609949 (+1)	lectin, galactoside-binding, soluble, 3 binding p	0	0	0	0	0	17
149	gi|12803709 (+2)	Keratin 14 [Homo sapiens], gi|17512236|gb|AA	0	0	0	0	0	11
150	gi|148676868 (+2)	tyrosine 3-monooxygenase/tryptophan 5-mono	19	18	4	0	3	0
151	gi|14548301 (+2)	RecName: Full=Cytochrome b-c1 complex sut	0	18	24	0	4	0
152	gi|152013069 (+5)	PCDH9 protein [Homo sapiens]	0	0	0	0	0	13
153	gi|312222784	voltage-dependent anion-selective channel prc	2	12	16	0	0	0
154	gi|70778976 (+1)	phosphoglycerate kinase 1 [Mus musculus], gi	14	16	0	0	0	0
155	gi|148342506 (+2)	ITGAV protein [Homo sapiens]	0	0	0	0	0	31
156	gi|148671436 (+1)	mCG55033 [Mus musculus]	4	16	19	0	0	0
157	gi|116063560 (+1)	contactin-associated protein 1 precursor [Mus	5	16	15	0	0	0
158	gi|148677082 (+8)	microtubule-associated protein 4, isoform CRA	4	7	2	0	0	0
159	gi|113204613	microtubule-associated protein 6 isoform 1 [Mu	7	21	3	0	0	0
160	gi|6678674	L-lactate dehydrogenase B chain [Mus muscul	11	17	3	0	0	0
161	gi|21313640 (+1)	AP-2 complex subunit beta isoform b [Mus mu:	15	25	13	0	0	0
162	gi|161168987 (+1)	synapsin-2 isoform IIa [Mus musculus], gi|7392	5	16	11	0	0	0
163	gi|21644575 (+1)	leucine-rich repeat LGI family member 3 precu	0	5	14	2	0	0

#	gi	Description						
164	gi|31982755 (+2)	vimentin [Mus musculus], gi|138536|sp|P20152	3	29	3	0	0	0
165	gi|6679593	ras-related protein Rab-3A [Mus musculus], gi|	5	10	6	0	2	0
166	gi|47059013	keratin, type II cytoskeletal 73 [Mus musculus],	2	2	0	0	0	0
167	gi|148703035 (+1)	claudin 11 [Mus musculus]	0	2	4	2	0	0
168	gi|21312994	mitochondrial 2-oxoglutarate/malate carrier pro	0	16	17	0	0	0
169	gi|12833077 (+3)	unnamed protein product [Mus musculus]	0	10	11	0	4	0
170	gi|122441 (+4)	RecName: Full=Hemoglobin subunit alpha; Alt	4	4	0	0	0	0
171	gi|13385942	citrate synthase, mitochondrial precursor [Mus	11	15	18	0	0	0
172	gi|30061381 (+3)	histone H2B type 1-F/J/L [Mus musculus], gi|30	5	10	3	0	0	2
173	gi|31560731 (+1)	V-type proton ATPase catalytic subunit A [Mus	20	21	8	0	0	0
174	gi|12843458 (+2)	unnamed protein product [Mus musculus]	3	6	14	0	0	0
175	gi|1171564 (+3)	metabotropic glutamate receptor type 3 (mGlul	0	0	0	0	0	16
176	gi|119466532 (+2)	laminin subunit alpha-2 isoform b precursor [H	0	0	0	0	0	37
177	gi|34740335	tubulin alpha-1B chain [Mus musculus], gi|570	2	3	0	0	0	0
178	gi|21450129	acetyl-CoA acetyltransferase, mitochondrial pr	7	11	22	0	0	0
179	gi|40795897 (+2)	hornerin precursor [Homo sapiens]	0	0	0	0	0	16
180	gi|10645195 (+10)	histone H2A type 1-B/E [Homo sapiens], gi|195	4	6	3	0	0	0
181	gi|1103585 (+2)	laminin beta 2 chain [Homo sapiens]	0	0	0	0	0	37
182	gi|20521652 (+2)	KIAA0778 protein [Homo sapiens]	0	0	0	0	0	7
183	gi|112181182 (+1)	cytochrome c oxidase subunit 5A, mitochondria	2	7	8	0	3	0
184	gi|21165514 (+3)	leucine zipper-EF-hand containing transmemb	0	15	25	0	0	0
185	gi|9845511 (+4)	ras-related C3 botulinum toxin substrate 1 isof	5	7	5	0	0	3
186	gi|13278096 (+3)	Ndufs2 protein [Mus musculus]	0	16	21	0	0	0
187	gi|114644568	PREDICTED: keratin 6A [Pan troglodytes], gi|1	0	0	0	0	0	18
188	gi|12832533 (+1)	unnamed protein product [Mus musculus]	3	16	16	0	3	0
189	gi|16716499	sideroflexin-3 isoform 1 [Mus musculus], gi|201	2	12	16	0	0	0
190	gi|6679299	prohibitin [Mus musculus], gi|13937353|ref|NP_	3	15	12	0	2	0
191	gi|13543186 (+1)	Ndufa9 protein [Mus musculus]	0	12	16	0	0	0
192	gi|119964726 (+1)	cation-independent mannose-6-phosphate rec	0	0	0	0	0	34
193	gi|28373122	contactin-4 precursor [Homo sapiens], gi|5597(	0	0	0	0	0	17
194	gi|2988422 (+1)	agrin precursor [Homo sapiens]	0	0	0	0	0	24
195	gi|4502201 (+6)	ADP-ribosylation factor 1 [Homo sapiens], gi|6(	5	4	4	0	0	11
196	gi|148704589 (+1)	reticulon 1, isoform CRA_b [Mus musculus]	5	14	0	0	0	0
197	gi|170014720 (+1)	D-beta-hydroxybutyrate dehydrogenase, mitoc	4	11	17	0	0	0
198	gi|18152793 (+1)	pyruvate dehydrogenase E1 component subur	9	10	11	0	0	0
199	gi|6754254 (+1)	heat shock protein HSP 90-alpha [Mus muscul	19	12	5	0	0	0
200	gi|148705576 (+2)	collapsin response mediator protein 1, isoform	14	15	2	0	0	0
201	gi|11528518	synaptic vesicle glycoprotein 2A [Mus musculu	3	18	5	0	0	0
202	gi|108796657 (+1)	calcium/calmodulin-dependent protein kinase t	5	14	5	0	0	0
203	gi|4758988 (+1)	ras-related protein Rab-1A isoform 1 [Homo sa	9	9	8	2	0	2
204	gi|148672085	mCG144996 [Mus musculus]	0	2	2	2	2	0
205	gi|6678359 (+1)	transketolase [Mus musculus], gi|730956|sp|P4	17	19	7	0	0	0
206	gi|33859811 (+1)	trifunctional enzyme subunit alpha, mitochondr	0	18	25	0	0	0
207	gi|119576784 (+4)	sortilin 1 [Homo sapiens]	0	0	0	0	0	15
208	gi|4504301 (+5)	histone H4 [Homo sapiens], gi|4504303|ref|NP	5	10	3	0	0	2
209	gi|6680924	cofilin-1 [Mus musculus], gi|116849|sp|P18760	11	10	0	0	0	0
210	gi|298286902	RecName: Full=Neuroplastin; AltName: Full=S	7	11	4	0	0	0
211	gi|124517716	solute carrier family 12 member 2 [Mus muscu	9	14	18	3	0	0
212	gi|238637277 (+2)	4F2 cell-surface antigen heavy chain isoform a	4	16	15	0	0	0
213	gi|27370360 (+1)	sodium- and chloride-dependent GABA transp	3	6	9	0	0	0
214	gi|110625761	AFG3-like protein 2 [Mus musculus], gi|819145	0	14	32	0	0	0
215	gi|21313618	coiled-coil-helix-coiled-coil-helix domain-contai	0	15	18	0	0	0
216	gi|27805887 (+1)	guanine nucleotide-binding protein G(i) subuni	9	15	9	0	0	5
217	gi|162461907 (+2)	stress-70 protein, mitochondrial [Mus musculu	11	14	22	0	0	0
218	gi|148680577 (+3)	discs, large homolog 4 (Drosophila), isoform C	0	17	13	0	0	0

219 gi|119587611	neural cell adhesion molecule 1, isoform CRA_	0	0	0	0	0	9
220 gi|237858634 (+1)	neurofascin isoform 4 precursor [Mus muscule	0	5	7	4	0	0
221 gi|110625954 (+1)	NADH dehydrogenase [ubiquinone] flavoprotei	0	10	15	0	0	0
222 gi|163310765 (+3)	serum albumin precursor [Mus musculus], gi|5!	28	11	0	0	0	0
223 gi|13195624 (+1)	NADH dehydrogenase [ubiquinone] 1 alpha su	2	12	23	0	2	0
224 gi|15029315 (+5)	CYFIP2 [Mus musculus]	11	19	7	0	0	0
225 gi|119600869 (+1)	CUB and Sushi multiple domains 1, isoform CF	0	0	0	0	0	20
226 gi|222352127	protein sidekick-2 [Homo sapiens], gi|2964529	0	0	0	0	0	35
227 gi|6679261	pyruvate dehydrogenase E1 component subur	5	13	16	2	0	0
228 gi|31982332 (+1)	glutamine synthetase [Mus musculus], gi|1455	14	20	10	0	0	0
229 gi|122889350 (+4)	microtubule-associated protein tau [Mus musc	8	10	2	0	0	0
230 gi|28628069 (+3)	long-chain acyl-CoA synthetase [Mus musculu	0	19	18	0	0	0
231 gi|119584273 (+5)	cell adhesion molecule with homology to L1CA	0	0	0	0	0	26
232 gi|33563266	NADH dehydrogenase [ubiquinone] 1 alpha su	0	9	10	0	2	0
233 gi|148702066 (+4)	mCG7879, isoform CRA_a [Mus musculus]	12	12	2	0	2	0
234 gi|9938002	leucine-rich glioma-inactivated protein 1 precu	4	19	10	0	0	0
235 gi|18700646	coat protein [Tomato leaf curl Gujarat virus-[Va	0	0	0	7	0	0
236 gi|49574491	sodium/potassium-transporting ATPase subun	0	0	0	0	0	13
237 gi|33469051	tubulin polymerization-promoting protein [Mus	3	8	6	0	0	0
238 gi|166235165	synaptophysin [Mus musculus], gi|41019466|s|	5	9	3	0	0	0
239 gi|12963633	NADH dehydrogenase [ubiquinone] 1 alpha su	0	13	14	0	0	0
240 gi|6671664 (+1)	calnexin precursor [Mus musculus], gi|160333:	8	14	7	0	0	0
241 gi|27370092	elongation factor Tu, mitochondrial isoform 1 [N	0	12	15	0	0	0
242 gi|148690579	mCG21690 [Mus musculus]	0	21	13	0	0	0
243 gi|119583171 (+4)	hCG1985052, isoform CRA_c [Homo sapiens]	0	0	0	0	0	15
244 gi|5803225	14-3-3 protein epsilon [Homo sapiens], gi|2780	16	10	4	0	4	0
245 gi|19526814	NADH dehydrogenase [ubiquinone] flavoprotei	2	16	18	0	0	0
246 gi|6680954	contactin-1 precursor [Mus musculus], gi|2274!	10	10	9	0	2	0
247 gi|197725013 (+24)	Chain C, Crystal Structure Of Human Amsh-Lp	2	2	0	0	0	0
248 gi|119582304 (+7)	protocadherin 1 (cadherin-like 1), isoform CRA	0	0	0	0	0	9
249 gi|193502 (+1)	G alpha q subunit [Mus musculus]	15	13	13	3	0	0
250 gi|254553344	6-phosphofructokinase, muscle type [Mus mus	9	21	5	0	0	0
251 gi|148703906 (+4)	succinate-Coenzyme A ligase, ADP-forming, b	5	19	18	0	0	0
252 gi|23957686	neuronal membrane glycoprotein M6-a [Mus m	5	10	6	0	0	0
253 gi|6755080	protein kinase C gamma type [Mus musculus],	8	18	5	0	0	0
254 gi|112807195 (+2)	cytochrome c oxidase subunit 5B, mitochondri:	2	8	7	0	0	0
255 gi|119631685 (+4)	low density lipoprotein-related protein 2 [Homo	0	0	0	0	0	21
256 gi|74215924	unnamed protein product [Mus musculus]	13	11	2	0	0	0
257 gi|119611411 (+2)	astrotactin, isoform CRA_a [Homo sapiens]	0	0	0	0	0	22
258 gi|122065423 (+1)	RecName: Full=Latrophilin-3; AltName: Full=L	0	0	0	0	0	0
259 gi|32189434 (+3)	immunoglobulin superfamily member 8 [Mus m	3	9	10	7	0	0
260 gi|28461135	heat shock 70 kDa protein 12A [Mus musculus	14	15	11	0	0	0
261 gi|210147430	electrogenic sodium bicarbonate cotransporter	0	11	10	0	0	0
262 gi|60687506 (+1)	fructose-bisphosphate aldolase C [Mus muscu	15	13	0	0	0	0
263 gi|7710086	ras-related protein Rab-10 [Mus musculus], gi|	3	8	6	0	0	3
264 gi|18700024	isocitrate dehydrogenase 3, beta subunit [Mus	3	12	16	2	0	0
265 gi|148696430 (+3)	phospholipase C, beta 1, isoform CRA_b [Mus	6	13	17	7	0	0
266 gi|21361647	putative adenosylhomocysteinase 2 [Homo saj	3	12	7	0	0	0
267 gi|251823978 (+5)	pyruvate carboxylase, mitochondrial isoform 2	0	16	25	0	0	0
268 gi|256773218 (+3)	synaptojanin-1 isoform b [Mus musculus]	16	20	0	0	0	0
269 gi|114318997 (+5)	protease serine 1 [Homo sapiens]	0	0	0	0	0	2
270 gi|7330691 (+1)	MOBP170 [Mus musculus]	5	4	8	2	0	0
271 gi|70794816	hypothetical protein LOC433182 [Mus muscule	19	6	4	0	0	0
272 gi|70778915	moesin [Mus musculus], gi|462608|sp|P26041.	10	6	12	3	0	0
273 gi|58037109	NADH dehydrogenase [ubiquinone] 1 beta sul	0	8	9	0	2	0

274 gi|16877778 (+3)	Neurochondrin [Mus musculus]	11	11	0	0	0	0
275 gi|27151644 (+2)	RecName: Full=Neurotrimin; Flags: Precursor,	8	8	0	0	0	0
276 gi|6679935	neuromodulin [Mus musculus], gi|128101|sp|P(	18	9	5	0	0	0
277 gi|116089329	SRC kinase signaling inhibitor 1 [Mus musculu	3	27	10	0	0	0
278 gi|12843074 (+3)	unnamed protein product [Mus musculus]	0	10	11	0	0	0
279 gi|148707401 (+2)	tenascin R [Mus musculus]	5	8	5	2	0	0
280 gi|34610235	reticulon-4 isoform A [Mus musculus], gi|9473(	6	16	6	0	0	0
281 gi|148704970 (+5)	dihydrolipoamide dehydrogenase [Mus muscul	6	12	12	0	0	0
282 gi|30519943 (+1)	sorting and assembly machinery component 5(	0	15	18	0	0	0
283 gi|31980832 (+1)	keratin, type II cuticular Hb5 [Mus musculus], g	2	21	4	0	3	0
284 gi|123298865 (+2)	apoptosis-inducing factor, mitochondrion-asso(	2	11	21	0	0	0
285 gi|148681386 (+4)	succinate dehydrogenase complex, subunit B,	0	10	13	0	0	0
286 gi|239985513 (+1)	ATPase family AAA domain-containing protein	0	9	23	0	0	0
287 gi|148670554 (+7)	valosin containing protein, isoform CRA_b [Mu	26	10	2	0	0	0
288 gi|148700326 (+3)	phosphofructokinase, platelet, isoform CRA_e	5	16	0	0	0	0
289 gi|118026911	myosin-Id [Mus musculus], gi|81871936|sp|Q5	0	11	23	0	0	0
290 gi|123121395 (+6)	glycerol kinase [Mus musculus], gi|123250362	0	13	17	0	0	0
291 gi|293686	epidermal keratin subunit II [Mus musculus]	3	3	2	2	0	0
292 gi|163644277 (+2)	AP-2 complex subunit alpha-2 [Mus musculus]	13	20	6	0	0	0
293 gi|269994079	erythrocyte protein band 4.1-like 3 isoform B [N	4	13	14	0	0	0
294 gi|13385726 (+1)	cytochrome b-c1 complex subunit 7 [Mus muso	2	9	11	0	0	0
295 gi|109731459 (+7)	Grm2 protein [Mus musculus]	0	2	0	0	0	5
296 gi|123229245 (+3)	solute carrier family 44, member 1 [Mus muscu	2	8	9	8	0	0
297 gi|21313536 (+1)	dihydrolipoyllysine-residue succinyltransferase	5	10	9	0	0	0
298 gi|124487483 (+1)	2-oxoglutarate dehydrogenase-like, mitochond	0	14	20	0	0	0
299 gi|188219589 (+1)	lamin-B1 [Mus musculus], gi|17865719|sp|P14	9	22	0	0	0	0
300 gi|267844804	coiled-coil-helix-coiled-coil-helix domain-contai	0	11	15	0	0	0
301 gi|83715998	ATP synthase subunit e, mitochondrial [Mus m	0	9	11	0	0	0
302 gi|10938016 (+1)	claudin-11 isoform 1 [Homo sapiens], gi|66853	0	0	0	0	0	4
303 gi|13937391	guanine nucleotide-binding protein G(I)/G(S)/G	8	8	6	0	0	2
304 gi|148693872 (+4)	isocitrate dehydrogenase 3 (NAD+) alpha, isof	4	8	11	0	0	0
305 gi|62954774	CSMD2 protein [Homo sapiens]	0	0	0	0	0	22
306 gi|148667348 (+2)	mCG134299, isoform CRA_b [Mus musculus]	9	10	4	0	0	0
307 gi|148665718 (+3)	activated leukocyte cell adhesion molecule [Mu	0	2	0	0	0	0
308 gi|259090165 (+2)	Chain A, Structural Basis Of Pp2a And Sgo Int	14	12	0	0	0	0
309 gi|148678069 (+4)	dihydropyrimidinase-like 3, isoform CRA_a [Mu	15	7	0	0	0	0
310 gi|41054806	guanine nucleotide-binding protein G(i) subunit	9	11	8	0	0	0
311 gi|17105370 (+5)	V-type proton ATPase subunit B, brain isoform	9	18	3	0	0	0
312 gi|114052913 (+5)	cell adhesion molecule 2 [Rattus norvegicus], (	3	5	3	0	0	0
313 gi|13385168	cytochrome b-c1 complex subunit Rieske, mito	0	5	11	0	0	0
314 gi|46195430	NADH dehydrogenase [ubiquinone] iron-sulfur	0	8	11	0	0	0
315 gi|6756037	14-3-3 protein eta [Mus musculus], gi|6981710	7	6	0	0	0	0
316 gi|6678483	ubiquitin-like modifier-activating enzyme 1 isof	15	14	0	0	0	0
317 gi|12832501 (+3)	unnamed protein product [Mus musculus]	0	6	14	0	0	0
318 gi|30519995	sideroflexin-5 [Mus musculus], gi|30581069|sp	0	7	9	0	0	0
319 gi|123236177 (+3)	brain-specific angiogenesis inhibitor 1-associat	0	17	10	0	0	0
320 gi|119587893 (+3)	Thy-1 cell surface antigen, isoform CRA_b [Ho	0	0	0	0	0	4
321 gi|12832758 (+2)	unnamed protein product [Mus musculus]	7	9	6	0	0	0
322 gi|110626109 (+1)	tyrosine-protein phosphatase non-receptor typ(	3	6	4	0	0	0
323 gi|31981304 (+1)	V-type proton ATPase subunit d 1 [Mus muscu	4	13	4	0	0	0
324 gi|26324898 (+7)	unnamed protein product [Mus musculus]	21	14	2	0	0	0
325 gi|169790797 (+1)	Fc fragment of IgG binding protein [Mus muscu	0	0	0	0	0	0
326 gi|148706752 (+2)	mCG115977 [Mus musculus]	4	8	10	0	0	0
327 gi|12842773 (+1)	unnamed protein product [Mus musculus]	2	4	4	0	0	0
328 gi|119850911 (+2)	Nckap1 protein [Mus musculus]	5	16	0	0	0	0

329	gi|24418919 (+4)	glycogen phosphorylase, brain form [Mus mus	8	19	0	0	0	0
330	gi|14589931 (+5)	protocadherin-7 isoform a precursor [Homo sa	0	0	0	0	0	9
331	gi|160707976 (+4)	protein piccolo isoform 1 [Mus musculus]	0	21	0	0	0	0
332	gi|281306830	immunoglobulin superfamily member 21 precu	0	0	0	0	0	12
333	gi|4503273	angiotensin-converting enzyme isoform 1 prec	0	0	0	0	0	14
334	gi|257743039 (+4)	L-lactate dehydrogenase A chain isoform 2 [M	9	7	2	0	0	0
335	gi|38325830 (+1)	CD90.1 [Mus musculus]	5	6	5	0	0	0
336	gi|221664641 (+3)	NADH dehydrogenase subunit 4 [Mus muscul	0	4	7	0	0	0
337	gi|257196228 (+2)	amine oxidase [flavin-containing] B [Mus musc	0	8	14	0	0	0
338	gi|112380628 (+5)	lysosome-associated membrane glycoprotein	0	0	0	0	0	8
339	gi|6755983	visinin-like protein 1 [Mus musculus], gi|21361!	11	12	0	0	0	2
340	gi|114326546 (+1)	phosphoglycerate mutase 1 [Mus musculus], g	10	5	0	0	0	0
341	gi|123288582 (+5)	G protein pathway suppressor 1 [Mus musculu	0	2	0	0	0	0
342	gi|148701361 (+3)	reticulon 3, isoform CRA_c [Mus musculus]	0	11	0	0	0	0
343	gi|148697948 (+1)	ATPase, Ca++ transporting, plasma membrane	3	10	6	0	0	0
344	gi|119584197 (+3)	N-acylsphingosine amidohydrolase (acid cerar	0	0	0	0	0	16
345	gi|1575347 (+2)	HU-K4 [Homo sapiens]	0	0	0	0	0	6
346	gi|12849385 (+1)	unnamed protein product [Mus musculus]	3	3	3	2	0	0
347	gi|18390323	ras-related protein Rab-14 [Mus musculus], gi|	3	10	5	0	0	3
348	gi|13278382 (+4)	Eukaryotic translation elongation factor 1 alph	5	6	3	3	0	0
349	gi|6679439 (+1)	peptidyl-prolyl cis-trans isomerase A [Mus mus	12	6	2	0	0	0
350	gi|45504359 (+1)	V-type proton ATPase subunit E 1 [Mus muscu	10	11	3	0	0	0
351	gi|6671684	catenin beta-1 [Mus musculus], gi|260166642|r	0	10	6	0	0	0
352	gi|10946620 (+2)	cell cycle exit and neuronal differentiation prote	0	5	5	0	0	0
353	gi|119615593 (+2)	dipeptidyl-peptidase 10, isoform CRA_b [Homo	0	0	0	0	0	13
354	gi|4506413 (+2)	ras-related protein Rap-1A precursor [Homo sa	9	9	10	0	0	0
355	gi|254540166 (+3)	78 kDa glucose-regulated protein precursor [M	11	16	5	0	0	0
356	gi|12843573	unnamed protein product [Mus musculus]	11	8	8	0	0	0
357	gi|148694562 (+7)	synaptosomal-associated protein 91, isoform C	4	6	2	0	0	0
358	gi|302331793	regulatory protein YycI [Staphylococcus aureu:	0	2	0	0	0	0
359	gi|120407048 (+5)	mitofusin-2 [Mus musculus], gi|47605852|sp|Q	0	11	19	0	0	0
360	gi|254039729 (+1)	mitochondrial Rho GTPase 1 isoform 3 [Mus m	0	9	14	0	0	0
361	gi|119580677 (+2)	neuronal pentraxin receptor, isoform CRA_a [F	0	0	0	0	0	9
362	gi|306991881 (+3)	Chain A, Molecular Mechanism Of Guidance C	0	0	0	0	0	11
363	gi|26328555 (+2)	unnamed protein product [Mus musculus], gi|2	0	7	9	0	0	0
364	gi|148703063 (+2)	NADH dehydrogenase (ubiquinone) 1 beta sut	0	6	8	0	2	0
365	gi|112293264 (+4)	protein disulfide-isomerase A3 precursor [Mus	10	10	5	0	0	0
366	gi|126506304 (+3)	CLIP-associating protein 2 isoform a [Mus mus	2	16	5	0	0	0
367	gi|148710162 (+2)	solute carrier family 8 (sodium/calcium exchan	4	9	2	0	0	0
368	gi|254553458 (+3)	glucose-6-phosphate isomerase [Mus musculu	10	10	0	0	0	0
369	gi|148697875 (+1)	guanosine diphosphate (GDP) dissociation inh	16	3	0	0	0	0
370	gi|255759902 (+2)	amine oxidase [flavin-containing] A [Mus musc	0	11	10	0	0	0
371	gi|29789104	beta-soluble NSF attachment protein [Mus mu:	8	8	2	0	0	5
372	gi|6753074 (+4)	AP-2 complex subunit mu [Mus musculus], gi|1	9	13	2	0	0	0
373	gi|112293279	neural cell adhesion molecule L1 [Mus muscul	9	8	0	0	0	0
374	gi|123793848 (+2)	RecName: Full=Vesicular glutamate transporte	0	5	0	0	0	0
375	gi|161086896 (+4)	voltage-dependent calcium channel subunit alp	7	6	0	0	0	0
376	gi|19526848	MOSC domain-containing protein 2, mitochonc	0	10	11	0	0	0
377	gi|1083569 (+7)	kappa-B motif-binding phosphoprotein - mouse	11	12	0	0	0	0
378	gi|148666875 (+2)	mCG128608 [Mus musculus]	0	13	2	0	0	0
379	gi|40548389	dickkopf-related protein 3 precursor [Homo sap	0	0	0	0	0	7
380	gi|9625037	rho-related GTP-binding protein RhoG precurs	4	6	6	2	0	4
381	gi|157951727 (+1)	catenin alpha-2 isoform 1 [Mus musculus], gi|1	5	13	5	0	0	0
382	gi|27754056	tubulin beta-6 chain [Mus musculus], gi|68775!	2	2	0	0	0	0
383	gi|8394030	serine/threonine-protein phosphatase 2B cataly	5	13	0	0	0	0

384	gi|134031976 (+2)	leucine-rich PPR motif-containing protein, mito	2	7	16	0	0	0
385	gi|13385322	NADH dehydrogenase [ubiquinone] 1 beta sub	0	6	8	0	0	0
386	gi|29789148	NADH dehydrogenase [ubiquinone] 1 beta sub	0	7	11	0	0	0
387	gi|148673973 (+3)	syntaphilin, isoform CRA_b [Mus musculus]	0	4	15	0	0	0
388	gi|14250196 (+2)	Nicotinamide nucleotide transhydrogenase [Mu	0	0	22	0	0	0
389	gi|17157993	noelin-2 precursor [Homo sapiens], gi|6747735	0	0	0	0	0	8
390	gi|62122917	filaggrin-2 [Homo sapiens], gi|74755309|sp|Q5	0	0	0	0	0	11
391	gi|74147849 (+1)	unnamed protein product [Mus musculus]	0	0	0	0	0	0
392	gi|15804627 (+3)	maltose ABC transporter periplasmic protein [E	0	2	4	0	2	4
393	gi|12855370 (+2)	unnamed protein product [Mus musculus]	3	4	2	0	0	0
394	gi|13242269 (+2)	sodium- and chloride-dependent GABA transp	2	7	4	0	0	0
395	gi|12832967 (+3)	unnamed protein product [Mus musculus]	0	7	10	0	0	0
396	gi|6753320	T-complex protein 1 subunit gamma [Mus mus	13	7	0	0	0	0
397	gi|112975 (+2)	RecName: Full=Aspartate aminotransferase, c	8	6	0	0	0	0
398	gi|4757764	rho-related GTP-binding protein RhoB precurs	5	4	7	0	0	0
399	gi|5031571 (+1)	actin-related protein 2 isoform b [Homo sapien	7	10	0	0	0	2
400	gi|122889796 (+3)	glutamate receptor ionotropic NMDA1 (zeta 1)	0	4	5	0	0	0
401	gi|116256491 (+8)	ankyrin 3, epithelial isoform a [Mus musculus],	0	14	6	0	0	0
402	gi|119395752 (+1)	potassium voltage-gated channel subfamily A	0	6	9	0	0	0
403	gi|158186704 (+3)	heterogeneous nuclear ribonucleoprotein M iso	4	17	0	0	0	0
404	gi|123244271	microtubule-actin crosslinking factor 1 [Mus mu	0	17	0	0	0	0
405	gi|22760207	unnamed protein product [Homo sapiens]	0	0	0	0	0	8
406	gi|4504779	integrin beta-8 precursor [Homo sapiens], gi|12	0	0	0	0	0	15
407	gi|1162922 (+12)	myelin basic protein [Homo sapiens]	0	0	0	0	0	2
408	gi|113866024 (+1)	ras-related protein Rab-5C [Mus musculus], gi|	6	7	6	0	0	0
409	gi|148667772 (+2)	a disintegrin and metallopeptidase domain 23 [	2	8	6	0	0	0
410	gi|4758984 (+3)	ras-related protein Rab-11A [Homo sapiens], g	5	5	5	0	0	0
411	gi|74139622 (+1)	unnamed protein product [Mus musculus]	2	4	0	0	0	0
412	gi|34147513	ras-related protein Rab-7a [Homo sapiens], gi|	6	9	6	0	0	0
413	gi|148697930 (+3)	isocitrate dehydrogenase 3 (NAD+), gamma, is	0	7	9	0	0	0
414	gi|19527228	CDGSH iron-sulfur domain-containing protein	0	6	9	0	0	0
415	gi|6753322 (+1)	T-complex protein 1 subunit delta [Mus muscu	10	10	0	0	0	0
416	gi|70778812	transmembrane protein 65 [Mus musculus], gi|	0	5	7	0	0	0
417	gi|292495011 (+1)	RecName: Full=Gamma-aminobutyric acid rec	0	3	0	0	0	0
418	gi|124487313 (+1)	glutaminase isoform 1 [Mus musculus]	0	6	15	0	0	0
419	gi|21312594	brain protein 44 [Mus musculus], gi|23396478|	0	4	5	0	0	0
420	gi|148666221	mCG119114, isoform CRA_a [Mus musculus]	6	12	0	0	0	0
421	gi|167716837 (+7)	NADH dehydrogenase subunit 1 [Mus muscul	0	4	3	0	0	0
422	gi|148680460 (+4)	olfactomedin 3, isoform CRA_c [Mus musculus	0	0	0	0	0	0
423	gi|6746357 (+3)	peroxisomal membrane protein 20 [Mus muscu	3	9	7	0	0	0
424	gi|29028581 (+1)	phi ETA orf 25-like protein [Staphylococcus ph	0	0	0	0	0	2
425	gi|148687555 (+3)	glioblastoma amplified sequence [Mus muscul	0	6	10	0	0	0
426	gi|40556608 (+1)	heat shock protein HSP 90-beta [Mus muscul	10	3	3	0	0	0
427	gi|30520019	probable saccharopine dehydrogenase [Mus m	2	11	10	0	0	0
428	gi|189409138 (+1)	cullin-associated NEDD8-dissociated protein 1	8	8	0	0	0	0
429	gi|21312950	NADH dehydrogenase [ubiquinone] iron-sulfur	0	7	8	0	0	0
430	gi|148697486 (+6)	brain-specific angiogenesis inhibitor 1 [Mus mu	0	0	0	0	0	2
431	gi|12963591	stomatin-like protein 2 [Mus musculus], gi|6041	0	8	17	0	0	0
432	gi|164565394 (+1)	dnaJ homolog subfamily C member 11 [Mus m	0	7	13	0	0	0
433	gi|148693677 (+1)	mCG1549, isoform CRA_b [Mus musculus]	0	4	5	0	0	0
434	gi|34148711 (+1)	melanoma chondroitin sulfate proteoglycan [Ho	0	0	0	0	0	10
435	gi|18087731 (+1)	dynein light chain 2, cytoplasmic [Mus muscult	0	7	5	0	0	2
436	gi|158508501 (+2)	septin-5 [Mus musculus], gi|83305642|sp|Q9Z2	3	9	4	0	0	0
437	gi|13385090	cytochrome c oxidase subunit 6B1 [Mus muscu	2	6	7	0	0	0
438	gi|148690793 (+4)	myosin, heavy polypeptide 14, isoform CRA_a	2	9	14	0	0	0

439	gi|26341092 (+1)	unnamed protein product [Mus musculus]	0	8	14	0	0	0
440	gi|1167982 (+3)	ABC transporter-7 [Mus musculus]	0	4	16	0	0	0
441	gi|12835914 (+2)	unnamed protein product [Mus musculus]	2	16	0	0	0	0
442	gi|11321166 (+1)	cardiac Ca2+ release channel [Mus musculus]	0	24	0	0	0	0
443	gi|1147813 (+1)	desmoplakin I [Homo sapiens]	0	0	0	0	0	16
444	gi|119611550 (+1)	laminin, gamma 1 (formerly LAMB2), isoform C	0	0	0	0	0	16
445	gi|13386238	keratin, type I cuticular Ha4 [Mus musculus], g	2	8	4	0	0	0
446	gi|5174447 (+3)	guanine nucleotide-binding protein subunit bet	7	7	0	0	0	6
447	gi|6754994	poly(rC)-binding protein 1 [Mus musculus], gi|6	5	6	0	0	0	3
448	gi|12851417 (+1)	unnamed protein product [Mus musculus]	7	6	5	0	0	0
449	gi|12003362 (+1)	NADP+-specific isocitrate dehydrogenase [Mus	0	5	11	0	0	0
450	gi|148684484 (+1)	phosphoglucomutase 2-like 1, isoform CRA_d	9	9	0	0	0	0
451	gi|148705512 (+5)	adducin 1 (alpha), isoform CRA_b [Mus muscu	2	7	0	0	0	0
452	gi|26390327 (+2)	unnamed protein product [Mus musculus]	0	2	0	0	0	0
453	gi|148705099 (+1)	mCG10028, isoform CRA_a [Mus musculus]	0	5	8	0	0	0
454	gi|148685332 (+1)	protein kinase C, beta 1, isoform CRA_b [Mus	4	12	0	0	0	0
455	gi|15147224	sideroflexin-1 [Mus musculus], gi|20140195|sp	0	9	8	0	0	0
456	gi|26344676 (+1)	unnamed protein product [Mus musculus]	3	8	0	0	0	0
457	gi|18605695 (+4)	Mtch1 protein [Mus musculus]	0	3	8	0	0	0
458	gi|48425844	Chain A, Crystal Structure Of Human Carboxy	0	0	0	0	0	13
459	gi|81908782	RecName: Full=Seizure 6-like protein 2; AltNa	0	0	0	0	0	0
460	gi|159572141	septin 8 [Mus musculus]	0	9	4	0	0	0
461	gi|10946940	ras-related protein Rab-2A [Mus musculus], gi|	5	6	5	0	0	0
462	gi|113680348	fascin [Mus musculus], gi|146345421|sp|Q615	11	5	0	0	0	0
463	gi|26325850 (+3)	unnamed protein product [Mus musculus]	4	13	3	0	0	0
464	gi|12746424 (+1)	dihydropyrimidinase-related protein 5 [Mus mu	13	5	0	0	0	0
465	gi|84781779	NADH dehydrogenase [ubiquinone] 1 beta sub	0	3	5	0	0	0
466	gi|118601017 (+2)	dynactin subunit 1 isoform 1 [Mus musculus]	9	8	0	0	0	0
467	gi|148707489 (+3)	DEAH (Asp-Glu-Ala-His) box polypeptide 9, iso	6	12	0	0	0	0
468	gi|148700394 (+2)	gamma-aminobutyric acid (GABA-A) receptor,	0	5	0	0	0	0
469	gi|82659196	alpha actinin 1a [Mus musculus]	0	18	0	0	0	0
470	gi|167001419 (+1)	glutamate receptor 1 isoform 1 precursor [Hom	0	0	0	0	0	8
471	gi|177870 (+5)	alpha-2-macroglobulin precursor [Homo sapier	0	0	0	0	0	12
472	gi|148271063 (+1)	dermcidin isoform 2 [Homo sapiens]	0	0	0	0	0	3
473	gi|27532946	guanine nucleotide-binding protein G(z) subun	7	9	4	0	0	0
474	gi|21431774 (+1)	RecName: Full=Fumarate hydratase, mitochor	4	7	11	0	0	0
475	gi|21314826 (+1)	NADH dehydrogenase [ubiquinone] 1 beta sub	0	5	7	0	0	0
476	gi|148705826 (+1)	ubiquitin carboxy-terminal hydrolase L1, isofor	8	7	0	0	0	0
477	gi|148705321 (+2)	mCG11629, isoform CRA_d [Mus musculus]	3	8	9	0	0	0
478	gi|61888838	3-hydroxyacyl-CoA dehydrogenase type-2 [Mu	0	9	6	0	0	0
479	gi|27261824	synaptic vesicle glycoprotein 2B [Mus musculu	2	11	0	0	0	0
480	gi|54607084 (+1)	contactin-2 precursor [Mus musculus], gi|5170	0	2	0	0	0	0
481	gi|100817933 (+1)	acyl-CoA dehydrogenase family member 9, mi	0	8	13	0	0	0
482	gi|120538559 (+4)	DEAD (Asp-Glu-Ala-Asp) box polypeptide 5 [M	5	11	0	0	0	0
483	gi|148685898 (+3)	dihydropyrimidinase-like 4, isoform CRA_d [Mu	10	11	0	0	0	0
484	gi|21312012	NADH dehydrogenase [ubiquinone] 1 alpha su	0	7	11	0	0	0
485	gi|21704242	caM kinase-like vesicle-associated protein [Mu	8	9	0	0	0	0
486	gi|148693866 (+2)	mCG130874, isoform CRA_a [Mus musculus]	0	14	0	0	0	0
487	gi|11934695 (+1)	CDA08 [Homo sapiens]	0	0	0	0	0	8
488	gi|158256826 (+2)	unnamed protein product [Homo sapiens]	0	0	0	0	0	10
489	gi|12857778 (+3)	unnamed protein product [Mus musculus]	0	2	3	2	0	0
490	gi|5031569	alpha-centractin [Homo sapiens], gi|8392847|r	5	5	0	0	0	4
491	gi|189339262 (+2)	V-type proton ATPase subunit C 1 [Mus muscu	4	11	0	0	0	0
492	gi|52221167 (+2)	Hepacam protein [Mus musculus]	0	8	5	0	0	0
493	gi|12846252 (+2)	unnamed protein product [Mus musculus]	7	5	0	0	0	0

494	gi|148686246 (+2)	CD 81 antigen, isoform CRA_a [Mus musculus	2	3	3	0	0	0
495	gi|13385492	NADH dehydrogenase [ubiquinone] 1 alpha su	0	7	7	0	0	0
496	gi|220468 (+3)	KIF2 protein [Mus musculus]	3	9	6	0	0	0
497	gi|148675904 (+2)	malate dehydrogenase 1, NAD (soluble), isofo	11	7	3	0	0	0
498	gi|74188195 (+1)	unnamed protein product [Mus musculus]	5	7	2	0	0	0
499	gi|148704504 (+3)	spectrin beta 1, isoform CRA_a [Mus musculus	0	10	10	0	0	0
500	gi|16716343	cytochrome c oxidase subunit 6C [Mus muscul	0	6	6	0	0	0
501	gi|148664714 (+4)	mCG121979, isoform CRA_b [Mus musculus]	0	18	0	0	0	0
502	gi|10312085 (+3)	HVEC cell-cell adhesion molecule/herpesvirus	0	0	0	0	0	7
503	gi|119395740 (+7)	integrin alpha-6 isoform a precursor [Homo sap	0	0	0	0	0	9
504	gi|119630936 (+2)	attractin, isoform CRA_b [Homo sapiens]	0	0	0	0	0	9
505	gi|42521647 (+1)	G protein coupled receptor 158 [Homo sapiens	0	0	0	0	0	9
506	gi|11225258 (+3)	myelin-associated glycoprotein isoform a precu	0	0	0	0	0	4
507	gi|4757952 (+2)	cell division control protein 42 homolog isoform	4	0	3	0	0	2
508	gi|6754382 (+1)	leukocyte surface antigen CD47 [Mus musculu	2	2	3	2	0	0
509	gi|148683963 (+2)	mCG145251 [Mus musculus]	5	7	5	0	0	0
510	gi|148676699 (+4)	gelsolin, isoform CRA_a [Mus musculus]	9	3	4	0	0	0
511	gi|148684443 (+1)	ribosomal protein S3, isoform CRA_e [Mus mu	6	13	0	0	0	0
512	gi|12859535 (+1)	unnamed protein product [Mus musculus]	0	8	10	0	0	0
513	gi|62948125 (+3)	Chaperonin containing Tcp1, subunit 6a (zeta)	6	7	0	0	0	0
514	gi|158631246 (+2)	NADH dehydrogenase [ubiquinone] 1 beta sub	0	5	6	0	0	0
515	gi|148670608 (+4)	ATP citrate lyase, isoform CRA_a [Mus muscu	12	10	0	0	0	0
516	gi|168823441	coiled-coil domain-containing protein 109A [Mu	0	4	8	0	0	0
517	gi|119577616 (+2)	immunoglobulin superfamily, member 4C, isofo	0	0	0	0	0	9
518	gi|148703351 (+4)	double cortin and calcium/calmodulin-depende	7	10	2	0	0	0
519	gi|27369922 (+1)	dynamin-3 isoform 2 [Mus musculus], gi|26340	5	2	11	0	0	0
520	gi|45597453	long-chain fatty acid transport protein 4 [Mus m	0	5	10	0	0	0
521	gi|112363090 (+2)	catenin delta-2 [Mus musculus]	0	10	2	0	0	0
522	gi|15011853 (+1)	syntaxin-1A [Mus musculus], gi|20141656|sp|C	5	13	0	0	0	0
523	gi|60360628 (+1)	mKIAA4233 protein [Mus musculus], gi|148705	0	12	0	0	0	0
524	gi|118200820 (+7)	NADH dehydrogenase subunit 5 [Mus muscul	0	5	5	0	0	0
525	gi|6679066	protein NipSnap homolog 1 [Mus musculus], g	0	4	6	0	0	0
526	gi|12963675 (+2)	OCIA domain-containing protein 1 isoform 1 [M	0	4	6	0	0	0
527	gi|189065500 (+2)	unnamed protein product [Homo sapiens]	0	0	0	0	0	11
528	gi|21750872 (+2)	unnamed protein product [Homo sapiens]	0	0	0	0	0	10
529	gi|283806778	Chain A, Crystal Structure Of The Human Lipo	0	0	0	0	0	5
530	gi|148672667 (+6)	synaptogyrin 1, isoform CRA_b [Mus musculus	2	2	0	0	0	2
531	gi|215983062 (+1)	EH domain-containing protein 3 [Mus musculu	4	6	5	0	0	0
532	gi|148664876 (+3)	4-aminobutyrate aminotransferase, isoform CR	3	4	7	0	0	0
533	gi|24638341 (+1)	RecName: Full=Vesicle-associated membrane	3	8	0	0	0	0
534	gi|163644296	PH and SEC7 domain-containing protein 3 isof	4	4	5	0	0	0
535	gi|22094989	mitochondrial import inner membrane transloca	0	6	8	0	0	0
536	gi|21312520	dihydropteridine reductase [Mus musculus], gi|	4	8	4	0	0	0
537	gi|148707043 (+1)	immunoglobulin superfamily, member 4B, isofo	3	4	4	0	0	0
538	gi|116014342 (+4)	basigin isoform 2 [Mus musculus], gi|1697908€	5	6	3	0	0	0
539	gi|238814391 (+3)	T-complex protein 1 subunit eta [Mus musculus	5	7	0	0	0	0
540	gi|269784615	plasma membrane calcium ATPase 4 isoform :	2	7	2	0	0	0
541	gi|16945962 (+1)	rabphilin-3A [Mus musculus], gi|21431839|sp|F	0	13	2	0	0	0
542	gi|148707278 (+3)	soluble adenylyl cyclase, isoform CRA_a [Mus	0	0	0	2	0	0
543	gi|22122795	cytoplasmic dynein 1 light intermediate chain 1	6	10	0	0	0	0
544	gi|116089322 (+3)	lon protease homolog, mitochondrial precursor	0	4	12	0	0	0
545	gi|13994195	serine/threonine-protein phosphatase PP1-alpl	3	8	0	0	0	0
546	gi|37537518	acylglycerol kinase, mitochondrial precursor [M	0	4	13	0	0	0
547	gi|113195686 (+1)	lamin-B2 [Mus musculus], gi|85700429|sp|P21	0	16	0	0	0	0
548	gi|119581273 (+1)	contactin associated protein 1, isoform CRA_b	0	0	0	0	0	6

549	gi|13173236 (+4)	ABC transporter ABCA2 [Homo sapiens]	0	0	0	0	0	9
550	gi|14715053 (+2)	Unknown (protein for IMAGE:3875338) [Homo	0	0	0	0	0	11
551	gi|157694524 (+1)	plexin-D1 precursor [Homo sapiens]	0	0	0	0	0	12
552	gi|200367	cAMP-dependent protein kinase catalytic subu	6	0	2	0	0	0
553	gi|15341745 (+2)	EH-domain containing 4 [Mus musculus]	2	3	9	4	0	0
554	gi|117959921 (+8)	protein ALEX isoform f [Mus musculus], gi|123	4	3	2	0	0	0
555	gi|31560541 (+1)	synaptogyrin-3 [Mus musculus], gi|54036519|s	3	4	0	0	0	0
556	gi|13195674	ras-related protein Rab-6A isoform 2 [Mus mus	2	7	0	0	0	0
557	gi|148707626 (+1)	cysteine and glycine-rich protein 1, isoform CR	2	7	4	0	0	0
558	gi|70794809 (+1)	neuronal proto-oncogene tyrosine-protein kinas	4	5	4	0	0	0
559	gi|163965382	neural cell adhesion molecule 2 isoform a [Mus	5	4	0	0	0	0
560	gi|158711690 (+3)	receptor-type tyrosine-protein phosphatase S p	0	14	0	0	0	0
561	gi|67463777 (+3)	Chain C, Paf-Ah Holoenzyme: Lis1ALFA2, gi|6	7	4	0	0	0	0
562	gi|14587839 (+5)	acyl-CoA hydrolase [Mus musculus], gi|154887	5	3	0	0	0	0
563	gi|16716465	long-chain-fatty-acid--CoA ligase ACSBG1 [Mu	2	12	4	0	0	0
564	gi|26333029 (+2)	unnamed protein product [Mus musculus]	2	8	3	0	0	0
565	gi|12963737	exportin-2 [Mus musculus], gi|20137950|sp|Q9	0	2	0	0	0	0
566	gi|13277927 (+1)	Ribosomal protein, large, P0 [Mus musculus],	5	8	0	0	0	0
567	gi|124494256 (+1)	prolow-density lipoprotein receptor-related prot	0	0	0	0	0	0
568	gi|28201978	pyruvate dehydrogenase protein X component	0	7	7	0	0	0
569	gi|254587960 (+3)	serine/threonine-protein phosphatase PGAM5,	0	4	6	0	0	0
570	gi|6753964 (+2)	ganglioside-induced differentiation-associated	0	6	9	0	0	0
571	gi|148701647 (+3)	ubiquinol-cytochrome c reductase, complex III	0	3	5	0	0	0
572	gi|149363636 (+1)	plexin-B2 precursor [Homo sapiens], gi|126302	0	0	0	0	0	14
573	gi|31874250 (+2)	hypothetical protein [Homo sapiens]	0	0	0	0	0	7
574	gi|68563515	keratinocyte proline-rich protein [Homo sapiens	0	0	0	0	0	7
575	gi|4506371 (+1)	ras-related protein Rab-5B [Homo sapiens], gi|	3	4	4	0	0	3
576	gi|4826659 (+5)	F-actin-capping protein subunit beta [Homo sa	3	4	0	0	0	2
577	gi|13097375 (+4)	Electron transferring flavoprotein, alpha polype	4	7	5	0	0	0
578	gi|6754004	guanine nucleotide-binding protein subunit alph	5	5	4	0	0	0
579	gi|38173745 (+1)	Nrxn3 protein [Mus musculus]	4	4	0	0	0	0
580	gi|110625979	elongation factor 1-gamma [Mus musculus], gi	8	4	0	0	0	0
581	gi|164419753 (+2)	glutamate receptor 4 isoform 2 precursor [Mus	0	0	2	0	0	0
582	gi|1695270 (+1)	K+ channel beta2 subunit [Mus musculus]	0	7	8	0	0	0
583	gi|12832230 (+3)	unnamed protein product [Mus musculus]	0	5	4	0	0	0
584	gi|21746161	tubulin beta-2B chain [Mus musculus], gi|2978	2	2	0	0	0	0
585	gi|148670196 (+1)	RIKEN cDNA 5230400G24, isoform CRA_f [M	0	4	7	0	0	0
586	gi|1398903 (+2)	Ca2+ dependent activator protein for secretion	5	7	0	0	0	0
587	gi|33286888 (+1)	Gja1 protein [Mus musculus]	0	10	7	0	0	0
588	gi|33585791 (+2)	Family with sequence similarity 82, member A2	0	7	8	0	0	0
589	gi|4895037 (+2)	coronin-1 [Mus musculus], gi|12805335|gb|AAI	5	9	0	0	0	0
590	gi|148695235 (+3)	metaxin 2, isoform CRA_a [Mus musculus]	0	5	11	0	0	0
591	gi|148671648 (+7)	methylenetetrahydrofolate dehydrogenase (NA	0	4	12	0	0	0
592	gi|31560705 (+1)	long-chain-fatty-acid--CoA ligase 1 [Mus musc	0	3	10	0	0	0
593	gi|18606009 (+1)	Metaxin 1 [Mus musculus], gi|21684682|gb|AA	0	2	9	0	0	0
594	gi|119612353 (+4)	CUB and Sushi multiple domains 3, isoform CF	0	0	0	0	0	9
595	gi|148699133 (+2)	astrotactin 2, isoform CRA_b [Mus musculus]	0	0	0	0	0	0
596	gi|223462499 (+1)	Contactin 3 (plasmacytoma associated) [Homo	0	0	0	0	0	10
597	gi|156071462 (+2)	ADP/ATP translocase 3 [Homo sapiens], gi|11	0	0	0	0	0	2
598	gi|12963613	junctional adhesion molecule C precursor [Mus	0	3	4	5	2	0
599	gi|148664644 (+1)	bridging integrator 1, isoform CRA_a [Mus mus	5	3	0	0	0	0
600	gi|148699102 (+3)	protein tyrosine phosphatase, receptor type, D	0	5	4	0	0	0
601	gi|18859597	NADH dehydrogenase [ubiquinone] 1 subunit C	0	3	5	0	0	0
602	gi|31982273 (+2)	peroxisomal multifunctional enzyme type 2 [Mu	3	8	2	0	0	0
603	gi|148684567 (+8)	phosphodiesterase 2A, cGMP-stimulated, isofo	5	7	0	0	0	0

604	gi|148686433 (+4)	NADH dehydrogenase (ubiquinone) Fe-S prote	0	6	8	0	0	0
605	gi|13385558	NADH dehydrogenase [ubiquinone] 1 beta sub	0	5	6	0	0	0
606	gi|158429419 (+2)	Chain A, Crystal Structure Of Human Cbr1 In C	0	0	0	0	0	10
607	gi|1709301 (+3)	amyloid precursor-like protein 1 [Homo sapiens	0	0	0	0	0	9
608	gi|27363458 (+3)	leucine-rich repeat and fibronectin type-III dom	0	0	0	0	0	6
609	gi|119605687 (+7)	mahogunin, ring finger 1, isoform CRA_c [Hom	0	0	0	0	0	5
610	gi|21758400	unnamed protein product [Homo sapiens], gi|8	0	0	0	0	0	4
611	gi|2507615	neural cell adhesion protein [Homo sapiens]	0	0	0	0	0	4
612	gi|4502277 (+2)	sodium/potassium-transporting ATPase subun	0	0	0	0	0	3
613	gi|148708988 (+1)	mCG20427 [Mus musculus]	0	3	2	2	0	0
614	gi|6754816	septin-2 a [Mus musculus], gi|228480251|ref|N	5	4	6	3	0	0
615	gi|122889413 (+3)	septin 9 [Mus musculus], gi|123244013|emb|C.	2	5	3	0	0	0
616	gi|2500063 (+2)	RecName: Full=GTPase HRas; AltName: Full=	6	4	3	0	0	0
617	gi|148674410 (+3)	tyrosine 3-monooxygenase/tryptophan 5-mono	5	5	2	0	0	0
618	gi|156523248	proline-rich transmembrane protein 2 [Mus mu	2	6	2	0	0	0
619	gi|6671672 (+1)	F-actin-capping protein subunit alpha-2 [Mus n	3	8	0	0	0	0
620	gi|148693838 (+4)	radixin [Mus musculus]	5	3	4	0	0	0
621	gi|12846591 (+1)	unnamed protein product [Mus musculus]	2	4	7	0	0	0
622	gi|126540842 (+1)	reticulon 1 [Mus musculus]	2	2	0	0	0	0
623	gi|30519971	atlastin-1 [Mus musculus], gi|37999666|sp|Q8E	2	6	0	0	0	0
624	gi|74186237 (+2)	unnamed protein product [Mus musculus]	0	10	3	0	0	0
625	gi|10181184	ATP synthase subunit f, mitochondrial [Mus mu	0	3	3	0	0	0
626	gi|27369748	succinate-semialdehyde dehydrogenase, mito	0	6	8	0	0	0
627	gi|100818161 (+5)	RAP1, GTP-GDP dissociation stimulator 1 isof	6	5	0	0	0	0
628	gi|123232765 (+2)	solute carrier family 25 (mitochondrial carrier, p	0	2	9	0	0	0
629	gi|14626498 (+8)	GABA(A) receptor gamma 2 subunit [Mus mus	0	3	0	0	0	0
630	gi|116268115 (+3)	methylglutaconyl-CoA hydratase, mitochondria	0	5	7	0	0	0
631	gi|123236356 (+3)	erythrocyte protein band 4.1-like 1 [Mus muscu	6	7	0	0	0	0
632	gi|123249051 (+5)	tyrosyl-tRNA synthetase [Mus musculus], gi|14	6	7	0	0	0	0
633	gi|21312524	NADH-cytochrome b5 reductase 1 [Mus muscu	0	5	9	0	0	0
634	gi|23956214	splicing factor, proline- and glutamine-rich [Mu	7	6	0	0	0	0
635	gi|74215259 (+1)	unnamed protein product [Mus musculus]	0	4	5	0	0	0
636	gi|27369613	nuclease EXOG, mitochondrial isoform 2 precu	0	5	8	0	0	0
637	gi|148681120 (+4)	glutamyl-prolyl-tRNA synthetase [Mus muscul	4	10	0	0	0	0
638	gi|10946928 (+2)	heterogeneous nuclear ribonucleoprotein H [M	4	6	0	0	0	0
639	gi|14250269 (+3)	Unknown (protein for IMAGE:3592890) [Mus n	8	4	0	0	0	0
640	gi|148686520 (+4)	mCG51413 [Mus musculus]	0	4	4	0	0	0
641	gi|12805413 (+1)	Echs1 protein [Mus musculus]	0	3	5	0	0	0
642	gi|160333553 (+2)	60S ribosomal protein L12 [Mus musculus], gi|	3	6	0	0	0	0
643	gi|219521150 (+2)	Ddx3x protein [Mus musculus]	2	10	0	0	0	0
644	gi|11863685 (+3)	neurobeachin [Mus musculus]	2	11	0	0	0	0
645	gi|168984393 (+2)	vesicle-associated membrane 2 [Mus muscul	0	5	0	0	0	0
646	gi|10864029 (+1)	junctional adhesion molecule B precursor [Hon	0	0	0	0	0	8
647	gi|157311649 (+2)	neogenin isoform 1 precursor [Homo sapiens],	0	0	0	0	0	8
648	gi|194382434 (+5)	unnamed protein product [Homo sapiens]	0	0	0	0	0	8
649	gi|4503057	alpha-crystallin B chain [Homo sapiens], gi|197	0	0	0	0	0	6
650	gi|118600983 (+3)	neurocan core protein precursor [Homo sapien	0	0	0	0	0	6
651	gi|162461738 (+1)	guanine nucleotide-binding protein G(o) subun	0	0	0	0	0	3
652	gi|237858675	neurofascin isoform 1 precursor [Homo sapien	0	0	0	0	0	2
653	gi|54607171	keratin, type II cytoskeletal 6A [Mus musculus]	2	2	0	2	0	0
654	gi|16923986 (+1)	transforming protein RhoA precursor [Rattus no	2	3	2	0	0	0
655	gi|6754632	mitogen-activated protein kinase 1 [Mus muscu	6	6	0	0	0	0
656	gi|110625609 (+3)	cadherin-13 precursor [Mus musculus], gi|2633	2	2	0	0	0	0
657	gi|198845	lipocortin I [Mus musculus]	0	0	0	0	2	0
658	gi|12832989 (+3)	unnamed protein product [Mus musculus]	4	3	6	0	0	0

659	gi|17390379 (+4)	Sod2 protein [Mus musculus]	3	3	3	0	0	0
660	gi|12963723 (+1)	ras-related protein Rab-3B [Mus musculus], gi|	3	5	3	0	0	0
661	gi|187954745 (+3)	AP2 associated kinase 1 [Mus musculus]	3	9	2	0	0	0
662	gi|148665339 (+5)	discs, large homolog 1 (Drosophila), isoform C	0	6	3	0	0	0
663	gi|148692965 (+2)	RIKEN cDNA 5730469M10, isoform CRA_b [M	0	6	0	0	0	0
664	gi|20070420	ES1 protein homolog, mitochondrial precursor	0	6	5	0	0	0
665	gi|114326446 (+2)	myosin-9 isoform 1 [Mus musculus], gi|205371	0	6	4	0	0	0
666	gi|1001011 (+5)	heat shock protein 105 kDa beta (42 degrees (	4	4	0	0	0	0
667	gi|148664998 (+9)	dynamin 1-like, isoform CRA_a [Mus musculus	3	10	0	0	0	0
668	gi|129535 (+3)	RecName: Full=Polyadenylate-binding protein	7	7	0	0	0	0
669	gi|148707802 (+4)	aspartyl-tRNA synthetase [Mus musculus]	6	7	0	0	0	0
670	gi|18204091 (+1)	Methylcrotonoyl-Coenzyme A carboxylase 1 (a	0	4	7	0	0	0
671	gi|283549150	SH3 and multiple ankyrin repeat domains 1 [M	0	5	3	0	0	0
672	gi|23943838 (+1)	solute carrier family 25, member 1 [Mus muscu	0	4	3	0	0	0
673	gi|118136297 (+3)	disks large homolog 2 [Mus musculus], gi|1478	0	5	4	0	0	0
674	gi|169403965 (+1)	SH3 and multiple ankyrin repeat domains prote	0	9	3	0	0	0
675	gi|148671187 (+1)	ATP-binding cassette, sub-family B (MDR/TAP	0	2	11	0	0	0
676	gi|119571613 (+4)	carboxypeptidase D, isoform CRA_b [Homo sa	0	0	0	0	0	7
677	gi|119575263 (+2)	hCG2002731, isoform CRA_e [Homo sapiens]	0	0	0	0	0	7
678	gi|158429456	Chain A, Crystal Structure Of Recombinant Fu	0	0	0	0	0	9
679	gi|193506632 (+3)	Chain A, Crystal Structure Of Human Phospho	0	0	0	0	0	7
680	gi|194385728 (+2)	unnamed protein product [Homo sapiens]	0	0	0	0	0	8
681	gi|119607674 (+2)	tweety homolog 3 (Drosophila), isoform CRA_	0	0	0	0	0	6
682	gi|4502313	V-type proton ATPase 16 kDa proteolipid subu	0	0	0	0	0	2
683	gi|37537562	hypothetical protein LOC73385 [Mus musculus	2	4	4	0	0	0
684	gi|26345686 (+1)	unnamed protein product [Mus musculus]	6	5	3	0	0	0
685	gi|4503529 (+9)	eukaryotic initiation factor 4A-I [Homo sapiens]	3	3	0	0	0	2
686	gi|149286309 (+35)	histone H3 [Bispira melanostigma]	4	3	0	0	0	0
687	gi|5453555 (+2)	GTP-binding nuclear protein Ran [Homo sapie	3	3	0	0	0	0
688	gi|19526936	lanC-like protein 2 [Mus musculus], gi|4711692	4	6	0	0	0	0
689	gi|58037395	secretory carrier-associated membrane protein	2	5	0	0	0	0
690	gi|31543797 (+1)	synaptotagmin-2 [Mus musculus], gi|20072029	0	6	2	0	0	0
691	gi|62000629 (+1)	CB1 cannabinoid receptor-interacting protein 1	4	0	0	0	0	0
692	gi|125987842 (+3)	RecName: Full=Myosin-XVIIIa; AltName: Full=	2	3	7	0	0	0
693	gi|14318722 (+1)	ATPase, H+ transporting, lysosomal V1 subun	4	6	0	0	0	0
694	gi|148664460 (+7)	mCG1031566 [Mus musculus]	4	5	2	0	0	0
695	gi|112363072	actin-related protein 2/3 complex subunit 2 [Mu	4	5	0	0	0	0
696	gi|6679809 (+1)	flotillin-1 [Mus musculus], gi|13124167|sp|O08!	4	7	0	0	0	0
697	gi|32766223 (+2)	Sept4 protein [Mus musculus], gi|56800078|en	0	4	5	0	0	0
698	gi|148677565 (+2)	acetyl-Coenzyme A acyltransferase 2 (mitocho	0	7	5	0	0	0
699	gi|74142229 (+2)	unnamed protein product [Mus musculus]	0	2	6	0	0	0
700	gi|7305027 (+1)	gamma-enolase [Mus musculus], gi|119348|sp	10	2	0	0	0	0
701	gi|171846263	homer protein homolog 1 isoform L [Mus muso	0	10	2	0	0	0
702	gi|129729 (+12)	RecName: Full=Protein disulfide-isomerase; S	6	5	0	0	0	0
703	gi|12851039 (+1)	unnamed protein product [Mus musculus]	0	4	3	0	0	0
704	gi|12963571	NADH dehydrogenase [ubiquinone] 1 alpha su	0	5	7	0	0	0
705	gi|147898512 (+5)	glucose transporter 14 [Xenopus laevis], gi|16!	0	3	0	0	0	0
706	gi|13928670 (+1)	vacuolar protein sorting-associated protein 35	2	8	0	0	0	0
707	gi|6671549	peroxiredoxin-6 [Mus musculus], gi|3719451|g	5	6	0	0	0	0
708	gi|31542413 (+2)	coronin-1C [Mus musculus], gi|54041071|sp|Q	5	7	0	0	0	0
709	gi|148681230 (+6)	heterogeneous nuclear ribonucleoprotein U, is	3	8	0	0	0	0
710	gi|124486670 (+1)	mitochondrial glutamate carrier 2 [Mus muscul	0	3	6	0	0	0
711	gi|167716839 (+6)	cytochrome c oxidase subunit I [Mus musculus	0	2	2	0	0	0
712	gi|165760848	Chain L, Crystal Structure Of Humanized Kr12	0	0	0	0	0	0
713	gi|145701025 (+2)	multiple epidermal growth factor-like domains	0	0	0	0	0	9

714	gi|162138936 (+2)	hyaluronan and proteoglycan link protein 1 pre	0	0	0	0	0	0
715	gi|5032223	plexin-C1 precursor [Homo sapiens], gi|747057	0	0	0	0	0	8
716	gi|18640734	contactin-associated protein-like 5 precursor [H	0	0	0	0	0	5
717	gi|26342759 (+2)	unnamed protein product [Mus musculus]	2	3	2	2	0	0
718	gi|5031595 (+4)	actin-related protein 2/3 complex subunit 4 isof	2	3	0	0	0	2
719	gi|133777734 (+5)	Adam22 protein [Mus musculus]	2	3	2	0	0	0
720	gi|148687772 (+5)	aldehyde dehydrogenase 2, mitochondrial, isof	2	4	6	0	0	0
721	gi|226958325 (+4)	neurexin-1-alpha isoform 1 [Mus musculus]	0	4	0	0	0	0
722	gi|6755448 (+1)	vesicle-trafficking protein SEC22b [Mus muscu	0	6	0	0	0	0
723	gi|126723461 (+6)	T-complex protein 1 subunit theta [Mus muscu	6	4	0	0	0	0
724	gi|110625624 (+2)	T-complex protein 1 subunit alpha [Mus muscu	8	3	0	0	0	0
725	gi|157909797 (+2)	mitochondrial import receptor subunit TOM40 l	0	3	7	0	0	0
726	gi|6754084	glutathione S-transferase Mu 1 [Mus musculus	5	7	0	0	0	0
727	gi|2829480 (+3)	RecName: Full=Importin subunit beta-1; AltNa	5	5	0	0	0	0
728	gi|26006171 (+3)	mKIAA0531 protein [Mus musculus]	4	6	0	0	0	0
729	gi|111598711 (+6)	Ckap5 protein [Mus musculus]	0	4	3	0	0	0
730	gi|12835959 (+5)	unnamed protein product [Mus musculus]	6	6	0	0	0	0
731	gi|148686691 (+3)	Cdc42 binding protein kinase beta, isoform CR	0	3	7	0	0	0
732	gi|226494598	WD repeat-containing protein 7 [Mus musculus	0	7	0	0	0	0
733	gi|45598396	cAMP-dependent protein kinase type II-beta re	9	5	0	0	0	0
734	gi|12842244 (+2)	unnamed protein product [Mus musculus]	0	4	5	0	0	0
735	gi|68226731 (+1)	puromycin-sensitive aminopeptidase [Mus mus	9	4	0	0	0	0
736	gi|31981600 (+1)	NADH dehydrogenase [ubiquinone] 1 alpha su	0	4	6	0	0	0
737	gi|23271467 (+1)	Aldh1l1 protein [Mus musculus]	6	3	0	0	0	0
738	gi|110625942 (+2)	tudor and KH domain-containing protein [Mus l	0	3	8	0	0	0
739	gi|148695059 (+1)	mCG129387 [Mus musculus]	0	7	0	0	0	0
740	gi|119576776 (+2)	cadherin, EGF LAG seven-pass G-type recept	0	0	0	0	0	8
741	gi|119589091 (+11)	tripeptidyl peptidase I, isoform CRA_a [Homo s	0	0	0	0	0	7
742	gi|119609220 (+4)	von Willebrand factor, isoform CRA_a [Homo s	0	0	0	0	0	10
743	gi|119703744 (+1)	desmoglein-1 preproprotein [Homo sapiens], g	0	0	0	0	0	7
744	gi|148683478 (+2)	fibrinogen, gamma polypeptide [Mus musculus	0	0	7	0	0	0
745	gi|256032280	Chain A, Crystal Structure Of The Human Iono	0	0	0	0	0	2
746	gi|123858154 (+11)	leucine rich repeat containing 57 [Mus muscul	2	3	2	0	0	0
747	gi|5803135	ras-related protein Rab-35 isoform 1 [Homo sa	2	3	2	0	0	0
748	gi|118150658 (+5)	protein NDRG1 [Mus musculus], gi|6093478|sp	2	5	5	2	0	0
749	gi|14714615 (+2)	Heat shock protein 90, beta (Grp94), member	6	2	0	0	0	0
750	gi|13385680	2,4-dienoyl-CoA reductase, mitochondrial prec	0	3	5	0	0	0
751	gi|148702406 (+4)	guanine nucleotide binding protein, alpha 13, i	2	3	2	0	0	0
752	gi|71725385	GTP-binding protein Di-Ras2 [Mus musculus],	5	5	2	0	0	0
753	gi|261862282 (+2)	solute carrier family 2, facilitated glucose trans	0	4	2	0	0	0
754	gi|12832367 (+1)	unnamed protein product [Mus musculus]	0	5	0	0	0	0
755	gi|21312006	mitochondrial uncoupling protein 4 [Mus muscu	0	2	8	0	0	0
756	gi|303232360	putative membrane protein [Atopobium vagina	0	0	2	0	0	0
757	gi|6755252	transcriptional activator protein Pur-beta [Mus	4	4	0	0	0	0
758	gi|118600805 (+4)	Pccb protein [Mus musculus]	0	3	5	0	0	0
759	gi|112293266 (+4)	heat shock 70 kDa protein 4 [Mus musculus], g	3	0	0	0	0	0
760	gi|5566087 (+1)	unknown [Mus musculus], gi|12834326|dbj|BA	2	8	0	0	0	0
761	gi|12849902 (+2)	unnamed protein product [Mus musculus]	0	5	7	0	0	0
762	gi|3342500 (+1)	protein phosphatase type 2A catalytic subunit a	6	2	0	0	0	0
763	gi|12833651 (+5)	unnamed protein product [Mus musculus]	3	4	0	0	0	0
764	gi|118601004 (+1)	proline dehydrogenase, mitochondrial [Mus mu	0	3	8	0	0	0
765	gi|123242697 (+3)	LIM and SH3 protein 1 [Mus musculus]	3	4	0	0	0	0
766	gi|31980939 (+1)	mitochondrial fission protein MTP18 [Mus mus	0	2	3	0	0	0
767	gi|19882201 (+6)	26S proteasome non-ATPase regulatory subur	5	2	0	0	0	0
768	gi|31980844 (+1)	dehydrogenase/reductase SDR family membe	0	3	7	0	0	0

769	gi|7305635	ATP-dependent zinc metalloprotease YME1L1	0	3	9	0	0	0
770	gi|242397501	metaxin 3 [Mus musculus]	0	3	4	0	0	0
771	gi|149241012 (+4)	Chain A, Crystal Structure Of Mouse Cytosolic	8	0	0	0	0	0
772	gi|125490380 (+2)	vesicular inhibitory amino acid transporter [Mus	0	6	0	0	0	0
773	gi|11182364	NCBE [Mus musculus]	0	11	0	0	0	0
774	gi|131412225 (+1)	keratin, type I cytoskeletal 13 isoform a [Homo	0	0	0	0	0	8
775	gi|1888354 (+7)	placental leucine aminopeptidase [Homo sapie	0	0	0	0	0	6
776	gi|221042868 (+5)	unnamed protein product [Homo sapiens]	0	0	0	0	0	9
777	gi|31645 (+3)	glyceraldehyde-3-phosphate dehydrogenase [H	0	0	0	0	0	6
778	gi|29427656	RecName: Full=Tyrosine-protein phosphatase	0	0	0	0	0	3
779	gi|13386338	ras-related protein Rap-2b precursor [Mus mus	3	4	2	0	0	0
780	gi|56961624	AP-2 complex subunit sigma [Rattus norvegicu	0	2	3	0	0	0
781	gi|4506005 (+3)	serine/threonine-protein phosphatase PP1-beta	3	3	0	0	0	0
782	gi|4506697	40S ribosomal protein S20 isoform 2 [Homo sa	2	2	0	0	0	0
783	gi|13173473 (+6)	major prion protein precursor [Mus musculus],	2	2	3	0	0	0
784	gi|23346547	cell adhesion molecule 4 precursor [Mus musc	0	0	0	2	2	0
785	gi|26327115 (+1)	unnamed protein product [Mus musculus]	3	5	0	0	0	0
786	gi|12044402 (+9)	voltage-dependent calcium channel alpha-2-de	4	3	0	0	0	0
787	gi|157821523 (+5)	septin-11 [Rattus norvegicus], gi|148673287|gl	3	4	3	0	0	0
788	gi|165377150 (+2)	contactin-associated protein-like 2 isoform a [M	0	4	2	0	0	0
789	gi|254281331 (+3)	neutral amino acid transporter A [Mus musculu	0	3	4	0	0	0
790	gi|110625902 (+1)	gamma-soluble NSF attachment protein [Mus r	4	5	0	0	0	0
791	gi|117168299 (+1)	glutamate [NMDA] receptor subunit epsilon-2 p	0	4	2	0	0	0
792	gi|15928589 (+1)	Capn5 protein [Mus musculus], gi|74199098|dl	2	0	5	0	0	0
793	gi|14165469 (+1)	40S ribosomal protein S15a [Homo sapiens], g	4	3	0	0	0	0
794	gi|219520939 (+3)	Sbf1 protein [Mus musculus]	0	4	0	0	0	0
795	gi|148696436 (+4)	phospholipase C, beta 4, isoform CRA_b [Mus	0	4	5	0	0	0
796	gi|19526878	pyrroline-5-carboxylate reductase 2 [Mus musc	0	2	6	0	0	0
797	gi|148707070 (+3)	mCG4485, isoform CRA_a [Mus musculus], gi	0	2	3	0	0	0
798	gi|6678768	myristoylated alanine-rich C-kinase substrate [	5	3	0	0	0	0
799	gi|148708561	adaptor protein complex AP-1, beta 1 subunit,	3	5	0	0	0	0
800	gi|12805339 (+1)	Abhd12 protein [Mus musculus]	0	6	0	0	0	0
801	gi|7710012	mu-crystallin homolog [Mus musculus], gi|3913	7	3	0	0	0	0
802	gi|124007127 (+6)	RecName: Full=CLIP-associating protein 1; Alt	0	5	5	0	0	0
803	gi|15029877 (+1)	Ncald protein [Mus musculus]	5	6	0	0	0	0
804	gi|157739867 (+2)	latrophilin-1 precursor [Mus musculus], gi|1220	0	5	0	0	0	0
805	gi|20270696 (+3)	guanine deaminase [Mus spretus]	5	4	0	0	0	0
806	gi|31982091	mitochondrial import receptor subunit TOM22 h	0	4	5	0	0	0
807	gi|52317148	AP-3 complex subunit beta-2 [Mus musculus],	4	6	0	0	0	0
808	gi|12963511 (+2)	40S ribosomal protein S19 [Mus musculus], gi|	5	6	0	0	0	0
809	gi|148700464 (+3)	mCG116671 [Mus musculus]	3	4	0	0	0	0
810	gi|23396700 (+3)	RecName: Full=Bcl-2-like protein 13; Short=Bc	0	4	6	0	0	0
811	gi|131889222 (+1)	epimerase family protein SDR39U1 [Mus musc	0	3	7	0	0	0
812	gi|148841191 (+1)	RecName: Full=SH3 and multiple ankyrin repe	0	6	3	0	0	0
813	gi|26006861 (+1)	pyridoxal kinase [Mus musculus], gi|61229841	2	6	0	0	0	0
814	gi|118200730 (+2)	ATP synthase F0 subunit 8 [Mus musculus], gi	0	2	2	0	0	0
815	gi|6679421	NADPH--cytochrome P450 reductase [Mus mu	0	10	2	0	0	0
816	gi|128678 (+2)	RecName: Full=NADH-ubiquinone oxidoreduct	0	2	2	0	0	0
817	gi|26667199 (+2)	calcium/calmodulin-dependent protein kinase t	0	3	0	0	0	0
818	gi|182627625 (+3)	RecName: Full=Ankyrin repeat and sterile alph	0	4	0	0	0	0
819	gi|148539988 (+8)	paraplegin [Mus musculus], gi|123784784|sp|C	0	0	10	0	0	0
820	gi|269973915	gephyrin isoform 2 [Mus musculus]	0	10	0	0	0	0
821	gi|114657944 (+2)	PREDICTED: pyruvate kinase 3 isoform 2 [Par	0	0	0	0	0	6
822	gi|116295258 (+2)	integrin alpha-2 precursor [Homo sapiens], gi|2	0	0	0	0	0	6
823	gi|119623974 (+5)	hCG2001591 [Homo sapiens]	0	0	0	0	0	9

#	ID	Description						
824	gi|120953219 (+2)	hypothetical protein LOC67412 precursor [Mus	0	9	0	0	0	0
825	gi|124486664 (+8)	dedicator of cytokinesis protein 9 isoform 1 [Mu	0	0	9	0	0	0
826	gi|148728162 (+3)	receptor-type tyrosine-protein phosphatase eta	0	0	0	0	0	10
827	gi|19548762 (+2)	myelin gene expression factor [Mus musculus]	0	8	0	0	0	0
828	gi|219518070 (+1)	OPCML protein [Homo sapiens]	0	0	0	0	0	6
829	gi|34527233	unnamed protein product [Homo sapiens]	0	0	0	0	0	7
830	gi|4758638	peroxiredoxin-6 [Homo sapiens], gi|114565483	0	0	0	0	0	8
831	gi|5031631	lysosome membrane protein 2 [Homo sapiens]	0	0	0	0	0	6
832	gi|194386666 (+2)	unnamed protein product [Homo sapiens]	0	0	0	0	0	3
833	gi|33859751 (+2)	ras-related protein Rab-21 [Mus musculus], gi|	2	3	3	0	0	2
834	gi|148666837	monoglyceride lipase, isoform CRA_a [Mus mu	3	4	3	0	0	0
835	gi|112181167 (+1)	complement component 1 Q subcomponent-bi	0	3	2	0	0	0
836	gi|23956396	erlin-2 [Mus musculus], gi|67461571|sp|Q8BFZ	2	6	0	0	0	0
837	gi|7949037	delta(3,5)-Delta(2,4)-dienoyl-CoA isomerase,	0	2	0	0	0	0
838	gi|6678794 (+3)	dual specificity mitogen-activated protein kinas	2	3	0	0	0	0
839	gi|33859662 (+3)	synaptic vesicle membrane protein VAT-1 hom	7	2	3	0	0	0
840	gi|157951596	carbonic anhydrase 2 [Mus musculus], gi|1463	2	4	2	0	0	0
841	gi|255522817 (+4)	TBC1 domain family member 24 isoform a [Mu	3	0	7	0	0	0
842	gi|125127 (+1)	RecName: Full=6-phosphofructokinase, liver ty	2	7	0	0	0	0
843	gi|187466257 (+2)	Parkinson disease (autosomal recessive, early	4	2	0	0	0	0
844	gi|90903233	phospholipid hydroperoxide glutathione peroxi	0	2	3	0	0	0
845	gi|13384998 (+2)	mitochondrial fission 1 protein isoform 1 [Mus	0	5	5	0	0	0
846	gi|119120890 (+5)	sodium/calcium exchanger 1 isoform A [Mus m	0	3	2	0	0	0
847	gi|10092608 (+4)	glutathione S-transferase P 1 [Mus musculus],	4	5	0	0	0	0
848	gi|26354941 (+3)	unnamed protein product [Mus musculus]	5	3	0	0	0	0
849	gi|148709667 (+3)	tight junction protein 2, isoform CRA_b [Mus m	0	3	6	0	0	0
850	gi|37359776 (+6)	mKIAA0098 protein [Mus musculus]	4	4	0	0	0	0
851	gi|21313668	adipocyte plasma membrane-associated prote	0	5	0	0	0	0
852	gi|114052104 (+10)	misshapen-like kinase 1 isoform 4 [Mus muscu	0	9	0	0	0	0
853	gi|29747890 (+1)	Atp6v0c protein [Mus musculus]	0	2	0	0	0	0
854	gi|148673649 (+1)	calbindin-28K, isoform CRA_a [Mus musculus]	7	5	0	0	0	0
855	gi|13435678 (+11)	Hnrpc protein [Mus musculus]	5	5	0	0	0	0
856	gi|165377065 (+3)	UMP-CMP kinase [Mus musculus], gi|1283257	5	5	0	0	0	0
857	gi|12851918 (+3)	unnamed protein product [Mus musculus]	3	6	0	0	0	0
858	gi|7305619 (+1)	ubiquitin carboxyl-terminal hydrolase 5 [Mus m	2	6	0	0	0	0
859	gi|12835802 (+4)	unnamed protein product [Mus musculus], gi|1	3	5	0	0	0	0
860	gi|261278094 (+1)	hyperpolarization-activated cation channel 2 [N	0	2	4	0	0	0
861	gi|123123581 (+6)	heterogeneous nuclear ribonucleoprotein A3 [N	3	4	0	0	0	0
862	gi|12835861 (+6)	unnamed protein product [Mus musculus]	0	6	0	0	0	0
863	gi|13399310 (+1)	40S ribosomal protein S10 [Mus musculus], gi|	3	3	0	0	0	0
864	gi|1079734 (+5)	citron [Mus musculus]	0	0	4	0	0	0
865	gi|33859809	fibrinogen beta chain precursor [Mus musculus	0	2	9	0	0	0
866	gi|122939194 (+1)	clathrin light chain A isoform b [Mus musculus]	0	6	0	0	0	0
867	gi|33859640	transaldolase [Mus musculus], gi|2851596|sp|C	6	0	0	0	0	0
868	gi|32469489 (+1)	metabotropic glutamate receptor 3 precursor [N	0	0	0	0	0	0
869	gi|209862919 (+3)	ciliary neurotrophic factor receptor subunit alph	0	0	0	0	0	0
870	gi|12833101 (+2)	unnamed protein product [Mus musculus]	0	0	6	0	0	0
871	gi|148665040	phosphatidylinositol 4-kinase, catalytic, alpha p	0	8	0	0	0	0
872	gi|13507622 (+1)	phosphatidylinositide phosphatase SAC1 [Mus	0	6	0	0	0	0
873	gi|13786849 (+3)	Chain A, Human Muscle L-Lactate Dehydroger	0	0	0	0	0	6
874	gi|148693018 (+4)	mCG142130 [Mus musculus]	0	0	0	0	0	0
875	gi|153266885 (+3)	gamma-glutamyltransferase 5 isoform b [Homo	0	0	0	0	0	7
876	gi|166007160	Chain C, Solution Structure Of Human Immuno	0	0	0	0	0	6
877	gi|17390079 (+3)	SERPINI1 protein [Homo sapiens]	0	0	0	0	0	7
878	gi|4503143	cathepsin D preproprotein [Homo sapiens], gi|	0	0	0	0	0	7

879	gi|15079348 (+7)	Angiotensinogen (serpin peptidase inhibitor, cl	0	0	0	0	0	5
880	gi|254588110 (+2)	histone H1.3 [Mus musculus], gi|1170155|sp|P	0	4	0	0	0	0
881	gi|21281681	leucine-rich repeat LGI family member 3 precu	0	0	0	0	0	4
882	gi|15080490 (+2)	CD9 molecule [Homo sapiens]	0	0	0	0	0	3
883	gi|114640414 (+7)	PREDICTED: hypothetical protein isoform 1 [P	0	0	0	0	0	3
884	gi|148707614 (+1)	plakophilin 1 [Mus musculus]	0	3	0	0	0	0
885	gi|6680744	sodium/potassium-transporting ATPase subun	0	2	2	0	0	0
886	gi|6678930 (+1)	ras-related protein M-Ras precursor [Mus mus	3	3	2	0	0	0
887	gi|5032051 (+1)	40S ribosomal protein S14 [Homo sapiens], gi|	0	5	0	0	0	0
888	gi|30841008	ras-related protein Rab-18 [Mus musculus], gi|	3	3	3	0	0	0
889	gi|148697407 (+1)	RIKEN cDNA 0910001A06, isoform CRA_b [M	4	2	0	0	0	0
890	gi|19527388 (+2)	ubiquitin thioesterase OTUB1 [Mus musculus],	2	2	0	0	0	0
891	gi|12833165 (+2)	unnamed protein product [Mus musculus]	2	5	2	0	0	0
892	gi|9790125	transgelin-3 [Mus musculus], gi|9910790|sp|Q9	4	4	0	0	0	0
893	gi|115424 (+3)	RecName: Full=Cadherin-2; AltName: Full=Ne	0	3	0	0	0	0
894	gi|148703639 (+2)	ectonucleotide pyrophosphatase/phosphodiest	0	3	0	0	0	0
895	gi|148700019 (+3)	phytanoyl-CoA hydroxylase interacting protein-	3	2	0	0	0	0
896	gi|9790141	actin-related protein 2/3 complex subunit 3 [Mu	3	5	0	0	0	0
897	gi|13385260	acyl-coenzyme A thioesterase 13 [Mus muscul	0	2	3	0	0	0
898	gi|148698877 (+2)	phosphatidic acid phosphatase type 2B, isofor	0	3	2	0	0	0
899	gi|14715019 (+3)	Syntaxin 12 [Mus musculus]	2	5	0	0	0	0
900	gi|226874865 (+4)	lethal(2) giant larvae protein homolog 1 isoforn	0	0	6	0	0	0
901	gi|148674381 (+2)	ganglioside-induced differentiation-associated	0	4	5	0	0	0
902	gi|115511018 (+1)	probable ubiquitin carboxyl-terminal hydrolase	3	3	0	0	0	0
903	gi|74223032	unnamed protein product [Mus musculus]	2	3	0	0	0	0
904	gi|117606375 (+5)	neuronal-specific septin-3 [Mus musculus], gi|3	0	3	0	0	0	0
905	gi|1098541 (+2)	osmotic stress protein 94 [Mus musculus]	6	5	0	0	0	0
906	gi|114842403 (+4)	TNF receptor-associated factor 3 isoform b [Mu	0	5	6	0	0	0
907	gi|23956084	very long-chain specific acyl-CoA dehydrogena	0	4	5	0	0	0
908	gi|126521835	T-complex protein 1 subunit beta [Mus muscul	6	4	0	0	0	0
909	gi|148694486 (+3)	mCG18842, isoform CRA_a [Mus musculus], g	0	2	4	0	0	0
910	gi|31560239	L-asparaginase [Mus musculus], gi|81875980|s	3	3	0	0	0	0
911	gi|148700758 (+2)	amphiphysin [Mus musculus]	3	5	0	0	0	0
912	gi|33468999	catechol O-methyltransferase domain-containir	0	3	3	0	0	0
913	gi|148700985 (+6)	carnitine palmitoyltransferase 1a, liver, isoform	0	3	4	0	0	5
914	gi|118490060 (+5)	inducible heat shock protein 70 [Mus musculus	0	3	0	0	0	0
915	gi|30519896	protein BAT5 [Mus musculus], gi|23813768|sp|	0	2	5	0	0	0
916	gi|148698451 (+3)	CAP, adenylate cyclase-associated protein 1 (y	7	3	0	0	0	0
917	gi|183980004 (+2)	heterogeneous nuclear ribonucleoprotein L [Mu	2	4	0	0	0	0
918	gi|15809016 (+1)	myosin regulatory light chain 12B [Homo sapie	2	4	0	0	0	0
919	gi|21313544	mitochondrial chaperone BCS1 [Mus musculus	0	2	7	0	0	0
920	gi|122065194 (+7)	RecName: Full=Glutamate receptor, ionotropic	0	2	0	0	0	0
921	gi|116089318 (+2)	disheveled-associated activator of morphogen	0	2	5	0	0	0
922	gi|110279023	RecName: Full=IQ motif and SEC7 domain-co	0	8	2	0	0	0
923	gi|13385672 (+2)	solute carrier family 25 member 46 [Mus musc	0	2	7	0	0	0
924	gi|21312546	growth and transformation-dependent protein [	0	0	5	0	0	0
925	gi|157909807	contactin-4 isoform 1 [Mus musculus], gi|55976	0	0	0	0	0	0
926	gi|35215309	neurofascin isoform 1 precursor [Mus musculu	0	0	0	0	0	0
927	gi|209862927	dipeptidyl aminopeptidase-like protein 6 isoforn	0	6	0	0	0	0
928	gi|134949013 (+1)	rho-associated protein kinase 2 [Mus musculus	0	8	0	0	0	0
929	gi|148700251 (+5)	calcium binding atopy-related autoantigen 1, is	0	0	8	0	0	0
930	gi|148669291 (+2)	cDNA sequence BC034204, isoform CRA_a [M	0	0	11	0	0	0
931	gi|158303335 (+5)	synaptopodin isoform A [Mus musculus], gi|741	0	7	0	0	0	0
932	gi|224922765 (+1)	BMP/retinoic acid-inducible neural-specific pro	0	0	0	0	0	0
933	gi|26333111	unnamed protein product [Mus musculus]	0	0	0	0	0	0

934 gi|282398110 (+1)	keratin, type II cuticular Hb2 [Mus musculus], g	0	8	0	0	0	0
935 gi|6755256	glycogen phosphorylase, muscle form [Mus mu	0	6	0	0	0	0
936 gi|16877071 (+2)	ATP synthase, H+ transporting, mitochondrial	0	0	0	0	0	4
937 gi|10863935 (+2)	reticulon-1 isoform A [Homo sapiens], gi|12643	0	0	0	0	0	4
938 gi|193784902	unnamed protein product [Homo sapiens]	0	0	0	0	0	3
939 gi|13385960 (+13)	ATP synthase lipid-binding protein, mitochondr	0	0	2	0	0	2
940 gi|303390013	alpha-tubulin [Encephalitozoon intestinalis ATC	2	0	0	0	0	0
941 gi|148697726 (+1)	thiosulfate sulfurtransferase, mitochondrial, iso	4	3	3	0	0	0
942 gi|148670856 (+4)	aldehyde dehydrogenase family 6, subfamily A	0	2	2	0	0	0
943 gi|148702497 (+3)	RIKEN cDNA 1500005I02, isoform CRA_a [Mu	2	4	0	0	0	0
944 gi|2801793 (+3)	putative membrane associated progesterone re	3	3	2	0	0	0
945 gi|161484610 (+2)	ectonucleoside triphosphate diphosphohydrola	0	2	3	0	0	0
946 gi|12848106 (+3)	unnamed protein product [Mus musculus]	4	3	0	0	0	0
947 gi|7305305	protein NDRG2 isoform 1 [Mus musculus], gi|8	2	5	0	0	0	0
948 gi|12846004 (+3)	unnamed protein product [Mus musculus], gi|1	2	5	0	0	0	0
949 gi|109809743	Golgin subfamily A member 7 [Mus musculus],	4	0	0	0	0	0
950 gi|12846524 (+2)	unnamed protein product [Mus musculus]	5	0	0	0	0	0
951 gi|6680309 (+1)	10 kDa heat shock protein, mitochondrial [Mus	3	0	3	0	0	0
952 gi|12963799 (+1)	V-type proton ATPase subunit D [Mus muscul	3	4	0	0	0	0
953 gi|12852148 (+4)	unnamed protein product [Mus musculus]	6	3	0	0	0	0
954 gi|6680836 (+2)	calreticulin precursor [Mus musculus], gi|11750	3	2	0	0	0	0
955 gi|123229396 (+2)	SH3-domain GRB2-like 2 [Mus musculus], gi|1	5	3	0	0	0	0
956 gi|12842709 (+1)	unnamed protein product [Mus musculus], gi|2	0	3	3	0	0	0
957 gi|9910194	dihydroorotate dehydrogenase, mitochondrial p	0	3	5	0	0	0
958 gi|12833936 (+3)	unnamed protein product [Mus musculus]	0	3	3	0	0	0
959 gi|149751320 (+1)	PREDICTED: similar to tropomyosin 3 isoform	4	2	0	0	0	0
960 gi|26336675 (+2)	unnamed protein product [Mus musculus]	0	4	2	0	0	0
961 gi|1709759 (+2)	RecName: Full=Proteasome subunit alpha type	7	2	0	0	0	0
962 gi|13879530 (+4)	Fech protein [Mus musculus]	0	2	5	0	0	0
963 gi|12963791	retinol dehydrogenase 14 [Mus musculus], gi|3	0	2	3	0	0	0
964 gi|13384642 (+6)	synaptojanin-2-binding protein [Mus musculus]	0	2	4	0	0	0
965 gi|28972680	mKIAA1232 protein [Mus musculus], gi|148682	0	5	2	0	0	0
966 gi|148707095 (+4)	coatomer protein complex subunit alpha, isofor	2	4	0	0	0	0
967 gi|160333877 (+5)	kinesin-like protein KIF1A isoform b [Mus musc	6	2	0	0	0	0
968 gi|14250287 (+2)	DEAD (Asp-Glu-Ala-Asp) box polypeptide 1 [M	0	5	0	0	0	0
969 gi|125660458 (+4)	zinc transporter 9 [Mus musculus], gi|1585638	0	0	6	0	0	0
970 gi|30424792	inactive hydroxysteroid dehydrogenase-like pro	0	0	7	0	0	0
971 gi|300857642	DNA topoisomerase I [Corynebacterium pseud	2	0	0	0	0	0
972 gi|148665540 (+4)	syntaxin binding protein 5-like, isoform CRA_a	0	6	0	0	0	0
973 gi|123297068 (+5)	ribophorin II [Mus musculus]	0	8	0	0	0	0
974 gi|6009521 (+3)	p100 co-activator [Mus musculus]	0	8	0	0	0	0
975 gi|31377644	ATPase family AAA domain-containing protein	0	0	6	0	0	0
976 gi|148675357 (+3)	proteasome (prosome, macropain) subunit, alp	4	0	0	0	0	0
977 gi|213688408 (+1)	leucine rich repeat and Ig domain containing 1	0	0	0	0	0	0
978 gi|148709253 (+2)	drebrin 1, isoform CRA_b [Mus musculus]	0	6	0	0	0	0
979 gi|148682448 (+5)	regulating synaptic membrane exocytosis 1 [M	0	6	0	0	0	0
980 gi|111154076	dystonin isoform b [Mus musculus]	0	7	0	0	0	0
981 gi|109255249 (+3)	keratin, type II cytoskeletal 4 [Homo sapiens]	0	0	0	0	0	9
982 gi|110224476 (+6)	proactivator polypeptide isoform b preprotein	0	0	0	0	0	8
983 gi|13111975 (+1)	Acid phosphatase 2, lysosomal [Homo sapiens	0	0	0	0	0	6
984 gi|177216 (+5)	4F2 heavy chain antigen [Homo sapiens]	0	0	0	0	0	6
985 gi|119571963 (+4)	ADAM metallopeptidase domain 11, isoform C	0	0	0	0	0	5
986 gi|134104498 (+1)	Chain A, Crystal Structure Of Human Mu_cryst	0	0	0	0	0	5
987 gi|196049886 (+2)	Chain A, Crystal Structure Of Human 3-Oxoac	0	0	0	0	0	4
988 gi|203282367 (+3)	Chain A, Crystal Structure Of Human Enolase	0	0	0	0	0	4

989	gi|50592988	cytochrome b-c1 complex subunit 2, mitochond	0	0	0	0	0	5
990	gi|145579640 (+5)	Chain A, Crystal Structure Of The Complex Fo	0	0	0	0	0	3
991	gi|148683476 (+3)	fibrinogen, alpha polypeptide, isoform CRA_a |	0	0	3	0	0	0
992	gi|119583097 (+6)	neurotrophic tyrosine kinase, receptor, type 2,	0	0	0	0	0	3
993	gi|13430254 (+3)	Niemann-Pick disease C1 protein [Homo sapie	0	0	0	0	0	3
994	gi|27764867 (+2)	synaptophysin [Homo sapiens], gi|135162|sp|F	0	0	0	0	0	3
995	gi|21614544 (+2)	protein S100-A8 [Homo sapiens], gi|11455969	0	0	0	0	0	2
996	gi|30424655	ras-related protein Rab-6B [Mus musculus], gi|	2	2	0	0	0	0
997	gi|76677920 (+1)	metallo-beta-lactamase domain-containing pro	0	4	0	0	0	0
998	gi|312596932	choline transporter-like protein 2 isoform 1 [Mu	0	2	2	0	0	0
999	gi|148671583 (+2)	mCG116242 [Mus musculus]	2	3	3	0	0	0
1000	gi|148703383 (+2)	profilin 2, isoform CRA_b [Mus musculus]	2	2	0	0	0	0
1001	gi|26347955 (+4)	unnamed protein product [Mus musculus]	2	2	2	0	0	0
1002	gi|12857969 (+4)	unnamed protein product [Mus musculus]	0	4	3	0	0	0
1003	gi|47168790 (+1)	Chain A, Crystal Structure Of The Extracellular	0	2	0	2	0	0
1004	gi|6677819	ras-related protein R-Ras precursor [Mus musc	3	0	3	0	0	0
1005	gi|148664250 (+1)	heterogeneous nuclear ribonucleoprotein D-lik	0	2	0	0	0	0
1006	gi|148694365 (+5)	guanine nucleotide binding protein, beta 5, isof	3	4	0	0	0	0
1007	gi|148692793 (+1)	calcium channel, voltage-dependent, alpha2/de	3	3	0	0	0	0
1008	gi|11230802 (+2)	alpha-actinin-4 [Mus musculus], gi|13123946|s	2	3	0	0	0	0
1009	gi|14210522 (+1)	microtubule-associated proteins 1A/1B light ch	0	2	0	0	0	0
1010	gi|11559579 (+3)	keratin intermediate filament 16a [Mus muscul	0	0	0	2	0	0
1011	gi|301156486	unnamed protein product [Haemophilus parain	0	2	0	0	0	0
1012	gi|157041260 (+5)	band 4.1-like protein 2 [Mus musculus], gi|3129	3	0	4	0	0	0
1013	gi|50511055 (+1)	mKIAA1699 protein [Mus musculus]	0	4	4	0	0	0
1014	gi|148679537 (+5)	alanyl-tRNA synthetase, isoform CRA_a [Mus	3	4	0	0	0	0
1015	gi|148678911 (+2)	mCG7984 [Mus musculus]	4	4	0	0	0	0
1016	gi|12846904 (+6)	unnamed protein product [Mus musculus]	3	4	0	0	0	0
1017	gi|148698427 (+2)	mCG5769, isoform CRA_a [Mus musculus]	0	3	3	0	0	0
1018	gi|13195630	coiled-coil domain-containing protein 127 isofo	0	3	4	0	0	0
1019	gi|123701966 (+1)	BTB/POZ domain-containing protein KCTD12	3	4	0	0	0	0
1020	gi|148690599 (+1)	protein kinase C and casein kinase substrate in	4	3	0	0	0	0
1021	gi|15029927 (+1)	Rps13 protein [Mus musculus], gi|148685152|g	2	5	0	0	0	0
1022	gi|148679269 (+2)	dynein, cytoplasmic 1 light intermediate chain 2	2	4	0	0	0	0
1023	gi|294610683 (+2)	mitochondrial carrier triple repeat protein 1 [Mu	0	2	4	0	0	0
1024	gi|11596855 (+1)	transferrin receptor protein 1 [Mus musculus],	2	5	0	0	0	0
1025	gi|6680690	thioredoxin-dependent peroxide reductase, mit	0	2	4	0	0	0
1026	gi|254553372 (+1)	isoleucyl-tRNA synthetase, cytoplasmic [Mus n	2	4	0	0	0	0
1027	gi|12851441 (+1)	unnamed protein product [Mus musculus]	2	3	0	0	0	0
1028	gi|116283229 (+3)	Pa2g4 protein [Mus musculus], gi|116283255|g	6	2	0	0	0	0
1029	gi|83921605	mitochondrial import receptor subunit TOM40E	0	2	5	0	0	0
1030	gi|225637533 (+1)	neuronal cell adhesion molecule isoform 1 [Mu	2	3	0	0	0	0
1031	gi|26328391 (+4)	unnamed protein product [Mus musculus]	2	5	0	0	0	0
1032	gi|12835839 (+5)	unnamed protein product [Mus musculus]	0	0	4	0	0	0
1033	gi|140972309 (+1)	NADH dehydrogenase [ubiquinone] flavoprotei	0	0	2	0	0	0
1034	gi|41680705	glutamate [NMDA] receptor subunit epsilon-1 p	0	0	0	0	0	0
1035	gi|58219050	OCIA domain-containing protein 2 [Mus muscu	0	2	5	0	0	0
1036	gi|148271067 (+3)	myeloid-associated differentiation marker [Mus	0	2	0	0	0	0
1037	gi|148695348 (+2)	thioredoxin domain containing 14, isoform CRA	0	5	0	0	0	0
1038	gi|21362277	CDP-diacylglycerol--inositol 3-phosphatidyltran	0	5	0	0	0	0
1039	gi|255003819	transmembrane emp24 protein transport doma	0	0	0	0	0	0
1040	gi|23346595	protein QIL1 [Mus musculus], gi|81901671|sp|(	0	0	3	0	0	0
1041	gi|299150259	cytochrome b [Heliophobius sp. CGF-2010a]	0	0	2	0	0	0
1042	gi|148703544 (+1)	mCG116006 [Mus musculus]	0	0	6	0	0	0
1043	gi|253763 (+1)	glutamic acid decarboxylase, GAD [mice, brain	0	8	0	0	0	0

1044	gi|161168996 (+2)	caskin-1 [Mus musculus], gi|61212969|sp|Q6P	0	8	0	0	0	0
1045	gi|13096987 (+5)	Me1 protein [Mus musculus]	7	0	0	0	0	0
1046	gi|148701560 (+6)	annexin A6, isoform CRA_b [Mus musculus]	6	0	0	0	0	0
1047	gi|170014689	VPS10 domain-containing receptor SorCS2 pr	0	0	0	0	0	6
1048	gi|21755908 (+2)	unnamed protein product [Homo sapiens]	0	0	0	0	0	6
1049	gi|123228108 (+4)	aconitase 2, mitochondrial [Homo sapiens], gi|	0	0	0	0	0	6
1050	gi|148706281 (+1)	solute carrier family 25 (mitochondrial carrier;	0	0	6	0	0	0
1051	gi|225697919 (+1)	Chain A, Crystal Structure Of Human Extracell	0	0	0	0	0	5
1052	gi|4826816	leucine-rich glioma-inactivated protein 1 precu	0	0	0	0	0	5
1053	gi|13543618 (+5)	ATP synthase, H+ transporting, mitochondrial	0	0	0	0	0	4
1054	gi|119593119 (+7)	ATPase, H+ transporting, lysosomal accessory	0	0	0	0	0	3
1055	gi|119627382 (+4)	peroxiredoxin 1, isoform CRA_b [Homo sapien	0	0	0	0	0	4
1056	gi|119631168 (+2)	cadherin 6, type 2, K-cadherin (fetal kidney), is	0	0	0	0	0	2
1057	gi|1638835 (+3)	vacuolar-type H(+)-ATPase 115 kDa subunit [H	0	0	0	0	0	2
1058	gi|148667828 (+2)	LanC (bacterial lantibiotic synthetase compone	0	3	2	0	0	0
1059	gi|148670001 (+1)	guanine nucleotide binding protein, alpha inhib	3	3	2	0	0	0
1060	gi|21313162	ras-related protein Rab-1B [Mus musculus], gi|	2	2	2	0	0	0
1061	gi|193436	G-protein beta subunit [Mus musculus], gi|193	3	0	2	0	0	0
1062	gi|133778953 (+3)	keratin, type II cytoskeletal 4 [Mus musculus],	0	0	2	3	0	0
1063	gi|111955312 (+4)	OX-2 membrane glycoprotein precursor [Mus r	3	0	0	0	0	0
1064	gi|18093102 (+1)	dynamin-1 [Rattus norvegicus], gi|56054|emb|(	0	0	2	0	0	0
1065	gi|27370248	prenylcysteine oxidase-like precursor [Mus mu	0	3	0	0	0	0
1066	gi|13385294 (+4)	prenylcysteine oxidase precursor [Mus muscul	0	5	0	0	0	0
1067	gi|168177243 (+2)	Chain A, Crystal Structure Of The Extracellular	0	4	0	0	0	0
1068	gi|10946936 (+1)	adenylate kinase isoenzyme 1 isoform 1 [Mus	3	2	0	0	0	0
1069	gi|307642237 (+1)	elongation factor 1 alpha [Acrolophus popeane	2	2	0	0	0	0
1070	gi|6754086	glutathione S-transferase Mu 5 [Mus musculus	2	2	0	0	0	0
1071	gi|13435867 (+2)	Epha4 protein [Mus musculus]	0	6	0	0	0	0
1072	gi|34098931	calretinin [Mus musculus], gi|13637964|sp|Q08	3	4	0	0	0	0
1073	gi|162138915 (+2)	carnitine O-palmitoyltransferase 2, mitochondr	0	3	5	0	0	0
1074	gi|21312260 (+1)	aldehyde dehydrogenase X, mitochondrial pre	0	3	4	0	0	0
1075	gi|148687862 (+2)	mCG7941, isoform CRA_b [Mus musculus]	4	3	0	0	0	0
1076	gi|1205976 (+7)	p162 protein [Mus musculus]	2	4	0	0	0	0
1077	gi|148681636 (+2)	single-stranded DNA binding protein 1, isoform	0	3	3	0	0	0
1078	gi|13507666 (+1)	serine beta-lactamase-like protein LACTB, mit	0	2	3	0	0	0
1079	gi|148700170 (+2)	mCG15755 [Mus musculus]	0	4	0	3	0	0
1080	gi|12836203 (+5)	unnamed protein product [Mus musculus]	2	3	0	0	0	0
1081	gi|30851559 (+1)	Mapre1 protein [Mus musculus]	3	2	0	0	0	0
1082	gi|53035 (+1)	cyclophilin CyP-S1 [Mus musculus], gi|192865	2	5	0	0	0	0
1083	gi|112491045 (+6)	Chain A, Crystal Structure Of Murine Carnitine	0	2	5	0	0	0
1084	gi|161016786 (+1)	liprin-alpha-3 [Mus musculus], gi|190148195|gl	2	5	0	0	0	0
1085	gi|148672368 (+8)	kinesin family member 21A, isoform CRA_a [M	2	5	0	0	0	0
1086	gi|148706135 (+4)	tripartite motif protein 28 [Mus musculus]	2	4	0	0	0	0
1087	gi|123248297 (+2)	discs, large (Drosophila) homolog-associated p	0	3	2	0	0	0
1088	gi|117647240 (+12)	MAP kinase-activating death domain protein is	2	4	0	0	0	0
1089	gi|18606328 (+2)	Biphenyl hydrolase-like (serine hydrolase, brea	0	2	2	0	0	0
1090	gi|13529464 (+12)	Nucleolin [Mus musculus]	5	2	0	0	0	0
1091	gi|134053905 (+2)	26S proteasome non-ATPase regulatory subur	4	0	0	0	0	0
1092	gi|12844972 (+4)	unnamed protein product [Mus musculus]	2	3	0	0	0	0
1093	gi|25742772 (+1)	potassium voltage-gated channel subfamily A r	0	0	3	0	0	0
1094	gi|160333729 (+2)	endonuclease domain-containing 1 protein pre	0	5	0	0	0	0
1095	gi|226958579	hypothetical protein LOC219189 isoform 1 [Mu	0	0	2	0	0	0
1096	gi|74178273	unnamed protein product [Mus musculus]	2	0	0	0	0	0
1097	gi|60360034 (+1)	mKIAA0167 protein [Mus musculus]	0	7	0	0	0	0
1098	gi|12849790 (+1)	unnamed protein product [Mus musculus]	0	0	5	0	0	0

1099 gi|148704781 (+2)	proteasome (prosome, macropain) subunit, alp	4	0	0	0	0	0
1100 gi|17505218 (+1)	growth hormone-inducible transmembrane pro	0	0	2	0	0	0
1101 gi|110626050 (+1)	thioesterase superfamily member 4 [Mus musc	0	0	2	0	0	0
1102 gi|148681362 (+1)	mCG140375 [Mus musculus]	0	3	0	0	0	0
1103 gi|6679339	membrane-associated phosphatidylinositol tran	0	6	0	0	0	0
1104 gi|68510034	coxsackievirus and adenovirus receptor homol	6	0	0	0	0	0
1105 gi|157830573 (+4)	Chain A, Structure Of A Soluble, Glycosylated	0	0	0	0	0	5
1106 gi|56090652	solute carrier family 25 member 42 [Mus musc	0	0	5	0	0	0
1107 gi|28435 (+6)	unnamed protein product [Homo sapiens]	0	0	0	0	0	4
1108 gi|123229264 (+1)	CDP-diacylglycerol synthase (phosphatidate cy	0	4	0	0	0	0
1109 gi|12833183 (+2)	unnamed protein product [Mus musculus]	3	0	0	0	0	0
1110 gi|19924101 (+3)	synapsin-2 isoform IIb [Homo sapiens]	0	0	0	0	0	3
1111 gi|115430112 (+3)	receptor expression-enhancing protein 5 [Hom	0	0	0	0	0	3
1112 gi|116666863 (+3)	Chain A, The Structure Of A Truncated, Solubl	0	0	0	0	0	3
1113 gi|28195384	neuronal pentraxin-2 precursor [Homo sapiens	0	0	0	0	0	2
1114 gi|194381454 (+4)	unnamed protein product [Homo sapiens]	0	0	0	0	0	2
1115 gi|20279132	plasmolipin [Mus musculus], gi|20978556|sp|Q	0	0	2	0	0	0
1116 gi|148670626 (+1)	mCG144006 [Mus musculus]	2	0	0	0	0	0
1117 gi|157951706 (+3)	hypoxia up-regulated protein 1 precursor [Mus	0	2	0	0	0	0
1118 gi|4501881 (+3)	actin, alpha skeletal muscle [Homo sapiens], g	2	0	0	0	0	0
1119 gi|148674574 (+3)	mCG20085, isoform CRA_a [Mus musculus]	3	2	0	0	0	0
1120 gi|26325436 (+5)	unnamed protein product [Mus musculus]	2	3	0	0	0	0
1121 gi|14028714 (+3)	Rho GTPase-activating protein [Mus musculus	2	3	0	0	0	0
1122 gi|148691088 (+2)	kinesin family member 5B [Mus musculus]	4	2	0	0	0	0
1123 gi|148685910 (+5)	inositol polyphosphate-5-phosphatase A, isofo	4	2	0	0	0	0
1124 gi|12861409 (+5)	unnamed protein product [Mus musculus]	2	2	0	0	0	0
1125 gi|293597551 (+6)	septin-6 isoform 3 [Mus musculus], gi|2633934	2	0	0	0	0	0
1126 gi|1256436 (+3)	APC-binding protein EB2 [Mus musculus]	0	3	0	0	0	0
1127 gi|148679920 (+3)	neuronal growth regulator 1, isoform CRA_b [M	2	0	0	0	0	0
1128 gi|13385012	mitochondrial import inner membrane transloca	0	3	3	0	0	0
1129 gi|12833259 (+3)	unnamed protein product [Mus musculus]	0	0	2	0	0	0
1130 gi|13435621 (+3)	Hypoxanthine guanine phosphoribosyl transfer	5	0	0	0	0	0
1131 gi|26333963	unnamed protein product [Mus musculus]	0	2	0	0	0	0
1132 gi|9790077	glycogen synthase kinase-3 beta [Mus muscul	3	2	0	0	0	0
1133 gi|10946902	sphingomyelin phosphodiesterase 3 [Mus mus	0	4	0	0	0	0
1134 gi|58037267 (+3)	protein disulfide-isomerase A6 [Mus musculus]	3	3	0	0	0	0
1135 gi|30520239 (+1)	neutral cholesterol ester hydrolase 1 [Mus mus	3	3	0	0	0	0
1136 gi|73622267 (+1)	methylcrotonoyl-CoA carboxylase beta chain, r	0	4	3	0	0	0
1137 gi|15030315 (+4)	Cttn protein [Mus musculus], gi|74223237|dbj|E	3	3	0	0	0	0
1138 gi|133778992 (+1)	potassium voltage-gated channel subfamily C	0	2	3	0	0	0
1139 gi|6679501	26S protease regulatory subunit 4 [Mus muscu	2	3	0	0	0	0
1140 gi|13124464 (+15)	RecName: Full=Prominin-1; AltName: Full=Ant	0	0	5	2	0	0
1141 gi|262050556 (+1)	FUN14 domain-containing protein 2 [Mus musc	0	2	5	0	0	0
1142 gi|12845784 (+5)	unnamed protein product [Mus musculus], gi|1	2	4	0	0	0	0
1143 gi|22550094	cAMP-dependent protein kinase type II-alpha r	4	2	0	0	0	0
1144 gi|157951741 (+3)	catalase [Mus musculus], gi|74139430|dbj|BAE	2	3	0	0	0	0
1145 gi|148704346 (+2)	copine VI, isoform CRA_a [Mus musculus]	3	2	0	0	0	0
1146 gi|124486885 (+3)	leucine-rich repeat-containing protein 7 [Mus m	0	3	0	0	0	0
1147 gi|111120337 (+3)	TBC1 domain family member 17 [Mus muscul	0	2	2	0	0	0
1148 gi|27923929	hippocalcin-like protein 4 [Mus musculus], gi|5	2	5	0	0	0	0
1149 gi|5107168 (+1)	small zinc finger-like protein [Mus musculus]	0	2	3	0	0	0
1150 gi|20071583 (+3)	Tspan7 protein [Mus musculus]	2	2	0	0	0	0
1151 gi|116734870 (+2)	leukotriene A-4 hydrolase [Mus musculus], gi|7	2	2	0	0	0	0
1152 gi|148671985 (+6)	mCG15678, isoform CRA_c [Mus musculus]	2	0	0	0	0	0
1153 gi|28077049	charged multivesicular body protein 4b [Mus m	2	4	0	0	0	0

1154	gi|9506911	NADH dehydrogenase [ubiquinone] 1 alpha su	0	2	2	0	0	0
1155	gi|26328385 (+3)	unnamed protein product [Mus musculus]	4	2	0	0	0	0
1156	gi|118196876 (+6)	2310061I04Rik protein [Mus musculus], gi|118	0	2	3	0	0	0
1157	gi|13435636 (+3)	Tmed9 protein [Mus musculus]	0	4	0	0	0	0
1158	gi|27229021 (+1)	succinate dehydrogenase [ubiquinone] cytochr	0	0	3	0	0	0
1159	gi|256985123 (+3)	synapsin-3 isoform 1 [Mus musculus]	0	3	0	0	0	0
1160	gi|307333935	beta-tubulin [Peronosclerospora maydis]	0	2	0	0	0	0
1161	gi|1022323 (+3)	collagen alpha-2(IV) chain [Mus musculus]	0	0	2	0	0	0
1162	gi|148681383 (+2)	peptidyl arginine deiminase, type II [Mus musc	0	0	4	0	0	0
1163	gi|15986733	GTP-binding protein RAB4 [Mus musculus]	0	4	0	0	0	0
1164	gi|6678437 (+4)	translationally-controlled tumor protein [Mus m	2	0	0	0	0	0
1165	gi|26453371 (+1)	axotomy induced glycoprotein 3 [Mus muscul	0	0	2	0	0	0
1166	gi|13994209 (+1)	wiskott-Aldrich syndrome protein family membe	0	6	0	0	0	0
1167	gi|131412178 (+2)	kinesin light chain 1 isoform 1D [Mus musculus	0	3	0	0	0	0
1168	gi|12836024 (+9)	unnamed protein product [Mus musculus]	0	3	0	0	0	0
1169	gi|22122427 (+1)	phytanoyl-CoA hydroxylase-interacting protein	0	3	0	0	0	0
1170	gi|125987790 (+7)	RecName: Full=Rho guanine nucleotide excha	0	6	0	0	0	0
1171	gi|148669655 (+2)	aquaporin 4, isoform CRA_c [Mus musculus]	0	2	0	0	0	0
1172	gi|209977076 (+1)	long-chain-fatty-acid--CoA ligase 3 isoform b [M	0	4	0	0	0	0
1173	gi|22122457	mitochondrial Rho GTPase 2 [Mus musculus],	0	0	6	0	0	0
1174	gi|7106387 (+2)	proteasome subunit alpha type-5 [Mus muscul	6	0	0	0	0	0
1175	gi|12832714 (+5)	unnamed protein product [Mus musculus]	4	0	0	0	0	0
1176	gi|148694205 (+3)	mCG141703, isoform CRA_a [Mus musculus]	5	0	0	0	0	0
1177	gi|148693260 (+1)	RIKEN cDNA 1810026J23 [Mus musculus]	0	0	5	0	0	0
1178	gi|21703770 (+1)	myeloid leukemia factor 2 [Mus musculus], gi|1	0	5	0	0	0	0
1179	gi|37360977 (+5)	ERC protein 2 [Mus musculus], gi|34783581|gb	0	6	0	0	0	0
1180	gi|226471 (+2)	Cu/Zn superoxide dismutase	4	0	0	0	0	0
1181	gi|52350563	probable G-protein coupled receptor 158 precu	0	2	0	0	0	0
1182	gi|238776842 (+1)	inactive dipeptidyl peptidase 10 [Mus musculus	0	4	0	0	0	0
1183	gi|54144633 (+1)	phosphatase and actin regulator 1 isoform 1 [M	0	4	0	0	0	0
1184	gi|111598731 (+1)	Gria3 protein [Mus musculus]	0	0	0	0	0	0
1185	gi|126340424 (+2)	PREDICTED: hypothetical protein [Monodelph	4	0	0	0	0	0
1186	gi|124486895 (+3)	6-phosphogluconate dehydrogenase, decarbox	3	0	0	0	0	0
1187	gi|145587082 (+1)	triple functional domain protein [Mus musculus	0	4	0	0	0	0
1188	gi|148699794 (+4)	1-acylglycerol-3-phosphate O-acyltransferase	0	4	0	0	0	0
1189	gi|21311871	nebulette [Mus musculus], gi|12835961|dbj|BA	0	5	0	0	0	0
1190	gi|109658664 (+23)	Fibronectin 1 [Homo sapiens], gi|119590942|gt	0	0	0	0	0	7
1191	gi|12841706 (+6)	unnamed protein product [Mus musculus]	7	0	0	0	0	0
1192	gi|118130807 (+3)	calcium-independent phospholipase A2-gamm	0	0	5	0	0	0
1193	gi|188497650 (+2)	malectin precursor [Mus musculus], gi|6290060	0	5	0	0	0	0
1194	gi|120537280 (+6)	C230096C10Rik protein [Mus musculus]	0	5	0	0	0	0
1195	gi|224809594 (+1)	family with sequence similarity 5, member C pr	0	0	0	0	0	0
1196	gi|6754450	fatty acid-binding protein, epidermal [Mus mus	5	0	0	0	0	0
1197	gi|119626065 (+22)	albumin, isoform CRA_b [Homo sapiens]	0	0	0	0	0	5
1198	gi|11141887	hyaluronan and proteoglycan link protein 2 pre	0	0	0	0	0	5
1199	gi|15215175 (+2)	Vacuolar protein sorting 45 (yeast) [Mus musc	0	4	0	0	0	0
1200	gi|159110562 (+2)	intercellular adhesion molecule 5 precursor [M	0	4	0	0	0	0
1201	gi|74188489	unnamed protein product [Mus musculus]	0	0	0	0	0	0
1202	gi|148669959 (+4)	solute carrier family 6 (neurotransmitter transp	0	3	0	0	0	0
1203	gi|10946856 (+7)	receptor-type tyrosine-protein phosphatase T [	0	0	0	0	0	0
1204	gi|11602963 (+5)	heparan sulfate proteoglycan perlecan [Homo	0	0	0	0	0	4
1205	gi|60097902	filaggrin [Homo sapiens], gi|84028206|sp|P209	0	0	0	0	0	4
1206	gi|157384998	low-density lipoprotein receptor-related protein	0	0	0	0	0	4
1207	gi|253314532 (+1)	synaptoporin isoform 1 [Mus musculus], gi|128	0	4	0	0	0	0
1208	gi|148747309 (+2)	adenylate cyclase type 5 [Mus musculus], gi|12	0	2	0	0	0	0

1209	gi|123233600 (+3)	reticulon 4 receptor-like 2 [Mus musculus]	0	0	0	0	0	0
1210	gi|15812198 (+3)	F-box only protein 2 [Homo sapiens], gi|51338:	0	0	0	0	0	3
1211	gi|4505047 (+1)	lumican precursor [Homo sapiens], gi|2014146	0	0	0	0	0	3
1212	gi|187956535 (+3)	SLIT and NTRK-like family, member 1 [Mus mu	0	0	0	0	0	0
1213	gi|110349752 (+1)	FERMRhoGEF (Arhgef) and pleckstrin domain	0	3	0	0	0	0
1214	gi|37182986 (+1)	NET-7 [Homo sapiens]	0	0	0	0	0	2
1215	gi|1335216	MOX2 [Homo sapiens]	0	0	0	0	0	2
1216	gi|115298665 (+6)	neurotrimin isoform 2 [Homo sapiens], gi|3718	0	0	0	0	0	2
1217	gi|163659858 (+1)	glutamate receptor 3 isoform 2 precursor [Hom	0	0	0	0	0	2
1218	gi|12847531 (+2)	unnamed protein product [Mus musculus]	2	2	0	0	0	0
1219	gi|148670996 (+3)	mCG17468, isoform CRA_d [Mus musculus]	2	0	0	0	0	0
1220	gi|148672092 (+2)	mCG144998 [Mus musculus]	2	0	0	0	0	0
1221	gi|113680352	carbonyl reductase [NADPH] 1 [Mus musculus	2	0	0	0	0	0
1222	gi|147904547	charged multivesicular body protein 6 [Mus mu	3	2	0	0	0	0
1223	gi|255958156 (+3)	cAMP-dependent protein kinase catalytic subu	2	2	0	0	0	0
1224	gi|119508431 (+5)	protein rogdi homolog [Mus musculus], gi|1662	0	3	0	0	0	0
1225	gi|5542285 (+2)	Chain A, Crystal Structure Of Macrophage Mig	2	0	0	0	0	0
1226	gi|13543176 (+5)	Gpd1 protein [Mus musculus]	2	3	0	0	0	0
1227	gi|148707097 (+5)	nicastrin [Mus musculus]	0	3	2	0	0	0
1228	gi|31982764 (+1)	large neutral amino acids transporter small sut	0	3	0	0	0	0
1229	gi|123226659 (+7)	neuroligin 3 [Mus musculus]	0	2	0	0	0	0
1230	gi|23463313	ras-related protein Rab-8B [Rattus norvegicus]	0	2	0	0	0	0
1231	gi|148694967	mCG14967 [Mus musculus]	0	0	3	0	0	0
1232	gi|6679803	peptidyl-prolyl cis-trans isomerase FKBP1A [M	2	0	0	0	0	0
1233	gi|148698122 (+3)	solute carrier family 9 (sodium/hydrogen excha	0	3	2	0	0	0
1234	gi|148704701 (+1)	FK506 binding protein 3, isoform CRA_a [Mus	2	3	0	0	0	0
1235	gi|26006275 (+2)	mKIAA1520 protein [Mus musculus]	0	2	3	0	0	0
1236	gi|148701025 (+3)	mCG3881, isoform CRA_b [Mus musculus]	0	2	4	0	0	0
1237	gi|148673911 (+10)	mCG144566 [Mus musculus]	2	4	0	0	0	0
1238	gi|148709204 (+4)	UBX domain containing 8, isoform CRA_a [Mu	0	2	3	0	0	0
1239	gi|40068493 (+1)	probable ATP-dependent RNA helicase DDX1	2	3	0	0	0	0
1240	gi|170172520 (+1)	lipoamide acyltransferase component of branc	0	2	2	0	0	0
1241	gi|148747410 (+1)	coatomer subunit delta [Mus musculus], gi|168	2	3	0	0	0	0
1242	gi|148667416 (+1)	CD9 antigen, isoform CRA_b [Mus musculus]	0	2	2	0	0	0
1243	gi|116283726 (+3)	Psmd1 protein [Mus musculus]	4	2	0	0	0	0
1244	gi|110626040 (+5)	cartilage acidic protein 1 precursor [Mus musc	2	3	0	0	0	0
1245	gi|119507488 (+3)	3-hydroxyisobutyrate dehydrogenase [Mus mu	0	2	2	0	0	0
1246	gi|15488707 (+1)	Acyl-Coenzyme A dehydrogenase, medium ch	2	4	0	0	0	0
1247	gi|148692550 (+3)	methionine-tRNA synthetase, isoform CRA_a [	2	4	0	0	0	0
1248	gi|28076935 (+2)	dynactin subunit 2 isoform 3 [Mus musculus], g	4	2	0	0	0	0
1249	gi|17223780 (+1)	phosphatidylinositol-4-phosphate 5-kinase type	3	2	0	0	0	0
1250	gi|12836323 (+1)	unnamed protein product [Mus musculus]	0	3	2	0	0	0
1251	gi|110625722 (+1)	optic atrophy 3 protein homolog [Mus musculu:	0	0	2	0	0	0
1252	gi|14141166 (+7)	poly(rC)-binding protein 2 isoform b [Homo sap	4	0	0	0	0	0
1253	gi|148690593 (+3)	mCG21680 [Mus musculus]	2	2	0	0	0	0
1254	gi|12846001 (+3)	unnamed protein product [Mus musculus]	3	0	0	0	0	0
1255	gi|148704343 (+4)	phosphoenolpyruvate carboxykinase 2 (mitoch	0	2	0	0	0	0
1256	gi|148664483 (+4)	tripeptidyl peptidase II, isoform CRA_c [Mus m	4	0	0	0	0	0
1257	gi|27369996 (+1)	hypothetical protein LOC230085 [Mus muscult	0	3	0	0	0	0
1258	gi|13435747 (+2)	Rho GDP dissociation inhibitor (GDI) alpha [M	2	0	0	0	0	0
1259	gi|13384870	transmembrane protein 126A [Mus musculus],	0	0	2	0	0	0
1260	gi|11527195 (+16)	sunday driver 2 [Mus musculus]	0	4	0	0	0	0
1261	gi|6677905	Golgi apparatus protein 1 precursor [Mus musc	0	4	0	0	0	0
1262	gi|13384904	28S ribosomal protein S22, mitochondrial [Mus	0	0	2	0	0	0
1263	gi|106507168 (+1)	ras-related protein Rab-12 [Mus musculus], gi|	0	2	0	0	0	0

1264 gi|4507789 (+6)	ubiquitin-conjugating enzyme E2 L3 [Homo sap	2	0	0	0	0	0
1265 gi|148699776 (+4)	ilvB (bacterial acetolactate synthase)-like, isofo	0	2	0	0	0	0
1266 gi|30794164 (+2)	clathrin light chain B [Mus musculus], gi|26325	0	4	0	0	0	0
1267 gi|160358864 (+5)	protein phosphatase 1H isoform 2 [Mus muscu	0	3	0	0	0	0
1268 gi|116284033 (+8)	Psip1 protein [Mus musculus]	0	2	0	0	0	0
1269 gi|33468961 (+1)	tripartite motif-containing protein 3 [Mus muscu	0	5	0	0	0	0
1270 gi|124487057 (+4)	endoplasmic reticulum metallopeptidase 1 [Mu	0	3	0	0	0	0
1271 gi|127800491 (+2)	Coiled-coil domain containing 51 [Mus muscul	0	0	4	0	0	0
1272 gi|73963667 (+4)	PREDICTED: similar to transmembrane traffick	0	2	0	0	0	0
1273 gi|41351529 (+3)	GPI transamidase component PIG-S [Mus mus	0	3	0	0	0	0
1274 gi|2149943 (+3)	Numblike [Mus musculus]	0	4	0	0	0	0
1275 gi|112817607 (+3)	thioredoxin-related transmembrane protein 4 p	0	3	0	0	0	0
1276 gi|8923415	E3 ubiquitin-protein ligase MARCH5 [Homo sa	0	0	4	0	0	0
1277 gi|74207672	unnamed protein product [Mus musculus]	0	2	0	0	0	0
1278 gi|1674501 (+3)	CD13/aminopeptidase N [Mus musculus]	4	0	0	0	0	0
1279 gi|13592009 (+2)	60S ribosomal protein L10a [Rattus norvegicus	0	2	0	0	0	0
1280 gi|148673159 (+7)	mCG10837 [Mus musculus]	0	4	0	0	0	0
1281 gi|164663791	protein kinase C alpha type [Mus musculus], g	0	3	0	0	0	0
1282 gi|148669281 (+2)	leucine rich repeat containing 4B [Mus muscul	0	0	0	0	0	0
1283 gi|12849613 (+1)	unnamed protein product [Mus musculus]	0	3	0	0	0	0
1284 gi|12836608 (+2)	unnamed protein product [Mus musculus]	0	4	0	0	0	0
1285 gi|148762971 (+1)	hypothetical protein LOC381353 [Mus muscul	0	3	0	0	0	0
1286 gi|148682723 (+4)	RIKEN cDNA B230315F11, isoform CRA_a [M	0	0	3	0	0	0
1287 gi|223633888	protein shisa-7 precursor [Mus musculus], gi|2:	0	4	0	0	0	0
1288 gi|12846177 (+3)	unnamed protein product [Mus musculus]	4	0	0	0	0	0
1289 gi|120587021 (+4)	GPI transamidase component PIG-T precursor	0	0	0	0	0	0
1290 gi|123857190 (+7)	SH3-domain GRB2-like endophilin B2 [Mus mu	0	4	0	0	0	0
1291 gi|148528987 (+2)	coronin-2B [Mus musculus], gi|254763263|sp|C	0	4	0	0	0	0
1292 gi|123228956 (+3)	O-linked N-acetylglucosamine (GlcNAc) transf	0	5	0	0	0	0
1293 gi|226442755 (+3)	phosphatidylinositol-4-phosphate 5-kinase type	0	5	0	0	0	0
1294 gi|148675298 (+3)	tight junction protein 1 [Mus musculus]	0	5	0	0	0	0
1295 gi|148695159 (+4)	Rap guanine nucleotide exchange factor (GEF	0	5	0	0	0	0
1296 gi|119632197 (+5)	immunoglobulin superfamily, member 1, isofor	0	0	0	0	0	5
1297 gi|227116358	trans-2-enoyl-CoA reductase, mitochondrial pr	0	0	5	0	0	0
1298 gi|148672872 (+4)	protein tyrosine phosphatase, receptor type, K	0	0	0	0	0	0
1299 gi|166795301 (+3)	prenylcysteine oxidase 1 precursor [Homo sap	0	0	0	0	0	5
1300 gi|190684703 (+2)	regulator of G-protein signaling 7 isoform 1 [Mu	0	4	0	0	0	0
1301 gi|133922561 (+3)	protein kinase C-binding protein NELL2 [Mus r	0	0	0	0	0	0
1302 gi|13905140 (+4)	Farsa protein [Mus musculus]	0	5	0	0	0	0
1303 gi|14192943 (+2)	multiple epidermal growth factor-like domains	0	0	0	0	0	4
1304 gi|62526118	cytoskeleton-associated protein 4 [Mus muscu	0	4	0	0	0	0
1305 gi|148687020 (+1)	aarF domain containing kinase 1, isoform CRA	0	0	5	0	0	0
1306 gi|4504067	aspartate aminotransferase, cytoplasmic [Hom	0	0	0	0	0	4
1307 gi|114615454 (+9)	PREDICTED: dihydrolipoamide dehydrogenas	0	0	0	0	0	4
1308 gi|200796 (+3)	16S ribosomal protein [Mus musculus]	0	4	0	0	0	0
1309 gi|13385998 (+6)	heat shock protein 75 kDa, mitochondrial precu	0	0	3	0	0	0
1310 gi|4506031	palmitoyl-protein thioesterase 1 isoform 1 prec	0	0	0	0	0	3
1311 gi|4557421 (+1)	ectonucleoside triphosphate diphosphohydrola	0	0	0	0	0	3
1312 gi|119583170 (+1)	hCG1985052, isoform CRA_b [Homo sapiens]	0	0	0	0	0	4
1313 gi|10432370 (+39)	CD44 molecule (Indian blood group) [Homo sa	0	0	0	0	0	3
1314 gi|114587605 (+7)	PREDICTED: hypothetical protein isoform 6 [P	0	0	0	0	0	3
1315 gi|10257437 (+5)	protein tweety homolog 1 isoform 1 [Homo sap	0	0	0	0	0	2
1316 gi|148922238 (+3)	Thrombospondin 2 [Homo sapiens]	0	0	0	0	0	2
1317 gi|6631112	synaptogyrin-3 [Homo sapiens], gi|14917042|s	0	0	0	0	0	2
1318 gi|119583561 (+8)	serpin peptidase inhibitor, clade B (ovalbumin)	0	0	0	0	0	2

1319	gi|493134	glutamate receptor 2 [Homo sapiens]	0	0	0	0	0	2
1320	gi|119588547 (+6)	solute carrier family 1 (glial high affinity glutam	0	0	0	0	0	2
1321	gi|6680878	lysosome membrane protein 2 [Mus musculus]	0	0	2	0	0	0
1322	gi|12837810 (+4)	unnamed protein product [Mus musculus], gi|1	2	2	0	0	0	0
1323	gi|148667974 (+3)	DnaJ (Hsp40) homolog, subfamily B, member	0	2	0	0	0	0
1324	gi|215260057 (+1)	heat shock protein 70-2 [Mus musculus]	0	0	0	0	0	0
1325	gi|148679159 (+2)	guanine nucleotide binding protein, alpha o, iso	0	3	0	0	0	0
1326	gi|6680908	cell division protein kinase 5 [Mus musculus], g	0	2	0	0	0	0
1327	gi|1346903 (+5)	RecName: Full=Receptor-type tyrosine-protein	0	3	0	0	0	0
1328	gi|38372905 (+1)	ras-related protein Rab-8A [Mus musculus], gi|	0	2	0	0	0	0
1329	gi|15530232	Proteasome (prosome, macropain) subunit, be	2	0	0	0	0	0
1330	gi|112363082 (+1)	neogenin isoform 1 [Mus musculus]	0	0	0	0	0	0
1331	gi|12060418 (+1)	ARG1 [Mus musculus], gi|71059879|emb|CAJ	0	0	2	0	0	0
1332	gi|113349 (+4)	RecName: Full=AP-1 complex subunit gamma	2	0	0	0	0	0
1333	gi|13277663 (+8)	FK506 binding protein 8 [Mus musculus], gi|20	0	2	3	0	0	0
1334	gi|153791547 (+6)	multidrug resistance protein 3 [Mus musculus],	2	3	0	0	0	0
1335	gi|148704655 (+4)	L-2-hydroxyglutarate dehydrogenase [Mus mu	0	2	3	0	0	0
1336	gi|148685669 (+6)	fusion, derived from t(12;16) malignant liposarc	2	3	0	0	0	0
1337	gi|187956944 (+1)	Isoc2a protein [Mus musculus]	0	2	2	0	0	0
1338	gi|126012517 (+2)	aminoacyl tRNA synthase complex-interacting	3	2	0	0	0	0
1339	gi|168984240 (+3)	active BCR-related gene [Mus musculus], gi|16	2	2	0	0	0	0
1340	gi|18490564 (+4)	Timm22 protein [Mus musculus]	0	2	2	0	0	0
1341	gi|140969946	NADH dehydrogenase [ubiquinone] flavoprotei	0	2	2	0	0	0
1342	gi|22256949 (+3)	RecName: Full=Dolichyl-diphosphooligosaccha	2	2	0	0	0	0
1343	gi|148672683 (+5)	mCG123838, isoform CRA_a [Mus musculus]	0	2	0	0	0	0
1344	gi|148677755 (+5)	asparaginyl-tRNA synthetase, isoform CRA_b	2	2	0	0	0	0
1345	gi|123226008 (+12)	proteasome (prosome, macropain) 26S subuni	2	2	0	0	0	0
1346	gi|14602601 (+2)	Prkcsh protein [Mus musculus], gi|148693295|	2	2	0	0	0	0
1347	gi|148708735	mCG1050441 [Mus musculus]	2	2	0	0	0	0
1348	gi|119508441 (+3)	26S proteasome non-ATPase regulatory subur	2	2	0	0	0	0
1349	gi|148699419 (+2)	mCG116065 [Mus musculus]	2	2	0	0	0	0
1350	gi|143811392 (+2)	RecName: Full=Tyrosine-protein kinase Fyn; A	2	3	0	0	0	0
1351	gi|161086922 (+1)	calcium/calmodulin-dependent protein kinase t	0	3	0	0	0	0
1352	gi|26354855 (+3)	unnamed protein product [Mus musculus]	2	2	0	0	0	0
1353	gi|110625719	histidine triad nucleotide-binding protein 2, mito	0	3	0	0	0	0
1354	gi|33468937 (+1)	mitochondrial import inner membrane transloca	0	0	2	0	0	0
1355	gi|148677001 (+7)	programmed cell death 6 interacting protein, is	0	2	0	0	0	0
1356	gi|4505813	dynein light chain 1, cytoplasmic [Homo sapier	0	0	2	0	0	0
1357	gi|6753490 (+1)	COP9 signalosome complex subunit 4 [Mus m	3	0	0	0	0	0
1358	gi|148673405 (+6)	RUN and FYVE domain containing 3, isoform (	0	3	0	0	0	0
1359	gi|12849707 (+3)	unnamed protein product [Mus musculus]	3	0	0	0	0	0
1360	gi|110625975 (+2)	pyruvate dehydrogenase kinase, isozyme 1 pr	0	0	3	0	0	0
1361	gi|148682887 (+4)	mCG16669, isoform CRA_e [Mus musculus]	0	2	0	0	0	0
1362	gi|9790221	actin-related protein 2/3 complex subunit 1A [M	2	0	0	0	0	0
1363	gi|148687481 (+3)	cytoplasmic linker 2, isoform CRA_c [Mus mus	0	3	0	0	0	0
1364	gi|40254507	phosphoglycolate phosphatase [Mus musculus	0	2	0	0	0	0
1365	gi|148672728 (+4)	eukaryotic translation initiation factor 3, subuni	2	0	0	0	0	0
1366	gi|902344	PMP68 [Mus musculus]	0	2	0	0	0	0
1367	gi|112181194	serine/threonine-protein kinase PAK 1 [Mus mi	2	0	0	0	0	0
1368	gi|20987211 (+3)	Vps26b protein [Mus musculus]	0	3	0	0	0	0
1369	gi|148680649 (+5)	profilin 1, isoform CRA_b [Mus musculus]	3	0	0	0	0	0
1370	gi|6680720	ADP-ribosylation factor 4 [Mus musculus], gi|1	2	0	0	0	0	0
1371	gi|225543409 (+2)	paraspeckle component 1 [Mus musculus], gi|8	0	3	0	0	0	0
1372	gi|226874869 (+2)	oligodendrocyte-myelin glycoprotein [Mus mus	0	3	0	0	0	0
1373	gi|13385196 (+1)	tetratricopeptide repeat protein 35 [Mus muscu	0	4	0	0	0	0

1374	gi|26353804 (+2)	unnamed protein product [Mus musculus]	0	0	0	0	0	0
1375	gi|226442772 (+1)	membrane-associated progesterone receptor c	0	4	0	0	0	0
1376	gi|148674270 (+2)	N-myc downstream regulated gene 3, isoform	0	3	0	0	0	0
1377	gi|148682195	mCG119680, isoform CRA_a [Mus musculus]	0	3	0	0	0	0
1378	gi|12859322 (+3)	unnamed protein product [Mus musculus]	0	2	0	0	0	0
1379	gi|20988736 (+1)	Lin7a protein [Mus musculus]	0	2	0	0	0	0
1380	gi|148696859 (+4)	homer homolog 3 (Drosophila), isoform CRA_a	0	4	0	0	0	0
1381	gi|148672440 (+2)	megalencephalic leukoencephalopathy with su	0	3	0	0	0	0
1382	gi|13879396 (+5)	Wdr48 protein [Mus musculus]	0	2	0	0	0	0
1383	gi|299522791	N(G),N(G)-dimethylarginine dimethylaminohyd	4	0	0	0	0	0
1384	gi|13124192 (+3)	RecName: Full=Elongation factor 1-delta; Shor	3	0	0	0	0	0
1385	gi|54873617	protein phosphatase 1E [Mus musculus], gi|14	3	0	0	0	0	0
1386	gi|148709892 (+7)	aldehyde dehydrogenase 18 family, member A	0	0	2	0	0	0
1387	gi|123794006 (+3)	RecName: Full=Far upstream element-binding	0	3	0	0	0	0
1388	gi|6755084	protein kinase C epsilon type [Mus musculus],	0	3	0	0	0	0
1389	gi|124007123 (+6)	RecName: Full=BR serine/threonine-protein ki	0	2	0	0	0	0
1390	gi|122890740 (+3)	HECT, UBA and WWE domain containing 1 [M	0	3	0	0	0	0
1391	gi|124517709 (+1)	glutamate decarboxylase 2 [Mus musculus], gi	0	3	0	0	0	0
1392	gi|148704663 (+1)	mCG3164 [Mus musculus]	0	3	0	0	0	0
1393	gi|124301217 (+2)	VPS10 domain-containing receptor SorCS2 pr	0	0	0	0	0	0
1394	gi|12248793 (+5)	sorting nexin 1 [Mus musculus]	0	4	0	0	0	0
1395	gi|13124606 (+4)	RecName: Full=Vesicle transport through inter	0	3	0	0	0	0
1396	gi|12841984 (+5)	unnamed protein product [Mus musculus]	0	2	0	0	0	0
1397	gi|37574048	cytochrome b-c1 complex subunit 9 [Mus muso	0	0	3	0	0	0
1398	gi|31982223	laminin subunit beta-2 precursor [Mus musculu	0	0	0	0	0	0
1399	gi|10946870 (+7)	alcohol dehydrogenase [NADP+] [Mus muscul	3	0	0	0	0	0
1400	gi|148704852 (+3)	mCG12232 [Mus musculus]	0	2	0	0	0	0
1401	gi|127548 (+2)	RecName: Full=Methylmalonyl-CoA mutase, m	0	0	3	0	0	0
1402	gi|148693657 (+2)	DEAD (Asp-Glu-Ala-Asp) box polypeptide 6, is	0	3	0	0	0	0
1403	gi|110347487 (+4)	cytoplasmic aconitate hydratase [Mus musculu	3	0	0	0	0	0
1404	gi|14715029 (+4)	Serine (or cysteine) peptidase inhibitor, clade E	0	0	0	0	0	0
1405	gi|126723102	protein EFR3 homolog B [Mus musculus], gi|16	0	3	0	0	0	0
1406	gi|13386026	hypothetical protein LOC68045 [Mus musculus	0	3	0	0	0	0
1407	gi|12836885 (+4)	nonsense mRNA reducing factor 1 NORF1 [Mu	0	2	0	0	0	0
1408	gi|148680404 (+4)	polypyrimidine tract binding protein 2, isoform C	0	4	0	0	0	0
1409	gi|6753022	adenylate kinase isoenzyme 4, mitochondrial [	0	0	2	0	0	0
1410	gi|148683989 (+5)	leucine rich repeat containing 59, isoform CRA	0	2	0	0	0	0
1411	gi|1246787 (+3)	UDP-galactose ceramide galactosyltransferase	0	0	0	0	0	0
1412	gi|260763900 (+1)	prostaglandin E synthase 2 [Mus musculus], gi	0	0	2	0	0	0
1413	gi|148702811 (+1)	solute carrier family 25 (mitochondrial carrier, c	0	0	4	0	0	0
1414	gi|19705424 (+4)	26S proteasome non-ATPase regulatory subur	3	0	0	0	0	0
1415	gi|119571401 (+2)	brain-specific protein p25 alpha, isoform CRA_	0	0	0	0	0	5
1416	gi|146345398 (+3)	RecName: Full=Collagen alpha-1(XIV) chain; F	0	0	0	0	0	0
1417	gi|122065166 (+2)	RecName: Full=Dedicator of cytokinesis protei	0	0	5	0	0	0
1418	gi|148699270 (+2)	tweety homolog 1 (Drosophila), isoform CRA_e	0	5	0	0	0	0
1419	gi|13544049 (+4)	SUMF2 protein [Homo sapiens]	0	0	0	0	0	4
1420	gi|148686389 (+5)	3-hydroxy-3-methylglutaryl-Coenzyme A synth	4	0	0	0	0	0
1421	gi|12842535 (+2)	unnamed protein product [Mus musculus], gi|2	0	4	0	0	0	0
1422	gi|12857783 (+4)	unnamed protein product [Mus musculus]	0	0	4	0	0	0
1423	gi|223461282 (+2)	Cttnbp2 protein [Mus musculus]	0	5	0	0	0	0
1424	gi|227908803 (+2)	nodal modulator 1 [Mus musculus], gi|8188476	0	4	0	0	0	0
1425	gi|148681158 (+5)	calpain 2 [Mus musculus]	0	4	0	0	0	0
1426	gi|26353732 (+1)	unnamed protein product [Mus musculus]	4	0	0	0	0	0
1427	gi|13277612 (+4)	Anxa5 protein [Mus musculus]	4	0	0	0	0	0
1428	gi|126517469 (+2)	methyl-CpG-binding protein 2 isoform 1 [Mus r	0	4	0	0	0	0

1429	gi|12836471 (+4)	unnamed protein product [Mus musculus]	0	4	0	0	0	0
1430	gi|74315985	keratin, type II cuticular Hb6 [Mus musculus], g	0	4	0	0	0	0
1431	gi|148697004 (+4)	unc-13 homolog A (C. elegans) [Mus musculus	0	4	0	0	0	0
1432	gi|50053703	neurabin-2 [Mus musculus], gi|81892818|sp|Q(	0	4	0	0	0	0
1433	gi|12845889 (+2)	unnamed protein product [Mus musculus]	4	0	0	0	0	0
1434	gi|19354292 (+1)	Arginyl-tRNA synthetase 2, mitochondrial [Mus	0	0	3	0	0	0
1435	gi|121949763 (+10)	lamina-associated polypeptide 2 isoform gamn	0	4	0	0	0	0
1436	gi|116642261 (+2)	prolactin-induced protein [Homo sapiens], gi|11	0	0	0	0	0	4
1437	gi|13905236 (+2)	Propionyl-Coenzyme A carboxylase, alpha poly	0	0	4	0	0	0
1438	gi|13623415 (+3)	Fascin homolog 1, actin-bundling protein (Stro	0	0	0	0	0	3
1439	gi|116089341 (+10)	abl interactor 1 isoform 1 [Mus musculus], gi|5(	0	4	0	0	0	0
1440	gi|120659964 (+4)	CNTN5 protein [Homo sapiens]	0	0	0	0	0	4
1441	gi|119581777 (+1)	sideroflexin 1, isoform CRA_c [Homo sapiens]	0	0	0	0	0	3
1442	gi|161086986	CUB and sushi domain-containing protein 3 [M	0	0	0	0	0	0
1443	gi|117647249	laminin subunit alpha-2 [Mus musculus], gi|225	0	0	0	0	0	0
1444	gi|119601993 (+13)	serpin peptidase inhibitor, clade A (alpha-1 ant	0	0	0	0	0	3
1445	gi|124530 (+2)	RecName: Full=Insulin receptor; Short=IR; Alt	0	0	0	0	0	0
1446	gi|148693326 (+5)	anillin, actin binding protein (scraps homolog, [	0	0	3	0	0	0
1447	gi|187954329 (+2)	Keratin 35 [Mus musculus]	0	3	0	0	0	0
1448	gi|14010849 (+5)	tripartite motif-containing protein 2 [Mus muscu	0	3	0	0	0	0
1449	gi|13096806 (+2)	Adrbk1 protein [Mus musculus]	0	2	0	0	0	0
1450	gi|119579401 (+5)	solute carrier family 44, member 1, isoform CR	0	0	0	0	0	3
1451	gi|119622488 (+5)	isocitrate dehydrogenase 2 (NADP+), mitochor	0	0	0	0	0	3
1452	gi|56203293 (+2)	F-box protein 6 [Homo sapiens]	0	0	0	0	0	3
1453	gi|7949027	dnaJ homolog subfamily C member 5 [Mus mu	0	3	0	0	0	0
1454	gi|118601085 (+3)	Atg9a protein [Mus musculus]	0	3	0	0	0	0
1455	gi|127796373 (+2)	Aldehyde dehydrogenase 7 family, member A1	0	0	0	0	0	3
1456	gi|188219544 (+1)	vesicular glutamate transporter 2 [Mus muscul	0	3	0	0	0	0
1457	gi|40254254	protein sidekick-2 precursor [Mus musculus], g	0	0	0	0	0	0
1458	gi|126116587 (+2)	type I inositol-3,4-bisphosphate 4-phosphatase	0	3	0	0	0	0
1459	gi|12859602 (+2)	unnamed protein product [Mus musculus]	0	2	0	0	0	0
1460	gi|86792774	dipeptidyl aminopeptidase-like protein 6 isoforr	0	0	0	0	0	2
1461	gi|1685051 (+9)	CD97 [Homo sapiens]	0	0	0	0	0	3
1462	gi|153791843 (+1)	receptor-type tyrosine-protein phosphatase ga	0	0	0	0	0	0
1463	gi|51243034 (+1)	oxysterol-binding protein-like protein 8 isoform	0	2	0	0	0	0
1464	gi|13435361 (+4)	desmocollin-1 isoform Dsc1a preproprotein [H(	0	0	0	0	0	2
1465	gi|189011546 (+1)	acid ceramidase isoform b [Homo sapiens]	0	0	0	0	0	2
1466	gi|12698039 (+2)	KIAA1747 protein [Homo sapiens]	0	0	0	0	0	2
1467	gi|127798841 (+2)	ATP synthase, H+ transporting, mitochondrial [	0	0	0	0	0	2
1468	gi|13194201 (+2)	reticulon-4 receptor precursor [Homo sapiens],	0	0	0	0	0	2
1469	gi|908801	keratin type II [Homo sapiens]	0	0	0	0	0	2
1470	gi|13195586 (+28)	hemoglobin alpha 1 globin chain [Homo sapier	0	0	0	0	0	2
1471	gi|47077659	FLJ00268 protein [Homo sapiens]	0	0	0	0	0	2
1472	gi|160298211 (+3)	probable G-protein coupled receptor 37 precur	0	2	0	0	0	0
1473	gi|126035631 (+2)	destrin [Mus spretus]	2	0	0	0	0	0
1474	gi|22477515 (+4)	EH-domain containing 1 [Mus musculus]	0	2	0	0	0	0
1475	gi|12838381 (+8)	unnamed protein product [Mus musculus]	0	2	0	0	0	0
1476	gi|148684930 (+1)	mCG114434 [Mus musculus]	2	2	0	0	0	0
1477	gi|148694750 (+4)	valyl-tRNA synthetase 2, isoform CRA_d [Mus	2	2	0	0	0	0
1478	gi|6671678 (+2)	carbonic anhydrase 4 precursor [Mus muscult	2	2	0	0	0	0
1479	gi|297342902	Chain A, Crystal Structure Of Mouse Mitochon	0	2	2	0	0	0
1480	gi|1583224 (+3)	RNA polymerase II elongation factor	2	2	0	0	0	0
1481	gi|1094400 (+3)	protein kinase CK2:SUBUNIT=alpha	2	2	0	0	0	0
1482	gi|13385408 (+5)	60S ribosomal protein L11 [Mus musculus], gi|	2	2	0	0	0	0
1483	gi|26326937 (+1)	unnamed protein product [Mus musculus]	0	2	0	0	0	0

1484 gi|148675899 (+3)	UDP-glucose pyrophosphorylase 2, isoform CF	0	2	0	0	0	0
1485 gi|1103844 (+7)	steroid dehydrogenase [Mus musculus]	0	0	2	0	0	0
1486 gi|16758754	V-type proton ATPase subunit F [Rattus norveg	0	2	0	0	0	0
1487 gi|29244192	leucine-rich repeat-containing protein 8A [Mus	0	2	2	0	0	0
1488 gi|12847642 (+2)	unnamed protein product [Mus musculus]	0	0	2	0	0	0
1489 gi|10863991 (+4)	60S ribosomal protein L35a [Rattus norvegicus	0	2	0	0	0	0
1490 gi|153941186	stage II sporulation protein D [Clostridium botu	0	0	0	0	0	2
1491 gi|115528975 (+1)	Keratin 77 [Mus musculus], gi|223461411|gb|A	0	0	0	0	0	0
1492 gi|7661678	ras-related protein Rap-1b precursor [Homo sa	0	0	2	0	0	0
1493 gi|12845883 (+1)	unnamed protein product [Mus musculus]	2	0	0	0	0	0
1494 gi|26389719 (+1)	unnamed protein product [Mus musculus]	0	2	0	0	0	0
1495 gi|3142331 (+1)	calcyclin binding protein [Mus musculus]	0	0	0	0	0	0
1496 gi|119508439 (+1)	pyrroline-5-carboxylate reductase 3 [Mus musc	0	2	0	0	0	0
1497 gi|123229439 (+6)	Rap1 GTPase-activating protein [Mus musculu	0	2	0	0	0	0
1498 gi|21362303	synaptosomal-associated protein 47 [Mus mus	0	3	0	0	0	0
1499 gi|149260643 (+7)	PREDICTED: 60S ribosomal protein L23a-like	0	3	0	0	0	0
1500 gi|148702098 (+3)	mCG20222, isoform CRA_b [Mus musculus]	0	2	0	0	0	0
1501 gi|119372300 (+4)	atlastin-2 isoform 1 [Mus musculus], gi|818854	0	2	0	0	0	0
1502 gi|12842359 (+3)	unnamed protein product [Mus musculus]	0	2	0	0	0	0
1503 gi|148679181 (+1)	mCG14657 [Mus musculus]	0	2	0	0	0	0
1504 gi|148747128 (+7)	dolichyl-diphosphooligosaccharide--protein gly	0	2	0	0	0	0
1505 gi|6677775	60S ribosomal protein L22 [Mus musculus], gi|	0	2	0	0	0	0
1506 gi|148678962 (+3)	mCG11048, isoform CRA_b [Mus musculus]	0	2	0	0	0	0
1507 gi|13435603 (+6)	Hnrpr protein [Mus musculus]	0	2	0	0	0	0
1508 gi|26353316 (+2)	unnamed protein product [Mus musculus]	0	2	0	0	0	0
1509 gi|12698456 (+9)	fatty aldehyde dehydrogenase [Mus musculus]	0	2	0	0	0	0
1510 gi|148708750 (+3)	holocytochrome c synthetase [Mus musculus]	0	0	3	0	0	0
1511 gi|9506367	ATP-binding cassette sub-family B member 10	0	0	3	0	0	2
1512 gi|111494223 (+2)	5'-nucleotidase domain-containing protein 3 [M	0	0	3	0	0	0
1513 gi|12845035 (+2)	unnamed protein product [Mus musculus]	3	0	0	0	0	0
1514 gi|11385994 (+2)	thimet oligopeptidase [Mus musculus]	2	0	0	0	0	0
1515 gi|6755210 (+1)	26S proteasome non-ATPase regulatory subur	2	0	0	0	0	0
1516 gi|148686508 (+2)	mCG10234, isoform CRA_b [Mus musculus]	0	0	2	0	0	0
1517 gi|123123374 (+3)	novel protein [Mus musculus], gi|123231646|en	0	0	0	0	0	0
1518 gi|6755202	proteasome subunit beta type-3 [Mus musculu	2	0	0	0	0	0
1519 gi|2970691 (+4)	thioredoxin-related protein [Mus musculus]	0	0	0	0	0	0
1520 gi|135290 (+6)	RecName: Full=Talin-1, gi|54258|emb|CAA395	2	0	0	0	0	0
1521 gi|247494171 (+1)	BTB/POZ domain-containing protein KCTD16	0	0	0	0	0	0
1522 gi|26329759 (+1)	unnamed protein product [Mus musculus]	0	0	2	0	0	0
1523 gi|31560618 (+1)	mitotic checkpoint protein BUB3 [Mus musculu	3	0	0	0	0	0
1524 gi|21312676 (+1)	armadillo repeat-containing protein 1 [Mus mus	0	0	3	0	0	2
1525 gi|125347376 (+6)	filamin-A [Mus musculus], gi|215406563|emb|(	0	2	0	0	0	0
1526 gi|12845617 (+2)	unnamed protein product [Mus musculus]	3	0	0	0	0	0
1527 gi|112181198 (+2)	phosphodiesterase 4B isoform 1 [Mus muscul	0	2	0	0	0	0
1528 gi|226958474 (+1)	plexin B2 [Mus musculus], gi|226958476|ref|NI	0	0	0	0	0	0
1529 gi|123207565 (+7)	dynein cytoplasmic 1 intermediate chain 2 [Mu	0	3	0	0	0	0
1530 gi|148689351 (+4)	glutaminyl-tRNA synthetase, isoform CRA_b [N	2	0	0	0	0	0
1531 gi|123213538 (+9)	calcium/calmodulin-dependent serine protein k	0	3	0	0	0	0
1532 gi|10048462 (+2)	mitochondrial carnitine/acylcarnitine carrier pro	0	0	2	0	0	0
1533 gi|148705710 (+4)	leucine-rich repeat LGI family, member 2, isofc	0	0	2	0	0	0
1534 gi|23943844 (+1)	opalin [Mus musculus], gi|62901445|sp|Q7M75	0	0	2	0	0	0
1535 gi|10764635 (+4)	glia maturation factor-beta [Mus musculus], gi|	0	0	0	0	0	0
1536 gi|12840795 (+7)	unnamed protein product [Mus musculus]	0	0	2	0	0	0
1537 gi|148700007 (+4)	transcription factor A, mitochondrial, isoform C	0	0	2	0	0	0
1538 gi|1170592 (+2)	RecName: Full=Integrin alpha-V; AltName: Ful	0	0	0	0	0	0

1539 gi|257153448 (+1)	proSAAS [Mus musculus], gi|117949769|sp|Q9	0	3	0	0	0	0
1540 gi	148704607 (+1)	translocase of inner mitochondrial membrane 9	0	0	2	0	0	0
1541 gi	304438843	conserved hypothetical protein [Peptoniphilus	0	0	2	0	0	0
1542 gi	18203570 (+1)	RecName: Full=Mitochondrial import inner mer	0	0	2	0	0	0
1543 gi|209862939 (+2)	heme oxygenase 2 [Mus musculus], gi|225007	0	3	0	0	0	0
1544 gi	17391158 (+2)	Transmembrane protein 30A [Mus musculus]	0	2	0	0	0	0
1545 gi|310688885 (+2)	abl interactor 2 isoform 1 [Mus musculus], gi|50	0	3	0	0	0	0
1546 gi	154550673 (+1)	expressed in non-metastatic cells 2 protein [Mu	2	0	0	0	0	0
1547 gi	13242255 (+8)	protein arginine N-methyltransferase 1 [Rattus	2	0	0	0	0	0
1548 gi	160285976	Chain A, Crystal Structure Of A Disulfide Trapp	0	2	0	0	0	0
1549 gi	148681126 (+5)	mCG12392 [Mus musculus]	0	3	0	0	0	0
1550 gi	12963653 (+1)	peptidyl-prolyl cis-trans isomerase NIMA-intera	0	2	0	0	0	0
1551 gi|126723792 (+3)	sorting nexin-27 isoform 1 [Mus musculus], gi|1	0	3	0	0	0	0
1552 gi	148700191 (+1)	pyrophosphatase (inorganic) 1 [Mus musculus]	2	0	0	0	0	0
1553 gi	10946572 (+2)	fatty acid-binding protein, brain [Mus musculus	4	0	0	0	0	0
1554 gi	12847965 (+6)	unnamed protein product [Mus musculus]	4	0	0	0	0	0
1555 gi	158256874 (+7)	unnamed protein product [Homo sapiens]	0	0	0	0	0	4
1556 gi	226443414 (+3)	kelch repeat and BTB domain-containing prote	0	4	0	0	0	0
1557 gi	26345256 (+2)	unnamed protein product [Mus musculus]	4	0	0	0	0	0
1558 gi	119607870 (+2)	hCG28560, isoform CRA_a [Homo sapiens]	0	0	0	0	0	4
1559 gi|154090989 (+3)	teneurin-2 [Mus musculus], gi|56800255|emb|C	0	0	0	0	0	0
1560 gi	148697878 (+5)	ATPase, H+ transporting, lysosomal accessory	0	4	0	0	0	0
1561 gi	109658940 (+5)	Carnosine dipeptidase 1 (metallopeptidase M2	0	0	0	0	0	4
1562 gi	283945572 (+3)	core histone macro-H2A.1 isoform 2 [Mus mus	0	4	0	0	0	0
1563 gi	12963569 (+2)	protein phosphatase 1 regulatory subunit 7 [Mu	4	0	0	0	0	0
1564 gi	31074631	keratin 1b [Homo sapiens]	0	0	0	0	0	4
1565 gi	148695677 (+1)	CD82 antigen, isoform CRA_b [Mus musculus]	0	0	3	0	0	0
1566 gi	262050625 (+1)	translocon-associated protein subunit delta iso	0	3	0	0	0	0
1567 gi	148698326 (+6)	expressed sequence AU040320, isoform CRA	0	0	0	0	0	0
1568 gi	49258190	NCK-interacting protein with SH3 domain [Mus	0	4	0	0	0	0
1569 gi	10337581 (+1)	keratin, type I cuticular Ha3-II [Homo sapiens],	0	0	0	0	0	3
1570 gi	10047273 (+2)	KIAA1599 protein [Homo sapiens]	0	0	0	0	0	3
1571 gi	6755196 (+1)	proteasome subunit alpha type-4 [Mus muscul	3	0	0	0	0	0
1572 gi	119604532 (+7)	solute carrier family 44, member 2, isoform CR	0	0	0	0	0	3
1573 gi	153792501 (+1)	glutamate receptor delta-1 subunit precursor [N	0	0	0	0	0	0
1574 gi	122889734 (+5)	SH3-domain GRB2-like (endophilin) interacting	0	3	0	0	0	0
1575 gi	103472025 (+1)	cleft lip and palate transmembrane protein 1 ho	0	3	0	0	0	0
1576 gi	148670038 (+2)	syntaxin binding protein 3A [Mus musculus]	0	0	3	0	0	0
1577 gi	148699231 (+1)	calcium channel, voltage-dependent, gamma s	0	3	0	0	0	0
1578 gi	77404294	up-regulated during skeletal muscle growth pro	0	0	3	0	0	0
1579 gi	148705521 (+4)	Huntington disease gene homolog, isoform CR	0	3	0	0	0	0
1580 gi	42542977 (+4)	Chain A, X-Ray Crystal Structure Of Human G	0	0	0	0	0	3
1581 gi	148691229 (+7)	apolipoprotein E, isoform CRA_a [Mus muscul	0	3	0	0	0	0
1582 gi	20379605 (+3)	Plcl2 protein [Mus musculus]	0	0	3	0	0	0
1583 gi	148698923 (+4)	DnaJ (Hsp40) homolog, subfamily C, member	0	4	0	0	0	0
1584 gi	163644321 (+2)	cytochrome b-c1 complex subunit Rieske, mito	0	0	0	0	0	3
1585 gi	148709445 (+5)	PRP19/PSO4 pre-mRNA processing factor 19	0	4	0	0	0	0
1586 gi	226823313	dual specificity protein phosphatase 15 isoform	0	0	2	0	0	0
1587 gi	148685189 (+2)	membrane interacting protein of RGS16, isofor	0	3	0	0	0	0
1588 gi	117558756 (+4)	FBLN7 protein [Homo sapiens]	0	0	0	0	0	3
1589 gi	200283 (+5)	protein disulfide isomerase-related protein [Mu	4	0	0	0	0	0
1590 gi	21361091	ubiquitin carboxyl-terminal hydrolase isozyme	0	0	0	0	0	3
1591 gi	46402175 (+1)	lysophospholipid acyltransferase LPCAT4 [Mu	0	3	0	0	0	0
1592 gi	3659901 (+1)	F1F0-type ATP synthase subunit g [Homo sap	0	0	0	0	0	2
1593 gi	122889566 (+2)	low density lipoprotein-related protein 1B (dele	0	0	0	0	0	0

1594 gi|119590894 (+4)	LanC lantibiotic synthetase component C-like	0	0	0	0	0	2
1595 gi|119581082 (+2)	keratin 25C [Homo sapiens]	0	0	0	0	0	2
1596 gi|194374129 (+2)	unnamed protein product [Homo sapiens]	0	0	0	0	0	2
1597 gi|67003568	skin-specific protein 32 [Homo sapiens], gi|747	0	0	0	0	0	2
1598 gi|15823094 (+2)	housekeeping protein DXS254E [Mus musculu	0	2	0	0	0	0
1599 gi|119613874 (+8)	CD46 antigen, complement regulatory protein,	0	0	0	0	0	2
1600 gi|338423 (+5)	small proline rich protein [Homo sapiens]	0	0	0	0	0	2
1601 gi|119602969 (+9)	fibroblast growth factor receptor 3 (achondropl	0	0	0	0	0	2
1602 gi|115527481 (+3)	Gliomedin [Mus musculus], gi|115528855|gb|A	0	0	0	0	0	0
1603 gi|193785329 (+3)	unnamed protein product [Homo sapiens]	0	0	0	0	0	2
1604 gi|116875858 (+2)	aggrecan core protein precursor [Mus musculu	0	0	0	0	0	0
1605 gi|13928664 (+1)	acetylcholinesterase precursor [Mus musculus	0	2	0	0	0	0
1606 gi|21704212 (+2)	protein NDRG4 isoform B [Mus musculus], gi|1	2	0	0	0	0	0
1607 gi|188035915 (+3)	alpha-aminoadipic semialdehyde dehydrogena	2	0	0	0	0	0
1608 gi|12852198 (+2)	unnamed protein product [Mus musculus]	0	2	0	0	0	0
1609 gi|74190754 (+7)	unnamed protein product [Mus musculus]	0	2	0	0	0	0
1610 gi|113680271 (+4)	voltage-dependent L-type calcium channel sub	0	2	0	0	0	0
1611 gi|12408324	complexin-1 [Rattus norvegicus], gi|227330544	0	2	0	0	0	0
1612 gi|13384730 (+2)	SAP domain-containing ribonucleoprotein [Mus	0	2	0	0	0	0
1613 gi|256000796 (+4)	tropomyosin alpha-1 chain isoform 10 [Mus mu	0	2	0	0	0	0
1614 gi|123238565 (+2)	dual specificity phosphatase 3 (vaccinia virus p	0	2	0	0	0	0
1615 gi|148667873 (+2)	mCG112980, isoform CRA_b [Mus musculus]	0	2	0	0	0	0
1616 gi|13591860 (+2)	toll-interacting protein [Mus musculus], gi|2014	0	2	0	0	0	0
1617 gi|148680839 (+4)	mCG1492, isoform CRA_b [Mus musculus]	0	2	0	0	0	0
1618 gi|12644592 (+7)	RecName: Full=Phenylalanyl-tRNA synthetase	0	2	0	0	0	0
1619 gi|148693689 (+1)	sodium channel, voltage-gated, type II, beta [M	0	2	0	0	0	0
1620 gi|146219835 (+8)	catenin delta-1 isoform 2 [Mus musculus], gi|74	0	2	0	0	0	0
1621 gi|148696995 (+3)	solute carrier family 27 (fatty acid transporter),	0	2	0	0	0	0
1622 gi|148666929 (+6)	mCG127318 [Mus musculus]	0	2	0	0	0	0
1623 gi|244789999 (+2)	3-mercaptopyruvate sulfurtransferase [Mus mu	2	0	0	0	0	0
1624 gi|11693154 (+3)	platelet-activating factor acetylhydrolase IB su	2	0	0	0	0	0
1625 gi|102468565 (+8)	thioredoxin reductase 2, mitochondrial precurs	0	0	2	0	0	0
1626 gi|307643829	glyceraldhyde-3-phosphate dehydrogenase [A	2	0	0	0	0	0
1627 gi|148670014 (+3)	sortilin 1 [Mus musculus]	0	0	0	0	0	0
1628 gi|148668374 (+3)	mCG119397 [Mus musculus]	2	0	0	0	0	0
1629 gi|148694470 (+1)	cytochrome c oxidase, subunit VIIa 2, isoform	0	0	2	0	0	0
1630 gi|148684490 (+4)	protein phosphatase methylesterase 1, isoform	2	0	0	0	0	0
1631 gi|13385872 (+1)	interleukin enhancer-binding factor 2 [Mus mus	2	0	0	0	0	0
1632 gi|148707494 (+2)	laminin, gamma 1, isoform CRA_a [Mus muscu	0	0	0	0	0	0
1633 gi|11762010 (+5)	cystatin C precursor [Mus musculus]	2	0	0	0	0	0
1634 gi|150378487 (+2)	adenylate cyclase type 9 [Mus musculus], gi|17	0	2	0	0	0	0
1635 gi|148692963 (+1)	tetraspanin 14, isoform CRA_b [Mus musculus	0	0	0	0	0	0
1636 gi|115583687 (+1)	pre-mRNA-processing-splicing factor 8 [Mus m	0	2	0	0	0	0
1637 gi|148690000 (+2)	trafficking protein particle complex 5 [Mus mus	0	2	0	0	0	0
1638 gi|6754240	neuron-specific calcium-binding protein hippoc	0	2	0	0	0	0
1639 gi|6755228	tyrosine-protein phosphatase non-receptor typ	0	2	0	0	0	0
1640 gi|124487059 (+5)	RIMS-binding protein 2 [Mus musculus], gi|157	0	2	0	0	0	0
1641 gi|148667132 (+3)	plexin D1, isoform CRA_a [Mus musculus]	0	0	0	0	0	0
1642 gi|6679120	neuronal pentraxin-1 precursor [Mus musculus	0	2	0	0	0	0
1643 gi|123229915 (+4)	discs, large homolog-associated protein 4 (Drc	0	2	0	0	0	0
1644 gi|21624617	NADH dehydrogenase [ubiquinone] 1 alpha su	0	0	2	0	0	0
1645 gi|148677080 (+5)	DEAH (Asp-Glu-Ala-His) box polypeptide 30 [M	0	2	0	0	0	0
1646 gi|151358090 (+5)	Eph receptor B2 [Mus musculus], gi|15135810	0	2	0	0	0	0
1647 gi|11132435 (+5)	RecName: Full=Galactokinase; AltName: Full=	2	0	0	0	0	0
1648 gi|13278438 (+6)	Strn4 protein [Mus musculus]	0	2	0	0	0	0

1649	gi|148676515 (+4)	RIKEN cDNA 5730472N09, isoform CRA_a [M	0	0	2	0	0	0
1650	gi|21450317	histone deacetylase 11 [Mus musculus], gi|263	0	0	2	0	0	0
1651	gi|148679226 (+2)	casein kinase II, alpha 2, polypeptide [Mus mu	0	2	0	0	0	0
1652	gi|291575137	keratin, type I cuticular Ha6 [Mus musculus], g	2	0	0	0	0	0
1653	gi|148677026 (+2)	EPM2A (laforin) interacting protein 1, isoform C	2	0	0	0	0	0
1654	gi|148698348 (+4)	arginine/proline rich coiled-coil 1, isoform CRA	0	2	0	0	0	0
1655	gi|123210959 (+8)	surfeit gene 1 [Mus musculus], gi|148676391|g	0	0	2	0	0	0
1656	gi|148685171 (+10)	ADP-ribosylation factor-like 6 interacting protei	0	2	0	0	0	0
1657	gi|304383311	DNA mismatch repair protein MutS2 [Prevotell	0	2	0	0	0	0
1658	gi|21311867	coiled-coil domain-containing protein 56 [Mus r	0	0	2	0	0	0
1659	gi|297209388 (+2)	immunoglobulin G binding protein A [Staphyloc	0	2	0	0	0	0
1660	gi|148680414 (+5)	DNA segment, Chr 3, Brigham & Women's Ge	0	2	0	0	0	0
1661	gi|124248570 (+5)	ras GTPase-activating protein-binding protein 2	0	2	0	0	0	0
1662	gi|148666704 (+4)	sepiapterin reductase, isoform CRA_a [Mus m	0	2	0	0	0	0
1663	gi|148692328 (+1)	mCG145770 [Mus musculus]	0	0	0	0	0	0
1664	gi|162329549	protein SCO2 homolog, mitochondrial precurso	0	0	2	0	0	0
1665	gi|148669288 (+4)	mCG21397, isoform CRA_a [Mus musculus]	0	0	2	0	0	0
1666	gi|12855312	unnamed protein product [Mus musculus]	0	2	0	0	0	0
1667	gi|119594653 (+9)	hCG2016877, isoform CRA_c [Homo sapiens]	0	0	0	0	0	3
1668	gi|1208433 (+9)	receptor-type tyrosine phosphatase [Mus muso	0	0	0	0	0	0
1669	gi|148667565 (+1)	3-hydroxyisobutyryl-Coenzyme A hydrolase [M	0	0	3	0	0	0
1670	gi|148670151 (+7)	phosphodiesterase 10A, isoform CRA_b [Mus	0	3	0	0	0	0
1671	gi|148673963 (+4)	mCG13192, isoform CRA_a [Mus musculus]	3	0	0	0	0	0
1672	gi|148679515 (+9)	Vac14 homolog (S. cerevisiae), isoform CRA_a	0	3	0	0	0	0
1673	gi|148683296 (+4)	death associated protein 3, isoform CRA_b [M	0	0	3	0	0	0
1674	gi|148685645 (+4)	syntaxin 4A (placental), isoform CRA_a [Mus r	0	0	3	0	0	0
1675	gi|221041140	unnamed protein product [Homo sapiens]	0	0	0	0	0	3
1676	gi|23065552 (+3)	glutathione S-transferase Mu 3 [Homo sapiens	0	0	0	0	0	3
1677	gi|189491653 (+3)	ubiquitin carboxyl-terminal hydrolase CYLD isc	0	3	0	0	0	0
1678	gi|123232549 (+6)	phosphoglucomutase 2 [Mus musculus]	3	0	0	0	0	0
1679	gi|148686768 (+2)	cytochrome P450, family 46, subfamily a, polyp	0	3	0	0	0	0
1680	gi|12836486 (+4)	unnamed protein product [Mus musculus]	0	3	0	0	0	0
1681	gi|116235485 (+4)	delta and Notch-like epidermal growth factor-re	0	0	0	0	0	3
1682	gi|13905142 (+4)	Fatty acid amide hydrolase [Mus musculus]	0	3	0	0	0	0
1683	gi|157057145 (+8)	actin-binding LIM protein 1 isoform 1 [Mus mus	0	3	0	0	0	0
1684	gi|26332266 (+3)	unnamed protein product [Mus musculus]	0	3	0	0	0	0
1685	gi|19526912 (+3)	hsc70-interacting protein [Mus musculus], gi|2(	3	0	0	0	0	0
1686	gi|21699068 (+6)	presequence protease, mitochondrial precurso	0	0	3	0	0	0
1687	gi|119630767 (+3)	chromosome 20 open reading frame 103, isofc	0	0	0	0	0	3
1688	gi|27370304 (+1)	probable cationic amino acid transporter [Mus	0	3	0	0	0	0
1689	gi|1255116 (+2)	heat-responsive protein [Mus musculus]	3	0	0	0	0	0
1690	gi|109287551 (+2)	Grik3 protein [Mus musculus]	0	0	0	0	0	0
1691	gi|124249058 (+1)	tectonin beta-propeller repeat-containing prote	0	3	0	0	0	0
1692	gi|6753618	D-dopachrome decarboxylase [Mus musculus]	3	0	0	0	0	0
1693	gi|169790983 (+1)	P2Y purinoceptor 12 [Mus musculus], gi|21263	3	0	0	0	0	0
1694	gi|194387028 (+4)	unnamed protein product [Homo sapiens]	0	0	0	0	0	3
1695	gi|12859995 (+2)	unnamed protein product [Mus musculus]	0	0	3	0	0	0
1696	gi|119577238 (+4)	sirtuin (silent mating type information regulation	0	0	0	0	0	3
1697	gi|116283304 (+10)	Add3 protein [Mus musculus]	0	3	0	0	0	0
1698	gi|1665773 (+4)	KIAA0253 [Homo sapiens]	0	0	0	0	0	3
1699	gi|148681543 (+1)	glutathione S-transferase kappa 1, isoform CR	0	3	0	0	0	0
1700	gi|4758788 (+3)	NADH dehydrogenase [ubiquinone] iron-sulfur	0	0	0	0	0	2
1701	gi|148678116 (+4)	Rho GTPase activating protein 26 [Mus muscu	0	3	0	0	0	0
1702	gi|6679201	platelet-activating factor acetylhydrolase IB sut	2	0	0	0	0	0
1703	gi|148698057 (+3)	RIKEN cDNA 2410166I05, isoform CRA_a [Mt	0	0	2	0	0	0

1704	gi|6680091	glutamate receptor delta-2 subunit precursor [N	0	3	0	0	0	0
1705	gi|12643331 (+6)	RecName: Full=Cytoplasmic dynein 1 intermed	0	3	0	0	0	0
1706	gi|118601011 (+7)	secretory carrier-associated membrane protein	0	2	0	0	0	0
1707	gi|118403322 (+4)	isobutyryl-CoA dehydrogenase, mitochondrial	0	2	0	0	0	0
1708	gi|148683291 (+4)	mCG17543, isoform CRA_a [Mus musculus]	3	0	0	0	0	0
1709	gi|158259621 (+1)	unnamed protein product [Homo sapiens]	0	0	0	0	0	2
1710	gi|119588732 (+8)	NEL-like 1 (chicken), isoform CRA_a [Homo sa	0	0	0	0	0	2
1711	gi|2253159 (+2)	peripherin [Mus musculus]	0	2	0	0	0	0
1712	gi|12847471 (+5)	unnamed protein product [Mus musculus]	0	2	0	0	0	0
1713	gi|119390389 (+1)	Chain A, The Crystal Structure Of The Bet3-Tr	0	2	0	0	0	0
1714	gi|15126735 (+2)	Heat shock 27kDa protein 1 [Homo sapiens]	0	0	0	0	0	2
1715	gi|61656188 (+1)	magnesium transporter MRS2 homolog, mitoch	0	0	2	0	0	0
1716	gi|257900520 (+2)	MAGUK p55 subfamily member 6 isoform b [M	0	2	0	0	0	0
1717	gi|1165123 (+1)	component C5 of proteasome [Mus musculus]	2	0	0	0	0	0
1718	gi|158937310 (+1)	hypothetical protein LOC380768 [Mus musculu	0	2	0	0	0	0
1719	gi|26328229 (+1)	unnamed protein product [Mus musculus]	0	0	0	0	0	0
1720	gi|148703976 (+3)	mCG3854, isoform CRA_a [Mus musculus]	0	2	0	0	0	0
1721	gi|187956876 (+2)	Slc6a5 protein [Mus musculus]	0	0	2	0	0	0
1722	gi|121309446 (+3)	acetoacetyl-CoA synthetase [Mus musculus]	2	0	0	0	0	0
1723	gi|14318638 (+3)	Brevican [Homo sapiens], gi|20380804|gb|AAF	0	0	0	0	0	2
1724	gi|126090932 (+7)	nucleolar protein 56 [Mus musculus], gi|30923	0	2	0	0	0	0
1725	gi|125958451 (+2)	RecName: Full=GPI inositol-deacylase; AltNan	0	2	0	0	0	0
1726	gi|148675658 (+8)	cold shock domain containing E1, RNA binding	2	0	0	0	0	0
1727	gi|16553735 (+3)	unnamed protein product [Homo sapiens]	0	0	0	0	0	2
1728	gi|148683592 (+3)	mCG63314 [Mus musculus]	0	0	2	0	0	0
1729	gi|148368976 (+4)	centaurin, alpha 1 [Mus musculus]	2	0	0	0	0	0
1730	gi|119587726 (+6)	Down syndrome cell adhesion molecule like 1,	0	0	0	0	0	2
1731	gi|12847616 (+8)	unnamed protein product [Mus musculus]	2	0	0	0	0	0
1732	gi|222831660	hypothetical protein LOC284069 precursor [Ho	0	0	0	0	0	2
1733	gi|22760412 (+4)	unnamed protein product [Homo sapiens]	0	0	0	0	0	2
1734	gi|15215021 (+6)	Eftud2 protein [Mus musculus]	0	2	0	0	0	0
1735	gi|31980998 (+1)	acyl-coenzyme A thioesterase 9, mitochondria	0	0	2	0	0	0
1736	gi|190360000 (+2)	RecName: Full=Trafficking protein particle com	0	2	0	0	0	0
1737	gi|187957326 (+10)	Sorbs2 protein [Mus musculus]	0	2	0	0	0	0
1738	gi|148705550 (+12)	actin-binding LIM protein 2, isoform CRA_a [M	0	3	0	0	0	0
1739	gi|105990539	neurofilament light polypeptide [Homo sapiens	0	0	0	0	0	2
1740	gi|110591399 (+14)	Chain A, Structure Of Human Ferritin L Chain,	0	0	0	0	0	2
1741	gi|119622432 (+7)	milk fat globule-EGF factor 8 protein, isoform C	0	0	0	0	0	2
1742	gi|12000323 (+3)	sodium-dependent vitamin C transporter type 2	0	2	0	0	0	0
1743	gi|12963559 (+1)	V-type proton ATPase subunit G 2 [Mus muscu	0	2	0	0	0	0
1744	gi|13124196 (+6)	RecName: Full=ELAV-like protein 1; AltName:	0	2	0	0	0	0
1745	gi|13236495 (+4)	quinone oxidoreductase isoform a [Homo sapie	0	0	0	0	0	2
1746	gi|13385436	reactive oxygen species modulator 1 [Mus mus	0	0	2	0	0	0
1747	gi|13786847 (+2)	Chain A, Human Heart L-Lactate Dehydrogena	0	0	0	0	0	2
1748	gi|148670202 (+4)	HIV-1 Rev binding protein [Mus musculus]	0	2	0	0	0	0
1749	gi|148699405 (+3)	ubiquilin 2, isoform CRA_b [Mus musculus]	2	0	0	0	0	0
1750	gi|148708252 (+5)	mCG8513 [Mus musculus]	0	2	0	0	0	0
1751	gi|16306530 (+1)	cadherin-10 preproprotein [Homo sapiens], gi|1	0	0	0	0	0	2
1752	gi|16554039	unnamed protein product [Homo sapiens]	0	0	0	0	0	2
1753	gi|189053201 (+3)	unnamed protein product [Homo sapiens]	0	0	0	0	0	2
1754	gi|28422739 (+3)	Wolfram syndrome 1 homolog (human) [Mus m	0	2	0	0	0	0
1755	gi|4504257 (+1)	histone H2B type 1-C/E/F/G/I [Homo sapiens],	0	2	0	0	0	0
1756	gi|4826962	ras-related C3 botulinum toxin substrate 3 prec	2	0	0	0	0	0
1757	gi|74138665 (+2)	unnamed protein product [Mus musculus]	2	0	0	0	0	0
1758	gi|8394493	tubulin alpha-8 chain [Mus musculus], gi|12585	0	2	0	0	0	0

1759	gi|26345374 (+3)	unnamed protein product [Mus musculus]	0	0	0	0	0	0
1760	gi|134035342 (+4)	RecName: Full=Ubiquitin-conjugating enzyme	2	0	0	0	0	0
1761	gi|194381492 (+4)	unnamed protein product [Homo sapiens]	0	0	0	0	0	2
1762	gi|12833090 (+4)	unnamed protein product [Mus musculus]	2	0	0	0	0	0
1763	gi|123858362 (+4)	NADH dehydrogenase (ubiquinone) 1 alpha su	0	0	2	0	0	0
1764	gi|21703854 (+2)	dehydrogenase/reductase SDR family membe	0	0	2	0	0	0
1765	gi|221041684 (+1)	unnamed protein product [Homo sapiens]	0	0	0	0	0	2
1766	gi|119594168 (+11)	serpin peptidase inhibitor, clade G (C1 inhibito	0	0	0	0	0	2
1767	gi|119620534 (+8)	reticulon 4, isoform CRA_h [Homo sapiens]	0	0	0	0	0	2
1768	gi|148676399 (+1)	surfeit gene 4, isoform CRA_b [Mus musculus]	0	2	0	0	0	0
1769	gi|109658490 (+14)	Insulin receptor [Homo sapiens]	0	0	0	0	0	2
1770	gi|109730745 (+2)	Leucine rich repeat containing 4 [Mus musculu	0	0	0	0	0	0
1771	gi|1923219 (+2)	ceramide UDPgalactosyltransferase [Homo sa	0	0	0	0	0	2
1772	gi|5729718	trophoblast glycoprotein [Homo sapiens], gi|26	0	0	0	0	0	2
1773	gi|11321583 (+9)	succinyl-CoA ligase [ADP-forming] subunit beta	0	0	0	0	0	2
1774	gi|148674178 (+2)	gamma-glutamyltransferase-like 3, isoform CR	0	2	0	0	0	0
1775	gi|34365085 (+1)	hypothetical protein [Homo sapiens]	0	0	0	0	0	2
1776	gi|109158017 (+4)	Chain A, Crystal Structure Of The Selenocyste	0	0	0	0	0	2
1777	gi|28173554 (+2)	histone H2B type 3-B [Homo sapiens], gi|1578	0	2	0	0	0	0
1778	gi|1096024 (+6)	isoAsp protein carboxyl methyltransferase	0	0	0	0	0	2
1779	gi|21313588 (+2)	small glutamine-rich tetratricopeptide repeat-co	2	0	0	0	0	0
1780	gi|124248566 (+1)	CUB and sushi domain-containing protein 1 pr	0	0	0	0	0	0
1781	gi|122066080	RecName: Full=Sacsin; AltName: Full=DnaJ h	0	2	0	0	0	0
1782	gi|109658736 (+5)	Interleukin 6 signal transducer (gp130, oncosta	0	0	0	0	0	2
1783	gi|109893891 (+55)	hemoglobin [Homo sapiens], gi|193244867|gb|	0	0	0	0	0	2
1784	gi|110225379 (+3)	ATP-binding cassette sub-family A member 2 [	0	0	0	0	0	0
1785	gi|11095441 (+3)	methylmalonate-semialdehyde dehydrogenase	0	0	0	0	0	2
1786	gi|114205611 (+7)	Syt7 protein [Mus musculus]	0	2	0	0	0	0
1787	gi|114648897 (+6)	PREDICTED: similar to lambda-crystallin isofo	0	0	0	0	0	2
1788	gi|118403314 (+8)	RNA-binding protein 39 [Mus musculus], gi|559	0	2	0	0	0	0
1789	gi|119570172 (+3)	sideroflexin 3 [Homo sapiens]	0	0	0	0	0	2
1790	gi|119574954 (+7)	voltage-dependent anion channel 2, isoform C	0	0	0	0	0	2
1791	gi|119587509 (+6)	acetyl-Coenzyme A acetyltransferase 1 (aceto	0	0	0	0	0	2
1792	gi|119589133 (+14)	sphingomyelin phosphodiesterase 1, acid lyso	0	0	0	0	0	2
1793	gi|119591511 (+10)	collagen, type VI, alpha 3, isoform CRA_c [Hor	0	0	0	0	0	2
1794	gi|119619155 (+3)	steroid sulfatase (microsomal), arylsulfatase C	0	0	0	0	0	2
1795	gi|120537241 (+2)	leucyl-tRNA synthetase, cytoplasmic [Mus mus	0	2	0	0	0	0
1796	gi|123209965 (+4)	diacylglycerol kinase zeta [Mus musculus], gi|1	0	2	0	0	0	0
1797	gi|123228991 (+2)	emerin [Mus musculus]	0	2	0	0	0	0
1798	gi|123239930 (+3)	acyl-CoA thioesterase 11 [Mus musculus]	0	2	0	0	0	0
1799	gi|123858142 (+14)	syndecan binding protein [Mus musculus]	0	2	0	0	0	0
1800	gi|124486712 (+3)	ribosome-binding protein 1 isoform a [Mus mus	2	0	0	0	0	0
1801	gi|124486789 (+4)	phosphoinositide 3-kinase regulatory subunit 4	0	2	0	0	0	0
1802	gi|126522466 (+1)	6430704M03Rik protein [Mus musculus]	0	2	0	0	0	0
1803	gi|127138858 (+6)	ras-related protein Rab-27B [Mus musculus], g	0	2	0	0	0	0
1804	gi|12833305 (+1)	unnamed protein product [Mus musculus]	0	0	2	0	0	0
1805	gi|12837563 (+1)	unnamed protein product [Mus musculus]	0	2	0	0	0	0
1806	gi|12847703 (+2)	unnamed protein product [Mus musculus]	0	2	0	0	0	0
1807	gi|12857304 (+3)	unnamed protein product [Mus musculus]	2	0	0	0	0	0
1808	gi|12963757	inositol-3-phosphate synthase 1 [Mus musculu	2	0	0	0	0	0
1809	gi|13277354 (+3)	UBX domain-containing protein 6 [Mus muscul	0	2	0	0	0	0
1810	gi|139948802 (+2)	ubiquitin carboxyl-terminal hydrolase isozyme	2	0	0	0	0	0
1811	gi|14486428 (+4)	phosphotyrosyl phosphatase activator [Mus mu	2	0	0	0	0	0
1812	gi|148665896 (+4)	mitochondrial ribosomal protein L39 [Mus mus	0	0	2	0	0	0
1813	gi|148675003 (+4)	mCG15301, isoform CRA_d [Mus musculus], g	0	2	0	0	0	0

1814 gi|148683488 (+3)	guanylate cyclase 1, soluble, beta 3, isoform C	0	2	0	0	0	0
1815 gi|148685766 (+2)	acyl-Coenzyme A dehydrogenase, short/branc	0	2	0	0	0	0
1816 gi|148686645 (+2)	adenylosuccinate synthetase like 1, isoform CF	0	2	0	0	0	0
1817 gi|148689643 (+1)	plexin C1 [Mus musculus]	0	0	0	0	0	0
1818 gi|148691044 (+2)	abhydrolase domain containing 3 [Mus muscul	0	2	0	0	0	0
1819 gi|148694894 (+3)	RIKEN cDNA A930041I02, isoform CRA_a [Mu	0	2	0	0	0	0
1820 gi|148695213 (+3)	limb and neural patterns, isoform CRA_a [Mus	0	2	0	0	0	0
1821 gi|148704518 (+1)	mCG52906 [Mus musculus]	0	2	0	0	0	0
1822 gi|15431316 (+2)	keratin, type II cuticular Hb4 [Homo sapiens], g	0	0	0	0	0	2
1823 gi|15489222 (+6)	Eukaryotic translation termination factor 1 [Mus	2	0	0	0	0	0
1824 gi|167466198 (+3)	intercellular adhesion molecule 1 precursor [Ho	0	0	0	0	0	2
1825 gi|170172546 (+2)	WD repeat-containing protein 47 [Mus muscul	0	2	0	0	0	0
1826 gi|1709933 (+2)	RecName: Full=Adenylosuccinate lyase; Short	0	2	0	0	0	0
1827 gi|189181759 (+2)	electron transfer flavoprotein subunit alpha, mi	0	0	0	0	0	2
1828 gi|191804 (+3)	aldehyde dehydrogenase II [Mus musculus]	0	2	0	0	0	0
1829 gi|193785685 (+2)	unnamed protein product [Homo sapiens]	0	0	0	0	0	2
1830 gi|223278387 (+2)	calmodulin-like protein 5 [Homo sapiens], gi|21	0	0	0	0	0	2
1831 gi|22761023 (+2)	unnamed protein product [Homo sapiens]	0	0	0	0	0	2
1832 gi|24212072 (+1)	RecName: Full=Mitochondrial import receptor s	0	2	0	0	0	0
1833 gi|242332593	ragulator complex protein PDRO [Mus muscul	0	2	0	0	0	0
1834 gi|260763997 (+1)	armadillo repeat-containing protein 8 isoform 1	0	2	0	0	0	0
1835 gi|26324293 (+2)	unnamed protein product [Mus musculus]	0	0	2	0	0	0
1836 gi|41393545 (+1)	ras-related protein Rab-5C isoform b [Homo sa	0	0	0	0	0	2
1837 gi|4503253 (+1)	dolichyl-diphosphooligosaccharide--protein gly	0	2	0	0	0	0
1838 gi|51476685	hypothetical protein [Homo sapiens]	0	0	0	0	0	2
1839 gi|6680522 (+1)	potassium voltage-gated channel subfamily C	0	2	0	0	0	0
1840 gi|6754480	keratin, type I cytoskeletal 13 [Mus musculus],	0	0	0	2	0	0
1841 gi|7106349	ly-6/neurotoxin-like protein 1 precursor [Mus m	0	2	0	0	0	0
1842 gi|12843407 (+10)	unnamed protein product [Mus musculus], gi|1	0	0	0	0	0	0
1843 gi|14278227 (+3)	Chain B, Nmr Structure Of Dff40 And Dff45 N-1	0	0	0	0	0	2
1844 gi|213511508 (+3)	B-cell receptor-associated protein 31 isoform a	0	0	0	0	0	2
1845 gi|148701161 (+4)	phosphofurin acidic cluster sorting protein 1 [M	0	2	0	0	0	0
1846 gi|26346504 (+3)	unnamed protein product [Mus musculus]	0	2	0	0	0	0
1847 gi|12835725 (+2)	unnamed protein product [Mus musculus]	0	2	0	0	0	0
1848 gi|10946722	cell differentiation protein RCD1 homolog [Mus	0	2	0	0	0	0
1849 gi|148670716 (+4)	exonuclease 3"-5" domain-like 2, isoform CRA	0	0	2	0	0	0
1850 gi|254675217 (+4)	vacuolar protein sorting-associated protein 18	0	2	0	0	0	0
1851 gi|193787420 (+3)	unnamed protein product [Homo sapiens]	0	0	0	0	0	2
1852 gi|119630986 (+6)	isocitrate dehydrogenase 3 (NAD+) beta, isofo	0	0	0	0	0	2
1853 gi|148683923 (+3)	diacylglycerol kinase, epsilon [Mus musculus]	0	2	0	0	0	0
1854 gi|124297703 (+2)	Reck protein [Mus musculus], gi|187953797|gb	0	0	0	0	0	0
1855 gi|14042242 (+4)	unnamed protein product [Homo sapiens]	0	0	0	0	0	2
1856 gi|110056 (+6)	transition protein - mouse	2	0	0	0	0	0
1857 gi|908803	keratin type II [Homo sapiens]	0	0	0	0	0	2
1858 gi|148689496 (+1)	mCG141936 [Mus musculus]	2	0	0	0	0	0
1859 gi|16118553 (+5)	ELMO2 [Mus musculus], gi|148674506|gb|EDL	0	2	0	0	0	0
1860 gi|123225318 (+5)	transformation related protein 53 inducible prot	0	2	0	0	0	0
1861 gi|119606585 (+3)	plexin domain containing 2, isoform CRA_c [Ho	0	0	0	0	0	2
1862 gi|16307535 (+3)	Lcmt1 protein [Mus musculus]	2	0	0	0	0	0
1863 gi|253683505 (+2)	brain-enriched guanylate kinase-associated pr	0	2	0	0	0	0
1864 gi|123210733 (+2)	gamma-aminobutyric acid (GABA-A) receptor,	0	2	0	0	0	0
1865 gi|148679603 (+3)	expressed sequence AI427515 [Mus musculus	2	0	0	0	0	0
1866 gi|148686999 (+3)	Sel1 (suppressor of lin-12) 1 homolog (C. elega	0	2	0	0	0	0
1867 gi|12832570 (+4)	unnamed protein product [Mus musculus]	0	2	0	0	0	0
1868 gi|33859690	ubiquinone biosynthesis protein COQ9, mitoch	0	0	2	0	0	0

1869	gi|12856544 (+1)	unnamed protein product [Mus musculus]	0	2	0	0	0	0
1870	gi|148705386 (+4)	solute carrier family 30 (zinc transporter), mem	0	2	0	0	0	0
1871	gi|61098100	tyrosine-protein phosphatase non-receptor typ	0	2	0	0	0	0
1872	gi|13385484 (+1)	ATP synthase subunit epsilon, mitochondrial [N	0	0	2	0	0	0
1873	gi|148696228 (+6)	activating signal cointegrator 1 complex subun	2	0	0	0	0	0
1874	gi|148669498 (+9)	mCG48640 [Mus musculus]	0	2	0	0	0	0
1875	gi|148707407 (+3)	astrotactin 1, isoform CRA_a [Mus musculus]	0	0	0	0	0	0
1876	gi|148668577 (+2)	mCG114899 [Mus musculus]	0	2	0	0	0	0
1877	gi|12963697 (+2)	fumarylacetoacetate hydrolase domain-contair	0	0	2	0	0	0
1878	gi|147904700 (+1)	semaphorin-5A precursor [Homo sapiens], gi|1	0	0	0	0	0	2
1879	gi|193787479 (+3)	unnamed protein product [Homo sapiens]	0	0	0	0	0	2
1880	gi|148691111 (+3)	cullin 2, isoform CRA_a [Mus musculus]	0	2	0	0	0	0
1881	gi|6755668 (+2)	signal transducing adapter molecule 1 [Mus mu	0	2	0	0	0	0
1882	gi|116248181 (+4)	RecName: Full=Protein FAM131B, gi|7418273	0	2	0	0	0	0
1883	gi|219518723 (+5)	Ankyrin repeat and FYVE domain containing 1	0	2	0	0	0	0
1884	gi|119590496 (+4)	fumarate hydratase, isoform CRA_a [Homo sa	0	0	0	0	0	2
1885	gi|114050895 (+2)	cadherin EGF LAG seven-pass G-type recepto	0	0	0	0	0	0
1886	gi|122114537	vacuolar protein sorting-associated protein 13(	0	2	0	0	0	0
1887	gi|148686944 (+6)	RIKEN cDNA 9030617O03, isoform CRA_a [N	0	0	2	0	0	0
1888	gi|119609562 (+1)	hCG30508, isoform CRA_b [Homo sapiens]	0	0	0	0	0	2
1889	gi|148683519 (+3)	mCG18109 [Mus musculus]	0	2	0	0	0	0
1890	gi|119368659 (+9)	RecName: Full=Diacylglycerol kinase beta; Sh	0	2	0	0	0	0
1891	gi|84040267	Keratin 6C [Homo sapiens]	0	0	0	0	0	2
1892	gi|20071563 (+2)	Saccharopine dehydrogenase (putative) [Hom	0	0	0	0	0	2
1893	gi|1709797 (+7)	RecName: Full=26S protease regulatory subur	0	2	0	0	0	0
1894	gi|12844196 (+1)	unnamed protein product [Mus musculus]	0	2	0	0	0	0
1895	gi|125660464 (+1)	dedicator of cytokinesis protein 11 [Mus muscu	0	0	2	0	0	0
1896	gi|148698234 (+1)	eukaryotic translation initiation factor 3, subuni	2	0	0	0	0	0
1897	gi|148672138 (+3)	LETM1 domain containing 1, isoform CRA_c [N	0	0	2	0	0	0
1898	gi|116512449	GntR family transcriptional regulator [Lactococ	0	2	0	0	0	0
1899	gi|12851714 (+4)	unnamed protein product [Mus musculus]	0	2	0	0	0	0
1900	gi|17975500	GMP reductase 1 [Mus musculus], gi|2500850	2	0	0	0	0	0
1901	gi|117938776 (+4)	Smc1a protein [Mus musculus], gi|118599981|	0	2	0	0	0	0
1902	gi|27753993	leucine-rich repeat transmembrane neuronal p	0	0	0	0	0	0
1903	gi|297161738	putative ABC transporter ATP-binding protein [	0	2	0	0	0	0
1904	gi|10438181 (+6)	unnamed protein product [Homo sapiens]	0	0	0	0	0	2

Bibliography

Aboitiz, F. and J. Montiel (2003). One hundred million years of interhemispheric communication: the history of the corpus callosum. *Brazilian Journal of Medical and Biological Research 36*, 409–420.

Aboul-Enein, F., P. Weiser, R. Höftberger, H. Lassmann, and M. Bradl (2006). Transient Axonal Injury in the Absence of Demyelination: A Correlate of Clinical Disease in Acute Experimental Autoimmune Encephalomyelitis. *Acta Neuropathologica 111*(6), 539–547.

Abrahams, P. J. and A. J. Van der Eb (1975, July). In vitro transformation of rat and mouse cells by DNA from simian virus 40. *Journal of virology 16*(1), 206–9.

Aggarwal, S., L. Yurlova, N. Snaidero, C. Reetz, S. Frey, J. Zimmermann, G. Pähler, A. Janshoff, J. Friedrichs, D. Müller, C. Goebel, and M. Simons (2011). A Size Barrier Limits Protein Diffusion at the Cell Surface to Generate Lipid-Rich Myelin-Membrane Sheets. *Developmental Cell 21*(3), 445–456.

Amor, S., M. F. Scallan, M. M. Morris, H. Dyson, and J. K. Fazakerley (1996). Role of immune responses in protection and pathogenesis during Semliki Forest virus encephalitis. *Journal of General Virology 77*(2), 281–291.

Antel, J., S. Antel, Z. Caramanos, D. Arnold, and T. Kuhlmann (2012). Primary progressive multiple sclerosis: part of the MS disease spectrum or separate disease entity? *Acta Neuropathologica 123*(5), 627–638.

Antony, J. M., G. van Marle, W. Opii, D. A. Butterfield, F. Mallet, V. W. Yong, J. L. Wallace, R. M. Deacon, K. Warren, and C. Power (2004). Human endogenous retrovirus glycoprotein-mediated induction of redox reactants causes oligodendrocyte death and demyelination. *Nature Neuroscience 7*(10), 1088–1095.

Arber, W. and S. Linn (1969, January). DNA modification and restriction. *Annual review of biochemistry 38*, 467–500.

Baer, A. S., Y. A. Syed, S. U. Kang, D. Mitteregger, R. Vig, C. Ffrench-Constant, R. J. M. Franklin, F. Altmann, G. Lubec, and M. R. Kotter (2009). Myelin-mediated inhibition of oligodendrocyte precursor differentiation can be overcome by pharmacological modulation of Fyn-RhoA and protein kinase C signalling. *Brain 132*(2), 465–481.

Barnett, M. H. and J. W. Prineas (2004). Relapsing and remitting multiple sclerosis: pathology of the newly forming lesion. *Annals of Neurology 55*(4), 458–468.

Baumann, N. and D. Pham-Dinh (2001). Biology of Oligodendrocyte and Myelin in the Mammalian Central Nervous System. *Physiol. Rev. 81*(2), 871–927.

Bitsch, A., J. Schuchardt, S. Bunkowski, T. Kuhlmann, and W. Bruck (2000). Acute axonal injury in multiple sclerosis: Correlation with demyelination and inflammation. *Brain 123*(6), 1174–1183.

Bjartmar, C. and B. Trapp (2003). Axonal degeneration and progressive neurologic disability in multiple sclerosis. *Neurotoxicity Research 5*(1), 157–164.

Blakemore, W. F. (1973a). Demyelination of the superior cerebellar peduncle in the mouse induced by cuprizone. *Journal of the Neurological Sciences 20*(1), 63–72.

Blakemore, W. F. (1973b). Remyelination of the superior cerebellar peduncle in the mouse following demyelination induced by feeding cuprizone. *Journal of the Neurological Sciences 20*(1), 73–83.

Blakemore, W. F. (1982). Ethidium bromide induced demyelination in the spinal cord of the cat. *Neuropathology and Applied Neurobiology 8*(5), 365–375.

Bolivar, V. J., S. R. Walters, and J. L. Phoenix (2007). Assessing autism-like behavior in mice: variations in social interactions among inbred strains. *Behavioural Brain Research 176*(1), 21–26.

Bourre, J. M., C. Jacque, A. Delassalle, J. Nguyen-Legros, O. Dumont, F. Lachapelle, M. Raoul, C. Alvarez, and N. Baumann (1980). Density Profile and Basic Protein Measurements in the Myelin Range of Particulate Material from Normal Developing Mouse Brain and from Neurological Mutants (Jimpy; Quaking; Trembler; Shiverer and its mid Allele) Obtained by Zonal Centrifugation. *Journal of Neurochemistry 35*(2), 458–464.

Bradford, M. M. (1976). A rapid and sensitive method for the quantitation of microgram quantities of protein utilizing the principle of protein-dye binding. *Analytical Biochemistry 72*(1-2), 248–254.

Brockschnieder, D., C. Lappe-Siefke, S. Goebbels, M. R. Boesl, K.-A. Nave, and D. Riethmacher (2004). Cell Depletion Due to Diphtheria Toxin Fragment A after Cre-Mediated Recombination. *Molecular and Cellular Biology 24*(17), 7636–7642.

Brück, W. (2005). Inflammatory demyelination is not central to the pathogenesis of multiple sclerosis. *Journal of Neurology 252*(0), v10–v15.

Brück, W., T. Kuhlmann, and C. Stadelmann (2003). Remyelination in multiple sclerosis. *Journal of the Neurological Sciences 206*(2), 181–185.

Buch, T., F. L. Heppner, C. Tertilt, T. Heinen, M. Kremer, F. T. Wunderlich, S. Jung, and A. Waisman (2005). A Cre-inducible diphtheria toxin receptor mediates cell lineage ablation after toxin administration. *Nature Methods 2*(6), 419–426.

Bunge, M. B., R. P. Bunge, and G. D. Pappas (1962). Electron Microscopic Demonstration of Connections between Glia and Myelin Sheaths in the Developing Mammalian Central Nervous System. *The Journal of Cell Biology 12*(2), 448–453.

Cahoy, J. D., B. Emery, A. Kaushal, L. C. Foo, J. L. Zamanian, K. S. Christopherson, Y. Xing, J. L. Lubischer, P. A. Krieg, S. A. Krupenko, W. J. Thompson, and B. A. Barres (2008). A Transcriptome Database for Astrocytes, Neurons, and Oligodendrocytes: A New Resource for Understanding Brain Development and Function. *The Journal of Neuroscience 28*(1), 264–278.

Cajal, S. R. Y. (1894). The Croonian Lecture: La Fine Structure des Centres Nerveux. *Proceedings of the Royal Society of London 55*(331-335), 444–468.

Cammer, W. (1999). The neurotoxicant, cuprizone, retards the differentiation of oligodendrocytes in vitro. *Journal of the Neurological Sciences 168*(2), 116–120.

Campagnoni, A. and W. Macklin (1988). Cellular and molecular aspects of myelin protein gene expression. *Molecular Neurobiology 2*(1), 41–89.

Chandross, K. J., R. I. Cohen, P. Paras, M. Gravel, P. E. Braun, and L. D. Hudson (1999, January). Identification and characterization of early glial progenitors using a transgenic selection strategy. *The Journal of neuroscience : the official journal of the Society for Neuroscience 19*(2), 759–74.

Chang, A., W. W. Tourtellotte, R. Rudick, and B. D. Trapp (2002). Premyelinating Oligodendrocytes in Chronic Lesions of Multiple Sclerosis. *New England Journal of Medicine 346*(3), 165–173.

Chastain, E. M. L. and S. D. Miller (2011). Molecular mimicry as an inducing trigger for CNS autoimmune demyelinating disease. *Immunological reviews 245*(1), 227–238.

Cobb, S. and M. Bielschowsky (1925). A method for intra-vital staining with silver ammonium oxide solution. *Journal für Psychologie und Neurologie 31*, 301–304.

Coetzee, T., N. Fujita, J. Dupree, R. Shi, A. Blight, K. Suzuki, K. Suzuki, and B. Popko (1996). Myelination in the Absence of Galactocerebroside and Sulfatide: Normal Structure with Abnormal Function and Regional Instability. *Cell 86*(2), 209–219.

Cohen, J. A., F. Barkhof, G. Comi, H.-P. Hartung, B. O. Khatri, X. Montalban, J. Pelletier, R. Capra, P. Gallo, G. Izquierdo, K. Tiel-Wilck, A. de Vera, J. Jin, T. Stites, S. Wu, S. Aradhye, and L. Kappos (2010). Oral Fingolimod or Intramuscular Interferon for Relapsing Multiple Sclerosis. *New England Journal of Medicine 362*(5), 402–415.

Colello, R. J., B. Fuss, M. A. Fox, and J. Alberti (2002). A proteomic approach to rapidly elucidate oligodendrocyte-associated proteins expressed in the myelinating rat optic nerve. *Electrophoresis 23*(1), 144–151.

Collier, R. J. (1967). Effect of diphtheria toxin on protein synthesis: Inactivation of one of the transfer factors. *Journal of Molecular Biology 25*(1), 83–98.

Compston, A. and A. Coles (2008). Multiple sclerosis. *The Lancet 372*(9648), 1502–1517.

Compston, A., J. Zajicek, J. O. N. Sussman, A. Webb, G. Hall, D. Muir, C. Shaw, A. Wood, and N. Scolding (1997). Review: Glial lineages and myelination in the central nervous system. *Journal of Anatomy 190*(2), 161–200.

Confavreux, C., G. Aimard, and M. Devic (1980). Course and prognosis of Multiple Sclerosis assessed by the computerized data processing of 349 patients. *Brain 103*(2), 281–300.

Confavreux, C., S. Vukusic, and P. Adeleine (2003). Early clinical predictors and progression of irreversible disability in multiple sclerosis: an amnesic process. *Brain 126*(4), 770–782.

Confavreux, C., S. Vukusic, T. Moreau, and P. Adeleine (2000). Relapses and Progression of Disability in Multiple Sclerosis. *New England Journal of Medicine 343*(20), 1430–1438.

Crawford, D. K., M. Mangiardi, X. Xia, H. E. López-Valdés, and S. K. Tiwari-Woodruff (2009). Functional recovery of callosal axons following demyelination: a critical window. *Neuroscience 164*(4), 1407–1421.

de Waegh, S. M., V. M. Lee, and S. T. Brady (1992, February). Local modulation of neurofilament phosphorylation, axonal caliber, and slow axonal transport by myelinating Schwann cells. *Cell 68*(3), 451–63.

Duncan, I. D., A. Brower, Y. Kondo, J. F. Curlee, and R. D. Schultz (2009). Extensive remyelination of the CNS leads to functional recovery. *Proceedings of the National Academy of Sciences 106*(16), 6832–6837.

Dutta, R., J. McDonough, X. Yin, J. Peterson, A. Chang, T. Torres, T. Gudz, W. B. Macklin, D. A. Lewis, R. J. Fox, R. Rudick, K. Mirnics, and B. D. Trapp (2006). Mitochondrial dysfunction as a cause of axonal degeneration in multiple sclerosis patients. *Annals of Neurology 59*(3), 478–489.

Edgar, J. M., M. McLaughlin, D. Yool, S.-C. Zhang, J. H. Fowler, P. Montague, J. A. Barrie, M. C. McCulloch, I. D. Duncan, J. Garbern, K. A. Nave, and I. R. Griffiths (2004). Oligodendroglial modulation of fast axonal transport in a mouse model of hereditary spastic paraplegia. *Journal of cell biology 166*(1), 121–131.

Eisenhaber, B., P. Bork, and F. Eisenhaber (1999, September). Prediction of potential GPI-modification sites in proprotein sequences. *Journal of molecular biology 292*(3), 741–58.

Emerson, M. R., S. Biswas, and S. M. LeVine (2001, October). Cuprizone and piperonyl butoxide, proposed inhibitors of T-cell function, attenuate experimental allergic encephalomyelitis in SJL mice. *Journal of neuroimmunology 119*(2), 205–13.

Evangelou, N., D. Konz, M. M. Esiri, S. Smith, J. Palace, and P. M. Matthews (2000). Regional axonal loss in the corpus callosum correlates with cerebral white matter lesion volume and distribution in multiple sclerosis. *Brain 123*(9), 1845–1849.

Evangelou, N., D. Konz, M. M. Esiri, S. Smith, J. Palace, and P. M. Matthews (2001). Size-selective neuronal changes in the anterior optic pathways suggest a differential susceptibility to injury in multiple sclerosis. *Brain 124*(9), 1813–1820.

Faivre, A., A. Rico, W. Zaaraoui, L. Crespy, F. Reuter, D. Wybrecht, E. Soulier, I. Malikova, S. Confort-Gouny, P. J. Cozzone, J. Pelletier, J.-P. Ranjeva, and B. Audoin (2012). Assessing brain connectivity at rest is clinically relevant in early multiple sclerosis. *Multiple Sclerosis Journal Publicatio.*

Fame, R. M., J. L. MacDonald, and J. D. Macklis (2010). Development, specification, and diversity of callosal projection neurons. *Trends in Neurosciences 34*(1), 41–50.

Ferguson, B., M. K. Matyszak, M. M. Esiri, and V. H. Perry (1997). Axonal damage in acute multiple sclerosis lesions. *Brain 120*, 393–399.

Fewou, S. N., H. Ramakrishnan, H. Büssow, V. Gieselmann, and M. Eckhardt (2007). Down-regulation of Polysialic Acid Is Required for Efficient Myelin Formation. *Journal of biological chemistry 282*(22), 16700–16711.

Fields, R. D. (2008). White matter in learning, cognition and psychiatric disorders. *Trends in Neurosciences 31*(7), 361–370.

Fitzner, D., A. Schneider, W. Kippert, W. Moebius, K. Willig, S. W. Hell, G. Bunt, K. Gaus, and M. Simons (2006). Myelin basic protein-dependent plasma membrane reorganization in the formation of myelin. *The EMBO Journal 25*, 5037–5048.

Fournier, A. E., T. Grandpre, and S. M. Strittmatter (2001). Identification of a receptor mediating Nogo-66 inhibition of axonal regeneration. *Nature 409*, 341–346.

Fox, E. J. (2004, December). Mechanism of action of mitoxantrone. *Neurology 63*(Issue 12, Supplement 6), S15–S18.

Franco-Pons, N., M. Torrente, M. T. Colomina, and E. Vilella (2007). Behavioral deficits in the cuprizone-induced murine model of demyelination/remyelination. *Toxicology Letters 169*(3), 205–213.

Franklin, R. J. M. (2002). Why does remyelination fail in multiple sclerosis? *Nature Reviews Neuroscience 3*(9), 705–714.

Franklin, R. J. M. and C. Ffrench-Constant (2008). Remyelination in the CNS: from biology to therapy. *Nature Reviews Neuroscience 9*(11), 839–855.

Friese, M. A. and L. Fugger (2005). Autoreactive CD8+ T cells in multiple sclerosis: a new target for therapy? *Brain 128*(8), 1747–1763.

Friese, M. A., X. Montalban, N. Willcox, J. I. Bell, R. Martin, and L. Fugger (2006). The value of animal models for drug development in multiple sclerosis. *Brain 129*(8), 1940–1952.

Frischer, J. M., S. Bramow, A. Dal-Bianco, C. F. Lucchinetti, H. Rauschka, M. Schmidbauer, H. Laursen, P. S. Sorensen, and H. Lassmann (2009). The relation between inflammation and neurodegeneration in multiple sclerosis brains. *Brain 132*(5), 1175–1189.

Gil, O. D., G. Zanazzi, A. F. Struyk, and J. L. Salzer (1998). Neurotrimin Mediates Bifunctional Effects on Neurite Outgrowth via Homophilic and Heterophilic Interactions. *The Journal of Neuroscience 18*(22), 9312–9325.

Gil, O. D., L. Zhang, S. Chen, Y. Q. Ren, A. Pimenta, G. Zanazzi, D. Hillman, P. Levitt, and J. L. Salzer (2002). Complementary expression and heterophilic interactions between igLON family members neurotrimin and LAMP. *Journal of Neurobiology 51*(3), 190–204.

Gold, R., C. Linington, and H. Lassmann (2006). Understanding pathogenesis and therapy of multiple sclerosis via animal models: 70 years of merits and culprits in experimental autoimmune encephalomyelitis research. *Brain 129*(8), 1953–1971.

Gourraud, P.-A., H. F. Harbo, S. L. Hauser, and S. E. Baranzini (2012). The genetics of multiple sclerosis: an up-to-date review. *Immunological reviews 248*(1), 87–103.

Graham, F. L., J. Smiley, W. C. Russell, and R. Nairn (1977, July). Characteristics of a human cell line transformed by DNA from human adenovirus type 5. *The Journal of general virology 36*(1), 59–74.

Griffiths, I., M. Klugmann, T. Anderson, D. Yool, C. Thomson, M. H. Schwab, A. Schneider, F. Zimmermann, M. McCulloch, N. Nadon, and K.-A. Nave (1998). Axonal Swellings and Degeneration in Mice Lacking the Major Proteolipid of Myelin. *Science 280*(5369), 1610–1613.

Group, T. I. M. S. S. (1993). Interferon beta1b is effective in relapsing-remitting multiple sclerosis. *Neurology 43*(4), 655.

Hall, S. M. (1972). The Effect of Injections of Lysophosphatidyl Choline into White Matter of the Adult Mouse Spinal Cord. *The Journal of Cell Science 10*(2), 535–546.

Hampton, D. W., N. Innes, D. Merkler, C. Zhao, R. J. M. Franklin, and S. Chandran (2012). Focal Immune-Mediated White Matter Demyelination Reveals an Age-Associated Increase in Axonal Vulnerability and Decreased Remyelination Efficiency. *The American Journal of Pathology 180*(5), 1897–1905.

Hanisch, U.-K. and H. Kettenmann (2007). Microglia: active sensor and versatile effector cells in the normal and pathologic brain. *Nature Neuroscience 10*(11), 1387–1394.

Hemmer, B., J. J. Archelos, and H.-P. Hartung (2002). New concepts in the immunopathogenesis of multiple sclerosis. *Nature Reviews Neuroscience 3*(4), 291–301.

Heppner, F. L., M. Greter, D. Marino, J. Falsig, G. Raivich, N. Hovelmeyer, A. Waisman, T. Rulicke, M. Prinz, J. Priller, B. Becher, and A. Aguzzi (2005). Experimental autoimmune encephalomyelitis repressed by microglial paralysis. *Nature Medicine 11*(2), 146–152.

Hibbits, N., R. Pannu, T. John Wu, and R. C. Armstrong (2009). Cuprizone demyelination of the corpus callosum in mice correlates with altered social interaction and impaired bilateral sensorimotor coordination. *ASN NEURO 1*(3), e00013.

Hiremath, M. M., Y. Saito, G. W. Knapp, J. P. Y. Ting, K. Suzuki, and G. K. Matsushima (1998). Microglial/macrophage accumulation during cuprizone-induced demyelination in C57BL/6 mice. *Journal of Neuroimmunology 92*, 38–49.

Hoehn, H. J., Y. Kress, A. Sohn, C. F. Brosnan, S. Bourdon, and B. Shafit-Zagardo (2008, November). Axl-/- mice have delayed recovery and prolonged axonal damage following cuprizone toxicity. *Brain research 1240*, 1–11.

Hoffmann, K., M. Lindner, I. Gröticke, M. Stangel, and W. Löscher (2008). Epileptic seizures and hippocampal damage after cuprizone-induced demyelination in C57BL/6 mice. *Experimental Neurology 210*(2), 308–321.

Holmes, R. K. (2000). Biology and Molecular Epidemiology of Diphtheria Toxin and the tox Gene. *Journal of Infectious Diseases 181*(Supplement 1), S156–S167.

Honjo, T., Y. Nishizuka, and O. Hayaishi (1969). Adenosine Diphosphoribosylation of Aminoacyl Transferase II by Diphtheria Toxin. *Cold Spring Harbor Symposia on Quantitative Biology 34*, 603–608.

Hovelmeyer, N., Z. Hao, K. Kranidioti, G. Kassiotis, T. Buch, F. Frommer, L. von Hoch, D. Kramer, L. Minichiello, G. Kollias, H. Lassmann, and A. Waisman (2005). Apoptosis of Oligodendrocytes via Fas and TNF-R1 Is a Key Event in the Induction of Experimental Autoimmune Encephalomyelitis. *The Journal of Immunology 175*(9), 5875–5884.

Huang, J., S. Fancy, C. Zhao, D. Rowitch, C. Ffrench-Constant, and R. Franklin (2011). Myelin Regeneration in Multiple Sclerosis: Targeting Endogenous Stem Cells. *Neurotherapeutics 8*(4), 650–658.

Huang, J. K., A. A. Jarjour, B. Nait Oumesmar, C. Kerninon, A. Williams, W. Krezel, H. Kagechika, J. Bauer, C. Zhao, A. B.-V. Evercooren, P. Chambon, C. Ffrench-Constant, and R. J. M. Franklin (2011, January). Retinoid X receptor gamma signaling accelerates CNS remyelination. *Nature Neuroscience 14*(1), 45–53.

Indra, A. K., X. Warot, J. Brocard, J. M. Bornert, J. H. Xiao, P. Chambon, and D. Metzger (1999, November). Temporally-controlled site-specific mutagenesis in the basal layer of the epidermis: comparison of the recombinase activity of the tamoxifen-inducible Cre-ER(T) and Cre-ER(T2) recombinases. *Nucleic acids research 27*(22), 4324–7.

Irvine, K. A. and W. F. Blakemore (2006). Age increases axon loss associated with primary demyelination in cuprizone-induced demyelination in C57BL/6 mice. *Journal of Neuroimmunology 175*(1-2), 69–76.

Irvine, K. A. and W. F. Blakemore (2008). Remyelination protects axons from demyelination-associated axon degeneration. *Brain 131*(6), 1464–1477.

Jahn, O., S. Tenzer, and H. Werner (2009a). Myelin Proteomics: Molecular Anatomy of an Insulating Sheath. *Molecular Neurobiology 40*(1), 55–72.

Jahn, O., S. Tenzer, and H. Werner (2009b). Myelin Proteomics: Molecular Anatomy of an Insulating Sheath. *Molecular Neurobiology 40*(1), 55–72.

Jessell, T. M. and E. R. Kandel (1993). Synaptic transmission: A bidirectional and self-modifiable form of cell-cell communication. *Cell 72, Supple*(0), 1–30.

John, G. R., S. L. Shankar, B. Shafit-Zagardo, A. Massimi, S. C. Lee, C. S. Raine, and C. F. Brosnan (2002). Multiple sclerosis: Re-expression of a developmental pathway that restricts oligodendrocyte maturation. *Nature Medicine 8*(10), 1115–1121.

Johnson, K. P., B. R. Brooks, J. A. Cohen, C. C. Ford, J. Goldstein, R. P. Lisak, L. W. Myers, H. S. Panitch, J. W. Rose, R. B. Schiffer, T. Vollmer, L. P. Weiner, J. S. Wolinsky, and C. . M. S. S. Group (1995). Copolymer 1 reduces relapse rate and improves disability in relapsing-remitting multiple sclerosis. *Neurology 45*(7), 1268–1276.

Käll, L., A. Krogh, and E. L. L. Sonnhammer (2004). A Combined Transmembrane Topology and Signal Peptide Prediction Method. *Journal of Molecular Biology 338*(5), 1027–1036.

Kandel, E. R., J. H. Schwartz, and T. M. Jessell (2000). *Principles of neural science.* New York: McGraw-Hill, Health Professions Division.

Keller, A., A. I. Nesvizhskii, E. Kolker, and R. Aebersold (2002, October). Empirical statistical model to estimate the accuracy of peptide identifications made by MS/MS and database search. *Analytical chemistry 74*(20), 5383–92.

Kiryu-Seo, S., N. Ohno, G. J. Kidd, H. Komuro, and B. D. Trapp (2010). Demyelination Increases Axonal Stationary Mitochondrial Size and the Speed of Axonal Mitochondrial Transport. *The Journal of Neuroscience 30*(19), 6658–6666.

Kornek, B., M. K. Storch, R. Weissert, E. Wallstroem, A. Stefferl, T. Olsson, C. Linington, M. Schmidbauer, and H. Lassmann (2000). Multiple Sclerosis and Chronic Autoimmune Encephalomyelitis : A Comparative Quantitative Study of Axonal Injury in Active, Inactive, and Remyelinated Lesions. *American Journal of Pathology 157*(1), 267–276.

Kotter, M. R., W.-W. Li, C. Zhao, and R. J. M. Franklin (2006). Myelin Impairs CNS Remyelination by Inhibiting Oligodendrocyte Precursor Cell Differentiation. *The Journal of Neuroscience 26*(1), 328–332.

Krämer, E. M., T. Koch, A. Niehaus, and J. Trotter (1997, April). Oligodendrocytes direct glycosyl phosphatidylinositol-anchored proteins to the myelin sheath in glycosphingolipid-rich complexes. *The Journal of biological chemistry 272*(14), 8937–45.

Kremenchutzky, M., G. P. A. Rice, J. Baskerville, D. M. Wingerchuk, and G. C. Ebers (2006). The natural history of multiple sclerosis: a geographically based study 9: Observations on the progressive phase of the disease. *Brain 129*(3), 584–594.

Kreutzberg, G. W. (1996). Microglia: A sensor for pathological events in the CNS. *Trends in Neurosciences 19*(8), 312–318.

Krogh, A., B. Larsson, G. von Heijne, and E. L. L. Sonnhammer (2001). Predicting transmembrane protein topology with a hidden markov model: application to complete genomes. *Journal of Molecular Biology 305*(3), 567–580.

Kuhlmann, T., G. Lingfeld, A. Bitsch, J. Schuchardt, and W. Bruck (2002). Acute axonal damage in multiple sclerosis is most extensive in early disease stages and decreases over time. *Brain 125*(10), 2202–2212.

Kurtzke, J. F. (1983). Rating neurologic impairment in multiple sclerosis. *Neurology 33*(11), 1444.

Lappe-Siefke, C., S. Goebbels, M. Gravel, E. Nicksch, J. Lee, P. E. Braun, I. R. Griffiths, and K.-A. Nave (2003). Disruption of Cnp1 uncouples oligodendroglial functions in axonal support and myelination. *Nature Genetics 33*(3), 366–374.

Lassmann, H., W. Bruck, and C. F. Lucchinetti (2007). The Immunopathology of Multiple Sclerosis: An Overview. *Brain Pathology 17*(2), 210–218.

Laursen, L. S., C. W. Chan, and C. Ffrench-Constant (2009, July). An integrin-contactin complex regulates CNS myelination by differential Fyn phosphorylation. *The Journal of neuroscience : the official journal of the Society for Neuroscience 29*(29), 9174–85.

Lavi, E., D. H. Gilden, Z. Wroblewska, L. B. Rorke, and S. R. Weiss (1984). Experimental demyelination produced by the A59 strain of mouse hepatitis virus. *Neurology 34*(5), 597–.

Levine, J. M., R. Reynolds, and J. W. Fawcett (2001). The oligodendrocyte precursor cell in health and disease. *Trends in Neurosciences 24*(1), 39–47.

Liebetanz, D. and D. Merkler (2006). Effects of commissural de- and remyelination on motor skill behaviour in the cuprizone mouse model of multiple sclerosis. *Experimental Neurology 202*(1), 217–224.

Liebscher, T., L. Schnell, D. Schnell, J. Scholl, R. Schneider, M. Gullo, K. Fouad, A. Mir, M. Rausch, D. Kindler, F. P. T. Hamers, and M. E. Schwab (2005, November). Nogo-A antibody improves regeneration and locomotion of spinal cord-injured rats. *Annals of Neurology 58*(5), 706–19.

Lindner, M., J. Fokuhl, F. Linsmeier, C. Trebst, and M. Stangel (2009). Chronic toxic demyelination in the central nervous system leads to axonal damage despite remyelination. *Neuroscience Letters 453*(2), 120–125.

Locatelli, G., S. Wörtge, T. Buch, B. Ingold, F. Frommer, B. Sobottka, M. Krüger, K. Karram, C. Bühlmann, I. Bechmann, F. L. Heppner, A. Waisman, and B. Becher (2012a). Primary oligodendrocyte death does not elicit anti-CNS immunity. *Nature Neuroscience 15*(4), 543–50.

Locatelli, G., S. Wörtge, T. Buch, B. Ingold, F. Frommer, B. Sobottka, M. Krüger, K. Karram, C. Bühlmann, I. Bechmann, F. L. Heppner, A. Waisman, and B. Becher (2012b, April). Primary oligodendrocyte death does not elicit anti-CNS immunity. *Nature Neuroscience 15*(4), 543–50.

Lodge, A. P., M. R. Howard, C. J. McNamee, and D. J. Moss (2000). Co-localisation, heterophilic interactions and regulated expression of IgLON family proteins in the chick nervous system. *Molecular Brain Research 82*(1-2), 84–94.

Lovas, G., N. Szilágyi, K. Majtényi, M. Palkovits, and S. Komoly (2000, February). Axonal changes in chronic demyelinated cervical spinal cord plaques. *Brain 123*, 308–17.

Lucchinetti, C., W. Bruck, J. Parisi, B. Scheithauer, M. Rodriguez, and H. Lassmann (2000). Heterogeneity of multiple sclerosis lesions: Implications for the pathogenesis of demyelination. *Annals of Neurology 47*(6), 707–717.

Maña, P., S. A. Fordham, M. A. Staykova, M. Correcha, D. Silva, D. O. Willenborg, and D. Liñares (2009). Demyelination caused by the copper chelator cuprizone halts T cell mediated autoimmune neuroinflammation. *Journal of Neuroimmunology 210*(1-2), 13–21.

Manrique-Hoyos, N., T. Jürgens, M. Grø nborg, M. Kreutzfeldt, M. Schedensack, T. Kuhlmann, C. Schrick, W. Brück, H. Urlaub, M. Simons, and D. Merkler (2011). Late motor decline after accomplished remyelination: Impact for progressive MS. *Annals of Neurology*, n/a–n/a.

Martin, R., H. F. McFarland, and D. E. McFarlin (1992). Immunological Aspects of Demyelinating Diseases. *Annual Review of Immunology 10*, 153–187.

Mason, J. L., C. Langaman, P. Morell, K. Suzuki, and G. K. Matsushima (2001). Episodic demyelination and subsequent remyelination within the murine central nervous system: changes in axonal calibre. *Neuropathology and Applied Neurobiology 27*(1), 50–58.

Mathey, E. K., T. Derfuss, M. K. Storch, K. R. Williams, K. Hales, D. R. Woolley, A. Al-Hayani, S. N. Davies, M. N. Rasband, T. Olsson, A. Moldenhauer, S. Velhin, R. Hohlfeld, E. Meinl, and C. Linington (2007). Neurofascin as a novel target for autoantibody-mediated axonal injury. *The Journal of Experimental Medicine 204*(10), 2363–2372.

Matsushima, G. K. and P. Morell (2001). The Neurotoxicant, Cuprizone, as a Model to Study Demyelination and Remyelination in the Central Nervous System. *Brain Pathology 11*(1), 107–116.

Matthews, P. M. and D. L. Arnold (2001). Magnetic resonance imaging of multiple sclerosis: new insights linking pathology to clinical evolution. *Current Opinion in Neurology 14*(3), 279–287.

Matthieu, J.-M., R. H. Quarles, R. O. Brady, and H. deF Webster (1973). Variation of proteins, enzyme markers and gangliosides in myelin subfractions. *Biochimica et Biophysica Acta (BBA) - General Subjects 329*(2), 305–317.

McMahon, E. J., K. Suzuki, and G. K. Matsushima (2002). Peripheral macrophage recruitment in cuprizone-induced CNS demyelination despite an intact blood-brain barrier. *Journal of Neuroimmunology 130*, 32–45.

McNamee, C. J., J. E. Reed, M. R. Howard, A. P. Lodge, and D. J. Moss (2002, March). Promotion of neuronal cell adhesion by members of the IgLON family occurs in the absence of either support or modification of neurite outgrowth. *Journal of neurochemistry 80*(6), 941–8.

Merkler, D., S. Boretius, C. Stadelmann, T. Ernsting, T. Michaelis, J. Frahm, and W. Brück (2005). Multicontrast MRI of remyelination in the central nervous system. *NMR in Biomedicine 18*(6), 395–403.

Merkler, D., T. Ernsting, and W. Brück (2006). A new focal EAE model of cortical demyelination: multiple sclerosis-like lesions with rapid resolution of inflammation and extensive remyelination. *Brain 129*, 1972–1983.

Meyer zu Hoerste, G., A. L. Zozulya, H. El-Haddad, H. C. Lehmann, H.-P. Hartung, H. Wiendl, and B. C. Kieseier (2010). Active immunization induces toxicity of diphtheria toxin in diphtheria resistant mice: Implications for neuroinflammatory models. *Journal of Immunological Methods 354*, 80–84.

Mi, S., X. Lee, Z. Shao, G. Thill, B. Ji, J. Relton, M. Levesque, N. Allaire, S. Perrin, B. Sands, T. Crowell, R. L. Cate, J. M. McCoy, and R. B. Pepinsky (2004, March). LINGO-1 is a component of the Nogo-66 receptor/p75 signaling complex. *Nature Neuroscience 7*(3), 221–8.

Mi, S., R. H. Miller, X. Lee, M. L. Scott, S. Shulag-Morskaya, Z. Shao, J. Chang, G. Thill, M. Levesque, M. Zhang, C. Hession, D. Sah, B. Trapp, Z. He, V. Jung, J. M. McCoy, and R. B. Pepinsky (2005). LINGO-1 negatively regulates myelination by oligodendrocytes. *Nature Neuroscience 8*(6), 745–751.

Middlebrook, J. L. and R. B. Dorland (1977). Response of cultured mammalian cells to the exotoxins of Pseudomonas aeruginosa and Corynebacterium diphtheriae: differential cytotoxicity. *Canadian Journal of Microbiology 23*(2), 183–189.

Miller, D. H. and S. M. Leary (2007). Primary-progressive multiple sclerosis. *The Lancet Neurology 6*(10), 903–912.

Miller, D. H., A. J. Thompson, and M. Filippi (2003). Magnetic resonance studies of abnormalities in the normal appearing white matter and grey matter in multiple sclerosis. *Journal of Neurology 250*(12), 1407–1419.

Mokhtarian, F., D. E. McFarlin, and C. S. Raine (1984). Adoptive transfer of myelin basic protein-sensitized T cells produces chronic relapsing demyelinating disease in mice. *Nature 309*(5966), 356–358.

Mullis, K., F. Faloona, S. Scharf, R. Saiki, G. Horn, and H. Erlich (1986, January). Specific enzymatic amplification of DNA in vitro: the polymerase chain reaction. *Cold Spring Harbor symposia on quantitative biology 51 Pt 1*, 263–73.

Naglich, J. G., J. M. Rolf, and L. Eidels (1992). Expression of functional diphtheria toxin receptors on highly toxin-sensitive mouse cells that specifically bind radioiodinated toxin. *Proceedings of the National Academy of Sciences 89*(6), 2170–2174.

Nakahara, J., M. Maeda, S. Aiso, and N. Suzuki (2012). Current Concepts in Multiple Sclerosis: Autoimmunity Versus Oligodendrogliopathy. *Clinical Reviews in Allergy and Immunology 42*(1), 26–34.

Narayanan, S., L. Fu, E. Pioro, N. De Stefano, D. L. Collins, G. S. Francis, J. P. Antel, P. M. Matthews, and D. L. Arnold (1997). Imaging of axonal damage in multiple sclerosis: Spatial distribution of magnetic resonance imaging lesions. *Annals of Neurology 41*(3), 385–391.

Nave, K.-A. (2010). Myelination and support of axonal integrity by glia. *Nature 468*(7321), 244–252.

Nave, K.-A. and B. D. Trapp (2008). Axon-Glial Signaling and the Glial Support of Axon Function. *Annual Review of Neuroscience 31*(1), 535–561.

Nesvizhskii, A. I., A. Keller, E. Kolker, and R. Aebersold (2003, September). A statistical model for identifying proteins by tandem mass spectrometry. *Analytical chemistry 75*(17), 4646–58.

Neumann, H., M. R. Kotter, and R. J. M. Franklin (2009, February). Debris clearance by microglia: an essential link between degeneration and regeneration. *Brain 132*(Pt 2), 288–95.

Nielsen, J. A., D. Maric, P. Lau, J. L. Barker, and L. D. Hudson (2006). Identification of a Novel Oligodendrocyte Cell Adhesion Protein Using Gene Expression Profiling. *The Journal of Neuroscience 26*(39), 9881–9891.

Nikic, I., D. Merkler, C. Sorbara, M. Brinkoetter, M. Kreutzfeldt, F. M. Bareyre, W. Bruck, D. Bishop, T. Misgeld, and M. Kerschensteiner (2011). A reversible form of axon damage in experimental autoimmune encephalomyelitis and multiple sclerosis. *Nature Medicine 17*(4), 495–499.

Norton, W. T. and S. E. Poduslo (1973). Myelination of rat brain: method of myelin isolation. *Journal of Neurochemistry 21*(4), 749–757.

Noseworthy, J. H., C. Lucchinetti, M. Rodriguez, and B. G. Weinshenker (2000). Multiple Sclerosis. *New England Journal of Medicine 343*(13), 938–952.

Oluich, L.-J., J. A. S. Stratton, Y. Lulu Xing, S. W. Ng, H. S. Cate, P. Sah, F. A. Windels, T. J. Kilpatrick, and T. D. Merson (2012). Targeted Ablation of Oligodendrocytes Induces Axonal Pathology Independent of Overt Demyelination. *The Journal of Neuroscience 32*(24), 8317–8330.

O'Sullivan, M., D. K. Jones, P. E. Summers, R. G. Morris, S. C. R. Williams, and H. S. Markus (2001). Evidence for cortical "disconnection" as a mechanism of age-related cognitive decline. *Neurology 57*(4), 632–638.

Owens, G. P., D. Gilden, M. P. Burgoon, X. Yu, and J. L. Bennett (2011). Viruses and Multiple Sclerosis. *The Neuroscientist 17*(6), 659–676.

Pappenheimer, A. M. and M. Gill (1973). Diphtheria: Recent studies have clarified the molecular mechanisms involved in its pathogenesis. *Science 128*(4110), 353–358.

Parazzini, C., C. Baldoli, G. Scotti, and F. Triulzi (2002). Terminal Zones of Myelination: MR Evaluation of Children Aged 20-40 Months. *American Journal of Neuroradiology 23*(10), 1669–1673.

Pasquini, L., C. Calatayud, A. Bertone Uña, V. Millet, J. Pasquini, and E. Soto (2007). The Neurotoxic Effect of Cuprizone on Oligodendrocytes Depends on the Presence of Pro-inflammatory Cytokines Secreted by Microglia. *Neurochemical Research 32*(2), 279–292.

Paty, D. W., D. K. B. Li, t. U. B. C. M. S. Group, and t. I. M. S. S. Group (1993). Interferon beta1b is effective in relapsing-remitting multiple sclerosis. *Neurology 43*(4), 662.

Peles, E. and J. L. Salzer (2000). Molecular domains of myelinated axons. *Current Opinion in Neurobiology 10*(5), 558–565.

Peters, A. (1996). Age-related changes in oligodendrocytes in monkey cerebral cortex. *Journal of comparative neurology 371*(1), 153–163.

Peters, A. (2002). The effects of normal aging on myelin and nerve fibers: A review. *Journal of Neurocytology 31*(8), 581–593.

Pfeiffer, S. E., A. E. Warrington, and R. Bansal (1993). The oligodendrocyte and its many cellular processes. *Trends in Cell Biology 3*(6), 191–197.

Pham-Dinh, D., O. Boespflug-Tanguy, C. Mimault, A. Cavagna, G. Giraud, G. Leberre, B. Lemarec, and A. Dautigny (1993). Pelizaeus – Merzbacher disease: a frameshift deletion/insertion event in the myelin proteolipid gene. *Hum. Mol. Genet. 2*(4), 465–467.

Piaton, G., M.-S. Aigrot, A. Williams, S. Moyon, V. Tepavcevic, I. Moutkine, J. Gras, K. S. Matho, A. Schmitt, H. Soellner, A. B. Huber, P. Ravassard, and C. Lubetzki (2011). Class 3 semaphorins influence oligodendrocyte precursor recruitment and remyelination in adult central nervous system. *Brain 134*(4), 1156–1167.

Pillai, A. M., C. Thaxton, A. L. Pribisko, J.-G. Cheng, J. L. Dupree, and M. A. Bhat (2009, June). Spatiotemporal ablation of myelinating glia-specific neurofascin (Nfasc NF155) in mice reveals gradual loss of paranodal axoglial junctions and concomitant disorganization of axonal domains. *Journal of Neuroscience Research 87*(8), 1773–93.

Pohl, H. B. F., C. Porcheri, T. Mueggler, L. C. Bachmann, G. Martino, D. Riethmacher, R. J. M. Franklin, M. Rudin, and U. Suter (2011). Genetically Induced Adult Oligodendrocyte Cell Death Is Associated with Poor Myelin Clearance, Reduced Remyelination, and Axonal Damage. *The Journal of Neuroscience 31*(3), 1069–1080.

Poliak, S. and E. Peles (2003). The local differentiation of myelinated axons at nodes of Ranvier. *Nature Reviews Neuroscience 4*(12), 968–980.

Polman, C. H., P. W. O'Connor, E. Havrdova, M. Hutchinson, L. Kappos, D. H. Miller, J. T. Phillips, F. D. Lublin, G. Giovannoni, A. Wajgt, M. Toal, F. Lynn, M. A. Panzara, and A. W. Sandrock (2006). A Randomized, Placebo-Controlled Trial of Natalizumab for Relapsing Multiple Sclerosis. *New England Journal of Medicine 354*(9), 899–910.

Poltorak, M., R. Sadoul, G. Keilhauer, C. Landa, T. Fahrig, and M. Schachner (1987, October). Myelin-associated glycoprotein, a member of the L2/HNK-1 family of neural cell adhesion molecules, is involved in neuron-oligodendrocyte and oligodendrocyte-oligodendrocyte interaction. *The Journal of cell biology 105*(4), 1893–9.

Popko, B., C. Puckett, E. Lai, H. D. Shine, C. Readhead, N. Takahashi, S. W. Hunt, R. L. Sidman, and L. Hood (1987). Myelin deficient mice: Expression of myelin basic protein and generation of mice with varying levels of myelin. *Cell 48*(4), 713–721.

Pruitt, K. D., T. Tatusova, and D. R. Maglott (2003). NCBI Reference Sequence Project: update and current status. *Nucleic Acids Research 31*(1), 34–37.

Ransohoff, R. M. (2012). Animal models of multiple sclerosis: the good, the bad and the bottom line. *Nature Neuroscience 15*(8), 1074–1077.

Reddy, H., S. Narayanan, R. Arnoutelis, M. Jenkinson, J. Antel, P. M. Matthews, and D. L. Arnold (2000). Evidence for adaptive functional changes in the cerebral cortex with axonal injury from multiple sclerosis. *Brain 123*(11), 2314–2320.

Reed, J., C. McNamee, S. Rackstraw, J. Jenkins, and D. Moss (2004). Diglons are heterodimeric proteins composed of IgLON subunits, and Diglon-CO inhibits neurite outgrowth from cerebellar granule cells. *Journal of Cell Science 117*(17), 3961–3973.

Reynolds, R. and G. P. Wilkin (1988). Development of macroglial cells in rat cerebellum. II. An in situ immunohistochemical study of oligodendroglial lineage from precursor to mature myelinating cell. *Development 102*(2), 409–425.

Ridge, S. C., A. E. Sloboda, R. A. McReynolds, S. Levine, A. L. Oronsky, and S. S. Kerwar (1985, April). Suppression of experimental allergic encephalomyelitis by mitoxantrone. *Clinical immunology and immunopathology 35*(1), 35–42.

Rios, J. C., C. V. Melendez-Vasquez, S. Einheber, M. Lustig, M. Grumet, J. Hemperly, E. Peles, and J. L. Salzer (2000). Contactin-Associated Protein (Caspr) and Contactin Form a Complex That Is Targeted to the Paranodal Junctions during Myelination. *The Journal of Neuroscience 20*(22), 8354–8364.

Roach, A., K. Boylan, S. Horvath, S. B. Prusiner, and L. E. Hood (1983). Characterization of cloned cDNA representing rat myelin basic protein: Absence of expression in brain of shiverer mutant mice. *Cell 34*(3), 799–806.

Rocca, M. A., A. Ceccarelli, M. Rodegher, P. Misci, G. Riccitelli, A. Falini, G. Comi, and M. Filippi (2010). Preserved brain adaptive properties in patients with benign multiple sclerosis. *Neurology 74*(2), 142–149.

Rocca, M. A., B. Colombo, A. Falini, A. Ghezzi, V. Martinelli, G. Scotti, G. Comi, and M. Filippi (2005). Cortical adaptation in patients with MS: a cross-sectional functional MRI study of disease phenotypes. *The Lancet Neurology 4*(10), 618–626.

Rovaris, M., C. Confavreux, R. Furlan, L. Kappos, G. Comi, and M. Filippi (2006). Secondary progressive multiple sclerosis: current knowledge and future challenges. *The Lancet Neurology 5*(4), 343–354.

Saito, M., T. Iwawaki, C. Taya, H. Yonekawa, M. Noda, Y. Inui, E. Mekada, Y. Kimata, A. Tsuru, and K. Kohno (2001). Diphtheria toxin receptor-mediated conditional and targeted cell ablation in transgenic mice. *Nature Biotechnology 19*(8), 746–750.

Salzer, J. L. (1997). Clustering Sodium Channels at the Node of Ranvier: Close Encounters of the Axon-Glia Kind. *Neuron 18*(6), 843–846.

Salzer, J. L. (2003). Polarized Domains of Myelinated Axons. *Neuron 40*(2), 297–318.

Salzer, J. L., P. J. Brophy, and E. Peles (2008). Molecular domains of myelinated axons in the peripheral nervous system. *Glia 56*(14), 1532–1540.

Sato, F., H. Tanaka, F. Hasanovic, and I. Tsunoda (2009). Theiler's virus infection: Pathophysiology of demyelination and neurodegeneration. *Pathophysiology 18*(1), 31–41.

Schalomon, P. M. and D. Wahlsten (2002). Wheel running behavior is impaired by both surgical section and genetic absence of the mouse corpus callosum. *Brain Research Bulletin 57*(1), 27–33.

Sharp, P. A., B. Sugden, and J. Sambrook (1973, July). Detection of two restriction endonuclease activities in Haemophilus parainfluenzae using analytical agarose-ethidium bromide electrophoresis. *Biochemistry 12*(16), 3055–63.

Shields, S. A., J. M. Gilson, W. F. Blakemore, and R. J. M. Franklin (1999). Remyelination occurs as extensively but more slowly in old rats compared to young rats following gliotoxin-induced CNS demyelination. *Glia 28*(1), 77–83.

Sim, F. J., C. Zhao, J. Penderis, and R. J. M. Franklin (2002). The Age-Related Decrease in CNS Remyelination Efficiency Is Attributable to an Impairment of Both Oligodendrocyte Progenitor Recruitment and Differentiation. *The Journal of Neuroscience 22*(7), 2451–2459.

Simons, K. and D. Toomre (2000, October). Lipid rafts and signal transduction. *Nature reviews. Molecular cell biology 1*(1), 31–9.

Sloane, J. A., C. Batt, Y. Ma, Z. M. Harris, B. Trapp, and T. Vartanian (2010). Hyaluronan blocks oligodendrocyte progenitor maturation and remyelination through TLR2. *Proceedings of the National Academy of Sciences 107*(25), 11555–11560.

Smith, K. J. (2006, December). Axonal protection in multiple sclerosis–a particular need during remyelination? *Brain 129*(Pt 12), 3147–9.

Smith, K. J., W. F. Blakemore, and W. I. McDonald (1979). Central remyelination restores secure conduction. *Nature 280*(5721), 395–396.

Smith, K. J., R. Kapoor, S. M. Hall, and M. Davies (2001, April). Electrically active axons degenerate when exposed to nitric oxide. *Annals of neurology 49*(4), 470–6.

Sommer, I. and M. Schachner (1981, April). Monoclonal antibodies (O1 to O4) to oligodendrocyte cell surfaces: an immunocytological study in the central nervous system. *Developmental biology 83*(2), 311–27.

Sospedra, M. and R. Martin (2005). Immunology of Multiple Sclerosis*. *Annual Review of Immunology 23*(1), 683–747.

Spiegel, I., K. Adamsky, Y. Eshed, R. Milo, H. Sabanay, O. Sarig-Nadir, I. Horresh, S. S. Scherer, M. N. Rasband, and E. Peles (2007). A central role for Necl4 (SynCAM4) in Schwann cell-axon interaction and myelination. *Nature Neuroscience 10*(7), 861–869.

Stefano, N. D., P. M. Matthews, and D. L. Arnold (1995). Reversible decreases in N-acetylaspartate after acute brain injury. *Magnetic Resonance in Medicine 34*(5), 721–727.

Steinman, L. (1999). Assessment of Animal Models for MS and Demyelinating Disease in the Design of Rational Therapy. *Neuron 24*(3), 511–514.

Steinman, L. and S. S. Zamvil (2006, July). How to successfully apply animal studies in experimental allergic encephalomyelitis to research on multiple sclerosis. *Annals of neurology 60*(1), 12–21.

Stys, P. K., G. W. Zamponi, J. van Minnen, and J. J. G. Geurts (2012). Will the real multiple sclerosis please stand up? *Nature Reviews Neuroscience 13*(7), 507–514.

Syed, Y. A., A. S. Baer, G. Lubec, H. Hoeger, G. Widhalm, and M. R. Kotter (2008). Inhibition of oligodendrocyte precursor cell differentiation by myelin-associated proteins. *Neurosurgical FOCUS 24*(3-4), E5.

Tait, S., F. Gunn-Moore, J. M. Collinson, J. Huang, C. Lubetzki, L. Pedraza, D. L. Sherman, D. R. Colman, and P. J. Brophy (2000). An Oligodendrocyte Cell Adhesion Molecule at the Site of Assembly of the Paranodal Axo-Glial Junction. *Journal of cell biology 150*(3), 657–666.

Taylor, C. M., C. B. Marta, R. J. Claycomb, D. K. Han, M. N. Rasband, T. Coetzee, and S. E. Pfeiffer (2004). Proteomic mapping provides powerful insights into functional myelin biology. *Proceedings of the National Academy of Sciences 101*(13), 4643–4648.

Teitelbaum, D., A. Meshorer, T. Hirshfeld, R. Arnon, and M. Sela (1971, August). Suppression of experimental allergic encephalomyelitis by a synthetic polypeptide. *European journal of immunology 1*(4), 242–8.

The UniProt Consortium (2008). The Universal Protein Resource (UniProt). *Nucleic Acids Research 36*(suppl_1), D190–195.

Trajkovic, K., A. S. Dhaunchak, J. T. Goncalves, D. Wenzel, A. Schneider, G. Bunt, K.-A. Nave, and M. Simons (2006, March). Neuron to glia signaling triggers myelin membrane exocytosis from endosomal storage sites. *The Journal of cell biology 172*(6), 937–48.

Traka, M., K. Arasi, R. L. Avila, J. R. Podojil, A. Christakos, S. D. Miller, B. Soliven, and B. Popko (2010). A genetic mouse model of adult-onset, pervasive central nervous system demyelination with robust remyelination. *Brain 133*(10), 3017–3029.

Trapp, B. D. and K.-A. Nave (2008). Multiple Sclerosis: An Immune or Neurodegenerative Disorder? *Annual Review of Neuroscience 31*(1), 247–269.

Trapp, B. D., J. Peterson, R. M. Ransohoff, R. Rudick, S. Mork, and L. Bo (1998). Axonal transection in the lesions of multiple sclerosis. *New England Journal of Medicine 338*(5), 278–285.

Trapp, B. D., R. M. Ransohoff, E. Fisher, and R. A. Rudick (1999). Neurodegeneration in Multiple Sclerosis: Relationship to Neurological Disability. *The Neuroscientist 5*(1), 48–57.

Tsiperson, V., X. Li, G. J. Schwartz, C. S. Raine, and B. Shafit-Zagardo (2010, January). GAS6 enhances repair following cuprizone-induced demyelination. *PLoS ONE 5*(12), e15748.

Tutuncu, M., J. Tang, N. A. Zeid, N. Kale, D. J. Crusan, E. J. Atkinson, A. Siva, S. J. Pittock, I. Pirko, B. M. Keegan, C. F. Lucchinetti, J. H. Noseworthy, M. Rodriguez, B. G. Weinshenker, and O. H. Kantarci (2012). Onset of progressive phase is an age-dependent clinical milestone in multiple sclerosis. *Multiple Sclerosis Journal Published*.

Verkhratsky, A. and A. Butt (2007). Introduction to Glia. In *Glial Neurobiology*, pp. 1–12. John Wiley & Sons, Ltd.

Virchow, R. L. (1846). Über das granulierte Ansehen der Wandungen der Gehirnventrikel. . *Allg Z Psychiatrie 3*, 242–250.

Vukusic, S. and C. Confavreux (2007). Natural history of multiple sclerosis : risk factors and prognostic indicators. *Current Opinion in Neurology 20*(3), 269–274.

Wahlsten, D. (1984, July). Growth of the mouse corpus callosum. *Brain research 317*(1), 59–67.

Wang, K. C., J. A. Kim, R. Sivasankaran, R. Segal, and Z. He (2002, November). P75 interacts with the Nogo receptor as a co-receptor for Nogo, MAG and OMgp. *Nature 420*(6911), 74–8.

Waxman, S. G. and J. M. Ritchie (1993). Molecular dissection of the myelinated axon. *Annals of Neurology 33*(2), 121–136.

Weinshenker, B. G., B. Bass, G. P. A. Rice, J. Noseworthy, W. Carriere, J. Baskerville, and G. C. Ebers (1989). The natural history of Multiple Sclerosis: a geographically based study. *Brain 112*(1), 133–146.

Werner, H. B., K. Kuhlmann, S. Shen, M. Uecker, A. Schardt, K. Dimova, F. Orfaniotou, A. Dhaunchak, B. G. Brinkmann, W. Mobius, L. Guarente, P. Casaccia-Bonnefil, O. Jahn, and K.-A. Nave (2007). Proteolipid Protein Is Required for Transport of Sirtuin 2 into CNS Myelin. *The Journal of Neuroscience 27*(29), 7717–7730.

Werner, S., J. Saha, C. Broderick, E. Zhen, R. Higgs, K. Duffin, and R. Smith (2010). Proteomic Analysis of Demyelinated and Remyelinating Brain Tissue following Dietary Cuprizone Administration. *Journal of Molecular Neuroscience 42*(2), 210–225.

Wigler, M., S. Silverstein, L. S. Lee, A. Pellicer, Y. c. Cheng, and R. Axel (1977, May). Transfer of purified herpes virus thymidine kinase gene to cultured mouse cells. *Cell 11*(1), 223–32.

Williams, A., G. A. Piaton, M.-S. A. Aigrot, A. Belhadi, M. Théaudin, F. Petermann, J.-L. A. Thomas, B. Zalc, and C. Lubetzki (2007). Semaphorin 3A and 3F: key players in myelin repair in multiple sclerosis? *Brain 130*(10), 2554–2565.

Wolswijk, G. (1998). Chronic Stage Multiple Sclerosis Lesions Contain a Relatively Quiescent Population of Oligodendrocyte Precursor Cells. *The Journal of Neuroscience 18*(2), 601–609.

Wybrecht, D., F. A. Reuter, W. Zaaraoui, A. Faivre, L. Crespy, A. Rico, I. Malikova, S. Confort-Gouny, E. Soulier, P. J. Cozzone, J. Pelletier, J.-P. Ranjeva, and B. Audoin (2012). Voxel-wise analysis of conventional magnetic resonance imaging to predict future disability in early relapsing-remitting multiple sclerosis. *Multiple Sclerosis Journal Published*.

Xu, H., H. Yang, B. McConomy, R. A. Browning, and X.-M. Li (2010). Behavioral and neurobiological changes in C57BL/6 mouse exposed to cuprizone: effects of antipsychotics. *Frontiers in Behavioral Neuroscience 4*(8), 1–10.

Xu, H., H.-J. Yang, Y. Zhang, R. Clough, R. Browning, and X.-M. Li (2009). Behavioral and neurobiological changes in C57BL/6 mice exposed to cuprizone. *Behavioral Neuroscience 123*(2), 418–429.

Yadav, V. and D. Bourdette (2012). New Disease-Modifying Therapies and New Challenges for MS. *Current Neurology and Neuroscience Reports Published*, 1–3.

Yamaizumi, M., E. Mekada, T. Uchida, and Y. Okada (1978). One molecule of diphtheria toxin fragment a introduced into a cell can kill the cell. *Cell 15*(1), 245–250.

Yednock, T. A., C. Cannon, L. C. Fritz, F. Sanchezmadrid, L. Steinman, and N. Karin (1992). Prevention of Experimental Autoimmune Encephalomyelitis by Antibodies against Alpha-4-Beta-1 Integrin. *Nature 356*(6364), 63–66.

Yin, X., T. O. Crawford, J. W. Griffin, P.-h. Tu, V. M.-Y. Lee, C. Li, J. Roder, and B. D. Trapp (1998). Myelin-Associated Glycoprotein Is a Myelin Signal that Modulates the Caliber of Myelinated Axons. *The Journal of Neuroscience 18*(6), 1953–1962.

Yoshikawa, K., S. Palumbo, C. D. Toscano, and F. Bosetti (2011, July). Inhibition of 5-lipoxygenase activity in mice during cuprizone-induced demyelination attenuates neuroinflammation, motor dysfunction and axonal damage. *Prostaglandins, leukotrienes, and essential fatty acids 85*(1), 43–52.

NATALIA MANRIQUE HOYOS

Phone: +49 (0) 551 3899-534   Hermann-Rein-Str. 3
manrique@em.mpg.de   Goettingen, Germany 37073

EDUCATION

PhD   **Georg-August University Goettingen**, Neuroscience.   *2009-expected November 2012*
Dissertation: "Neurodegeneration in toxin-mediated demyelinating animal models of MS"
Committee: Dr. Mikael Simons (advisor), Dr. Wolfgang Brück, Dr. Till Marquardt

MS   **Georg-August University Goettingen**, Neuroscience.   *2007-2009*
Thesis: "Proteomic analysis of myelin in aging and demyelinating disease"
Committee: Dr. Mikael Simons (advisor), Dr. Wolfgang Brück, Dr. Till Marquardt

BS   **Pontificia Universidad Javeriana**, Biology   *2002-2007*
GPA: 4.24 (out of 5).

RESEARCH EXPERIENCE

PhD (in progress)   *April 2009-present*
"Glial-mediated axonal support in animal models of multiple sclerosis"
Department of Cellular Neuroscience. Max Planck Institute for Experimental Medicine, Göttingen. Advisor: Dr. Mikael Simons.

Master Thesis   *October 2008-March 2009*
"Proteomic analysis of myelin in aging and demyelinating disease".
Department of Cellular Neuroscience. Max Planck Institute for Experimental Medicine, Göttingen. Advisor: Dr. Mikael Simons.

Graduate School Lab Rotation   *May- June 2008*
"Expression of MHC class I in the brain of common marmoset (*Callithrix jacchus*)". Clinical Neurobiology Laboratory, German Primate Center, Göttingen. Advisor: Dr Eberhard Fuchs.

Graduate School Lab Rotation   *March-April 2008*
"Proteolipids interactions in Pelizaeus-Merzbacher disease". Department of Neurogenetics Max Planck Institute for Experimental Medicine, Göttingen. Advisor: Dr. Hauke Werner.

Graduate School Lab Rotation   *January-March 2008*
"Assessment of Beta-Synuclein-induced Experimental Autoimmune Encephalomyelitis in CD8-deficient Lewis rats". Department of Neuropathology, Göttingen Georg-August-Universität. Advisor: Dr. Christine Stadelmann.

Undergraduate Thesis Project   *September 2006 -May 2007*
"Genetic structure and connectivity of *Palythoa caribaeorum* populations in the Colombia Caribbean using nuclear rDNA markers". Population Genetics and Evolutionary Biology Laboratory, Javeriana University. Advisor: Dr. Alberto Acosta.

Internship   *January - May 2006*
"Standardization of heterologue rDNA nuclear and microsatellite markers PCR protocol for *Palythoa caribaeorum*". Population Genetics and Evolutionary Biology Laboratory, Javeriana University. Coordinated by Dr. Alberto Acosta and Dr. Manuel Ruiz-Garcia.

HONORS AND AWARDS

PhD Excellence Stipend   *2009-Present*
Awarded by the Göttingen Graduate School for Neurosciences and Molecular Neurosciences (GGNB), Georg-August University Goettingen (4 awarded per semester).

MSc Stipend   *2007 – 2008*
Excellence Foundation for the Promotion of the Max Planck Society, International Master's/PhD/MD-PhD IMPRS Neuroscience Program (15-20 awarded per year).

3rd best national score, Biology undergraduate studies examination ECAES Colombia *2006*.
Acknowledgement granted on August 4th, 2006 by the Javeriana University.

11th best national score in the examination for university entrance (ICFES), Colombia, *2001*
Diploma granted on November 29th, 2001 by the Education Ministry to the best 50 scores.

TEACHING EXPERIENCE

Mentoring   *May-June 2011*
Designed and mentored a 2-month lab rotation student. Department of Cellular Neuroscience, Max Planck Institute for Experimental Medicine, Göttingen, Germany.

Teaching Assistant   *January-June 2005*
Genetics undergraduate course. Department of Biology, Javeriana University, Colombia.

PUBLICATIONS

Manrique-Hoyos, N., T. Jürgens, M. Grønborg, M. Kreutzfeldt, M. Schedensack, T. Kuhlmann, C. Schrick, W. Brück, H. Urlaub, M. Simons and D. Merkler. 2012. Late motor   decline   after accomplished remyelination: Impact for progressive multiple sclerosis. Ann Neurol. 71: 227 – 244.

Ghosh A*, **N. Manrique-Hoyos***, A. Voigt, J. Schulz, M. Kreutzfeldt, D. Merkler and M. Simons. 2011. Targeted Ablation of Oligodendrocytes Triggers Axonal Damage. PLoS ONE 6(7): e22735.

Hsu, C., Y. Morohashi, S. Yoshimura, **N. Manrique-Hoyos**, S. Jung, M. Lauterbach, M. Bakhti, M. Groenborg, W. Möbius, J. Rhee, F. Barr and M. Simons. 2010. Regulation of exosome secretion by Rab35 and its GTPase-activating proteins TBC1D10A-C. J. Cell Biol. 189(2): 223-32.

PRESENTATIONS

Seminars
• Progress reports at IMPRS Neuroscience retreat, and at the departments of Neurogenetics and Cellular Neuroscience, MPI of Experimental Medicine, Goettingen. 2008-present.
• EMBO Young Investigator Programme PhD workshop, Heidelberg, Germany. 2010.

Poster presentation
• 26th Congress of the European Committee for Treatment and Research in Multiple Sclerosis (ECTRIMS), Goteburg, Sweden. 2010.
• Neurizons 2011: From Molecules to Mind, Goettingen, Germany. 2011
• EMBO Young Investigator Programme PhD workshop, Heidelberg, Germany. 2010.
• Glia in Health & Disease Meeting. Cold Spring Harbor Laboratory, NY. 2012.

PROFESSIONAL SERVICE

International Scientific Conference Co-Organizer   *2011*
International symposium "Neurizons 2011: From Molecules to Mind".
May 25th- 28th, 2011. Goettingen, Germany. Over 250 participants, responsibilities included public relations, logistics, invitation and introduction of international speakers.

List of Publications

Manrique-Hoyos, N., T. Jürgens, M. Grønborg, M. Kreutzfeldt, M. Schedensack, T. Kuhlmann, C. Schrick, W. Brück, H. Urlaub, M. Simons and D. Merkler. (2012).Late motor decline after accomplished remyelination: Impact for progressive multiple sclerosis. *Ann Neurol.*; 71: 227 – 244.

Ghosh A.*, **N. Manrique-Hoyos***, A. Voigt, J. Schulz, M. Kreutzfeldt, D. Merkler and M. Simons. (2011) Targeted Ablation of Oligodendrocytes Triggers Axonal Damage. *PLoS ONE*; 6(7): e22735.
*These authors contributed equally to this work.

Hsu C., Y. Morohashi, S. Yoshimura, **N. Manrique-Hoyos**, S. Jung, M. Lauterbach, M. Bakhti, M. Grønborg M, W. Möobius, J. Rhee, F. Barr, M. Simons. (2010) Regulation of exosome secretion by Rab35 and its GTPase-activating proteins TBC1D10A-C. *J Cell Biol.* 189:223 – 32.